Syntaxin – Munc18 Interaction

by

Angela McDonald

Thesis for degree of

Doctor of Philosophy

School of Medicine and Veterinary Medicine

University of Edinburgh

July 2005

Declaration of Originality

I declare that, unless otherwise stated, this thesis represents my own work and was composed by me. No part of this work has been, or is being submitted for any other degree or qualification.

Angela McDonald

16th July 2005

Acknowledgements

I would like to thank my supervisors, Dr. David K. Apps and Prof. Michael J. Shipston for their guidance and constructive advice throughout this project. I thank Dr. Rory Duncan for his invaluable help and encouragement over the last four years. I would like to thank all the members of the Membrane Biology Group both past and present for their friendship and support. Thanks are also due to Linda W. Wilson for technical assistance with the confocal microscopy facility. Finally, I would like to express my thanks to my family and Richard for their encouragement and patience throughout my studies. This work was funded by a University of Edinburgh research scholarship and the Wellcome Trust.

Abbreviations

A	absorbance
A	adenine
ANF	atrial natriuretic factor
ATP	adenosine triphosphate
AtT20 cells	anterior pituitary corticotroph tumour cell-line
BCC	bovine chromaffin cell
BFP	blue fluorescent protein
bp	base pair(s)
BP	band pass
BSA	bovine serum albumin
C	carboxy
C	cytosine
CD	circular dichroism
Cdk5	cyclin-dependent Kinase 5
cDNA	complementary DNA
CLSM	confocal laser scanning microscopy
°C	degrees Celsius
cyt	cytoplasmic
DEPC	diethyl pyrocarbonate
DMEM	Dulbecco's modified Eagle's medium
DMSO	dimethyl sulphoxide
DNA	deoxyribonucleic acid
dNTP	2'-deoxynucleoside 5'-triphosphate
DSRed	*Discosoma striata* red fluorescent protein

DTT	dithiothreitol
ECFP	Enhanced cyan fluorescent protein
ECL	Enhanced-chemiluminescence
EDTA	ethylenediaminetetraacetic acid
EGFP	enhance green fluorescent protein
EGTA	ethylene glycol bis(β-aminoethyl ether)-N,N,N',N-tetraacetate)
ER	endoplasmic reticulum
EYFP	enhanced yellow fluorescent protein
4α-PMA	phorbol 4α-myristoyl
FLIM	fluorescent lifetime imaging
FM-dyes	Fei Mao dyes
FRET	fluorescent resonant energy transfer
fs	femtosecond
fwhm	full width half maximal
G	guanidine
GABA	gamma-aminobutyric acid
GFP	green fluorescent protein
GST	glutathione S-transferase
GSH	Glutathione Sepharose 4B
h	hours
HcRed	*Heteractis crispa* red fluorescent protein
HEK293	transformed human embryonic kidney cell-line
His	histidine
HRP	horseradish peroxidase
H_2O	water
IgG	immunoglobulin G

INS-1 β-cells	insulin secreting beta cells
IPTG	isopropyl-β-thiogalactopyranoside
IR	infrared
Kb	kilobase-pair(s)
kDa	kiloDalton(s)
l	litre
λ	wavelength
LB	Luria-Bertani medium
LDCV	large dense-core vesicle
LP	long pass
LTR	LysoTracker Red
M	molar
MCS	multiple cloning site
MCP-PMT	multichannel plate-photomuliplier tube
mg	milligram
mins	minutes
minis	spontaneous miniature release events
μM	micromolar
N	amino
NAD(P)H	nicotinamide adenine dinucleotide phosphate (reduced form)
NDSB	non detergent sulfobutane
ng	nanogram
NGF	nerve growth factor
nm	nanometre
NSF	soluble-N-ethyl-maleimide sensitive factor
PBS	phosphate-buffered saline buffer

PC12	Pheochromocytoma cells
PCR	polymerase chain reaction
PKC	protein kinase C
PMA	phorbol myristoyl acetate
PMSF	phenyl methyl sulfonyl fluoride
PSF	point spread function
PVDF	polyvinylidene difluoride
pmol	picomoles
RNA	ribonucleic acid
RNasin	ribonuclease inhibitor
RP	reserve pool
RRP	readily releasable pool
s	second(s)
SDCV	small dense-cored vesicle
SDS	sodium dodecyl sulphate
SDS-PAGE	sodium dodecyl sulphate-polyacrylamide gel electrophoresis
SM protein	Sec1/munc18 protein
SNAP-25	synaptosomal-associated protein of 25kDa
SNARE	soluble N-ethylmaleimide-sensitive fusion protein-attachment protein receptor
SV	synaptic vesicle
T	thymine
TAC	time-amplitude-converter
TB	terrific broth
TBS	tris-buffered saline
TBST	tris-buffered saline-Tween buffer

TCA	trichloroacetic acid
TCSPC	time-correlated single photon counting
TEMED	N, N, N', N-tetramethylenediamine
3D	three dimensional
TGN	trans Golgi network
TIRFM	Total Internal Reflection Fluorescence Microscopy
Tm	melting temperature
TMD	transmembrane domain
Tris	tris[hydroxymethyl]aminomethane
Triton X-100	octylphenyl-nonaoxyethylene
tRNA	transfer RNA
TTS	transit time spread
Tween-20	polyoxyethylene-sorbitan monolaurate
2D	two dimensional
UV	ultraviolet
VAMP	vesicle associated membrane protein
vs	verses
wt	wild-type
v/v	volume per volume
w/v	weight per volume
w/w	weight per weight

Abstract

Regulated exocytosis is spatially and temporally regulated by a cascade of protein-protein interactions. The minimal machinery required for membrane fusion is the SNARE complex, formed between three membrane proteins: syntaxin, synaptobrevin (VAMP) and SNAP-25. The conformation of syntaxin 1a, which exists in 'open' and 'closed' states, is believed to play a role in SNARE complex assembly in neuronal and neuroendocrine cells, through regulation of the interconversion between its different conformational states by the cytoplasmic protein munc18-1. Recent work has also demonstrated that phosphorylation of munc18-1 by protein kinase C on serines 306 and 313 weakens its affinity for syntaxin 1a *in vitro*.

To further understand the role of the syntaxin 1a – munc18-1 complex, the interaction of these two proteins was studied *in vitro* and *in vivo*. These studies utilized munc18-1 and syntaxin 1a chimeras containing the fluorescent proteins EGFP and EYFP. Use of radiolabelled munc18-1, EGFP-munc18-1, munc18-1_{R39C} (mutated in a residue that is important for interaction with syntaxin 1a and for maintaining munc18-1s conformation), EGFP-munc18-1_{R39C}, EYFP-munc18-$1_{S306E:S313E}$ (a phosphomimetic mutant) and EYFP-munc18-$1_{R39C:S306E:S313E}$ in *in vitro* binding studies revealed that the addition of the fluorescent proteins to syntaxin 1a and munc18-1 had little effect on their interaction in comparison with wild-type proteins. The munc18-1_{R39C} and the phosphomimetic munc18-1 mutants had a reduced affinity for syntaxin 1a. In order to study protein interaction within cells, using a cell line with no endogenous protein background, munc18-1 and syntaxin 1a variants were expressed in HEK293 cells and imaged using confocal laser scanning microscopy. These studies showed that phosphorylation of munc18-1 reorganised the cellular localisation of the syntaxin 1a – munc18-1 complex from the cytoplasm to the plasma membrane. Finally FRET and FLIM analysis of the interaction between ECFP-syntaxin 1a and EYFP-munc18-1, and its mutants, revealed that the conformation of the syntaxin 1a – munc18-1complex depended on its cellular location, and that PKC phosphorylation of munc18-1 occurred in a

spatially restricted manner in HEK293 cells, altering the intracellular conformation. Also the syntaxin 1a – munc18-1 complex can assume at least one other spatially defined conformation on the plasma membrane.

Contents

List of Figures

Chapter 1

Chapter 2

Chapter 3

Chapter 7

Chapter 1

Introduction

1.1 The Secretory Pathway

One of the defining features of eukaryotic cells is their compartmentalisation into membrane-bound organelles. Cellular life and differentiation depend on keeping the boundaries of a cell and its organelles intact at all times. There is, however, a dynamic flux of membrane constituents and cargo transported between these organelles and to the plasma membrane without compromising membrane integrity (Bock and Scheller 1999; Jahn and Sudhof 1999). With the advent of electron microscopy in the 1960s and 1970s, and following the development of cell-free systems for the study of protein synthesis, the hypothesis of the secretory pathway was developed, which posited that proteins to be secreted were synthesised on ribosomes bound to the endoplasmic reticulum, co-translationally translocated into the lumen, moved to and through the Golgi apparatus then packaged into secretory vesicles and finally secreted (Blobel, Walter et al. 1979). This process is largely mediated by the budding of transport vesicles from a donor compartment followed by the trafficking to and fusion with an acceptor compartment, and the transfer of soluble vesicular constituents (Figure 1.1) (Bock and Scheller 1999). Limited progress made in understanding the secretory pathway was largely due to two approaches: the biochemical dissection of the secretory machinery of mammalian cells, including vertebrate synapses, and the genetic dissection of the secretory pathway in yeast. Both approaches revealed that a key event in intracellular membrane traffic is membrane fusion. This suggested a common underlying mechanism for all trafficking reactions between intracellular organelles during constitutive and regulated secretory pathways within cell types ranging from yeast to man, with some pathways having specialised features (Jahn and Sudhof 1999).

1.2 Exocytosis

Exocytosis forms the basis of intercellular communication in multicellular organisms through the release of a wide array of signalling molecules. The fusion of secretory vesicles with the plasma membrane is essential for normal cellular function and occurs in most cells

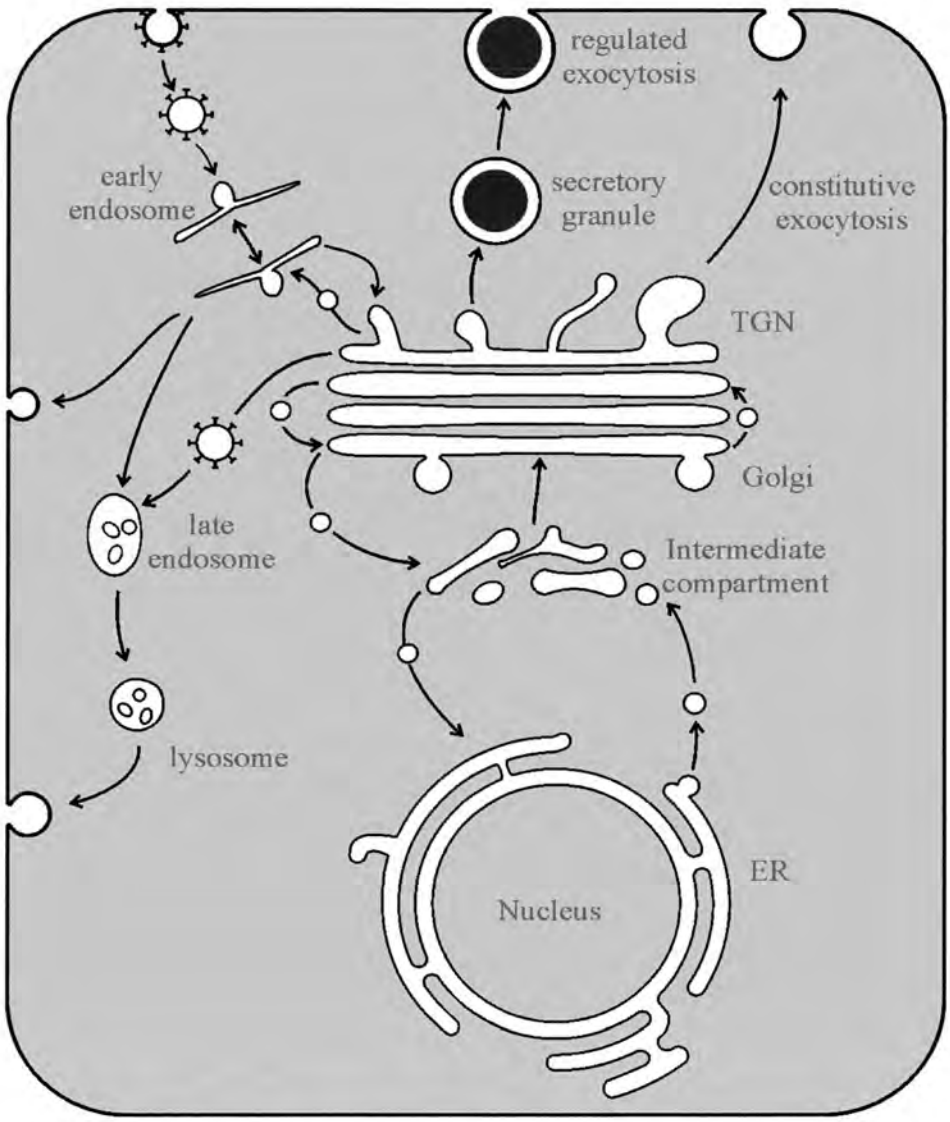

Figure 1.1: Overview of the secretory pathway

Proteins are translated on bound ribosomes and co-translationally translocated into the endoplasmic reticulum (ER). The proteins travel through the ER then onto and through the Golgi apparatus. In the Golgi the proteins are packaged into secretory vesicles that travel to the plasma membrane, where they fuse releasing their contents into the extracellular space. Transport between organelles occurs by the budding of vesicles from the donor compartment followed by the subsequent trafficking and fusion with the appropriate acceptor compartment

in the form of constitutive exocytosis, allowing the maintenance of plasma membrane lipids, proteins and the extracellular environment. In addition, some cells perform more specialised forms of exocytosis: regulated exocytosis, used to release materials, such as neurotransmitters, neuropeptides, cytokines, hormones, and also to control levels of different lipids, receptors and transporters in the plasma membrane, in a highly regulated manner. Regulated exocytosis occurs in response to a range of physiological signals, which usually result in an increase in the intracellular free calcium concentration. Although the regulation differs, the fundamental pathway and the basic machinery involved in constitutive and regulated exocytosis and for membrane fusion throughout the secretory pathway are similar (Brunger 2000; Lin and Scheller 2000; Burgoyne and Morgan 2003).

1.3 Types of secretory vesicles

The ability of secretory cells to release material by exocytosis, strictly on demand, is accomplished by the selective exclusion of regulated secretory proteins from constitutive secretory vesicles. Therefore an alternative organelle capable of stimulus-induced exocytosis is used, known as the secretory vesicle. There are different types of secretory vesicles present in different types of secretory cells (Burgoyne and Morgan 2003). Neuronal cells contain two types of secretory vesicles, synaptic vesicles (SVs) and large dense-cored vesicles (LDCVs), also found in neuroendocrine cells. SVs are approximately spherical with a diameter of 50 nm and store non-peptide transmitters. Within neurons each synapse is thought to contain 200-250 SVs. LDCVs store peptide hormones and biogenic amines and have a diameter of 150-300 nm. Exocytosis of SVs and LDCVs is separately controlled via differences in sensitivity to Ca^{2+} although probably through a common mechanism. In addition to SVs and LDCVs, peripheral neurons contain secretory vesicles of intermediate size (60-80 nm) called small dense-cored vesicles (SDCVs), which store catecholamines (Apps 2004).

1.3.1 Vesicle biogenesis

Both SVs and LDCVs are generated from the Golgi apparatus, although with significant differences. The cargo proteins of LDCVs accumulate in the trans Golgi network (TGN) forming aggregates, resulting in the deformation of the TGN membrane, condensation of the granule matrix and membrane budding to form immature secretory granules. Newly formed LDCVs then mature by fusing with other immature granules, and undergoing membrane remodelling, with the removal of mis-sorted material via clathrin coated vesicles (Burgoyne and Morgan 2003; Apps 2004). SVs also bud from the Golgi as immature vesicles with morphology and protein composition different from mature SVs. They reach synapses by axonal transport where they undergo processing and remodelling.

The major difference between SVs and LDCVs lies in their fate following fusion with the plasma membrane. After LDCV fusion, vesicle membrane components are retrieved and recycled to the Golgi, where they collect new cargo, thus generating vesicles *de novo* in each cycle. In contrast SVs are used many times, being locally recycled up to 1-2000 times prior to degradation, because most central nerve synapses are far from the cell body. Therefore, *de novo* generation of SVs after fusion would not produce enough SVs to maintain prolonged stimulation. Also some transmitters, such as GABA are synthesised in nerve terminals. SVs use proton-coupled transporters for neurotransmitter uptake. This proton motive force is generated by a V-type H^+-translocating ATPase (Apps 2004).

1.4 Regulated exocytosis

Regulated exocytosis consists of a sequence of functionally defined steps (Figure 1.2). Before any event at the plasma membrane, secretory vesicles may need to be mobilized by dissolution of cytoskeletal barriers to movement, and thereafter transported to their site of fusion (Cheek and Burgoyne 1987; Greengard, Valtorta et al. 1993; Vitale, Seward et al. 1995). The first step in exocytosis proper, membrane attachment, also known as tethering, requires that the secretory vesicles and the plasma membrane "recognise" each other. This

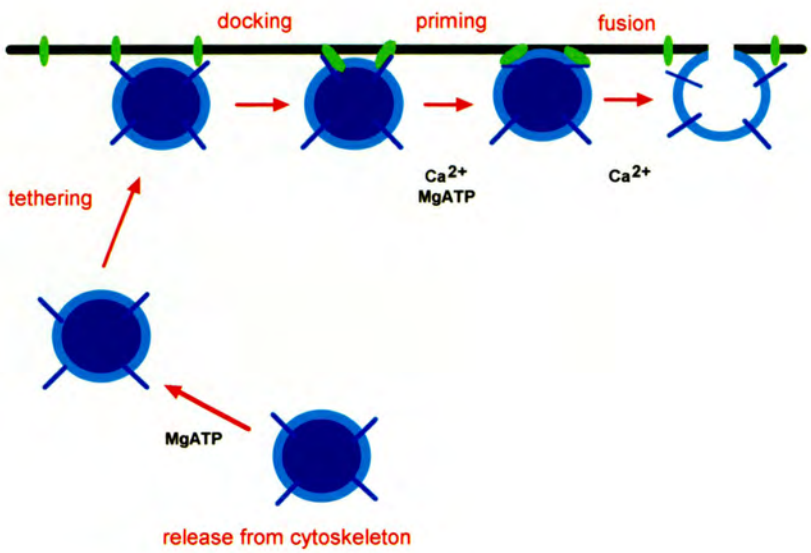

Figure 1.2: The steps involved in regulated exocytosis

Secretory vesicles are initially mobilised, move towards the plasma membrane and associate with it in a process known as *tethering*. Proteins on the vesicles then undergo specific interactions with proteins present on the plasma membrane (*docking*) which is followed by the *priming* of the vesicles into a fusion-competent state, through several steps that require Ca^{2+} and MgATP. The vesicles then undergo *fusion* with the plasma membrane through the opening of a fusion pore that either expands, resulting in *full fusion*, or closes again *(kiss and run)*.

step results in the vesicles becoming "morphologically docked", i.e. closely associated with the membrane; but docking itself, i.e. direct engagement with the fusion machinery, may be a separate process. After docking secretory vesicles undergo priming, which probably contains multiple events and requires both ATP hydrolysis and a low concentration of Ca^{2+}. The final stage in regulated exocytosis is membrane fusion, the signal for which is invariably increased free [Ca^{2+}], at a higher concentration than is needed for priming, typically in the 2-30 μM range for most types of regulated exocytosis. Fusion then proceeds through the formation of a fusion pore that can open transiently or expand, leading to full fusion. The molecular nature of the fusion pore is still a matter for debate (Lindau and Alvarez de Toledo 2003) although it has recently been proposed that the pore initially formed contains the transmembrane domains of several syntaxin molecules (Han, Wang et al. 2004). The opening of the fusion pore is probably the most tightly regulated step since it mediates the release of the secretory materials. In the case of neurotransmitter release, acute triggering of release has to act on the very last step of exocytosis simply because Ca^{2+}-triggered release is so fast (<100 μs in some synapses) that there is probably insufficient time for it to act on earlier steps. Based on this speed, it has been argued that synaptic vesicle exocytosis is arrested at a late step in fusion, i.e. largely completed during priming, and that elevated [Ca^{2+}] acts at a point in exocytosis at which only fusion pore opening is required for release (Gerber and Sudhof 2002; Burgoyne and Morgan 2003). Extensive evidence suggests, however, that the steps prior to fusion are also tightly regulated.

Functional studies of secretion kinetics, in a variety of cells, have led to the proposal of distinct functional pools of vesicles (Heinemann, Chow et al. 1994; Eliasson, Renstrom et al. 1997; Nelson, Robinson et al. 2002). Only a small fraction of the synaptic vesicles docked at the plasma membrane, referred to as the readily releasable pool (RRP) are ready/available for immediate release upon Ca^{2+} influx. The remaining vesicles belong to a reserve pool (RP), perhaps retained by a cytoskeletal network, which requires recruitment in an ATP-,

Ca^{2+}-, and temperature-dependent fashion prior to release (Holz, Bittner et al. 1989; Bittner and Holz 1992; Barg, Olofsson et al. 2002).

Through studies of membrane trafficking in yeast and *in vitro* fusion reactions of intracellular organelles, similarities between all eukaryotic fusion reactions have emerged, where four protein families play key roles: NSF and its adaptor proteins (α-soluble NSF attachment protein, α-SNAP), soluble N-ethylmalemide-sensitive factor attachment protein receptors (SNAREs), Sec1/munc18 (SM Proteins) and Rab proteins (Sudhof 1995; Gerber and Sudhof 2002; Burgoyne and Morgan 2003).

1.5 NSF and SNAPs

The discovery of NSF followed the development of a cell-free assay for vesicular traffic between mammalian ER and Golgi (Beckers, Block et al. 1989), the sensitivity of this process to the alkylating agent N-ethyl maleimide permitting the isolation of its target. NSF is a hexameric ATPase, homologous to sec18p in yeast, which was independently discovered by mutational analysis (Wilson, Wilcox et al. 1989; Kaiser and Schekman 1990). The three SNAPS (α, β and γ) were then discovered as soluble brain proteins that bound to NSF, as part of a stoichiometric 20S-complex that contained the SNAREs (see below) α-SNAP, which stimulates the ATPase activity of NSF, is homologous to the yeast protein sec17p.

1.6 SNARE proteins

SNARE proteins were discovered independently in yeast and neurons and were originally classified on the basis of their subcellular localisation, either as t-SNAREs (found on the target membrane) or as v-SNAREs (located on the vesicle membrane) (Figure 1.3A). Sequence analysis revealed that they all contained a characteristic heptad repeat of ~70 residues, known as the SNARE motif, which mediates the association of SNAREs into core complexes (see below). In addition to the SNARE motifs, SNAREs contain flanking

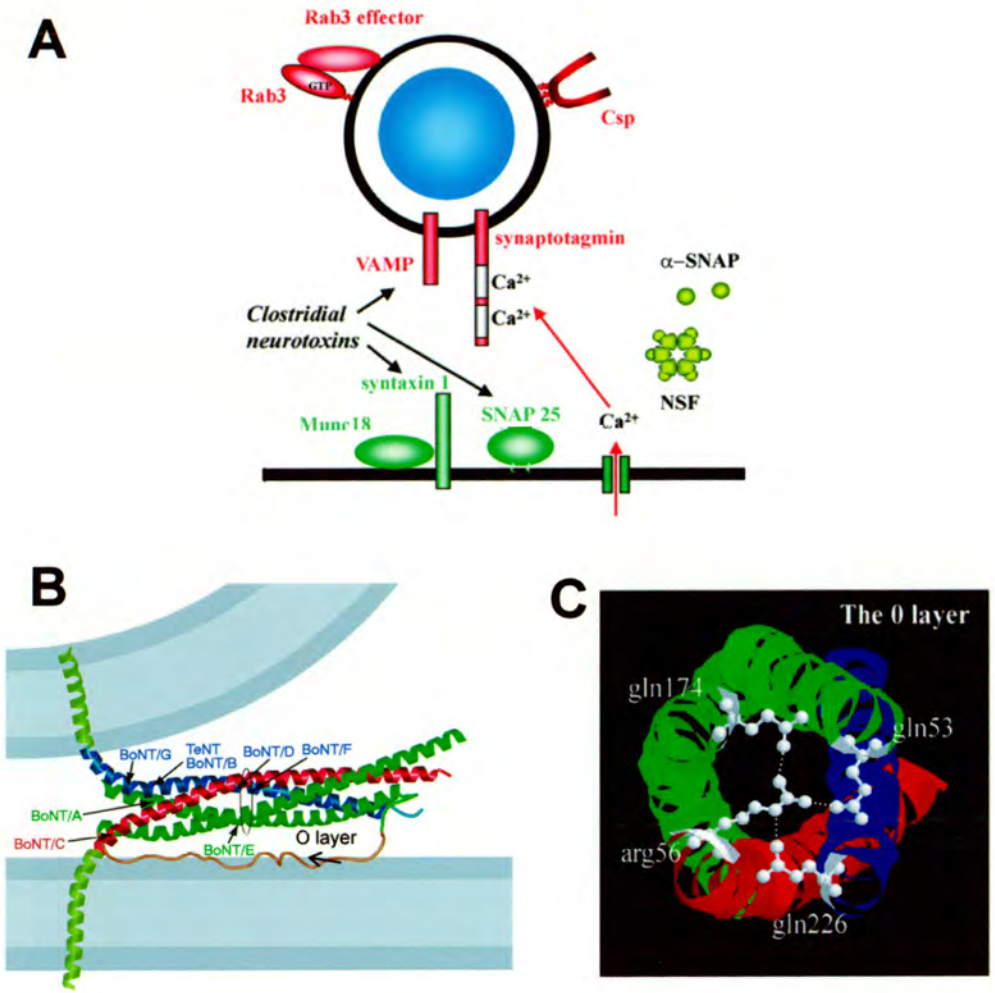

Figure 1.3: The SNARE proteins

Figure A is a diagrammatic representation of the localisation of the SNARE proteins on either the vesicle or the plasma membrane (Burgoyne and Morgan, 2002).

Figure B illustrates how the SNARE proteins assemble into the core complex and the sites of clostridial neurotoxin cleavage (Rizo and Südhof, 2002)

Figure C shows the coordination of the three glutamine and one arginine residue present in the ionic layer of the core complex (Burgoyne and Morgan, 2002)

sequences that attach them to membranes and partake in additional protein-protein interactions (Sollner, Bennett et al. 1993; Terrian and White 1997; Weimbs, Low et al. 1997; Weimbs, Mostov et al. 1998; Pelham 1999; Bock, Matern et al. 2001).

SNAREs were divided into families based on whether they contained one or two SNARE motifs, on the sequences of the SNARE motifs and on the type and sequences of the flanking domains. Most SNAREs contain a single SNARE motif preceded by a variable N-terminal domain, followed by a single transmembrane domain as seen in the syntaxin and synaptobrevin/VAMP families. Other SNAREs do not contain a transmembrane domain, but interact with the membrane via post-translationally attached lipids, for example SNAP-25 is attached to the membrane by palmitoylated cysteine residues. SNAREs are also classified as Q or R SNAREs based on whether they contain a conserved glutamine (Q) or arginine (R) in the SNARE motif in the so called zero layer (see below) (Hess, Slater et al. 1992; Fasshauer, Sutton et al. 1998; Pelham 1999; Bock, Matern et al. 2001).

1.6.1 The core complex of SNAREs

The human genome encodes 35 SNAREs compared with 22 in the yeast genome. The synaptic SNARE complex remains the most intensively studied and is the model for how other SNARE complexes in the secretory pathway may assemble. It is composed of the three proteins: VAMP/synaptobrevin, located on the vesicle membrane, and syntaxin 1a and SNAP-25, located on the plasma membrane. These assemble into a stable ternary complex with a 1:1:1 stoichiometry that is referred to as the core complex (Wilson, Whiteheart et al. 1992) (Figure 1.3B). The core complex is formed by the four SNARE motifs (one SNARE motif each from syntaxin and synaptobrevin and two from SNAP-25) twisted into a parallel four-helical bundle approximately 12 nm long. The interactions in the core of this bundle are mainly hydrophobic apart from a central ionic layer (known as the zero layer) that is constructed from an arginine residue contributed by the SNARE motif of synaptobrevin and three glutamine residues contributed by each of the three SNARE motifs of syntaxin 1a and

SNAP-25 hence the sub-classification into Q and R SNAREs (Figure 1.3C). All SNARE complexes consist of 1R and 3Q SNARE motifs. This ionic layer is shielded from its aqueous surroundings by the flanking leucine zipper layers and the polypeptide backbones of the proteins, greatly increasing the stability of this complex. Furthermore, the asymmetric ionic layer fixes the positions of the hydrophobic layer in the centre of the bundle, ensuring that the helices of the SNARE motifs are placed in the correct register during assembly (Sutton, Fasshauer et al. 1998). Before core complex assembly, the cytoplasmic regions of synaptobrevin and SNAP-25 are largely unstructured and a binary complex between syntaxin 1a and SNAP-25 forms before the ternary complex. The formation of the binary complex induces secondary structure in SNAP-25 and *in vitro* data has suggested that secondary structure in synaptobrevin is then induced by its interaction with the binary complex during formation of the core complex (Fasshauer, Bruns et al. 1997), a process known as 'zippering'. The assembled SNARE complex is unusually stable, with a 'melting' temperature of 70-90 °C, and is resistant to SDS. It is believed to function in all cellular fusion reactions, since SNAREs are ubiquitous, and each SNARE exhibits a characteristic subcellular distribution. The requirement for SNAREs in membrane fusion has been further proved by genetic studies in the yeast, *Saccharomyces cerevisiae*, where deletion of SNAREs is usually lethal (Gerst 1999). Similarly genetic ablation of synaptic SNAREs in *Drosophila melanogaster*, *Caenorhabditis elegans* and *Mus musculus* abolishes evoked neurotransmission (Schulze, Broadie et al. 1995; Nonet, Saifee et al. 1998; Schoch, Deak et al. 2001; Washbourne, Thompson et al. 2002). Furthermore, the identification of the SNARE proteins as substrates for the Botulinum and Tetanus neurotoxins revealed an essential role for these proteins in exocytosis. The light chains of these toxins are metalloproteinases that enter target neurons and inhibit neurotransmission through degradation of SNAREs. Synaptobrevin is cleaved by Tetanus toxin and Botulinum toxin types B, D, F and G; SNAP-25 is cleaved by Botulinum toxins A, C and E and syntaxin 1a is

cleaved by Botulinum toxin C (Hayashi, McMahon et al. 1994). These results, with the additional observation that synaptobrevin, syntaxin and SNAP-25 form a stoichiometric complex (the 20S complex) with NSF and SNAPs, led to a model of intracellular membrane traffic known as the 'SNARE hypothesis'.

1.6.2 The SNARE hypothesis

The SNARE hypothesis was an early attempt to explain the events leading up to membrane fusion and postulated that the assembly of the SNARE proteins synaptobrevin, syntaxin 1a and SNAP-25 into the stable core complex, bringing the vesicle and plasma membrane into close proximity, supplied the energy required to overcome the repulsive forces of the two lipid bilayers resulting in membrane fusion. This was supported by studies of *in vitro* fusion reactions in which the SNARE proteins synaptobrevin, syntaxin 1a and SNAP-25 were found to be both necessary and sufficient to promote lipid bilayer fusion (Weber, Zemelman et al. 1998). The fusion of proteoliposomes has also been demonstrated with specific combinations of core SNAREs (McNew, Parlati et al. 2000; Parlati, McNew et al. 2000). These *in vitro* fusion reactions were extremely slow, and the inclusion of synaptotagmin produced only a modest acceleration of fusion (Tucker, Weber et al. 2004), suggesting that additional factors might be required; but in recent work (E. Chapman, personal communication) much faster fusion of SNARE-containing proteoliposomes has been achieved, by use of much smaller protein:lipid ratios and thus avoiding the formation of refractory SNARE aggregates.

In the original formulation of the SNARE hypothesis, ATP hydrolysis by NSF was supposed to drive the fusion reaction itself, and for a while NSF was taken to mean 'NEM-sensitive fusion protein'. This idea, however, was confounded by the observation that the rate of ATP hydrolysis by NSF, even when stimulated by α-SNAP, was far too slow, and then by the finding that the rapid phase of LDCV fusion occurred even after removal of ATP (Holz,

Bittner et al. 1989). It was later suggested that following membrane fusion, SNARE complex disassembly was catalysed by the binding of α-SNAP and NSF. Following ATP hydrolysis, NSF and α-SNAP are released and the dissociated individual SNAREs can participate in further fusion reactions. The study of stage-specific exocytosis in chromaffin cells and high resolution electrophysiological approaches have suggested, however, that α-SNAP/NSF acts in an early ATP-dependent priming reaction that precedes the later Ca^{2+}-dependent fusion step (Chamberlain, Roth et al. 1995; Banerjee, Barry et al. 1996; Xu, Rammner et al. 1999).

Despite the general agreement that SNARE complex assembly has an essential role in exocytosis, some studies have suggested it has a pre-fusion role, in which it is not directly involved in the opening of the fusion pore and the SNARE proteins themselves do not confer specificity on membrane fusion. In studies of fusion between two populations of vacuoles that contained either v-SNAREs or t-SNAREs, trans-core complexes were formed and could be disassembled by Sec18/Sec17 without inhibiting the subsequent mixing of vacuolar contents (Ungermann, Sato et al. 1998). Also experiments with sea urchin egg secretory vesicles indicated that core complexes were, in fact disrupted by Ca^{2+} in a step before membrane fusion (Tahara, Coorssen et al. 1998). In *Drosophila* the deletion of synaptobrevin abolishes evoked neurotransmitter release, but spontaneous miniature release events (minis) still occurred and *C.elegans* synaptobrevin mutants still had some movement and were not totally paralysed (Harter, James et al. 1989; Ferro-Novick and Jahn 1994; Steyer, Horstmann et al. 1997; Oheim, Loerke et al. 1998; Rizo and Sudhof 2002).

The SNARE hypothesis also stated that the SNARE proteins themselves conferred the specificity for the different fusion events throughout the secretory pathway ensuring that the vesicles fused with the correct target membranes. Several yeast SNAREs have, however, been implicated in multiple SNARE complexes (Gaudin, Ruigrok et al. 1995). In addition,

synaptic vesicles release neurotransmitters only at active zones, despite the presence of syntaxin 1a and SNAP-25 throughout the plasma membrane (Weimbs, Low et al. 1997). More recently, a model for how SNAREs participate in neurotransmitter release has been proposed (Figure 1.4). In this model SNARE complex assembly forces synaptic vesicles into an unstable fusion intermediate that is stabilised by complexin. The two complexins, I and II, are closely related ~15 kDa cytosolic proteins, expressed specifically in the brain. Double knockout mice studies have suggested complexins positively regulate a late step in exocytosis by binding to the assembled trimeric SNARE complex. Synaptotagmin (see below) could then bind in the absence of Ca^{2+}, but switch to the phospholipid membrane as $[Ca^{2+}]$ concentration increases. Binding of the synaptotagmin C_2-domains to the phospholipids, with partial insertion of synaptotagmin hydrophobic sequences into the membrane, could then induce a mechanical stress that destabilises the fusion intermediate, opening the fusion pore. This speculative model, however, is far from proven (Sudhof 2004).

There is little doubt that the role the SNAREs play is specific, but their specificity could arise from sequences outside of the SNARE motif, or from surface residues of the SNARE motif that do not participate in core complex assembly as SNARE proteins also differ from each other in sequences surrounding the SNARE motifs and the membrane attachment domains. Syntaxin, one of the SNARE proteins, and its homologues contain an N-terminal domain that plays an important role by interacting with other synaptic proteins, which regulate membrane fusion.

1.7 Syntaxin

Syntaxin 1 was discovered as a protein that interacts with the synaptic vesicle membrane protein synaptotagmin and by immunocytochemistry as a surface protein of various neurons (Bennett, Calakos et al. 1992; Inoue, Obata et al. 1992) and since then many syntaxin 1 homologues have been identified that work at all transport steps throughout the secretory

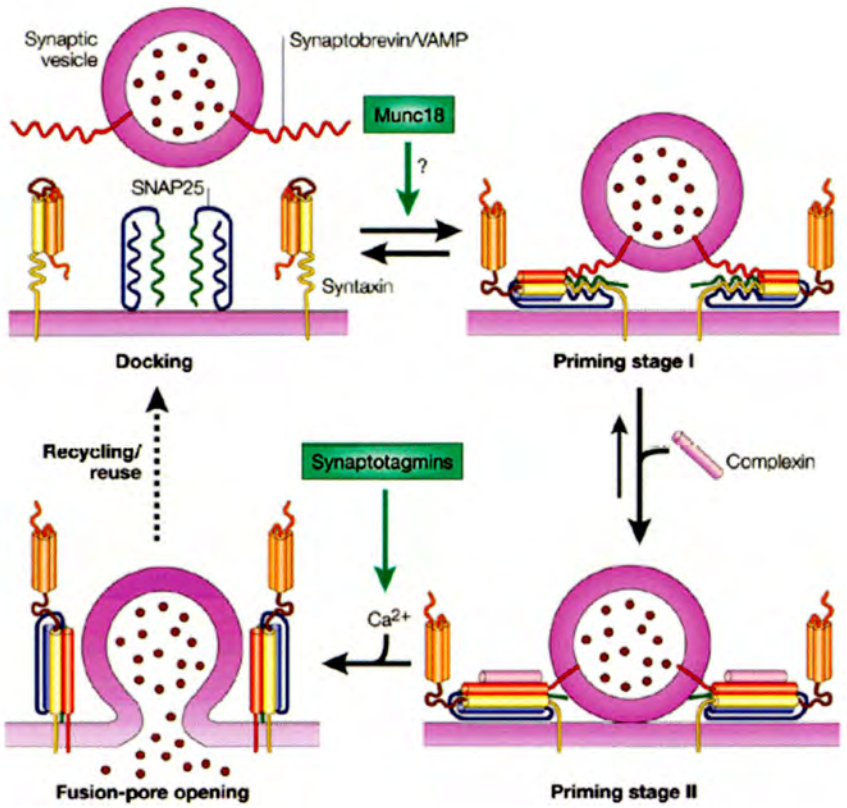

Figure 1.4: The role of SNAREs in neurotransmission

In this model SNARE complex assemble forces the synaptic vesicle into an unstable fusion intermediate, followed by the binding of synaptotagmin to the core complex in the absence of Ca^{2+}. Upon an increase in [Ca^{2+}] synaptotagmin binds and partially inserts its hydrophobic sequences into the plasma membrane, inducing a mechanical stress resulting in the opening of the fusion pore (figure taken from Rizo and Sudhof, 2002).

pathway. Unlike the other SNARE proteins, syntaxin-null mutants have no evoked and spontaneous neurotransmission and are paralysed in *Drosophila* and *C.elegans* respectively (Schulze, Broadie et al. 1995; Nonet, Saifee et al. 1998), indicating that the syntaxin family of proteins are essential for membrane fusion.

In addition to the SNARE motif and a C-terminal transmembrane region, all syntaxins contain a characteristic N-terminal domain. These domains are conserved between syntaxins that function at the same trafficking step, but differ between syntaxins that function at distinct trafficking steps, while the SNARE motifs of all syntaxins are homologous, suggesting that the N-terminal domains of syntaxins are specific for a given trafficking step (Weimbs, Low et al. 1997). The presence of an evolutionarily conserved autonomously folding N-terminal domain in syntaxins suggests that these proteins have additional roles besides core complex formation, which are thought to be mediated through the interaction of syntaxins with various other proteins involved in membrane fusion (Jahn and Sudhof 1999). This idea was further supported when the synaptic syntaxin, syntaxin 1a, was found to have more binding partners than any other synaptic protein, interacting with at least nine other neuronal proteins, including munc18/n-Sec1, Ca^{2+} channels, synaptotagmin, complexins, α-SNAP, rsec6/rsec8, CIRL/latrophilin, tomosyn and munc13, in addition to synaptobrevin and SNAP-25 (Chapman, Hanson et al. 1995; McMahon, Missler et al. 1995; Hsu and Jackson 1996; Krasnoperov, Bittner et al. 1997; Betz, Ashery et al. 1998; Fujita, Shirataki et al. 1998).

1.7.1 Syntaxin 1a

The N-terminal domain of syntaxin 1a spans two-thirds of its sequence and is composed of a three- helical bundle called the Habc domain, which is preceded by a short amino-terminal sequence and is followed by a linker region that separates it from the SNARE motif and the C-terminal trans-membrane domain. Syntaxin 1a (Figure 1.5) was found to exist in two

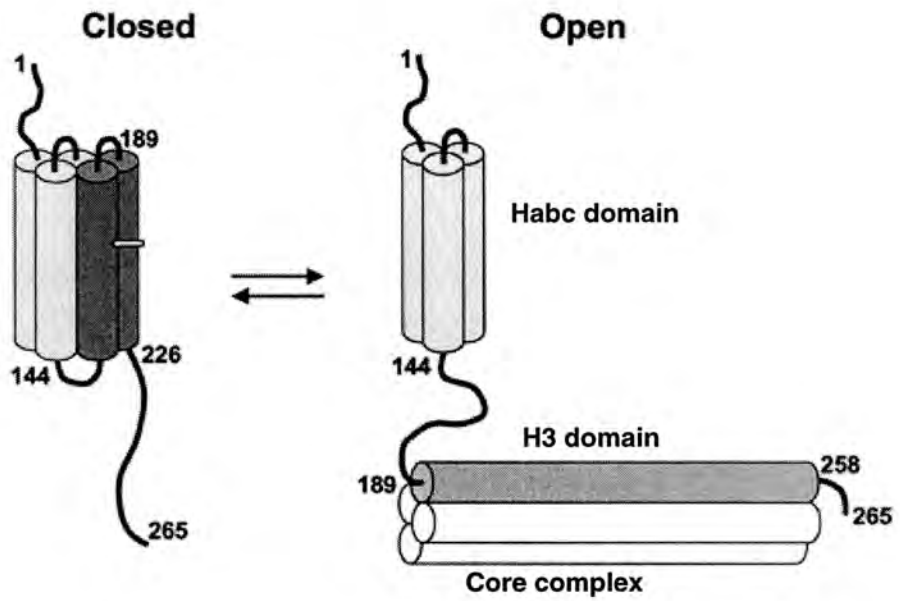

Figure 1.5: The conformations of syntaxin 1a

Syntaxin 1a has a large N-terminal domain, consisting of a 3 helical bundle termed the Habc domain.

Syntaxin 1a exists in two conformations: 'closed', in which the Habc domain folds back and interacts with the H3 domain, and 'open', in which the H3 helix can participate in core complex assembly (adapted from Dulubova et al, 1999).

conformations, the open conformation, which can interact with the other SNARE proteins in the core complex, and the closed conformation, in which the Habc domain folds back onto the SNARE motif and prevents such interactions (Fernandez, Ubach et al. 1998; Dulubova, Sugita et al. 1999). Isolated syntaxin 1a was found to switch between the closed and the open conformation suggesting that regulatory proteins were required to hold it in the closed inactive conformation (Margittai, Widengren et al. 2003). The SM protein munc18-1 binds to syntaxin 1a, stabilising it in the closed conformation and thereby preventing interaction with the other SNAREs. This finding has led to the theory that regulation of the conformational state of syntaxin 1a plays a key role in regulating exocytosis.

1.8 Munc18-1

Munc18-1 is a member of the Sec1/munc18 (SM) protein family and was first identified by its ability to bind syntaxin 1a with nanomolar affinity (Hata, Slaughter et al. 1993) and was later cloned based on its similarity to *Drosophila* Rop and *C.elegans* unc-18 using homology screening (Halachmi and Lev 1996). In vertebrates three isoforms of munc18-1 have been discovered; munc18-1, -2 and -3 (also known as munc18a, 18b and 18c).

SM proteins are 60-70 kDa hydrophilic soluble proteins with high sequence homology that is distributed evenly over their entire sequence, suggesting that they have a similar structure. SM proteins were first discovered during genetic screens in *C.elegans* for uncoordinated (unc) phenotypes that were fully or partially paralysed (UNC-18) (Brenner 1974) and as secretion mutants in *S.cerevisiae* (Sec1) (Novick and Schekman 1979). Since then genetic studies have established a general requirement for SM proteins in membrane fusion in a wide variety of organisms, operating throughout the secretory pathway (Jahn 2000), including yeast, plants, nematodes, flies and mice (Halachmi and Lev 1996; Verhage, Maia et al. 2000), although their precise role remains elusive. Exocytosis is completely blocked in *S.cerevisiae* Sec1 mutants and *Drosophila* Rop null mutants suggesting a positive role for SM proteins in membrane fusion. Over-expression of *Drosophila* Rop, however, leads to a

decrease in neurotransmitter release (Schulze, Littleton et al. 1994), which is representative of a more negative role for SM proteins. This idea was further supported when munc18-1 was found to bind to the closed conformation of syntaxin 1a, preventing it from interacting with the other SNAREs. Furthermore, in PC12 cells, syntaxin is unable to leave the Golgi in the absence of munc18 (Rowe, Calegari et al. 2001).

The action of SM proteins remains controversial, most experimental evidence indicating that they have multiple functions in vesicle trafficking through their interactions with several other proteins. Such a notion is supported by observations in yeast, where a genetic interaction between Sly1 and the Rab-like GTPase YPT suggests an involvement in the early event of vesicle recruitment, whereas Sec1p acts at a very late stage in exocytosis, downstream of SNARE complex assembly (Dascher, Ossig et al. 1991; Ossig, Dascher et al. 1991; Carr, Grote et al. 1999; Grote, Carr et al. 2000). An additional role in docking has been suggested for SM proteins since in *C.elegans* unc-18 mutant synapses there is a reduced number of docked vesicles, which was mirrored in munc18-1 knockout mice by a similar reduction in docked dense core granules in chromaffin cells (Verhage, Maia et al. 2000; Voets, Moser et al. 2001; Weimer, Richmond et al. 2003). In these mice, although there was no effect on synaptic vesicle docking, there was a complete block of neurotransmission, implying an additional post-docking role for munc18-1 in the late stages of exocytosis (Verhage, Maia et al. 2000; Ciufo, Barclay et al. 2005). Despite the different phenotypes seen for different SM protein mutants, a conserved function among all SM proteins in membrane fusion is its interaction with the corresponding syntaxin homologue.

1.8.1 SM Proteins and syntaxin protein interactions

Generally SM proteins interact with their respective syntaxins with high specificity and high affinity, although the way in which these proteins interact appear to be fundamentally different among different pairs (Toonen and Verhage 2003). So far at least four binding modes have been identified (Figure 1.6):

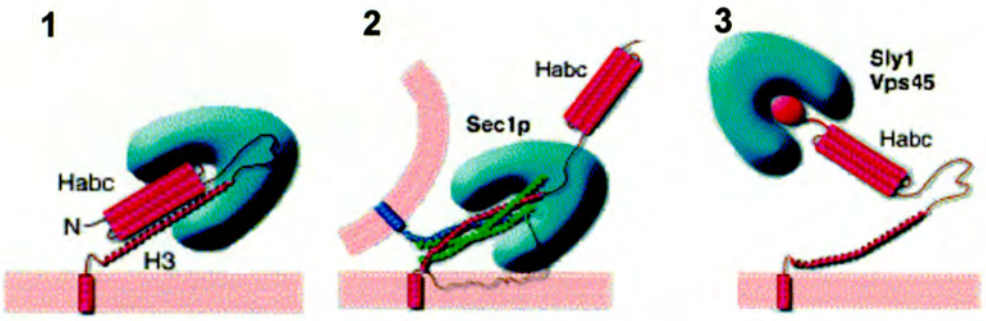

Figure 1.6: Modes of syntaxin – SM protein interactions

1. SM protein binding to the closed conformation of syntaxin
2. SM protein binding to assembled SNARE complexes
3. SM protein binding to the conserved N-terminus irrespective of syntaxin 1a conformation

(adapted from Toonen and Verhage, 2003)

1. Binding to the closed conformation of syntaxin. This is exemplified by the way in which munc18-1 interacts with syntaxin 1a (Misura, Scheller et al. 2000).
2. Binding to assembled SNARE complexes. In the yeast *S.cerevisiae* the corresponding SM protein, Sec1p, interacts with the assembled SNARE complex, even though the syntaxin homologue, Sso1p adopts a closed conformation when free (Carr, Grote et al. 1999).
3. Binding to the conserved N-terminus irrespective of the conformation of syntaxin. Examples of this have been observed in both yeast and mammals where the SM protein involved in membrane traffic events to and from the Golgi, Sly1p/mSly1 and Vps45p/mVps45, bind to a conserved N-terminal motif of their respective syntaxins. This binding mode allows the simultaneous binding of SM protein and SNARE complex members and seems to represent the most general mode of syntaxin – SM protein coupling (Bryant and James 2001; Peng and Gallwitz 2002; Rizo and Sudhof 2002).
4. Binding via multiprotein complexes. In *S.cerevisiae* another yeast SM protein, Vps33p is part of a complex (C-Vps complex) that functions in Golgi to vacuole transport and interacts with the Syntaxin homologue Vam3p (Sato, Rehling et al. 2000). The same interactions are observed with homologues of Vps33p and members of the C-Vps complex in *Drosophila* (Sevrioukov, He et al. 1999).

These different binding modes might be an evolutionary adaptation to prevent the binding of SM proteins to non-cognate syntaxins. Since only munc18/UNC18 bind to monomeric syntaxins this binding mode might be necessary to meet the specific requirements and regulation of fast exocytosis of neurotransmitters (Toonen and Verhage 2003). Furthermore the crystal structure of the syntaxin 1a – munc18-1 complex has made this interaction of particular interest since it appears to represent a specialised mode of interaction between SM proteins and syntaxins (Misura, Scheller et al. 2000).

1.9 Syntaxin1A – Munc18-1 interaction

The crystal structure of the syntaxin 1a – munc18-1 complex (Figure 1.7) (Misura, Scheller et al. 2000) revealed that the interaction between syntaxin 1a and munc18-1 requires most of the cytoplasmic domain of syntaxin 1a, including the Habc and the H3 domains and almost all of munc18-1 (Hanson 2000; Misura, Scheller et al. 2000). Munc18-1 is a horseshoe-, or arch-shaped molecule, containing three domains arranged around a ~15 Å central cavity that wraps around syntaxin 1a (Misura, Scheller et al. 2000). The syntaxin 1a – munc18-1 interaction is believed to stabilise the closed conformation of syntaxin 1a and may help prevent premature or inappropriate SNARE complex assembly. This structural work led to the idea that additional factors must be involved in the regulation of this complex, resulting in conformational changes in either or both syntaxin 1a and munc18-1 to allow SNARE complex assembly.

1.9.1 Disassembly of the syntaxin 1a – munc18-1 interaction

To date several candidates for mediating the dissociation of the syntaxin 1a – munc18-1 complex, which is necessary for membrane fusion to occur, have been investigated, such as phosphorylation, UNC13/munc13 proteins, Rab and Rab effectors, and Tomosyn.

1.9.1.1 Munc18-1 phosphorylation

Destabilisation of munc18-1 – syntaxin 1a interaction could be promoted by phosphorylation, as munc18-1 has been shown to be phosphorylated by Cyclin-dependent Kinase 5 (Cdk5) *in vitro* (Fletcher, Shuang et al. 1999) and by Protein Kinase C (PKC) both *in vitro* and *in vivo* (Fujita, Sasaki et al. 1996; Barclay, Craig et al. 2003; Craig, Evans et al. 2003). PKC has been shown to stimulate Ca^{2+}-dependent exocytosis in various types of secretory cells and was found to phosphorylate munc18-1 on Ser306 and Ser313 (Figure1.8), the latter being conserved in *Drosophila* Rop (Fujita, Sasaki et al. 1996). Munc18-1

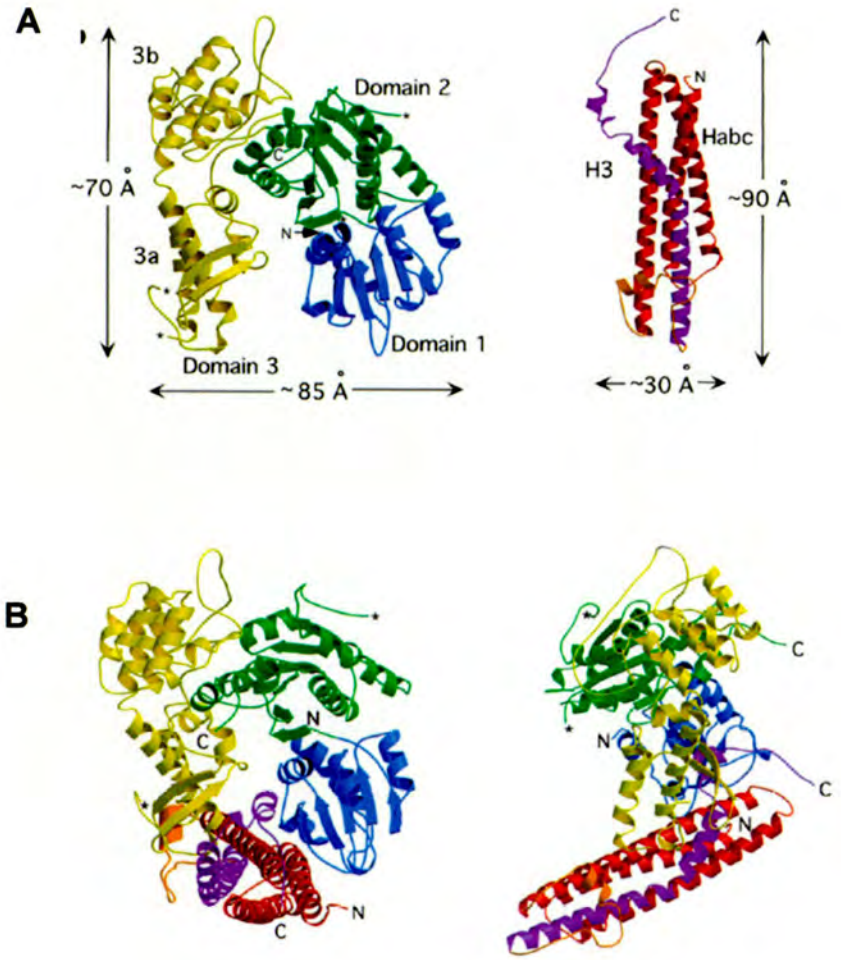

Figure 1.7: Crystal structure of syntaxin 1a – munc18-1 complex

Figure A shows the structures of both syntaxin 1a and munc18-1

Figure B is the crystal structure of the syntaxin 1a – munc18-1 bimolecular complex from two different angles, revealing how munc18-1 wraps around syntaxin 1a (Misura et al, 2000)

Munc18-1 is shown in blue: domain 1, green: domain 2 and yellow: domain 3.

Syntaxin 1a is shown in red: Habc domain and purple: H3 domain.

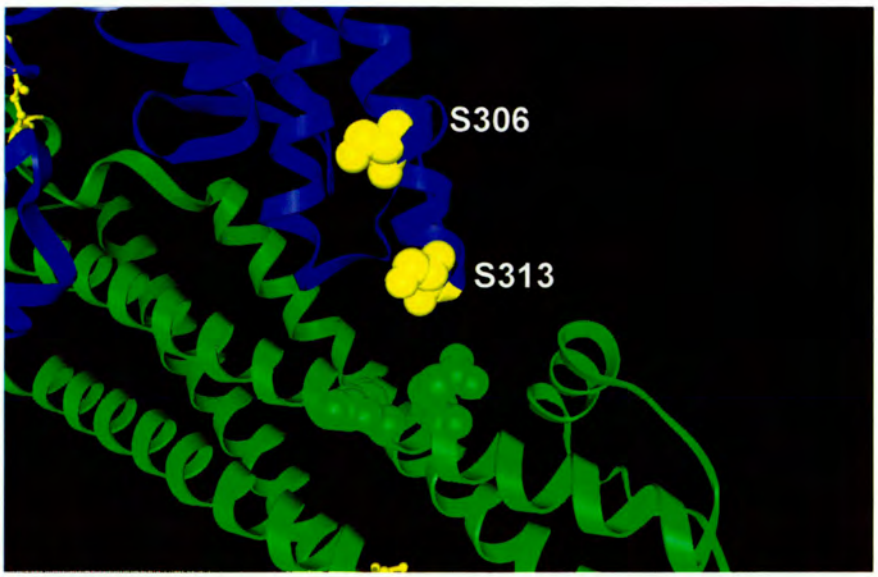

Figure 1.8: Phosphorylation sites on munc18-1

This shows the phosphorylation sites Ser306 and Ser313 on munc18-1 (shown in blue) and their position in relation to syntaxin 1a (shown in green).

phosphorylation has been shown to reduce the affinity of munc18-1 for syntaxin 1a and occurs in response to histamine and Ca^{2+} in permeabilised chromaffin cells, altering the release kinetics of single vesicles (Barclay, Craig et al. 2003; Craig, Evans et al. 2003).

1.9.1.2 UNC-13/munc13 proteins

C.elegans UNC-13 and its mammalian homologue have been implicated in priming synaptic vesicles to a fusion competent state. Munc13-1 has been shown to interact with the N-terminal domain of syntaxin 1a in the open conformation, and this interaction and the interaction of syntaxin 1a with munc18-1 are mutually exclusive. This idea was reinforced when *C.elegans* UNC-13 was shown to displace UNC-18 from its complex with syntaxin *in vitro* (Sassa, Harada et al. 1999). Furthermore, UNC-13 mutations in *C.elegans* and *Drosophila,* and double knockout of munc13-1 and munc13-2 in mice, completely block neurotransmitter release, apparently through a defect in synaptic vesicle priming (Rizo and Sudhof 2002). Finally, the importance of UNC-13 as a priming factor was demonstrated by the successful rescue of the *unc-13* null phenotype by the introduction of syntaxin mutant that is locked in the open conformation (Richmond, Weimer et al. 2001).

1.9.1.3 Rab and Rab effectors

Rab proteins are small GTPases that are believed to be involved in vesicle docking. This idea is supported by studies in *S.cerevisiae* where SEC1 genetically interacts with the Rab-like GTPase SEC4 and the absence of Rab proteins results in a block in fusion at defined stages (Jahn and Sudhof 1999). Also, *C. elegans* mutants in the Rab effector RIM (Rab3 interacting molecule) suffer a severe decrease in neurotransmitter release, which was restored by the mutant syntaxin with the open conformation. Furthermore RIM has been found to interact with munc13 functionally, suggesting that RIM may have a role in regulating the priming activity of munc13 (Betz, Thakur et al. 2001).

1.9.1.4 Tomosyn

Tomosyn is a large, neuron-specific SNARE protein regulator that has been shown to bind syntaxin 1a, displacing munc18-1 *in vitro* (Fujita, Shirataki et al. 1998). Although it is unknown whether this interaction is physiologically relevant, SRO7 and SRO77, putative tomosyn orthologues in yeast, are essential for vesicle exocytosis, suggesting that these proteins may have conserved roles in regulating SNARE-dependent trafficking (Lehman, Rossi et al. 1999).

1.9.1.5 Other proteins that interact with munc18

Munc18 has also been shown to interact with a number of other proteins and whether such interactions have any effect on the syntaxin 1a – munc18-1 interaction or whether they participate in the other multiple roles of munc18 remains unclear. One such group of proteins are Mints, which contain a munc18 interacting domain followed by a sequence that binds to CASK, a cellular junction protein enriched in synapses. Mint 1 and Mint 2 were detected in brain in a complex with syntaxin 1a and munc18-1 and may function by recruiting munc18-1 to neurexin-containing regions of the plasma membrane through its association with CASK (Okamoto and Sudhof 1997; Biederer and Sudhof 2000).
The second protein family to be identified was that of the Doc2 proteins namely, Doc2α and Doc2β, which are synaptic proteins that contain two C2 domains thought to associate with intracellular membranes. Doc2 proteins have been implicated in regulating exocytosis through their interaction with other exocytotic proteins. In addition, over expression of Doc2 in PC12 cells enhances exocytosis (Duncan, Apps et al. 2000). As well as munc18-1, Doc2 has been shown to interact with munc13 and undergo a munc13-dependent redistribution from the cytoplasm to the plasma membrane in response to stimulation of PC12 cells with phorbol ester (Duncan, Betz et al. 1999).

Finally munc18-1 has been shown to interact with granuphilin, a protein identified in pancreatic beta cells that associates with dense-core granules and also Rab3A and Rab27 (Fukuda, Kanno et al. 2002), providing a potential mechanism for the modulation of munc18-1 function through Rab activity (Ciufo, Barclay et al. 2005).

1.10 Synaptotagmins as the Ca^{2+} sensors in regulated exocytosis

Most forms of regulated exocytosis are Ca^{2+}-dependent and this dependence has been most closely studied for neurotransmitter release, which is extremely rapid, with a steep [Ca^{2+}] dependence. In contrast, Ca^{2+}-triggered exocytosis of peptidergic vesicles in endocrine cells is multiphasic and sustained, although a small component of their secretion is through fast Ca^{2+}-dependent exocytosis. Thus, there are major differences in the time course of Ca^{2+}-triggered exocytosis between endocrine and synaptic systems, however the Ca^{2+} dependence and cooperativity appear to be similar (Gerber and Sudhof 2002).

At present the favoured candidates for the calcium trigger are the synaptotagmins, which in humans constitute a family of at least 19 proteins, with similar domain organisation. All synaptotagmins contain an N-terminal glycosylated domain, a single transmembrane sequence, a central linker sequence and two C-terminal C_2-domains referred to as C_2A- and C_2B-domains. These C_2 domains are the most highly conserved parts of synaptotagmins (Gerber and Sudhof 2002).

Synaptotagmin 1 and 2, the first synaptotagmins to be purified and cloned, are highly homologous. These two synaptotagmins are detectable only in the brain and endocrine tissues where they are expressed in overlapping but distinct sets of cells (Gerber and Sudhof 2002). Furthermore, evidence from genetic studies in mice, *Drosophila melanogaster* and *Caenorhabditis elegans* as well as microinjection studies in squid giant synapses indicated that synaptotagmin 1 plays an essential role in fast Ca^{2+}-triggered synaptic vesicle exocytosis. The C_2A-domain of synaptotagmin 1 binds 3 Ca^{2+} ions (Ubach, Zhang et al. 1998) and the C_2B-domain 2 Ca^{2+} ions (Fernandez, Arac et al. 2001). The intrinsic Ca^{2+}

affinities of the C_2-domains are very low (0.5-5 mM) because the coordination spheres for the Ca^{2+} ions are incomplete. The apparent Ca^{2+} affinity of the C_2-domains increases dramatically (up to 1000-fold) when the C_2-domains bind to phospholipid membranes as the negatively charged headgroups provide additional coordination sites for the bound Ca^{2+} (Sudhof 2004). In addition to phospholipids, synaptotagmin exhibits Ca^{2+}-dependent interactions with a variety of other molecules including synaptotagmins, the SNARE complex (which it also binds in a Ca^{2+}-independent manner), syntaxin 1a, SNAP-25, Ca^{2+} channels, calmodulin, RIM and phosphoinositides (Li and Chin 2003).

Even if synaptotagmins are, as appears likely, the Ca^{2+}-sensors of regulated exocytosis, it is not known how they fulfil this function at a molecular level. An early suggestion was that synaptotagmin acts as a "fusion clamp", its association with the SNARE complex preventing exocytosis until released by the binding of Ca^{2+}. Acute photolytic knockout of synaptotagmin I was accomplished by incorporating a tetracysteine motif that binds to a fluoroscein derivative FIAsH, upon illumination of FIAsH synaptotagmin 1 was inactivated, blocking Ca^{2+}-induced fusion without increasing the frequency of spontaneous fusion events (Marek and Davis 2002) which argues for a positive role for synaptotagmin in fusion, such as a Ca^{2+}-induced conformation change causing insertion of some loops of the C_2A domain into the membrane (Bai, Wang et al. 2002).

Although synaptotagmins 1 and 2 play a key role in fast-triggered exocytosis, other Ca^{2+} sensors must also be present. The most likely candidates for this are other synaptotagmins. namely synaptotagmins 3, 6 and 7. The best current model is that the different synaptotagmins have distinct but complementary roles in exocytosis, with synaptotagmins 1 and 2 specialised for fast synaptic vesicle exocytosis, whereas synaptotagmins 3, 6 and 7 (and possibly others) may be responsible for slower exocytosis, such as in endocrine cells (Gerber and Sudhof 2002). In mouse neurons, knockout of synaptotagmin I blocks the rapid phase of exocytosis. This can, however, still be induced by treatment with high concentrations of sucrose, which induces fusion in a Ca^{2+}-independent manner and therefore

by-passing the regulated fusion step, indicating that the knockout blocks the fusion reaction itself and not vesicle docking. Although, in *Drosophila* and *C.elegans*, knockout of synaptotagmin I prevents SNARE complex assembly, which suggests that other synaptotagmins may control these in mouse.

1.11 Investigating exocytosis

So far, investigations into the formation and dissociation of the syntaxin 1a – munc18-1 complex have relied on *in vitro* biochemical assays of protein-protein interactions, in which protein fragments and chimeras are used, and on mechanistic interpretations of alterations in functional responses using genetic approaches in isolated cells or whole animals. Although such studies have provided valuable information an approach is required that will impart spatial and temporal information on the state of the bimolecular syntaxin 1a – munc18-1 complex in response to secretory pathway activation in intact cells. The development of high-resolution imaging systems has already enabled various aspects of exocytosis to be investigated, but with the advent of FRET and FLIM microscopy the interaction between these two proteins can be studied in greater depth.

1.12 Fluorescent proteins

1.12.1 Green Fluorescent Protein

Green fluorescent protein (GFP) was discovered (Shimomura, Johnson et al. 1962) in the jellyfish *Aequorea victoria* as one of two closely associated proteins, aequorin and GFP, that are responsible for the bluish green light that emits from its umbrella margin. Aequorin binds Ca^{2+} and emits blue light, which is absorbed through fluorescent energy transfer by GFP to produce green light (Morise, Shimomura et al. 1974). GFP is a 238 amino acid protein with an apparent molecular weight of 27-30 kDa on SDS PAGE. It absorbs blue light maximally at 395 nm, with a smaller absorbance peak at 475 nm and emits green light

at 508 nm (Cubitt, Heim et al. 1995). Its fluorescence is due to the presence of a p-hydroxybenzylidene-imidazolidinone chromophore, which is formed by the posttranslational autocatalytic cyclisation of the polypeptide backbone between residues Ser65 and Gly67 and the oxidation of the α-β bond of Tyr66 in a maturation process that takes 2-4 hours and requires oxygen (Prasher, Eckenrode et al. 1992; Cody, Prasher et al. 1993). The crystal structure of GFP (Ormo, Cubitt et al. 1996; Yang, Moss et al. 1996) revealed a tightly packed cylindrical structure of 11 β-strands surrounding a helical segment containing the imidazolidinone chromophore.

Widespread interest in GFP as a biological tool did not develop until 1992 when its cDNA was cloned and sequenced (Prasher, Eckenrode et al. 1992) followed by its expression in a wide range of prokaryotic and eukaryotic cells (Chalfie, Tu et al. 1994), in which a diffuse green fluorescence was detected distributed throughout the cytoplasm. The ability of GFP to fluoresce in a wide variety of organisms indicated that its fluorescence was not species-specific and that the assembly of the chromophore did not require additional cofactors specific to jellyfish. In addition, GFP was found to be a resilient protein, remaining stable for many hours in the presence of denaturants (1 % SDS or 6 M guanidium chloride), as well as over a broad range of pH values (2 to 11) and high temperatures (up to 65 °C) (Cubitt, Heim et al. 1995).

For use in biological systems, however, wild-type GFP is not ideal as its signal is relatively faint, susceptible to photobleaching and subject to photoisomerisation, resulting in instability in the emission wavelength. Furthermore, misfolding of GFP is not uncommon when it is expressed in mammalian cells at their optimal culture temperature of 37 °C. Mammalian cells also autofluoresce (Aubin 1979) due mainly to mitochondrial NAD(P)H (Andersson, Baechi et al. 1998) and endogenous flavins (Benson, Meyer et al. 1979). This fluorescence is excited and emitted in the near UV and has a wide emission peak, appearing yellow-green; it can become problematic when the wtGFP signal is very faint, or when attempting

quantitative fluorescent microscopy (Niswender, Blackman et al. 1995). The possibility that these problems associated with wtGFP could be overcome and the desire for additional fluorescent proteins with different spectral properties prompted investigations into GFP variants (Bajno and Grinstein 1999).

1.12.1.1 Variants of GFP

Genetic manipulations of wtGFP cDNA were made, leading to the generation of mutants with altered excitation and emission spectra and enhanced fluorescence. These were created by mutagenesis of the Ser-Tyr-Gly sequence that make up the chromophore and of the amino acids that interact with the chromophore. To increase the expression of such favourable GFP variants the GFP gene sequence was re-engineered so as to incorporate codons that have preferred usage in humans. Examples of GFP variants used today are: (1) the F64L/S65L mutant, enhanced GFP (EGFP), which has 6-fold greater brightness, 4-fold faster maturation, less photoisomerisation, reduced photobleaching and better folding in mammalian cells than wtGFP (Cubitt et al, 1995); (2) the Y66H mutant, which generated a blue shifted GFP called (E)nhanced B(lue)FP; (3) the Y66W mutant, (E)nhanced C(yan)FP, which is much brighter than EBFP; and (4) the (E)nhanced Y(ellow)FP mutant, with an aromatic amino acid at position 203, which has the most red-shifted emission spectra of all the GFP variants (Pollok and Heim 1999). The generation of such variants of GFP allow the separate labelling of different subcellular compartments; expression of differently-labelled protein constructs in the same cell, enabling colocalisation experiments to be performed; and the study of protein-protein interactions by fluorescence resonance energy transfer (FRET).

1.12.1.2 Applications of GFP and its variants

Such developments revealed the potential of GFP and its variants as tools for imaging intracellular structures and protein localisation within living cells and as a transcriptional reporter for studies of gene expression. The GFP gene can be fused in-frame with the gene

encoding the protein or targeting domain of interest. The resulting chimera can then be expressed and visualised in the cell of choice, and ideally without affecting the targeting and physiological functions of the host protein or domain (Cubitt, Heim et al. 1995; Bajno and Grinstein 1999). GFP has been successfully fused to both the N- and the C-termini of a wide range of cytoplasmic, cytoskeletal and membrane proteins and can be used as an *in vivo* marker for subcellular structures such as the endoplasmic reticulum and the Golgi, through its fusion to targeting domains.

1.12.1.3 Advantages of using GFP and its variants

The use of GFP and its variants has several advantages over other reporter genes or for use in cellular structure and protein labelling. For instance GFP does not require any additional factors for it to fluoresce. The major advantage of GFP over other reporter genes is its ability to reveal the presence of the gene product in living cells by its fluorescence. Most other commonly used reporter genes encode enzymes, for example chloramphenicol acetyl transferase, luciferase and β-galactosidase, which can be quantified only in the presence of the appropriate substrate and cofactors, which requires cellular lysis or fixation for detection of the desired activity. The detection of these reporters *in situ* is complicated by variable penetration of substrates that may lead to detection artefacts (Niswender, Blackman et al. 1995).

The advantage of using GFP chimeras compared to other protein labelling techniques is that they can be visualised in living, unperturbed cells. Most other available techniques for visualising proteins in cells require fixation and often permeabilisation. These procedures preclude continuous visualisation and can potentially damage the protein and/or redistribute it to an artifactual location, whereas GFP chimeras can be used to visualise trafficking between membrane-bound organelles, the translocation of proteins involved in signal transduction, and many other cellular processes (Bajno and Grinstein 1999). In a typical

example, Persley et al. (1997) were able to monitor endoplasmic reticulum-to-Golgi transport in live cells by following the distribution of a GFP fused to a temperature sensitive mutant protein from vesicular stomatis virus (Presley, Cole et al. 1997).

1.13 Other labelling techniques used in cells

1.13.1 Other fluorescent proteins

Yellow and red-orange proteins have also been cloned from fluorescent but nonbiolouminescent corals from the Indian and Pacific oceans (Matz, Fradkov et al. 1999). One example, DsRed, from the anemone *Discosoma striata,* is a red fluorescent protein that has ~25 % sequence identity with *Aequorea* GFP, with a peak emission around 583 nm. Unfortunately, several problems associated with DsRed have emerged, including slow protein maturation and a strong tendency to form tetramers (Baird, Zacharias et al. 2000). Another red fluorescent protein from the indo-pacific sea anemone *Heteractis crispa*, HcRed, is the most red-shifted GFP-like protein identified to date with excitation and emission maxima of 592 nm and 645 nm respectively (Gurskaya, Fradkov et al. 2001).

1.13.2 Fluorescent stains

Most stains used as tools for imaging in cells are small organic molecules and are generally acidophilic or lipophilic probes, but they have poor subcellular specificity and resolution. For example the acidophilic probes LysoTracker Red and Acridine Orange have been used to visualise chromaffin granules and other types of secretory vesicle, but they also stain other acidic compartments such as lysosomes, endosomes and the *trans* Golgi. Lipophilic probes, including FM dyes such as FM1-43, are often used to study endocytosis and exocytosis as they fluoresce following insertion into lipid bilayers and therefore report plasma membrane area changes consequent upon exocytosis or membrane retrieval (Burgoyne and Morgan 2003).

1.13.3 Immunofluorescence

An alternative approach to visualising proteins within cells is to use indirect immunofluorescence, in which a polyclonal or monoclonal antibody specifically directed against the protein of interest is recognised by a secondary antibody conjugated to a fluorescent dye such as fluorescein or rhodamine. This technique is good for investigating endogenous proteins, although the cells have to be fixed and permeabilised, therefore protein dynamics cannot generally be studied. Furthermore it is often difficult to look at direct protein-protein interactions by use of FRET, as the fluorescent tags on the secondary antibodies are often too far apart for FRET to occur between the fluorophores.

1.14 Fluorescence microscopy

1.14.1 Confocal microscopy

With the discovery of GFP and the development of its variants as well as other fluorescent proteins a system was required for the visualisation of these fluorochromes, which led to the development of confocal laser scanning microscopy (CLSM).

Confocal microscopy was developed and patented by Marvin Minsky in the 1950s, but it was not until the 1980s that the potential of confocal microscopy was realised, through advances in computer technology that permitted control of laser operation alongside the microscope's optical system, resulting in the emergence of a new microscopic concept: digital imaging. Confocal microscopes can be used for studying complex biological structures in 3D producing high-resolution images without the out-of-focus blur often associated with standard fluorescent microscopes. Because of the ease in which it can detect fluorescent proteins, combined with optical sectioning in live and fixed tissues, 3D rendering and the high resolution, confocal microscopy is now a successful and widely used tool.

In confocal microscopy a laser beam is expanded to make full use of the optics of the objective and is turned into a scanning beam by an x-y deflection mechanism while an

objective lens focuses it to a small spot within the specimen of interest. Emitted fluorescent light and reflected light are collected by this same objective and converted into a static beam by the x-y scanner device. The emitted photons are passed through an appropriate filter (dependent of the emission spectra of the fluorescent specimen) and focussed, via a dichroic mirror (beam splitter), onto a photodetector (photomultiplier). This dichroic mirror blocks the reflected light while allowing the emitted fluorescent light to pass through in the direction of the photomultiplier. The confocal microscope uses a pinhole placed in front of the photo-detector to exclude the out-of-focus signal. The pinhole prevents fluorescent light originating from points in the specimen that are not within the focal plane of the focussed laser beam from passing through reaching the photodetector. Therefore, only the region of the specimen in focus is detected. Finally, the photomultiplier converts the analogue light signal into a digital signal that is displayed on a computer monitor attached to the microscope as a 2D pixel-based image. A computer-controlled motor moves the microscope stage up and down selecting the plane of focus (the x-y plane). By moving the stage in the z-axis in a number of measured steps while performing lateral scanning of the specimen, a series of optical steps through the specimen are generated. These 2D optical sections, collected in a series, can be reconstructed into a 3D 'stack' by the computer, with every section in focus. To ensure that the x, y and z-axes of the reconstructed specimen reflect the biological sample of interest, the sampling in each plane of the specimen should match the sampling in the other two planes, like Nyquist sampling rate.

When collecting an image stack selective bleaching by the laser can occur in the x-y plane and non-selective bleaching in the other planes. While such bleaching cannot be avoided, it can be minimized by using the lowest possible laser power. Coincidentally, software packages have been developed that can improve image quality and restore lost data. Median and Gaussian filters can be used to reduce noise and background artefacts, while deconvolution software uses mathematical algorithms, removing any remaining haze and increasing the resolution of the acquired image. The ideal result is a 3D image that is a

faithful representation of the specimen imaged. Finally, colocalisation software can be used to generate statistics relating to the number of voxels that overlap in 3D, providing a measure of the amount of fluorescence from different fluorochromes in the same volume. Also 3D software can be used to rotate and animate the image, volume-render it or make parts of it transparent, allowing a more detailed analysis of the structure.

1.15 Microscopic techniques used in the study of exocytosis

1.15.1 Confocal microscopy

Standard confocal microscopy as described above has been used to study neuropeptide release in PC12 cells (Burke, Han et al. 1997). Neuropeptide release is not associated with active zones, is relatively slow and usually requires bouts of action potentials. Granule dynamics in nerve growth factor (NGF)-treated PC12 cells was studied using an ANF-EGFP fusion protein revealing that secretion is associated with depletion of granules distributed throughout the terminal. Furthermore, recovery after photobleaching and time-lapse particle tracking revealed that only a subpopulation of cytoplasmic secretory granules, similar in size to the releasable pool, can move quickly enough to support release (Burke, Han et al. 1997). Confocal microscopy has also been used to study the behaviour of dense-core secretory granules before exocytosis in insulin-secreting INS-1 β-cells and in PC12 cells using a phogrin-EGFP chimera (Pouli, Emmanouilidou et al. 1998). The phogrin-EGFP chimera was targeted to secretory vesicles in both cell types. In unstimulated INS-1 cells the movement of the granules was restricted to 2-3 granule diameters from the starting location, whereas when stimulated by Ca^{2+} the vesicles underwent longer, saltatory excursions. By contrast, in PC12 cells, long saltatory granule movements were apparent, even in the absence of stimulus. These appeared to be directed from the cell interior outwards, i.e. towards the

plasma membrane. This apparent, predominantly anterograde movement is therefore compatible with previous observations (Pouli, Emmanouilidou et al. 1998).

Confocal microscopy has also been used to study the localisation of the EYFP-syntaxin 1a, ECFP-munc18-1 and EGFP-munc13-1 when expressed singularly or co-expressed in different combinations in HEK293 cells (Gladycheva, Ho et al. 2004). These studies revealed that when expressed on their own EYFP-syntaxin 1a and ECFP-munc18-1 remain trapped within the cell. EYFP-syntaxin 1a was found to be associated with membranous structure whereas ECFP-munc18-1 was cytosolic, but when they were expressed together they were found to colocalise on the plasma membrane. These results support the view that munc18s act as chaperones to syntaxin proteins enabling them to reach their correct cellular localisation. EGFP-munc13-1 was found in the cytoplasm and no change on its distribution occurred when it was co-expressed with either EYFP-syntaxin 1a or ECFP-munc18-1. Gladycheva et al. also reported that EYFP-syntaxin 1a was able to shift the localisation of a SNAP-25 mutant lacking its membrane anchor from the cytoplasm to the plasma membrane, although in the presence of ECFP-munc18-1 this effect was reversed and the SNAP-25 mutant remained in the cytoplasm. When EGFP-munc13-1 was also expressed, however, the plasma membrane localisation of the SNAP-25 mutant was restored. They concluded from this that munc13-1 disrupts the syntaxin 1a – munc18-1 complex allowing syntaxin1a to interact with its cognate SNAREs.

Confocal microscopy in conjunction with a "fluorescent timer" probe, (ANF)-timer, which is targeted to large dense-core vesicles (LDCVs) in bovine chromaffin cells (BCC), revealed that LDCVs were segregated into different vesicle pools dependent on their age (Duncan, Greaves et al. 2003; Wiegand, Duncan et al. 2003). Atrial natriuretic factor (ANF), a cargo protein that is targeted to the vesicle lumen of endocrine cells was fused to the fluorescent protein DsRed-E5. DsRed-E5 is a mutant of the red fluorescent coral protein DsRed, and is characterised by unusually slow maturation during which the initial green emission changes to red over approximately 16 hours. Thus newly assembled LDCVs appear green, those of

intermediate age are yellow and older vesicles (>16 h) are red. The use of (ANF)-timer made it possible to investigate the location of differently aged LDCVs in BCCs the LDCVs depending on their age revealing that newly synthesised LDCVs are located in the peripheral areas of BCCs suggesting newly synthesised peptides are preferentially secreted. LDCVs that were not released within 16 hours of assembly retreated from the cell membrane and entered the reserve vesicle pool (Duncan, Greaves et al. 2003; Wiegand, Duncan et al. 2003).

1.15.2 Total Internal Reflection Fluorescence Microscopy

A less widely used microscopic technique for the study of exocytosis is Total Internal Reflection Fluorescence Microscopy (TIRFM), which makes it possible to observe individual dye-loaded dense-core vesicles prior to exocytosis. TIRFM can be used to selectively excite dye molecules in an aqueous environment directly adjacent to a glass interface. In TIRFM a light beam striking an interface between two media, 1 (e.g. glass) and 2 (e.g. aqueous solution), with refractive indices n_1 and n_2, respectively, is totally internally reflected if $n1>n2$ and if the angle of incidence θ_i exceeds the critical angle θ_c. Owing to the interference of the incident and reflected light beam a standing wave is generated in the optically rarer medium and is known as the evanescent wave, which is used to excite the sample. The evanescent wave decays exponentially with distance and penetrates about 70-300 nm into the specimen depending on media refractive indices, incidence angle and illumination wavelength (Oheim, Loerke et al. 1998).

As applied to biological cell cultures, TIRF microscopy allows selective visualisation of cell/substrate contact regions. By restricting fluorescence excitation to a thin optical layer adjacent to the interface to which cells adhere, TIRF microscopy eliminates out-of-focus fluorescence present in conventional epifluorescence excitation. Thus TIRFM can be used to visualise the position, extent and motion of these contact regions or to determine dynamics. For some applications TIRFM has distinct advantages over confocal microscopy, which

places a high radiation burden on cells, as the entire cell is illuminated with fluorescence excitation light and most of the fluorescence emission is rejected by the confocal pinhole. In contrast TIRFM only illuminates a thin layer of the cell and all the emitted light is collected by the objective (Steyer and Almers 1999).

TIRFM has been successfully used to study vesicle dynamics next to the plasma membrane preceding exocytosis. The trajectories of single-dense-core vesicles were analysed as they approached the plasma membrane and revealed that as they got closer to the plasma membrane, a 100-fold decrease in 3D-mobility was observed. This was interpreted as the vesicle undergoing docking at the plasma membrane (Oheim, Loerke et al. 1999). In the absence of stimulation, vesicles changed from a less mobile to a more mobile state and vice versa, while some vesicles disappeared and were replaced by others, suggesting a dynamic equilibrium between the docked and free vesicle pools. Upon stimulation, readily releasable vesicles fused with the plasma membrane in a cloud of released dye molecules and despite the exocytotic fusion of a large number of vesicles during prolonged stimulation the number of vesicles at the plasma membrane remained constant due to the recruitment of new vesicles from the invisible reserve pool (Oheim, Loerke et al. 1999).

TIRFM was also used to image single-vesicle exocytosis in a preparation of 'unroofed' bovine adrenal chromaffin cells, in which part of the plasma membrane had been removed with a jet of liquid, leaving a patch of membrane, with attached LDCVs, adhering to a glass coverslip (Wiegand, Don-Wauchope et al. 2002). These vesicles were induced to fuse by an increase in $[Ca^{2+}]$.

More recently TIRFM was used to monitor individual fusion events between proteoliposomes containing SNAREs and a supported planar bilayer containing cognate target SNAREs (Fix, Melia et al. 2004). Approach, docking and fusion of individual vesicles to the target membrane were quantified revealing that fusion was initiated within <100 ms of the rise in of Ca^{2+} and membrane mixing was complete within 300 ms. Removal of the N-terminal domain of syntaxin 1a increased the fusion probability > 30-fold compared

to the full-length protein. This suggested that formation of the SNARE core complex is sufficient to fuse opposing membrane bilayers at a speed commensurate with most fusion processes in cells (Fix, Melia et al. 2004).

Although the above techniques are very powerful and have imparted valuable information regarding exocytosis, when used to study the interaction between specific proteins, they can only report on the location of the proteins of interest. They can show whether two proteins share the same space within a cell, but they cannot show whether these proteins are interacting. An advanced technique that can give information about the interactions between proteins is FRET microscopy.

1.15.3 Fluorescence Resonance Energy Transfer Microscopy and Fluorescence Lifetime Imaging Microscopy

Fluorescence resonance energy transfer (FRET) is a physical effect that can be measured and thus used for quantifying the distance between two different fluorophores. FRET describes the non-radiative energy transfer from a 'donor' fluorophore (e.g. ECFP) to an 'acceptor' (EYFP), when there is overlap between the emission spectrum of the donor and the excitation spectrum of the acceptor. When the two excited-state dipoles, in a favourable mutual orientation, come within a critical distance (usually between 2-8 nm), the fluorescent lifetime of the donor fluorophore is shortened (Pollok and Heim 1999; Elangovan, Day et al. 2002; Duncan, Bergmann et al. 2004). At the critical distance where 50 % of the donor energy is transferred to an acceptor – the Förster radius – the donor emission and fluorescent lifetime are each reduced by 50 %, and sensitised emission (acceptor emission specifically under donor excitation) is increased. FRET is inversely proportional to the 6th-power of inter-dipole distance, and can therefore be used as a quantitative spectroscopic measure of protein-protein proximity. The possibility of FRET measurement and quantification between spectrally distinct fluorescent proteins means that this approach has become used widely in cell biology to visualise protein-protein interactions in intact cells. FRET is predictable,

quantitative and can be imaged in single cells with high temporal and spatial resolution; it is therefore ideal for monitoring the dynamic association of macromolecular partners. It needs, however, a general method for labelling one macromolecule participant with a donor fluorophore and the other with an acceptor fluorophore, such as expressing fusions of the two prospective partners with differently coloured GFP variants (Cubitt, Heim et al. 1995). Two GFP pairs have so far been used in FRET-based biological systems; BFP (donor) and EGFP (acceptor) have been widely used, however BFP is only weakly fluorescent, which limits its usefulness. An alternative FRET pair is ECFP (donor) and EYFP (acceptor). ECFP is significantly brighter than BFP, permitting accurate ratiometric measurements of both donor and acceptor fluorophores by a variety of fluorescent detectors (Pollok and Heim 1999).

To date FRET has been used to study the equilibrium between the open and the closed conformation of syntaxin 1a (Margittai, Widengren et al. 2003) and the interaction between syntaxin1a and munc18-1 in HEK293 cells (Liu, Ernst et al. 2004), but in these studies FRET images were not collected, so there was no spatial information.

Margittai et al (2003) showed that there is a dynamic equilibrium between the open and the closed conformation of syntaxin 1a in isolation with a relaxation time of 0.8 ms, suggesting a rationale for regulatory proteins that stabilise it in one conformation or the other during exocytosis.

Studies in HEK293 cells revealed that syntaxin 1a and munc18-1 interacted with each other in the Golgi complex at early expression time points, with strong plasma membrane colocalisation apparent at later times. Also the trafficking of syntaxin 1a was found to be dependent on the presence of munc18-1. Furthermore the use of phosphomimetic mutants of munc18-1 suggested that Ser313, a protein kinase C phosphorylation site, and Thr574, a Cdk5 phosphorylation site, regulate the syntaxin 1a – munc18-1 interaction (Liu, Ernst et al. 2004).

Although FRET is a powerful tool for investigating the interaction between proteins, it requires complicated arithmetical manipulations of the donor, acceptor and sensitised emission data to correct for spectral bleed-through and cross-talk. In addition FRET measurements using steady-state fluorescence emission intensity data are affected by photobleaching and uncorrected data can be influenced by relative donor/acceptor concentration changes. An alternative to this approach is fluorescence lifetime imaging microscopy (FLIM). The fluorescence lifetime of a fluorophore is the mean time that it spends in the excited state. This is usually a few nanoseconds, but is strongly dependent on microenvironmental factors; any energy transfer between an excited molecule and environment changes the fluorescence lifetime in a predictable way, independent of chromophore concentration. Importantly FRET shortens the fluorescence lifetime of a donor fluorophore, therefore FLIM is a direct approach quantifying effects that involve energy transfer. FLIM is not affected by photo-bleaching, relative donor/acceptor concentration changes or excitation intensity and since only the donor lifetime is measured, spectral bleed-through is not an issue. The combination of FRET and FLIM provides high spatial (micrometer) and temporal (nanosecond) resolution for studying the association of macromolecules in single cells (Elangovan, Day et al. 2002; Duncan, Bergmann et al. 2004). Duncan et al used time-correlated single photon counting (TCSPC)-FLIM to measure ECFP fluorescent lifetime and energy transfer. (TCSPC)-FLIM requires two-photon excitation (TPE) microscopy, which uses near-infra-red excitation energy, exciting the fluorophore when two photons, each contributing half the energy required to excite fluorescence, are absorbed by the molecule in quick succession (10^{-18} seconds), and can be less phototoxic to cells than conventional laser energy (Cahalan, Parker et al. 2002; Duncan, Greaves et al. 2003). PC12 or HEK293 cells, transfected with ECFP or CY24, were imaged as described using 800 nm TPE, enabling efficient excitation of ECFP and no detectable excitation or emission from EYFP in the absence of FRET. This revealed that ECFP or the CY24 fusion was distributed throughout the cell cytoplasm. Duncan et al quantified donor fluorescence

lifetime and energy transfer in the fixed-distance construct, by applying TCSPC FLIM to cells expressing the ECFP alone or CY24 constructs, acquiring data from a 512 x 512 pixel image (146 nm x 146 nm pixel dimensions) using 128 x 128 binned TCSPC pixels (i.e. 4 x TCSPC binning) and 256 time bin per pixel. TCSPC data acquisition using different BP or LP filters to separate spectral components of the ECFP emission revealed that of ECFP (alone) fluorescent decay data were best fit using the Levenberg – Marquardt algorithm to a bi-exponential decay (average reduced weighted chi-squared residual (χ^2) value <1.1), as previously described (Pepperkok, Squire et al. 1999; Tramier, Gautier et al. 2002); Figure 1.9). These data yielded a long lifetime component of 2.19 ± 0.24 ns (τ_2). A short lifetime component (τ_1) was also present, with lifetime of 0.42 ± 0.12 ns. These combined data yielded a mean time constant value, τ, of 1.57 ± 0.06 ns (mean ± SD, n = 12). TCSPC analysis of intramolecular FRET between tandem ECFP and EYFP moieties revealed a specific, significant decrease in the donor lifetime participating in FRET. Duncan et al provided further evidence that the donor-specific decreases in the mean fluorescent lifetime was due to energy transfer, they specifically photo-bleached the acceptor, EYFP fluorophore (Figure 1.10). Photo-bleaching required 500 iterations from a 514 nm laser line, at 100% laser power, in a defined intracellular region of interest. FLIM imaging after acceptor photo-bleaching revealed that the mean fluorescence lifetime of the donor, ECFP, fluorophore had increased within the photo-bleached region. These data were plotted as lifetime vs. pixel frequency distributions, emphasising the appearance of a longer mean donor lifetime (~1500 ps, comparable with that measured for ECFP alone in a non-FRET system) in the image after photobleaching (Duncan 2003).

Since TCSPC-FLIM has been used extensively in the present work, its theory and practice are described in more detail in the next Chapter.

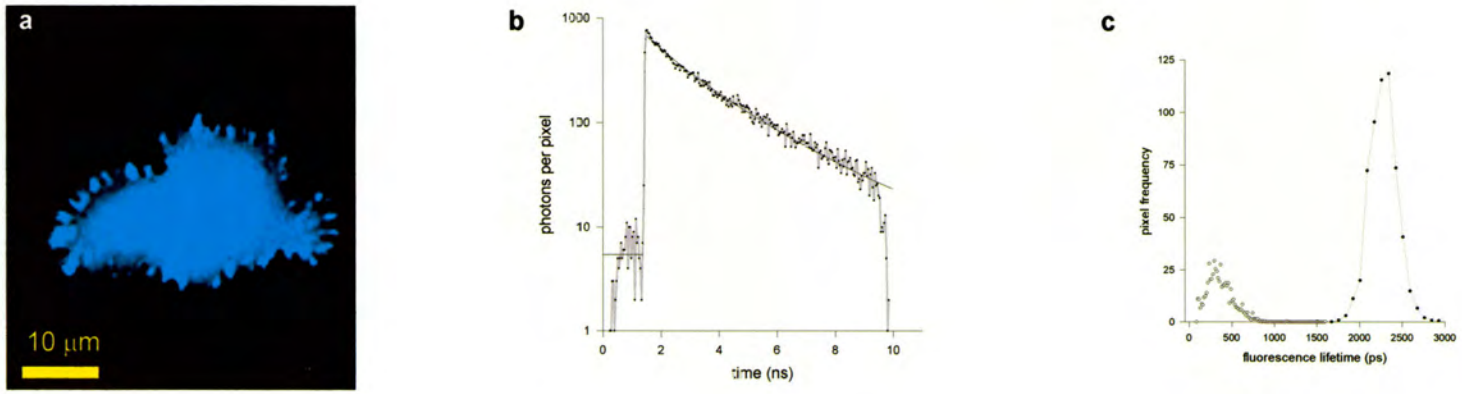

Figure 1.9: TCSPC imaging of a PC12 cell expressing ECFP

Data were acquired as described, using 10 s recording time, a long pass 470nm emission filter and a Zeiss C-Apochromat 1.2 NA 63 x water-corrected immersion objective lens.

a: A non-descanned TPE intensity image, acquired using the TCSPC card, showed a fluorescence throughout the cell

b: The fluorescence decay data from three-binned pixels from a 128 x 128 pixel image were fit to a bio-exponential curve

c: A frequency distribution plot revealed two lifetime populations in the image, a fast component and a slow component (Duncan at al, 2004)

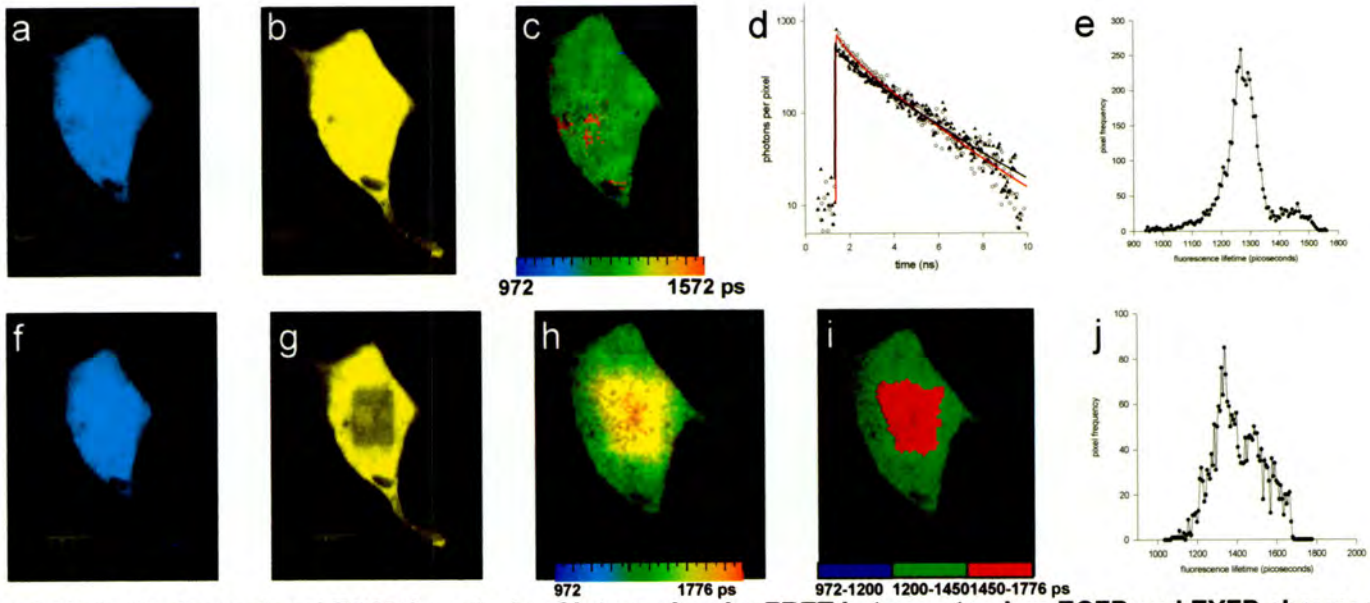

Figure 1.10: Multi-dimensional TCSPC analysis of intramolecular FRET between tandem ECFP and EYFP chromophores in HEK293 cells

(a,b) The non-descanned TPE intensity images in the 435-458 nm and the LP530nm channels, respectively. (c) A FLIM map for the donor, 435-458 nm channel. (d) the normalised fluorescence decay data for ECFP alone (black filled triangles) and CY24 (open circles), plotted from three-binned TCSPC pixels. (e) The fluorescence lifetime vs pixel frequency distribution shows a major peak centred around the τ lifetime mean of ~1300 ps, with a minor peak at ~1400-1500 ps. (f-j) the respective intensity images, τ FLIM map and frequency distribution for the same cell with a region of interest photobleached in the acceptor, EYFP. Two FLIM maps are shown (h.i), each indicating that the donor lifetime has increased in the region where the acceptor was photobleached. This was emphasised particularly by applying discrete colours to the FLIM map (i).

1.16 Project Aims

When starting the project years of biochemical studies had shown that syntaxin 1a and munc18-1 interacted with each other with nanomolar affinity. However most of these studies were done using a fragment of syntaxin 1a and their interaction had not been investigated in cells, which led to several questions: Do syntaxin 1a and munc18-1 interact in cells? Where in cells does this interaction occur? What regulates this interaction in cells? To address some of these questions, the interaction between endogenous and fluorescently labelled proteins was investigated using confocal microscopy in conjuction with colocalisation analysis and Fluorescence Lifetime Imaging Microscopy in absence and presence of the PKC activation, which has been shown to enhance exocytosis.

Chapter 2

Materials and Methods

2.1 Chemicals and Biochemicals

Amersham Biosciences Ltd, Bucks, U.K

[^{35}S]-methionine, (cat. no. AG1094) GSH- Sepharose. HiTrap affinity columns

BD Biosciences, CA, U.S.A

BD TALON Metal Affinity Resin, CHROMA SPIN-30 DEPC H_2O columns

QIAGEN Ltd, Dorking, Surrey, U.K

Ni-superflow columns

Roche Diagnostics Ltd, East Sussex, U.K

Complete protease inhibitor tablets and Complete protease inhibitor tablets EDTA-free

Sigma-Aldrich Chemical Company, Dorset, U.K

All general chemicals used. Kodak Biomax film for autoradiography, leupeptin and pepstatin protease inhibitors, Protease inhibitor cocktail (purification of poly(histidine)-tagged proteins, cat. no. P-8849), Protease inhibitor cocktail (cat. no. P-8340), Phosphoramidon.

2.1.1 Molecular Biology Reagents

Eppendorf, Cambridge, U.K

The Perfectprep® Gel Cleanup Kit

Gibco BRL, Paisley, U.K

All reagents and media for mammalian cell culture

Invitrogen, Paisley, U.K

All vectors used. Top10 competent cells

New England Biolabs, Herts, U.K

All restriction endonucleases used: Age I, BamHI, BsrGI, EcoRI, Hind III, NheI, NdeI, XbaI, XhoI

Novagen, Nottingham, U.K

Bugbuster® Protein Extraction Reagent

Pharmacia Biotech, Cambridge, UK.

Deoxyribonucleotide triphosphates

Promega Corporation UK, Southhampton, U.K

Pfu polymerase. Taq polymerase. T4 DNA Ligase. RNasin. *In vitro* Coupled Transcription Translation Kit

QIAGEN Ltd, Dorking, Surrey, U.K

QIAfilter™ Plasmid Maxi Kit, Ni-NTA Superflow column

Roche, Lewes, East Sussex, U.K

Expand High fidelity PCR System

Strategene Europe, Amersterdam, The Netherlands

Quickchange® II XL Site-directed Mutagenisis Kit

2.1.2 *Escherichia coli* Strains Used

Top10, BL21 RIL, BL21 DE3, M15[pREP4]

2.1.3 Culture Media

Media were prepared according to standard recipes (Sambrook, Fritsch et al. 1989). The media used in this study were Luria-Bertani (LB) (10 g NaCl, 10 g Tryptone, 5 g Yeast extract, pH7.0 made up to 1 litre with dH_2O), Terrific Broth (TB) (12 g Tryptone, 24 g Yeast extract, 4 ml Glycerol made up to 900 ml with dH_2O). Following autoclaving the media was left to cool to 60 °C then 100 ml of a sterile solution of 0.17 M KH_2PO_4, 0.72 M K_2HPO_4 (2.31 g KH_2PO_4, 12.54 g K_2HPO_4 in 90 ml of dH_2O) was added) and Supermedia (5 g NaCl, 15 g Tryptone, 25 g Yeast extract, pH7.0 made up to 1 litre with dH_2O)

2.1.4 Antibodies

Mouse monoclonal antibodies were directed against V5 epitope (Invitrogen, cat no: R960-25, 1 in 1000 dilution), munc18 (BD Biosciences, cat no: 610336, 1 in 500 dilution) and

syntaxin 1a (HPC-1, cat no: S0664, 1 in 500 dilution). Rabbit anti-mouse IgGs were horseradish peroxidase-coupled (SAPU, product no: S081-201, 1 in 4000 dilution) and alexa546-coupled (Molecular Probes, Invitrogen, cat no: A-21123, 1 in 1000 dilution).

2.2 Standard DNA manipulations

Several of the protocols used were as described (Sambrook, Fritsch et al. 1989). These included phenol extraction of nucleic acids, (ppE3-E4), nucleic acid precipitation, (ppE10-E15), agarose gel electrophoresis, (pp6.9-6.12) and restriction endonuclease digestion (pp5.28-5.32). DNA was extracted from agarose gels using a commercial kit (Eppendorf) according to the manufacturer's protocol.

2.3 Polymerase chain reaction (PCR)

PCR was performed on an Applied Biosystems GeneAmp PCR system 9700 PCR machine and for all the work reported in this thesis the PCR reaction mixes, dependent on the DNA polymerase used, were as follows:

2.3.1 Expand High Fidelity PCR System™ reaction mix

component	*µl*
10 X PCR Buffer	5
dNTP mixture (10 mM each)	1
forward primer (10 µM)	1
reverse primer (10 µM)	1
template DNA (10 ng/µl)	1
DEPC treated H_2O	40.25

The reaction mix was placed in the PCR machine and incubated at 95 °C for 1 min to separate the two strands of the DNA double helix, 0.75 µl Taq/Rho polymerase (Roche) was

then added, followed by a suitable PCR cycle dependent on the size of the PCR template, which is described in the relevant chapters.

2.3.2 Pfu polymerase reaction mix

Component	*µl*
10 X PCR Buffer	5
dNTP mixture (10 mM)	1
EGFP/munc18-1 forward primer (10 µM)	1
Munc18-1 reverse primer (10 µM)	1
Munc18-1-EGFP-C2/Munc18-1_{R39C}-EGFP-C2 (10 ng/µl)	1
DEPC treated H_2O	40

The reaction mix was incubated at 95 °C for 1 minute to separate the DNA template strands then 1 µl Pfu was added followed by a suitable PCR cycle dependent on the DNA template used described in the relevant chapter.

2.3.3 Taq polymerase reaction mix

component	*µl*	*master mix (x13) µl*
10 x Buffer	5	65
$MgCl_2$	3	39
dNTP mixture (10 mM each)	1	13
ECFP Forward Primer (10 µM)	2.5	32.5
Syn 1a-(cyt) Reverse Primer (10 µM)	2.5	32.5
DEPC-treated H_2O	35.5	461
Taq polymerase	0.5	6.5

The master mix was assembled on ice, mixed thoroughly before being aliquoted into PCR tubes. 10 colonies were picked and each one was dipped into a different PCR tube before

being spotted onto a LB-agar plate containing ampicillin (100 μg/ml) and a suitable PCR cycle was used, described in the relevant chapter.

2.3.4 Deoxynucleotide primers

Oligodeoxynucleotide primers used for sequencing were generally 16-24 nucleotides long. The forward primer was a direct copy of the DNA sequence at the overlapping the start codon of the DNA template, sometimes containing a restriction endonuclease site 5' to the start codon. The reverse primer was a direct copy of the DNA template complementary strand written 5'-3'. All PCR primers were ordered from MWG Biotech (0.05 μmol, MALDI purification). Oligodeoxynucleotide primers used for sequencing reactions were approximately 20 nucleotides long, preferentially containing a GC and AT content that gave a melting temperature of less than 60 °C, as recommended by MWG Biotech. Sequencing primers were designed so that they overlapped the vector:insert junction, with subsequent primers overlapping the end of the previous sequencing round by ~200 bp and were ordered from MWG Biotech.

2.3.5 Site directed mutagenesis PCR

For this the oligonucleotide primers were complementary to each other, containing the desired mutation with 15 bp on either side and were ordered from MWG Biotech. PCR was performed using the Quickchange II XL Site-Directed Mutagenesis kit (Strategene) following the manufacturer's instructions with the reaction mix components as follows:

Component	*µl*
10 X Buffer	5
dNTP mixture	1
Forward primer	1.25
Reverse primer	1.25
Quick solution	3
Munc18-1_{R39C}-V5-His_6/EGFP-munc18-1_{R39C}-V5-His_6 (5 ng/µl)	1
DEPC-treated H_2O	37.5

The reaction mix was incubated at 95 °C for 1 min, followed by the addition of 1 µl Turbo Pfu (Stratagene) followed by the appropriate PCR cycle dependent on the DNA template used and is described in the relevant chapter.

2.4 Cloning in TOPO plasmid vectors

Two types of TOPO vectors were used during this study. The pCR T7/CT TOPO vector was used for non-directional cloning in which the vector has T-overhangs and the insert has A-overhangs, added during the PCR reaction by Expand™ polymerase (Roche). The other vector used was pET directional TOPO, which allows directional cloning by having one overhanging end and one blunt end. The vectors were linearised and have Topoisomerase I from *Vaccinia* virus attached to the 3' ends (Shuman 1991). The bond between the enzyme and the DNA can be broken by the 5' hydroxyl of the original cleaved strand reversing the reaction and releasing the enzyme (Shuman 1994). TOPO cloning exploits this process to allow the insertion of DNA fragments into vectors.

2.5 Cloning in plasmid vectors

Both non-directional and directional cloning were used, depending on the vector. In non-directional cloning the inserts generated by PCR contain A-overhangs and the vectors are linearised therefore no preparation for both the vector and the insert DNA was required.

With directional cloning both the vector and the insert were digested by two different restriction endonucleases, usually resulting in the insert annealing into the vector in the correct orientation in a T4 Ligase-dependent reaction. In both cases the resulting recombinant plasmids were then used to transform bacteria. Plasmids containing the insert in the correct orientation were distinguished from those where the insert has inserted in the wrong orientation or from recircularised vector with no insert by restriction endonuclease analysis of small scale plasmid preparations (see below)

2.5.1 Preparation of vector DNA for cloning

With non-directional cloning the PCR product was ligated directly into the vector without any preparation since the vectors are supplied linearised.

In directional cloning, the vector was first cleaved by appropriate restriction endonucleases, usually two. Normally 1-5 μg of the vector and 10 units of each restriction enzyme was used in a 20 μl reaction mix for two hours at 37 °C. Depending on the restriction endonucleases used, both enzymes could be added to the same mix if they worked well in a common buffer. If not the enzymes were used sequentially, starting with the enzyme that required the buffer of lower ionic strength. The reaction products were analysed and then purified from an agarose gel using the Eppendorf kit.

2.5.2 Preparation of the DNA fragments for ligation

No preparation of the DNA fragments was required for non-directional cloning since A-overhangs are added during the PCR reaction therefore the insert can be ligated directly into a linearised vector. For directional cloning the DNA fragment was prepared in the same way as the vector.

2.6 Ligation of insert DNA and plasmid vector

The ligation reaction was optimised using various ratios for each individual ligation and was based on the following equation:

$$ng\ insert = \frac{ng\ vector \times insert\ size(kb)}{vector\ size(kb)} \times molar\ ratio \frac{insert}{vector}$$

Usually a molar mass ratio of 1:1 or 1:3 of vector:insert works best. For this the DNA concentration of the linearised vector and the insert were estimated by agarose gel electrophoresis and comparison with DNA weight markers of known concentration. The ligation reaction was then set up in a 10 µl reaction mix using the appropriate vector:insert ratios and was performed according to the T4 DNA Ligase manufacturers protocol (Promega) The mix was incubated overnight at 16 °C and terminated by incubation for 10 min at 70 °C.

2.7 Production of competent Escherichia coli

E.coli cells were made competent for transformation using rubidium chloride following the protocol in the Promega Protocols and Applications Guide (p.45).

2.8 Transformation of Escherichia coli

The TOPO vectors came with competent *E.coli* TOP10 cells (Invitrogen) and were transformed following the manufacturer's protocol.

Competent cells produced in-house were used with the other vectors used. The 10 µl ligation reaction mix was added to a 100 µl aliquot of the cells. This was then incubated on ice for 20 min, followed by a heat shock at 42 °C for 30 seconds. The cells were allowed to recover on ice for 2 min before 500 µl of Luria-Bertani (LB) medium (Sambrook, Fritsch et al. 1989) was added followed by incubation at 37 °C for 30-60 min, depending on the antibiotic selection. 200 µl of the transformed cells were plated on a pre-warmed LB/agar plate containing the appropriate antibiotic.

2.9 Analysis of transformants

2.9.1 Small-scale plasmid preparation: 'miniprep'

The routinely used method for identifying the insert in recombinant vectors was to purify the plasmid DNA from individual clones and check for its presence using restriction digestion and agarose gel electrophoresis. The miniprep protocol used in this study, which is described elsewhere, was the Alkaline Lysis method (Sambrook, Fritsch et al. 1989) (pp1.25-1.28).

2.9.2 Analysis of transformants by restriction digests

Restriction digests were performed to check that recombinant vectors had been made and to ensure that the DNA fragment had inserted in the correct orientation. This was especially important when non-directional cloning was used. In most cases two enzymes, one known to cut the vector and the other known to cut the insert at a unique site, were used. The enzymes were also chosen so that they would produce fragments of appropriate size that would indicate whether or not the DNA fragment had inserted into the vector in the correct orientation. In each reaction 10 µl of the 'miniprep' DNA was used. The results were analysed by running 10 % (v/v) of the digested plasmid on an agarose gel.

2.9.3 Large scale plasmid preparations

The large-scale plasmid preparations followed the Alkaline Lysis protocol (Sambrook, Fritsch et al. 1989) using the QIAGEN QIAfilter™ Plasmid Maxi Kit according to the manufacturer's instructions (Qiagen).

2.10 Quantification of plasmid DNA

Plasmid DNA concentration was measured by spectrophotometry, at 260 nm and 280 nm. Absorbance at 260 nm allowed the calculation of the concentration of nucleic acid in the

sample, an absorbance of 1 corresponding to approximately 50 µg/ml for double stranded DNA. The ratio between absorbances at 260 nm and 280 nm (A_{260}/A_{280}) provides an estimate of the purity of the nucleic acid, the value for pure DNA being 1.8. Contamination with protein results in a smaller value of A_{260}/A_{280} (Sambrook, Fritsch et al. 1989).

2.11 DNA sequencing

When PCR is used to amplify a fragment of DNA for cloning the polymerase can make errors, introducing mutations in the sequence. The error frequency depends on the polymerase used: the error frequency for Pfu, for example, is 1 x 10^{-6} /bp/duplication (Cline, Braman et al. 1996). In this study all PCR products were sequenced by MWG Biotech and the DNA was prepared following their instructions. 1 µg of DNA was precipitated using 0.5 vol of 7.5 M ammonium acetate and 2 x vol of 100 % ethanol in the freezer for 20 min. The DNA was pelleted by centrifugation at 13000 rpm for 15 min, followed by washing with 70 % (v/v) ethanol and centrifugation. The pellet was then left to dry in air before being sent off.

2.12 Electrophoretic separation and detection of proteins

SDS polyacrylamide gels (SDS-PAGE) were used for the separation of proteins, using the protocol of Laemmli, (1970). The Hoeffer Tall Mighty Small apparatus was used with the following solutions for a 10 % acrylamide gel. The separating gel (appendix 1.1.1) was poured between glass plates to the appropriate level and then was overlaid with water-saturated butan-2-ol and left to polymerise. Once polymerised the butan-2-ol was removed and the gel was rinsed with water before the stacking gel (appendix 1.1.2) was poured, followed by insertion of a comb allowing wells to form before the gel polymerised. The samples were denatured by heating to 100 °C for 5 min in 1 x SDS sample buffer (appendix 1.1.3).

Once the stacking gel had polymerised the tank was filled with electrophoresis buffer (appendix 1.1.4). The comb was then carefully removed and the samples loaded. A potential of 50 mV was then applied until the dye front entered the separating gel, and then increased to 200 mV until the dye front reached the bottom of the gel.

2.12.1 Coomassie blue R staining

Following electrophoretic separation the protein bands were visualised by Coomassie blue staining. First the gels were fixed by immersing them in fixing solution (appendix 1.2.1) for 15 min. Next the gels were covered in Coomassie blue R250 stain (appendix 1.2.2) for 20 min. Following this the gel was destained (appendix 1.2.3), and the destaining solution changed every 15 min until the protein bands were clear. The gel was then dried onto filter paper using a heated bed vacuum gel drier at 65 °C for 1 hour (Biorad)

2.12.2 Silver staining

When there was not enough protein on a polyacrylamide gel to be visualised by Coomassie staining, silver staining was used as it is more sensitive (Wray, Boulikas et al. 1981). The polyacrylamide gel was run and fixed as before. The gel was then immersed in 50 % (v/v) methanol for 30 min followed by rinsing in water for 5 min. This procedure was repeated three times. The staining solution C was then prepared by adding solution A (appendix 1.3.1) drop wise, with vigorous stirring, to solution B (appendix 1.3.2). The gel was stained in solution C for 15 min followed by washing in H_2O for 5 min. The stained gel is then developed using solution D (appendix 1.3.4) until the protein bands have appeared. Development was stopped by rinsing the gel in 50 % (v/v) methanol, 10 % (v/v) acetic acid followed by rinsing in H_2O. The gel was then dried as before.

2.13 Transfer of proteins from gels to solid supports: immunological detection of immobilised proteins (Western blotting)

The transfer of proteins from a polyacrylamide gel to a membrane was achieved by electrophoretic elution (Towbin, Staehelin et al. 1979). The method used in this study was *wet* transfer, in which the gel sandwich (2 pieces of blotting paper, gel, membrane, 2 pieces of blotting paper) is fully immersed in transfer buffer (appendix 1.4.1) in a tank between platinum electrodes with the membrane closest to the anode. This was done using a LKB Transfer apparatus and a current of 0.8 mA for 2 hours. The membrane used was Hybond-P (Amersham), which had been pre-soaked in methanol.

2.13.1 Blocking

Following transfer of the proteins, the membrane was blocked to prevent any non-specific binding of the antibody. The membrane was fully immersed in 5 % (w/v) Marvel in TBS containing 0.5 % Tween-20 (v/v) (appendix 1.4.3) for 1 hour at room temperature.

2.13.2 Antibody Incubations

After the blocking solution was removed the membrane was washed 3 x in TBST (appendix 1.4.3) followed by incubation in the primary antibody, diluted appropriately depending on the antibody (appendix 1.4.4), for at least 3 hours at room temperature or usually overnight at 4 °C. The primary antibody was then removed and the membrane was washed three times over 5 min in TBST (appendix 1.4.3) as before, followed by further washing for 1 hour changing the wash every 10 min. After washing the membrane was then incubated with the secondary antibody, horseradish peroxidase conjugated anti-mouse IgG (SEPA), diluted 1:4000 in blocking buffer, for 1 hour. The membrane was then washed as with the primary antibody.

2.13.3 Detection of immune complexes on immunoblots

The detection of the horseradish conjugate used enhanced chemiluminescent reagent (ECL), which involved incubating the membrane for 1 min using 2 solutions in a 1:1 ratio, ECL solution 1 (appendix 1.4.5) and ECL solution 2 (appendix 1.4.6). Following this the protein bands were visualised by exposing the membrane to Konica x-ray film for an appropriate length of time, depending on how much protein is on the membrane, typically 1-5 min. The film was then developed (Konica SRX-101A developer).

2.14 Production of fusion proteins in *Escherichia coli*

2.14.1 Induction of expression from a lac promoter

The expression plasmid, containing a gene under the control of the *lac* promoter, was first transformed into *E.coli* strain BL21 RIL (see 2.8). A bacterial culture, harbouring the expression plasmid, was grown in selective medium at 37 °C to an optical density 0.6-0.8 (measurement at 600 nm). Expression was then induced using 0.5-1 mM IPTG. Cells were grown at an appropriate temperature and time dependent on the protein being expressed, as discussed in subsequent chapters.

2.14.2 Lysis and fractionation of a bacterial culture

Following induction the bacteria were harvested by centrifugation at 5000 x g for 10 min. The bacteria were then resuspended in 1/20 of the original culture volume in Bugbuster® containing 1 µl Benzonase® Nuclease per 1 ml Bugbuster reagent, complete protease inhibitor tablets (from 10x stock), 1 mM PMSF, 10 µg/ml pepstatin and 10 µg/ml leupeptin, following the manufacturer's instructions. Bugbuster Protein Extraction Reagent is formulated for the gentle disruption of the cell wall of *E.coli*, resulting in the liberation of soluble proteins.

The lysate was centrifuged at 50000 rpm for 15 min to separate the soluble and insoluble fractions.

2.14.3 The purification of oligohistidine-tagged proteins

During this study three methods were used for purifying oligohistidine-tagged proteins, the HiTrap affinity column (Amersham) and BD TALON™ Metal Affinity Resin (BD Biosciences) and the Ni-NTA Superflow columns (Qiagen). With both the HiTrap columns and the BD Talon the soluble fraction from bacterial lysis using Bugbuster was used without further treatment and was fractionated according to the manufacturer's instructions, but with the Ni-NTA Superflow columns the bacteria were lysed and the soluble fraction was treated following the manufacturer's instructions.

2.14.3.1 Purification of oligohistidine-tagged proteins using HiTrap columns

With the HiTrap (Amersham) columns the soluble protein sample, obtained by ultracentrifugation, was passed through a 0.2 micron syringe filter, loaded and recirculated through the column using a peristaltic pump. The column was then washed with 5 column volumes of wash buffer (appendix 1.5.1.1). The oligohistidine-tagged protein was eluted using a step gradient of imidazole in elution buffer (appendix 1.5.1.2). The individual steps used were 2 mls of each of the following, 50 mM, 100 mM, 350 mM and 500 mM imidazole, collected as 1 ml fractions. The purification was analysed by SDS PAGE followed by Coomassie staining.

2.14.3.2 Purification of oligohistidine-tagged proteins using BD Talon

With the BD TALON™ (BD Biosciences) resin a batch elution method was used. The soluble protein fraction (10 ml) obtained by ultracentrifugation was passed through a 0.2 micron syringe filter then incubated with 500 µl slurry of resin in a 50 ml Falcon tube with

rolling at 4 °C for 2 hours. Following incubation the resin was harvested by centrifugation at 700 x g and then washed twice with 10 x bed volumes in wash buffer (appendix 1.5.2.1). The resin was then resuspended as 1:1 slurry with wash buffer and transferred to a 1 ml gravity-flow column. The resin was washed with a further 5 bed volumes of wash buffer. The oligohistidine-tagged protein was then eluted using a step imidazole gradient of 50 mM, 150 mM and 500 mM in elution buffer (appendix 1.5.2.2), collected as 500 µl fractions. The results of the purification were assessed using SDS-PAGE and Coomassie blue staining.

2.14.3.3 Purification of oligohistidine-tagged proteins using Ni-NTA Superflow columns

When using the Ni-NTA Superflow columns (Qiagen) the bacterial pellet was resuspended in 1/50 of the original culture volume in lysis buffer (Appendix 1.5.3.1) containing protease inhibitors (Sigma), 200 µl for 500 ml starting culture and Benzonase (1/100 dilution). Lysozyme was then added to a final concentration of 1 mg/ml and the slurry kept on ice for 30 mins. The bacterial lysate was then sonicated, 8 x 10 secs at 6 microns, with cooling at 0 °C for 10 secs between each burst. The lysate was then separated into soluble and insoluble fractions with centrifugation at 10000 x g for 30 mins. During this time the NI-NTA matrix was removed from the column and washed 3 x with 10 mls of lysis buffer in a 15ml falcon tube. The bacterial supernatant was then incubated with the washed beads for 2 h at 4 °C with rolling. Following incubation, the beads were packed into the supplied column and the supernatant was left to flow by gravity through the column. The beads were washed with 20 mls of wash buffer (Appendix 1.5.3.2) before being eluted with 3 mls of elution buffer (Appendix 1.5.3.3), which was collected as 500 µl fractions. Samples were then prepared for SDS PAGE analysis followed by Coomassie staining.

2.14.4 Purification of GST-tagged proteins

For the purification of GST fusion proteins, Glutathione Sepharose 4B (GSH) (Amersham) was used. The GST fusion proteins used in this study were used in pull-down experiments so were not removed from the Glutathione Sepharose 4B. The soluble protein fraction (10ml) was incubated with 500 µl of the resin in a 50 ml Falcon tube with rolling at 4 °C for 2 hrs. The resin was then harvested by centrifugation at 500 x g for 5 min, washed five times with 10 x bed volumes. The first wash was with PBS pH7.5, followed by three washes with wash buffer (appendix 1.6.1) and a final wash with PBS, these washes were performed to remove non-specific binding. The resin was resuspended in 1:1 slurry with PBS. The results of the purification was analysed using SDS-PAGE and Coomassie blue staining.

2.15 Estimation of protein concentration

For several applications it was important to measure the concentration of purified protein. During this study two methods were used.

2.15.1 Bradford method

The Bradford method is a fast and fairly sensitive way to measure protein concentration. The method used here was adapted from Methods in Molecular Biology, Vol.32, Basic Protein and Peptide Protocols. First a standard curve was generated using known concentrations of a BSA standard (120 mg/ml), the concentration of which was calculated from its absorbance at 280 nm ($A_{280}^{1\%} = 6.60$). Samples were made using BSA concentrations ranging from 0 – 80 µg per sample made up to a final volume of 100 µl. To this 1 ml of Bradford's Reagent (appendix 1.7.1) was added and vortexed. The absorbance at 595 nm of the samples relative to a blank was measured up to 60 min after the reagent was added. These measurements were used to plot a standard curve of protein concentration vs absorbance at 595 nm. The unknown protein sample concentration was measured in the

same way using different volumes of the sample, each in triplicate. This method proved unsuitable for determining the concentrations of protein coupled to Sepharose.

2.15.2 Lowry method

The Lowry method was used to measure the protein concentration of a GST fusion proteins still attached to Glutathione Sepharose as it elutes the fusion protein from the beads, which are then removed. The method used was adapted from Lowry et al, (Peterson 1977). BSA standards were made ranging in concentration from 0 – 100 µg per sample. To each of these 50 µl of 10 % (w/v) sodium deoxycholate was added followed by vortexing. 1 ml of TCA was added, to precipitate the protein, followed by vortexing. The samples were centrifuged at maximum speed for 2 min in a microfuge and the supernatant removed. 1 ml of solution C (appendix 1.8.3) was added, followed by vortexing. 100 µl of solution D (appendix 1.8.4) was added and each sample must be vortexed immediately. The samples were then incubated at room temperature for 1 hour before the absorbance at 750 nm was measured. The BSA standards were used to plot a standard curve, which was used to determine the protein concentration of the fusion protein samples, also assayed in triplicate.

2.16 Solubilisation and refolding of insoluble fusion proteins

2.16.1 Solubilising and refolding of insoluble fusion proteins using non detergent sulfobutane

It is often difficult to obtain soluble and active proteins from expression in prokaryotes, as they often misfold and form aggregates, known as inclusion bodies. These can easily be purified because of known size and density, however solubilisation of the expressed protein can usually only be obtained using strongly denaturing conditions and it is difficult to achieve efficient folding *in vitro*. In most cases the denaturant is removed by dialysis but this exposes the protein to a decreasing denaturant concentration over a few hours leading to

the protein being exposed to an intermediate denaturant concentration where they are not yet folded and are prone to aggregate. In an attempt to avoid this, the solubilised protein in denaturant was diluted 10-fold in a mild solubilising agent, non detergent sulfobutane (NDSB), which aids refolding.

First the inclusion bodies were washed twice with 2 ml PBS / 0.1% Triton X-100 followed by centrifugation at 30000 rpm for 30 min. The pellet was then solubilised by incubating for 1 hour at 4 °C in 2 ml solubilising solution (appendix 1.9.1). Insoluble material was then removed by centrifugation at 100000 x g for 10 min. The protein concentration was determined using Bradford's method and adjusted to 1 mg/ml with solubilising solution. The solubilised protein was then diluted as quickly as possible 1 in 10 into cold folding buffer (appendix 1.9.2) with vigorous stirring during and for 2 min after addition. This was then left at 4 °C for 1 hour. The remaining guanidine and NDSB were the removed through dialysis into a phosphate buffer (appendix 1.9.3). The solubilised protein was then purified using the BD TALON resin. The solubilisation and purification was analysed with SDS-PAGE and Coomassie blue staining and circular dichroism spectroscopy was used to determine whether the protein had refolded properly.

2.16.2 Solubilising and refolding of insoluble GST-fusion proteins using Q-Sepharose

It has been documented, (Hoess, Arthur et al. 1988), that GST-fusion proteins can be recovered from inclusion bodies in a soluble and biologically active by using ion exchange resins such as Q-Sepharose. The inclusion bodies were harvested and the insoluble protein was resuspended in 3 ml of Buffer A (appendix1.10.1). 1.5 ml of the resuspended pellet was incubated in 1.5 ml of Q-Sepharose (pre-washed in Buffer A) at 4 °C with rolling for 2 hours. The beads were then harvested by centrifugation at 2000 x g for 5 minutes and the supernatant removed and kept for analysis. The beads were then washed with 3 ml of Buffer A and harvested as before. The wash was removed and added to the first supernatant. The

beads were then incubated for a further 30 minutes at 4 °C rolling in 3 ml of high salt buffer A (appendix 1.10.2), then harvested as before. The supernatant, which should contain the GST-Fusion protein, was kept. The solubilisation and purification was analysed with SDS-PAGE and Coomassie blue staining.

2.17 Circular Dichroism

Purified protein samples were dialysed into 50 mM sodium phosphate pH8.0 and Circular Dichroism spectra were obtained in a Jasco J-810 spectropolarimeter using 0.05 cm cells, scanning between 260 and 190 nm at 10 nm/min and a data pitch of 0.2 nm. For each sample, 5 spectra were accumulated, the buffer-only baseline spectrum was subtracted and the data were analysed using CDSSTR (Compton and Johnson 1986; Manavalan and Johnson 1987), CONTINLL (Provencher and Glockner 1981) and SELCON3 (Sreerama and Woody 2000) and reference set 7 (Sreerama and Woody 2000) from the Dichroweb website (Lobley, Whitmore et al. 2002).

2.18 Coupled *in vitro* transcription and translation

This process expresses [^{35}S]-methionine labelled proteins from a desired gene under the control of the bateriophage Lambda T7 promoter. The reaction was carried out according to the manufacturer's instructions (Promega). The following components were assembled into a 1.5 ml tube:

TnT Rabbit Reticulocyte Lysate	25 µl
TnT reaction buffer	2 µl
TnT RNA T7 polymerase	1 µl
Amino acid mixture minus methionine	1 µl
RNasin	1 µl
DNA template (0.5 µg/µl)	2 µl
[^{35}S]-methionine (370 MBq/ml, >37 TBq/mmol)	2 µl

Nuclease-free deionised water was added to a final volume of 50 µl. The reaction mix was then incubated at 30 °C for 1 hour. Following this the reaction mix was passed through a size exclusion column (CHROMA SPIN-30 DEPC H_2O columns, BD Biosciences) to remove the unincorporated [^{35}S]-methionine. 5 µl aliquots of the eluate were then taken to either be analysed by SDS-PAGE and autoradiography or used in binding experiments described below.

2.18.1 Binding of [^{35}S]-methionine labelled munc18-1, EGFP-munc18-1, munc18-1$_{R39C}$ and EGFP-munc18-1$_{R39C}$ to GST-syntaxin 1a-(cyt)

In this study a comparison between the binding to GST-syntaxin 1a-(cyt), which is 1-799 bp of syntaxin 1a, and of either wild-type munc18-1, EGFP-munc18-1, munc18-1$_{R39C}$ and EGFP-munc18-1$_{R39C}$ was made, in order to determine whether the addition of the green fluorescent protein had any effect on the interaction of these two proteins and also to investigate the effect of a point mutation on this interaction. Full length syntaxin 1a was not used in this study because when expressed in bacteria it was insoluble, but the removal of the transmembrane domain overcomes this problem, and therefore the cytoplasmic domain of syntaxin 1a was fused to the C-terminus of GST. First the interaction between the proteins was looked at and the following reaction was set up:

GST-syntaxin 1a-(cyt)-GSH Sepharose (0.5 mg/ml)	5 µl
Munc18-1 variant *in vitro* transcription translation reaction	5 µl
Binding Buffer (Appendix 1.11.1)	40 µl

This mixture was incubated at 4 °C for 2 hours with rolling. The beads were harvested by centrifugation 6000 rpm for 2 min. The beads were then washed with 5 x 500 µl binding buffer with incubation at 4 °C, rolling for 15 min for each wash. The final wash was removed leaving approximately 40 µl of liquid in the tube, which was then totally removed from the Sepharose Beads using a piece of tissue paper. The beads were resuspended in 15 µl of 1 x SDS PAGE loading buffer and boiled for 5 min. The bound proteins were analysed by SDS-PAGE followed by drying the gel and autoradiography. To quantify the bands a phosphorimager was used.

2.18.2 Competition Binding Between [^{35}S]-methionine labelled munc18-1, EGFP-munc18-1 and munc18-1 peptides for binding to GST-syntaxin1a-(cyt)

To further investigate differences between the wild-type munc18-1 and EGFP-munc18-1 binding to GST-syntaxin 1a-(cyt), their relative binding affinity was assessed. This was done using a munc18-1-derived peptide that was reported to compete for binding to syntaxin 1a (Dresbach, Burns et al. 1998). The *in vitro* transcription and translation were performed and the binding experiment was set up as before but with the addition of increasing concentration of the competitive peptide similar to the concentrations described previously, with a scrambled peptide as a control. The results were analysed in the same way as before, except that before drying the gels they were Coomassie Blue stained so that each binding reaction could be normalised with respect to the amount of GST-syntaxin 1a-(cyt) present.

2.18.3 Competitive Binding Between [^{35}S]-methionine labelled munc18-1, EGFP-munc18-1 and munc18-1-His$_6$ for GST-syntaxin 1a-(cyt)

This experiment was done in the same way as before, but instead of using a peptide as competitor purified munc18-1-His$_6$ (munc18-1 fused to a hexahistidine tag), at suitable concentrations to compete off the radiolabelled munc18-1 and EGFP-munc18-1, was used. The results were analysed in the same way as before.

2.19 Autoradiography

Autoradiography was performed using Kodak biomax film, which was exposed to the radioactive gels for a suitable time depending on how hot the gel, which was determined using a Geiger counter (Morgan series 900 mini monitor) in a Kodak x-ray cassette. The film was then developed using a Konica SRX-101A developer.

2.20 Phosphorimager

The radioactive gels were exposed to the filter for an appropriate length of time, depending on how hot the gels were as with autoradiography; typically they were exposed for approximately 24 hours. Following exposure the filter was scanned using the phosphorimager (Fujifilm FLA2000) and the densities of the protein bands were analysed using the Aida programme by drawing a rectangle around the band of interest and also another rectangle of the same size above the band to acquire a background value. For each experiment the exact same size of rectangle was used to select each band.

2.21 Mammalian cell culture

2.21.1 HEK293 cells

HEK293 (transformed human embryonic kidney cell-line) were cultured in DMEM (Gibco BRL) supplemented with 10 % (v/v) foetal calf serum (Invitrogen) and 2 mM L-glutamine

(Gibco BRL). Cells were cultured and passaged according to standard procedures (Doyle, Griffiths et al. 1994)

2.21.2 AtT20 cells

AtT20 cells (anterior pituitary corticotroph tumour cell-line) were cultured in DMEM with L-glutamine, Na pyruvate (Gibco BRL) supplemented with 5 % (v/v) foetal calf serum (Harlen Serolabs). Cells were cultured and passaged according to standard procedures (Booth, Tian et al. 1998).

2.22 Transfection of mammalian cells

During this study cells were transfected using Lipofectamine 2000 (Invitrogen) and the manufacturer's protocol was followed. Cells to be transfected were cultured in a 6 or 12 well tissue culture dish on 12 or 16 mm glass coverslips, which allows the cells to adhere to the coverslip so they can be visualised easily using an upright confocal microscope.

2.22.1 Fixation of transfected cells using 4 % paraformaldehyde

Following transfection the cells were incubated for 48 h before being fixed in 4 % paraformaldehyde. The culture medium was removed and the cells were washed three times with PBS, 50 mM $CaCl_2$ (PBS tablets, Sigma), followed by fixing (4 % (w/v) paraformaldehyde in PBS). The fixative was removed by aspiration and the cells were washed three times in PBS. Following washing the cells were immersed in 50 mM NH_4Cl in PBS for 10 min, to quench autofluorescence. The cells were then washed three times with PBS before being mounted in Mowiol and stored in the fridge until imaged using CLSM.

2.23 Indirect immunofluorescence

Transfection was carried out 48 hours before immunofluorescence. The cells were fixed as above and then incubated for 4 min with PBS containing 0.1 % Triton X-100 to permeabilise

the cell membranes. The cells were washed another three times with PBS followed by washing the cells three times over 5 min with 0.2 % (v/v) fish skin gelatin / PBS. The cells were then incubated with a monoclonal antibody against syntaxin 1a, diluted 500 fold in 0.2 % (v/v) fish skin gelatin / PBS, for 3 hours. After the incubation the cells were washed three times in 0.2 % (v/v) fish skin gelatin / PBS over 5 min followed by three times with PBS over 5 min. The cells were then incubated with rabbit anti-mouse IgG rhodamine-conjugated secondary (Molecular Probes) diluted 1:1000 in PBS/0.2 % (v/v) fish skin gelatin and washed as before with the primary antibody. The cells were then mounted in Mowiol and kept at 4 °C until imaged.

2.24 Imaging fixed cells by confocal laser scanning microscopy

Paraformaldehyde-fixed cells on glass coverslips, mounted in Mowiol, were imaged with a Zeiss LSM Axioscope 510 confocal laser scanning microscope. In AtT20 cells FITC (EGFP) emission was collected through a reflection short pass (RSP) filter 580 nm then through a Band Pass (BP) filter 500-550 and Alexa 546 excitation was with the 546 nm line of a Kr-ion laser, with emission collected through a Long Pass 560 nm filter. In HEK293 cells, ECFP image data were acquired using the 458nm excitation line of an Argon ion laser with filtering through BP 480-520 and EYFP image data were acquired using the 514 nm excitation line of an Argon laser and emission collected through a BP 535-590 filter. Co-localisation image data were sampled at Nyquist rates and deconvoluted using the Huygens II package (Scientific Volume Imaging, The Netherlands) to remove the out-of-focus haze, which is characterised by the microscope's point spread function (PSF). The deconvoluted images were analysed using the Bitplane suite of image analysis software (Bitplane AG, Zürich, Switzerland) on Silicon Graphics Octane 2 workstations. The PSF, optical aberration and thresholding levels were determined in advance using 200 nm diameter fluorescent latex beads (490 nm excitation/517 nm emission; Molecular Probes).

2.25 Fluorescence lifetime imaging

2.25.1 Fluorescence imaging

All fluorescence lifetime imaging experiments were performed and analysed by Dr Rory Duncan using a Zeiss LSM 510 Axiovert confocal laser scanning microscope, equipped with a pulsed excitation source (MIRA 900 Ti:Sapphire femtosecond pulsed laser, with a coupled VERDI 10 W pump laser (Coherent, Ely, UK) (Figure 2.1). The laser was tuned to provide a TPE wavelength of 800 nm, which efficiently excited ECFP, without any detectable excitation/emission from EYFP in the absence of FRET from a donor. Live cells on coverslips (37 mm) were imaged in an incubation chamber (H. Saur, Reutlingen, Germany);

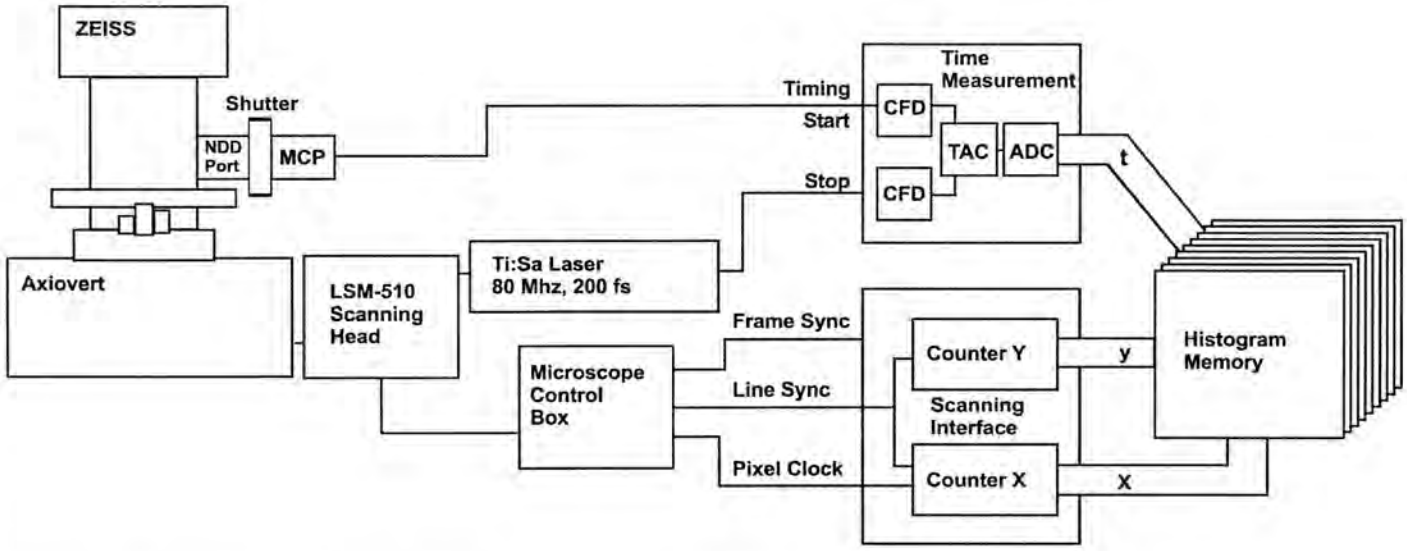

Figure 2.1: Schematic representation of the multi-dimensional TCSPC microscope

The recording circuit consists of a time measurement channel, a scanning interface, and a large histogram memory. The time measurement channel contains the usual TCSPC building blocks. Two constant fraction discriminators, CFD, receive the single photon pulses from the detector and the reference pulses from the laser. The time-to-amplitude converter, TAC, measures the time from the detection of a photon to the next laser pulse. The analogue-to-digital converter, ADC, converts the TAC output voltage into an address for the memory. The scanning interface is a system of counters. When a photon is detected the device determines the time, t, within the fluorescence decay curve and the location of the laser spot within the scanning area, x, y. The result can be interpreted as a stack of images for different times after the excitation pulse or as an array of pixels containing a complete fluorescence decay function each.

fixed cells were mounted using FLUORSAVE (Calbiochem, San Diego, CA). TPE data acquisition was performed using 512 x 512 or 1024 x 1024 pixel image sizes, with 4 x frame averaging, using a Zeiss Plan NeoFLUAR 1.3 NA 40 x oil immersion, or a Zeiss C-Apochromat 1.2 NA 63 x water corrected immersion objective lens. Band pass and long pass (480 – 520 nm for cyan) emission filters were used in conjunction with a Schott (New York, NY) BG39 IR filter to attenuate the TPE light.

2.25.2 TCSPC-FLIM

TCSPC imaging requires that the scan control pulses of the microscope, i.e. the frame clock, line clock, and, if possible the pixel clocks be available. TCSPC measurements were made under 800 nm TPE, using a non-descanned detector (Hamamatsu R3809U-50; Hamamatsu Photonics UK Ltd, Herts, UK) multichannel plate-photomuliplier tube (MCP-PMT), coupled directly to the rear port of the Axiovert microscope and protected from room light and other sources of overload with a Uniblitz shutter (Rochester, NY) (Figure 2.1). This MCP-PMT is a key to measuring very fast fluorescent lifetimes as it achieves a transit time spread (TTS; the limiting factor for TCSPC measurements) of 30 ps, and is free of after-pulses. Dark count rates were $10^2 - 10^3$ photons per second. The MCP-PMT was operated at 3 kV, and signal pulses were pre-amplified using a Becker & Hickl HFAC-26 26 dB, 1.6 GHz preamplifier. TCSPC recording used the "reversed start stop" approach, with accurate laser synchronisation using a Becker & Hickl SPC-730 card together with a PHD-400 reference photodiode, routinely at 79.4 MHz. In contrast to conventional TCSPC devices, the SPC boards use a novel analogue-to-digital (AD) conversion (ADC) technique that cancels the unavoidable errors of an ultra-fast ADC chip. Together with a speed-optimised time-amplitude-converter (TAC), this achieves an overall dead time of only 25 ns per photon. BP and LP filters were used to dissect the components of ECFP emission and also to enable spectral separation of donor and acceptor FRET- and sensitised-emissions. 3-6 mm Schott BG39 filters were positioned directly in front of the MCP-PMT. TCSPC recordings were

acquired routinely for between 5 s and 25 s, mean photon counts were between $10^5 - 10^6$ counts per second. Images were recorded routinely with 128 x 128 pixels from a 512 x 512 scan, with 256 time bins per pixel, or 256 x 256 pixels from a 1024 x 1024 image scan with 64 time bins.

2.25.3 FLIM data analysis and FRET calculations

Off-line FLIM data analysis used pixel-based fitting software (SPCImage, Becker & Hickl), able to import the binary data generated by the FLIM module.

The fluorescence was assumed to follow a multi-exponential decay. In addition an adaptive offset-correction was performed. A constant offset takes into consideration the time-independent baseline due to dark noise of the detector and the background caused by room light, calculated from the average number of photons per channel in front of the rising part of the fluorescence trace. To fit the parameters of the multi-exponential decay to the fluorescence decay trace measured by the system, a convolution with the instrumental response function was carried out. The optimisation of the fit parameters was performed by using the Levenberg-Marquardt algorithm, minimising the weighted chi-squared (χ^2) quantity.

2.25.4 Features of TCSPC imaging technique

2.25.4.1 Time resolution

The time resolution of TCSPC technique is given by the transit time spread in the detector. A system response shorter than 30 ps full width half maximal (fwhm) is achieved with MCP PMTs, which in conjunction with the minimum time channel width in TCSPC modules of 813 fs, allowed lifetimes down to a few picoseconds to be determined (see below).

2.25.4.2 Acquisition time

TCSPC data were acquired at the full scanning rate of the microscope, with scan times of approximately 900 ms at 512 x 512 frame size. The FLIM image was recorded by accumulating over several frames with a lower pixel resolution of 128 x 128 pixels using a non-descanned detector couple to the rear port of the microscope. Non-descanned detection resulted in mean photon counts of ~10^4 – 10^6 per second (Elangovan, Day et al. 2002; van Kuppeveld, Melchers et al. 2002).

Chapter 3

Expression and Purification of syntaxin 1a constructs

3.1 Introduction

Exocytosis is a multistep process that requires a large number of proteins interacting with each other, presumably in a complex series of steps, the details of which are still unclear. One protein that is believed to have a pivotal role in exocytosis is syntaxin. Syntaxin 1a is integral to the plasma membrane of mammalian neuronal and neuroendocrine cells and is known to interact with many proteins that are involved in exocytosis. Although there is still debate about the molecular mechanism of membrane fusion, it is well established that SNARE complex formation is essential in the exocytotic fusion process, and syntaxin 1a has even been proposed to be a component of the fusion pore itself (Han, Wang et al. 2004). The function of syntaxin 1a appears to be regulated by its interaction with various regulatory proteins, including munc18-1 (Jahn 2000). A major aim of the work reported in this thesis was to further understand the role of syntaxin 1a in exocytosis, by investigating its interactions with other exocytotic proteins, such as munc18-1, both *in vitro* and *in vivo*. Recent developments in molecular biological and biochemical techniques have facilitated the investigation of such protein interactions; in particular the addition of protein 'tags', such as oligohistidine, GST and the V5 epitope, allows the identification, purification and experimental manipulation of proteins of interest. Furthermore, the arrival of high resolution imaging systems makes it possible to visualise and investigate the behaviour of proteins, particularly those bearing fluorescent tags, *in vivo*. This technique requires the use of fluorescently coupled antibodies and/or the fusion of fluorescent proteins, for example EGFP, ECFP or EYFP to the C- or the N -terminus of the proteins of interest.

In this chapter I describe the attempted cloning and expression of full-length syntaxin fused to EGFP and carrying a hexahistidine tag, for use in binding experiments with munc-18 *in vitro*; the expression of GST-syntaxin 1a (cytoplasmic domain), the fusion protein that was eventually chosen for the *in vitro* work; and the expression and purification of GST-ECFP-syntaxin 1a (cytoplasmic domain), which was also required for *in vitro* binding studies to complement work with intact cells. EGFP-syntaxin1a and ECFP-syntaxin 1a fusion protein

clones were available, by courtesy of Dr Rory Duncan, but before they could be used in *in vivo* experiments the effect of the addition of such a large protein on syntaxin 1a's behaviour and on its interactions with other exocytotic proteins had to be investigated. This involved the cloning and expression in bacteria of oligohistidine- and GST- fusions syntaxin 1a and EGFP/ECFP-syntaxin 1a followed by their purification for use in binding experiments.

3.2 GST-syntaxin 1a-cytoplasmic domain (cyt) fusion protein expression and purification

A plasmid encoding the cytoplasmic domain of syntaxin 1a fused to GST in a pGEX-KG vector was obtained from Dr R D Burgoyne, University of Liverpool, which was used for *in vitro* binding experiments, for two reasons: first, syntaxin 1a without its transmembrane domain is known to be more soluble, and therefore easier to express and purify, than full-length syntaxin 1a; and second, it was reported (R D Burgoyne, personal communication) that when hexahistine-tagged constructs are used in pull-down experiments, there are often high background levels of non-specifically-bound proteins, giving false positives. GST-syntaxin 1a-(cyt) was transformed into *E.coli* BL21 RIL cells, chosen because they carry extra copies of the genes encoding tRNAs for arginine, isoleucine and leucine. This aids in the production of recombinant proteins, which can be inefficient when the codon use in the recombinant gene differs from the codon use in the host cell. High-level expression of a gene containing codons that are rarely used in *E.coli* ('codon bias') results in depletion of the internal tRNA pools with consequent delay in the translation of the recombinant protein and its eventual degradation. A colony was picked for an overnight 5 ml LB culture with ampicillin (100 μg/ml), 1 ml of which was used to seed 100 ml Supermedia culture, containing ampicillin. This was grown at 37 °C until A_{600} was 0.6-0.8. Protein expression was then induced, using 1 mM IPTG, at 37 °C for 3 hours followed by cell harvesting by centrifugation at 5000 x g for 10 minutes. The bacteria were lysed using Bugbuster followed by centrifugation at 50000 rpm for 15 minutes to separate the soluble and insoluble fractions.

Samples were then prepared for analysis by SDS PAGE and Coomassie staining (Figure 3.1). The gel revealed that the GST-syntaxin 1a-(cyt) was expressed at a high level, but that it was insoluble, probably in inclusion bodies. It has been documented, (Hoess, Arthur et al. 1988), that GST-fusion proteins can be recovered from inclusion bodies in a soluble and biologically active form using ion exchange resins such as Q-Sepharose. GST-syntaxin 1a-(cyt) was induced and the bacteria were processed as before, however the insoluble fraction was kept for attempted solubilisation of the GST-syntaxin 1a-(cyt) using Q-Sepharose (Chapter 2.16.2). Samples were made and analysed by 10 % SDS PAGE and Coomassie staining, (Figure 3.2A). The gel showed that most of the GST-syntaxin 1a-(cyt) was in the insoluble fraction following induction and after incubation with Q-Sepharose the protein was not eluted by any of the washing steps, suggesting it was either still bound to the Q-Sepharose or in inclusion bodies. To determine whether the GST-syntaxin 1a-(cyt) was bound to the Q-Sepharose or in inclusion bodies 200 µl samples of the Q-Sepharose were taken and treated either with SDS, 2 M NaCl, 4 M Urea or 2 M Guanidine thiocyanate for 30 minutes at 4 °C with rolling. The beads were then harvested as before and the supernatants removed and analysed by SDS PAGE and Coomassie staining (Figure 3.2B) The gel revealed that GST-syntaxin 1a-(cyt) remained bound to the Q-Sepharose and that even treatment with high concentrations of salt, urea or guanidine thiocyanate failed to elute it. Since the recovery of the GST-syntaxin 1a-(cyt) from inclusion bodies was unsuccessful different induction conditions were investigated to reduce the amount of GST-syntaxin 1a-(cyt) produced to prevent the formation of inclusion bodies. The induction was repeated at 37 °C as before but only for 1 hour to determine whether the product was more soluble than after a 4 hour induction. It was also repeated at 16 °C overnight, which slows the rate of bacterial growth and hence protein synthesis, inhibiting reformation of inclusion bodies. Both inductions were done using Supermedia and the bacteria were harvested, lysed and centrifuged as before. Samples were made for SDS PAGE analysis and Coomassie staining

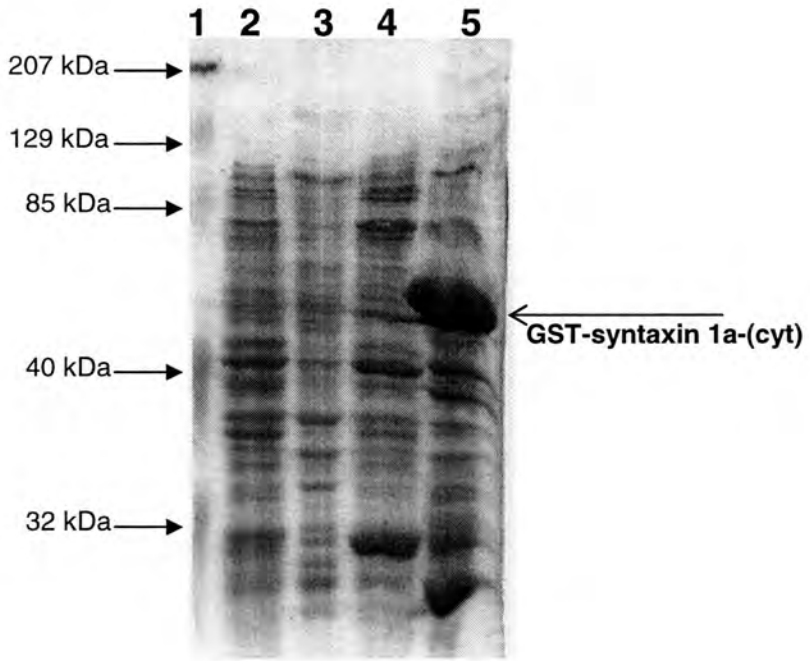

Lane

1: Markers

2: No induction: soluble fraction

3: No induction: pellet fraction

4: Induction: soluble fraction

5: Induction: insoluble fraction

Figure 3.1: GST-syntaxin 1a-(cyt) induction

Coomassie blue-stained gel. GST-syntaxin 1a-(cyt) was induced using 1 mM IPTG in BL21 RIL grown in Supermedia at 37 ^{oC} for 3 hours.

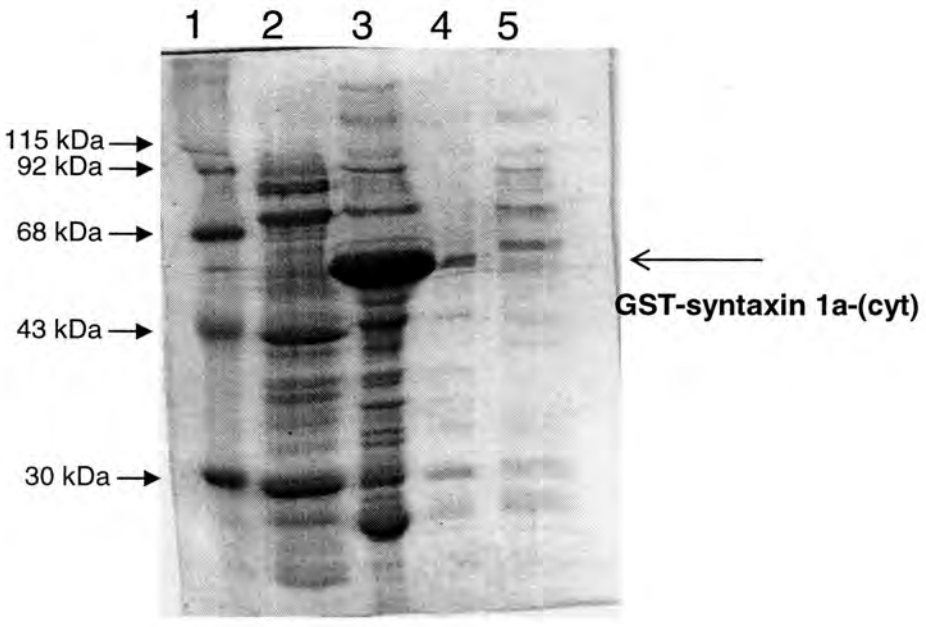

Lane

1: Markers

2: Supernatant fraction

3: Pellet fraction

4: Supernatant after Q-Sepharose treatment of pellet

5: Supernatant after high salt wash of Q-Sepharose

Figure 3.2A: Attempted solubilisation of GST-syntaxin 1a-(cyt) using Q-Sepharose

Coomassie stained gel of the attempted solubilisation of GST-syntaxin 1a-(cyt) revealing that the high salt wash was unsuccessful in eluting the GST-syntaxin 1a-(cyt) from the Q-Sepharose.

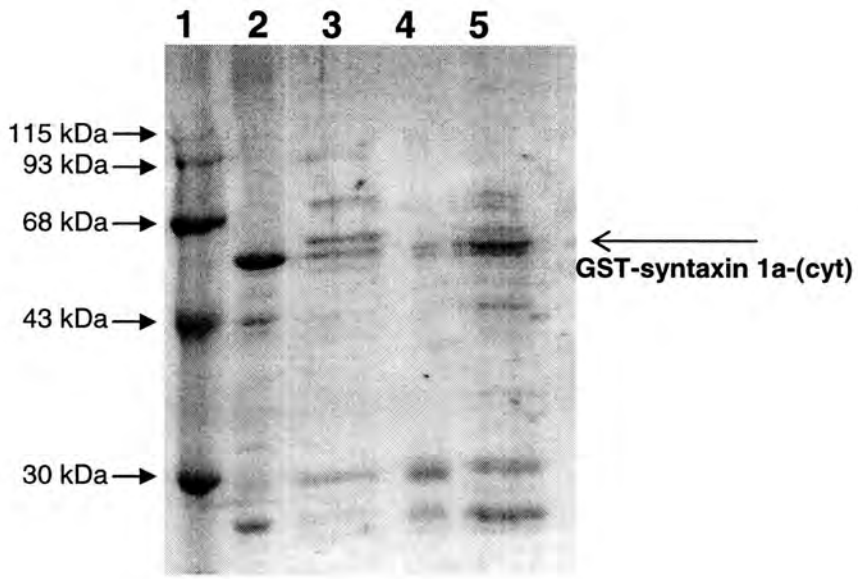

Lane

1: Markers

2: Q-sepharose + SDS

3: Q-sepharose + 2M NaCl

4: Q-sepharose + 4M Urea

5: Q-sepharose + 2M Guanidine thiocyanate

Figure 3.2B: Attempted solubilisation of GST-syntaxin 1a-(cyt) using Q-Sepharose

Coomassie blue-stained gel analysing the various washes used to try and remove the GST-syntaxin 1a-(cyt) from the Q-Sepharose.

(Figure 3.3). The gel revealed that GST-syntaxin 1a-(cyt) was still mainly insoluble under these different induction conditions.

Another method for reducing protein production rates is to reduce the IPTG concentration used for the induction, so the different IPTG concentrations investigated were: 0.1, 0.2, 0.5 mM in inductions at 37 °C for 1, 2, 3 and 4 hours or 16 °C overnight. Following these inductions samples were analysed as before (Figure 3.4 A-D). The gels revealed that the GST-syntaxin 1a-(cyt) was still mainly insoluble when the IPTG concentration and the length of the induction were varied at 37 °C. When these conditions were varied during a 16 °C overnight induction, there was more soluble protein produced with the highest yield at 0.5 mM IPTG, although most of the protein was still insoluble. To slow down the protein production further the induction was repeated using LB instead of Supermedia. An 8 hour time course was carried out at 16 °C to investigate the optimum length of expression required. After induction samples were taken every 2 hours and the bacteria were harvested and samples prepared for SDS PAGE analysis (Figure 3.5 A-B). The gels revealed that using LB media instead of Supermedia did produce more soluble protein and after an overnight expression there were similar amounts of protein in the soluble and insoluble fractions, which was the most soluble protein that had so far been generated. This protocol , using LB and induction with 0.5 mM IPTG at 16 °C overnight, was used continuously throughout the remainder of the study to produce soluble GST-syntaxin 1a-(cyt) for use in binding studies *in vitro*.

Before the GST-syntaxin 1a-(cyt) could be used in future experiments it had to be purified. This was done using Glutathione Sepharose 4B (GSH) (Amersham). A 250 ml LB culture of BL21 (RIL), transformed with GST-syntaxin 1a-(cyt), was induced at 16 °C overnight with 0.5 mM IPTG. The bacteria were harvested and lysed using Bugbuster (Chapter 2.13.2) followed by centrifugation as before. The soluble fraction was then incubated with 500 µl of a 50 % (v/v) suspension of Glutathione Sepharose 4B as previously described (Chapter 2.13.4), and the beads washed: 3 x with PBS, 0.1 % Triton X-100 (15 ml), 5 mM DTT

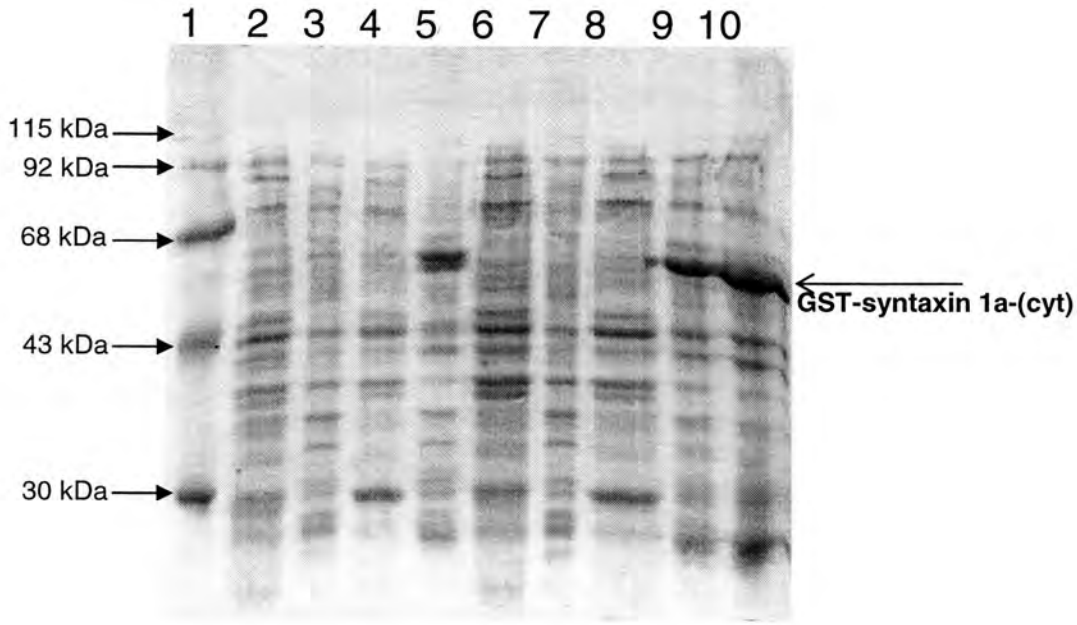

Lane

1: Markers

2: No induction, 16 °C, o/n supernatant

3: No induction, 16 °C, o/n pellet

4: Induction, 16 °C, o/n supernatant

5: Induction, 16 °C, o/n pellet

6: No induction, 37 °C, 1 hr, supernatant

7: No induction, 37 °C, 1 hr pellet

8: Induction, 37 °C, 1 hr, supernatant

9: Induction, 37 °C, 1 hr pellet

10: Induction, 37 °C, 4 hrs pellet

Figure 3.3: Induction of GST-syntaxin 1a-(cyt) expression at 37 °C for 1 hour and 16 °C overnight

Coomassie stained gel analysing the induction of GST-syntaxin 1a-(cyt) at 37 °C for 1 h and 16 °C overnight.

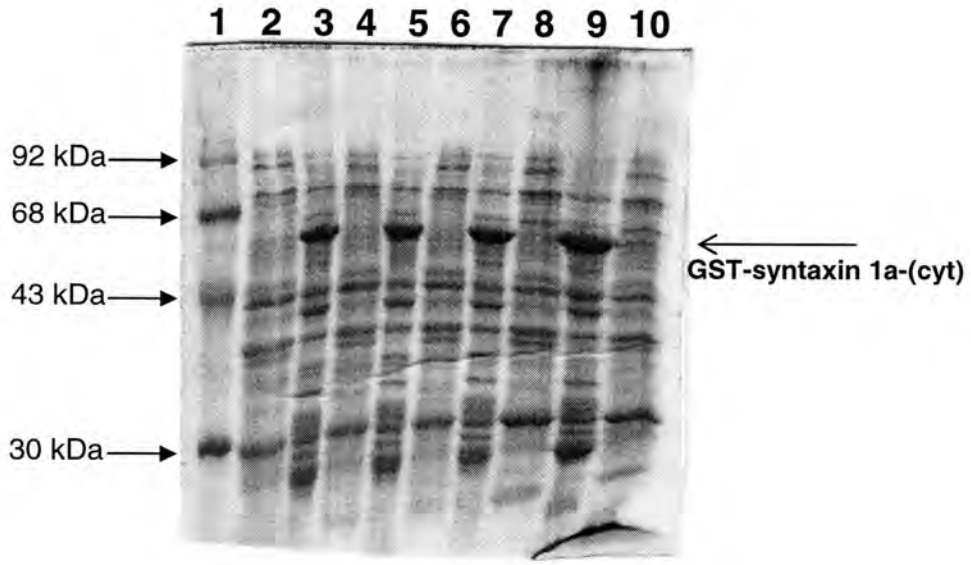

Lane

1: Markers

2: 1 h induction, 0.1 mM IPTG, 37 °C, S

3: 1 h induction, 0.1 mM IPTG, 37 °C, P

4: 1 h induction, 0.2 mM IPTG, 37 °C, S

5: 1 h induction, 0.2 mM IPTG, 37°C, P

6: 1 h induction, 0.5 mM IPTG, 37 °C, S

7: 1 h induction, 0.5 mM IPTG, 37 °C, P

8: 2 h induction, 0.1 mM IPTG, 37 °C, S

9: 2 h induction, 0.1 mM IPTG, 37 °C, P

10: 2 h induction, 0.2 mM IPTG, 37 °C, S

Figure 3.4 A: Induction of GST-syntaxin 1a-(cyt) expression with varying time, IPTG concentration at 37 °C.

A Coomassie stained gel for GST-syntaxin 1a-(cyt) induction using different IPTG concentrations; 0.1, 0.2 or 0.5 mM, for different time periods, 1 or 2 hours at 37 °C.

S = Supernatant fraction, P = Pellet fraction

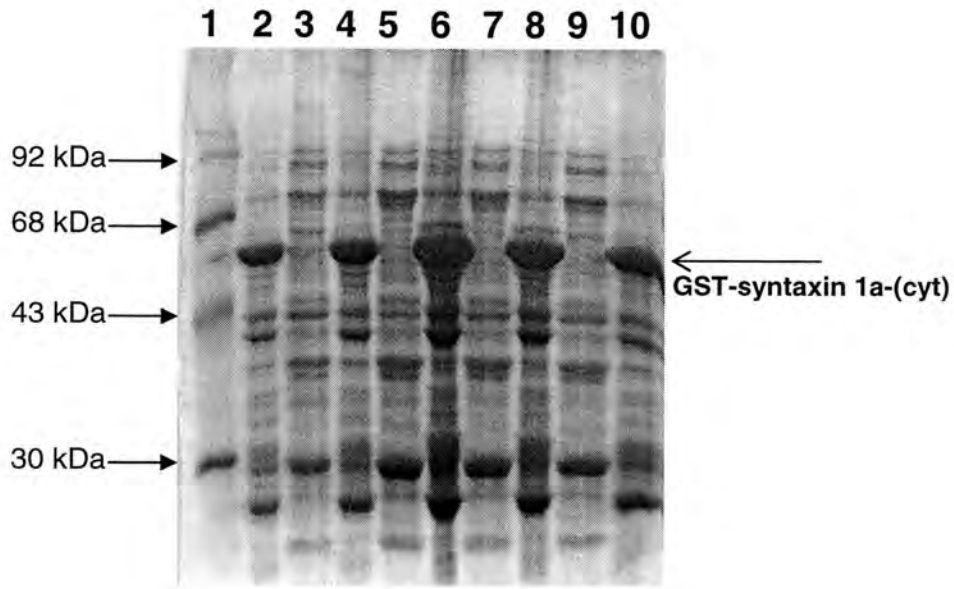

Lane

1: Markers

2: 2 h induction, 0.2 mM IPTG, 37 °C, P

3: 2 h induction, 0.5 mM IPTG, 37°C, S

4: 2 h induction, 0.5 mM IPTG, 37 °C, P

5: 3 h induction, 0.1 mM IPTG, 37 °C, S

6: 3 h induction, 0.1 mM IPTG, 37 °C, P

7: 3 h induction, 0.2 mM IPTG, 37 °C, S

8: 3 h induction, 0.2 mM IPTG, 37 °C, P

9: 3 h induction, 0.5 mM IPTG, 37 °C, S

10: 3 h induction, 0.5 mM IPTG, 37 °C, P

Figure 3.4 B: Induction of GST-syntaxin 1a-(cyt) expression with varying time, IPTG concentration at 37 °C.

A Coomassie stained gel for GST-syntaxin 1a-(cyt) induction using different IPTG concentrations; 0.1, 0.2 or 0.5 mM, for different time periods, 2 or 3 hours at 37 °C.

S = Supernatant fraction, P = Pellet fraction

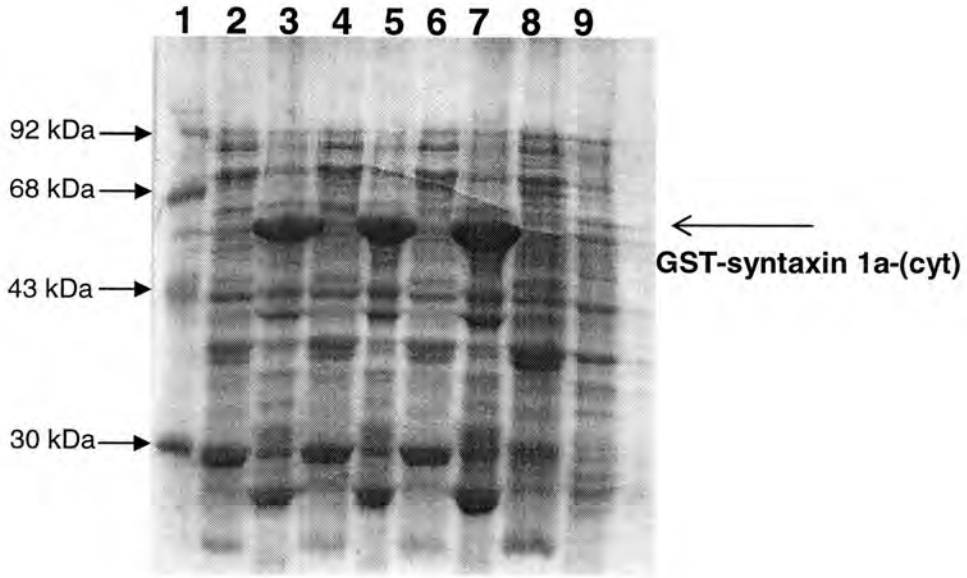

Lane

1: Markers

2: 4 h induction, 0.1 mM IPTG, 37°C, S

3: 4 h induction,0.1 mM IPTG, 37 °C, P

4: 4 h induction, 0.2 mM IPTG, 37 °C, S

5: 4 h induction, 0.2 mM IPTG, 37 °C, P

6: 4 h induction, 0.5 mM IPTG, 37 °C,S

7: 4 h induction, 0.5 mM IPTG, 37 °C, P

8: 4 h no induction, 37 °C, S

9: 4 h no induction, 37°C, P

Figure 3.4C: Induction of GST-syntaxin 1a-(cyt) expression with varying IPTG concentration for 4 hours at 37 °C.

Coomassie stained gel of GST-syntaxin 1a-(cyt) inductions at 37 °C for 4 h with different IPTG concentrations: 0.1, 0.2 or 0.5 mM.

S = Supernatant fraction, P = Pellet fraction

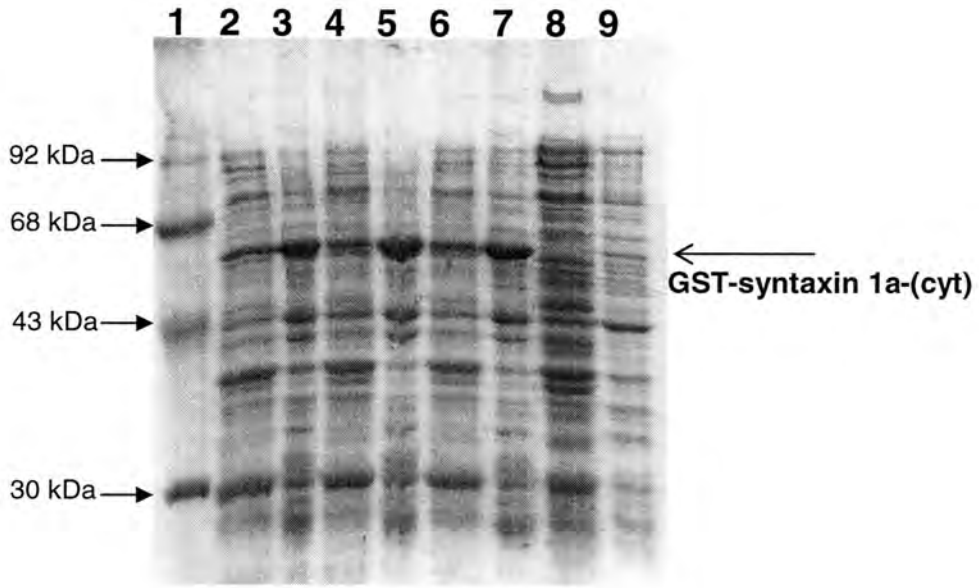

Lane

1: Markers

2: Overnight induction, 0.1 mM IPTG, 16 °C, S

3: Overnight induction, 0.1 mM IPTG, 16 °C, P

4: Overnight induction, 0.2 mM IPTG, 16 °C, S

5: Overnight induction, 0.2 mM IPTG, 16 °C, P

6: Overnight induction, 0.5 mM IPTG, 16 °C, S

7: Overnight induction, 0.5 mM IPTG, 16°C, P

8: Overnight no induction, 16 °C, S

9: Overnight no induction, 16°C,P

Figure 3.4D: Induction of GST-syntaxin 1a-(cyt) expression with varying IPTG concentration overnight at 16 °C.

Coomassie stained gel analysing the results of GST-syntaxin 1a-(cyt) inductions performed at 16° overnight.

S = Supernatant fraction, P = Pellet fraction

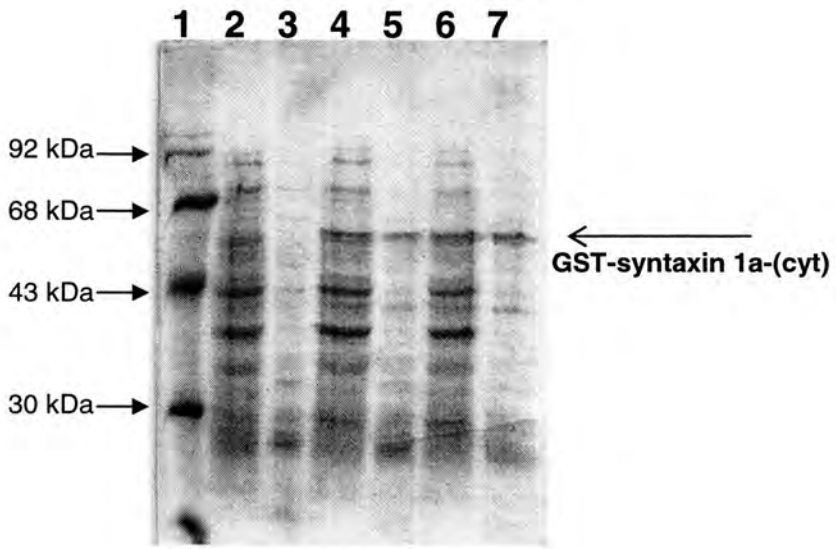

Lane

1: Markers

2: No induction, 16 °C S

3: No induction, 16 °C P

4: 2hr induction, 16 °C S

5: 2hr induction, 16 °C P

6: 4hr induction, 16 °C S

7: 4hr induction, 16 °C P

Figure 3.5A: Induction of GST-syntaxin 1a-(cyt) expression using LB medium at 16° time course.

Coomassie stained gel analysing GST-syntaxin 1a-(cyt) time course induction using 0.5 mM IPTG at 16 °C.

S = Supernatant fraction, P = Pellet fraction

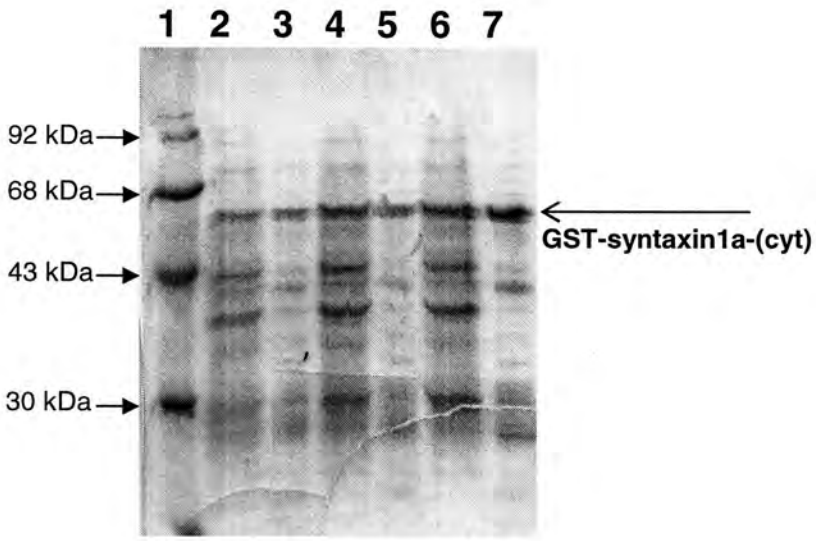

Lane

1: Markers

2: 6 hr induction, 16 °C, S

3: 6 hr induction, 16 °C, P

4: 8 hr induction, 16 °C, S

5: 8 hr induction, 16 °C, P

6: Overnight induction, 16 °C, S

7: Overnight induction, 16 °C, P

Figure 3.5B: Time course of induction of GST-syntaxin1a-(cyt) expression using LB medium at 16 °C.

Coomassie blue-stained gel of an induction time course of GST-syntaxin 1a-(cyt) analysing the results from the time points 6 and 8 hours and overnight.

S = Supernatant fraction, P = Pellet fraction

followed by 2 washes in PBS (15 ml). The products were analysed by SDS PAGE and Coomassie staining (Figure 3.6). The results showed that the purification worked well and that GST-syntaxin 1a-(cyt) accounted for about 95 % of the gel-bound protein. Accordingly, GST-syntaxin 1a-(cyt) was not eluted from the Glutathione Sepharose 4B, but stored as protein-loaded beads in PBS with 0.1 % azide at 4 °C, ready for use in future binding experiments, although it was possible to elute the GST-syntaxin 1a-(cyt) using glutathione. Following purification of GST-syntaxin 1a-(cyt), the protein concentration was determined using a modification of the Folin-Lowry method, (Chapter 2.15.2). First a standard curve was obtained using BSA standards. 3 different volumes of the protein loaded GSH beads were used; 10, 15 and 20 µl, all done in triplicate and A_{750} was measured. The standard curve was used to calculate the concentration of GST-syntaxin 1a-(cyt), which was typically about 0.5 mg/ml suspension.

3.3 Production of GST-ECFP-syntaxin1a-(cyt)

To compare the munc18-1-binding affinity of ECFP-syntaxin 1a, used in the cell imaging experiments, with that of native syntaxin 1a, the production of a GST ECFP-syntaxin 1a cytoplasmic domain fusion protein was required. The cytoplasmic domain only of syntaxin 1a was used because, as described above, it had already been decided to use GST-syntaxin 1a-(cyt) in binding experiments *in vitro*. To produce the fusion protein ECFP-syntaxin 1a-(cyt) had to be cloned in to a vector allowing the addition of GST so pGEX-5X-1 was chosen, which would attach GST to the N-terminus of the protein, the same arrangement as in GST-syntaxin 1a-(cyt). First ECFP-syntaxin 1a-(cyt) had to be generated with suitable restriction enzyme sites added to the 5' and 3'of the coding sequence. These had to be sites that occurred in the multiple cloning site of the pGEX-5X-1, allowing the insertion of ECFP-syntaxin 1a-(cyt) into the pGEX-5X-1 vector in frame using directional cloning. This was done using PCR with suitable primers.

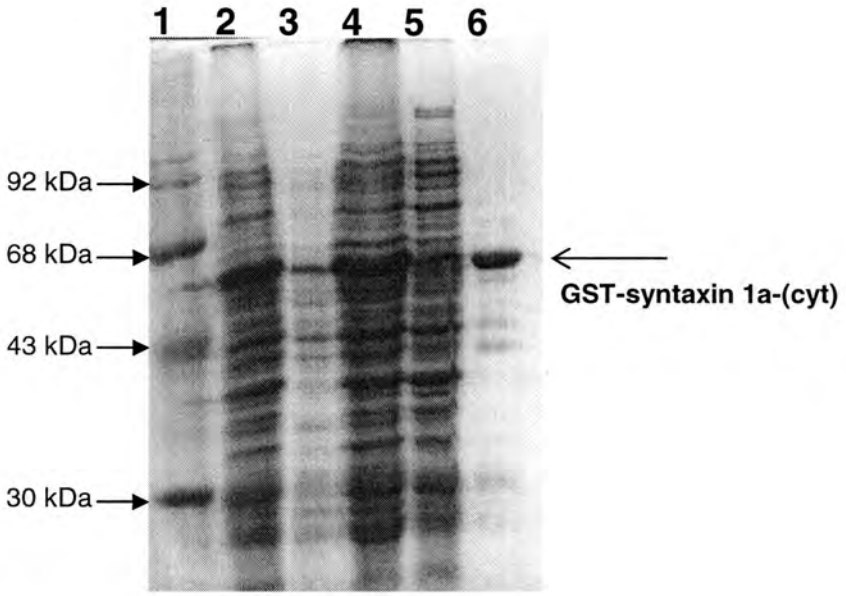

Lane

1: Markers

2: Bacterial Lysate

3: Supernatant fraction

4: Pellet fraction

5: Flow through

6: GSH-GST-syntaxin 1a-(cyt)

Figure 3.6 GST-syntaxin 1a-(cyt) expression and purification

Coomassie blue-stained gel analysing the purification of GST-syntaxin 1a-(cyt) using Glutathione Sepharose 4B.

3.3.1 PCR for production of ECFP-syntaxin 1a-(cyt) flanked by the restriction sites for Sal1 and Not1

To generate ECFP-syntaxin 1a-(cyt) PCR was performed using full length ECFP-syntaxin 1a, (supplied by Dr Rory Duncan) as the template, using a forward ECFP primer with a Sal1 site and a reverse syntaxin 1a primer which annealed to syntaxin 1a at the end of its cytoplasmic domain, at 71 bp from the C-terminus and just ahead of the transmembrane domain. This contained a Not1 site. Initially the ECFP-syntaxin 1a was cloned into pCR2.1 (Invitrogen), so it would be easy to determine whether digestion by Sal1 and Not1 was complete. This required the addition of 3' A-overhangs so the Expand High Fidelity PCR System™ (Roche) was used and the PCR reaction mix was assembled (Chapter 2.3.1). The reaction mixes were then heated to 95 °C for 1 min to separate the DNA double helix before 0.75 µl of Taq/Rho was added followed by 25 cycles of 95 °C, 30 secs, 60 °C, 30 secs, 72 °C, 70 secs. The PCR was completed by incubation at 72 °C for 7 mins and the products were then left at 4 °C until needed. A parallel negative control was also done in the same way omitting the template DNA. 5 µl of each PCR reaction was analysed by a 1 % (w/v) agarose gel alongside a 1 kb DNA ladder, which was also used to estimate the concentration of the amplified product. The gel revealed a product of ~1500 bp as expected and there was no product in the negative control lane. The PCR products were then cloned into pCR2.1 (Invitrogen).

3.3.2 Cloning of ECFP-syntaxin 1a-(cyt) PCR product into pCR2.1

The amplified product of the PCR reaction was ligated into the pCR2.1 vector (Invitrogen) using the estimated concentration and the equation below to calculate the required volume as stated in the Manufacture's instruction,where a 50 times molar ratio of PCR product to vector was used.

The ligation reaction mix was set up containing the appropriate volume of amplified PCR product, 1 µl 10 X ligation buffer, 1 µl T4 DNA ligase (Invitrogen) and 2 µl pCR2.1 then

made up to a final volume of 10 µl with dH_2O before being incubated overnight at 16 °C. 5 µl of each ligation reaction mix was used to transform TOP10 *E.coli* cells (Chapter 2.8) and 200 µl was spread on to an LB-agar plate containing ampicillin then incubated overnight at 37 °C. Positive clones were detected using PCR to screen colonies (Chapter 2.3.3). The master mix was mixed thoroughly and 49 µl aliquots were then pipetted into 12 PCR tubes on ice. 10 colonies were picked and each one was dipped into a different PCR tube before being spotted onto a LB-agar plate containing ampicillin (100 µg/ml). A positive control, containing 1 µl ECFP-syntaxin 1a (10 ng/µl) and a negative control with no DNA were set up in the remaining two tubes. The heating block of the PCR machine was brought to 95 °C before the tubes were place inside and incubated for 1 min to lyse the bacteria and separate the DNA strands followed by 25 cycles of 95 °C, 30 secs, 60 °C, 30 secs, 72 °C, 70csecs. The reaction was completed with incubation at 72 °C for 7 mins then the products were stored at 4 °C until analysed. The LB-agar plate with the spotted on bacteria was incubated at 37 °C. 5 µl of each of the PCR products was analysed by 1 % (w/v) agarose gel electrophoresis alongside a 1 kb DNA ladder revealing that several of the lanes were from positive clones, having a PCR product of ~1500 bp as expected for ECFP-syntaxin 1a-(cyt). A positive colony was chosen and used to seed a 100 ml LB-ampicillin culture, which was incubated overnight at 37 °C for "maxiprep". The "maxiprep" (Qiagen) was done according to the manufacturer's instructions. The ECFP-syntaxin 1a-(cyt) was then restriction digested from the pCR2.1 vector using the restriction endonucleases Sal1 and Not1, so that it could be sub-cloned into the pGEX-5X-1 vector, which was also cut with the same enzymes. 3 µg each of pCR2.1-ECFP-syntaxin 1a-(cyt) and pGEX-5X-1 were incubated with 10 units Sal1 and 10 units Not1 at 37 °C for 2 h before being analysed by 1 % (w/v) agarose gel electrophoresis, which revealed that the restriction digestions had been successful. The bands corresponding to ECFP-syntaxin 1a-(cyt) and pGEX-5X-1 were excised and the DNA was purified using a gel extraction kit (Eppendorf) and its concentration was estimated

(Chapter 2.6). Following purification the ECFP-syntaxin 1a-(cyt) was the cloned into the pGEX-5X-1 vector.

3.3.3 Cloning of ECFP-syntaxin 1a-(cyt) into pGEX-5X-1

Once the concentration of the restriction digested ECFP-syntaxin 1a-(cyt) and pGEX-5X-1 DNA had been estimated, ligation reactions were set up with vector:insert ratios of 1:1, 3:1 and 1:3, produced by adding the appropriate volume of both insert and vector DNA (Chapter 2.6). The ligation reaction mixes were incubated overnight at 4 °C. 5 µl of each ligation reaction mix was used to transform competent *E.coli* TOP10 cells (Chapter 2.8) and then 200 µl of each transformation was plated on a LB-agar plate containing ampicillin followed by incubation at 37 °C overnight. Colonies were then picked and used to seed 5 ml LB-ampicillin (100 µg/ml) cultures for "minipreps" (Chapter 2.9.1), which were incubated overnight at 37 °C. The purified plasmid DNA from the "minipreps" was then restriction digested to check for positive clones, with the ECFP-syntaxin 1a-(cyt) inserted into the pGEX-5X-1 vector in the correct orientation. 10µl of each "miniprep" was digested with 10 units of BamH1 for 2 h at 37 °C before being analysed by 1 % (w/v) agarose gel electrophoresis alongside a 1 kb DNA ladder. The gel revealed several positive clones where a DNA fragment ~1100 bp in size had been excised, as expected. One of the positive clones was chosen and the remainder of the "miniprep" culture was used to seed a 100 ml LB-ampicillin culture (1:100 dilution), which was grown overnight at 37 °C for "maxiprep" (Qiagen), done according to the manufacturer's instructions.

3.3.4 Sequencing of ECFP-syntaxin 1a-(cyt) in pGEX-5X-1

The production of this construct involved the use of PCR so it was important to sequence the insert to confirm that no mutations had been introduced during that process, and that the insert was correctly oriented in the vector. Primers were designed that would cover the

GST:ECFP, ECFP:syntaxin 1a-(cyt) and syntaxin 1a:Vector junctions. Samples of DNA were prepared (Chapter 2.11) and sequenced by MWG Biotech revealing that ECFP-syntaxin 1a had been accurately amplified and correctly inserted into the pGEX-5X-1 vector, in frame with GST. The protein could then be expressed in bacteria.

3.3.5 Expression of GST-ECFP-syntaxin 1a-(cyt) in *E.coli* BL21 RIL and purification using Glutathione Sepharose 4B

Since the conditions for expressing GST-syntaxin 1a-(cyt) had already been optimised (Chapter 3.3) these conditions were used for the expression and purification of GST-ECFP-syntaxin 1a-(cyt). It was transformed into *E.coli* BL21 RIL cells grown in LB-ampicillin (100 μg/ml) and induced at 16 °C overnight using 0.5 mM IPTG. The cells were harvested and lysed using Bugbuster (Amersham) before being separated into soluble and insoluble fractions using ultracentrifugation. The soluble fraction was incubated with 300 μl slurry of Glutathione Sepharose 4B for 2 h before being washed five times (Chapter 2.14.4). Finally 0.1 % NaN_3 was added and the Glutathione Sepharose 4B coupled with GST-ECFP-syntaxin 1a-(cyt) was stored at 4 °C. SDS PAGE followed by Coomassie staining (Figure 3.7) revealed that the expression and purification protocol developed for GST-syntaxin 1a-(cyt) also worked well for GST-ECFP-syntaxin 1a-(cyt). The GST-ECFP-syntaxin 1a-(cyt) was not eluted from the Glutathione Sepharose 4B but was used directly in binding experiments (Chapter 5).

Following purification, the concentration of the GST-ECFP-syntaxin 1a-(cyt) coupled Glutathione Sepharose 4B was determined using the modified Folin-Lowry method (Chapter 2.15.2). A standard curve was plotted using BSA standards first, which was then used to determine the concentration of GST-ECFP-syntaxin 1a-(cyt). 3 different volumes; 10, 15 and 20 μl, of the protein-coupled Sepharose, each in triplicate, were used. The concentration of GST-ECFP-syntaxin 1a-(cyt) was typically 1 mg/ml of suspension.

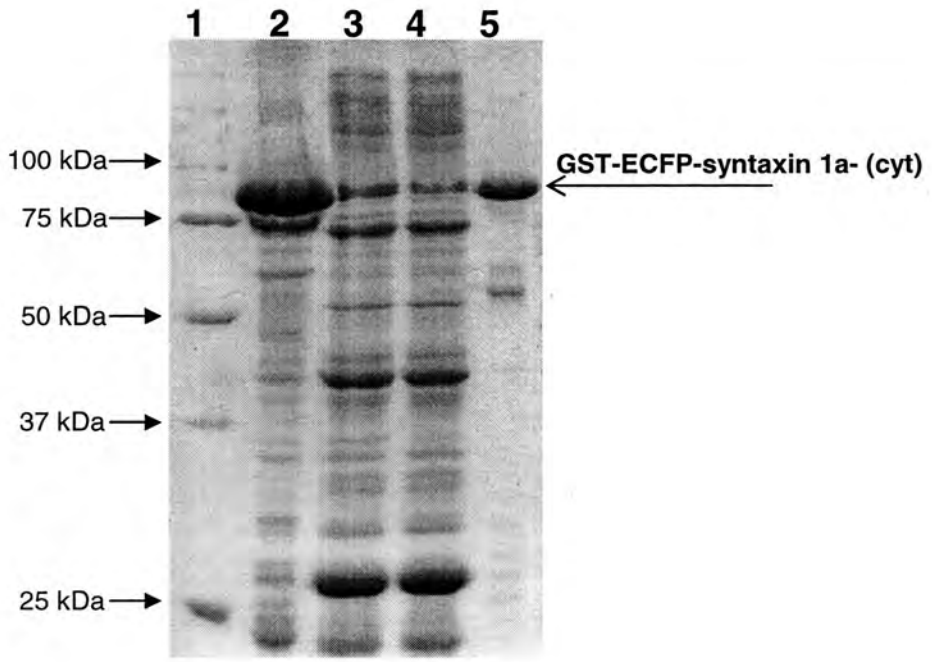

Lane

1: Markers

2: Pellet fraction

3: Supernatant fraction

4: Flow through

5: GSH-GST-ECFP-syntaxin 1a- (cyt)

Figure 3.7: GST-ECFP-syntaxin 1a-(cyt) expression and purification

Coomassie blue-stained gel analysing the purification of GST-syntaxin 1a-(cyt) using Glutathione Sepharose 4B.

3.4 Summary

A protocol is described for the production and expression of constructs encoding GST-syntaxin 1a-(cyt) and GST-ECFP-syntaxin 1a-(cyt), for use in pull-down experiments to measure the binding of munc18-1. These *in vitro* binding controls are an essential complement to the use of ECFP-syntaxin 1a in cellular imaging.

Chapter 4

Cloning, Expression and Purification of munc18-1 constructs

4.1 Introduction

Regulated exocytosis requires the interaction of a large number of proteins, some of which are directly responsible for membrane fusion while others have regulatory roles. One protein known to have a key role in exocytosis is syntaxin 1a (Chapter 3). A major aim of this thesis was to investigate more fully the way in which syntaxin 1a participates in exocytosis, and in particular how it is regulated by its interaction with other proteins, such as munc18-1. Munc18-1 is essential for exocytosis in yeast, *C.elegans*, *Drosophila* and mouse. Munc18-1 has a very high affinity for syntaxin 1a and has been reported to have both positive and negative effects on exocytosis (Brenner 1974; Novick and Schekman 1979; Hata, Slaughter et al. 1993; Schulze, Littleton et al. 1994; Halachmi and Lev 1996; Jahn 2000; Verhage, Maia et al. 2000; Rowe, Calegari et al. 2001) presumably through its interaction with syntaxin 1a, although interactions with other proteins cannot be excluded. Munc18-1 binding maintains syntaxin 1a in its 'closed' conformation, preventing it from interacting with the other SNARE proteins and hence blocking membrane fusion (Margittai, Fasshauer et al. 2003). In order for exocytosis to occur the interaction between munc18-1 and syntaxin 1a must change, so that syntaxin1a can adopt its open conformation and bind the other SNARE proteins, but the process by which this occurs remains unclear. The work reported in this thesis made use of confocal microscopic imaging techniques to study the interaction between munc18-1 and syntaxin 1a in secretory cells in the presence and absence of various stimuli, using fluorescent fusion proteins, (i.e. EGFP, EYFP and ECFP) based on munc18-1 itself and a munc18-1 mutant form, munc18-1_{R39C}, which has a lower affinity for syntaxin 1a (Fisher, Pevsner et al. 2001).

In vitro studies of protein interactions have been facilitated by recent advances in biochemical and molecular biological techniques, which enable the bacterial production and affinity purification of proteins with oligohistidine tags and the cell free production of radiolabelled proteins.

This chapter describes the attempted production and purification of a hexahistidine tagged munc18-1 for bacterial expression for use in *in vitro* competitive binding experiments. EGFP-munc18-1 and EGFP-munc18-1_{R39C} fusion protein clones were made available by Dr Rory Duncan. These were cloned into a vector suitable for the expression of the proteins *in vitro* and then modified so as to produce EYFP-munc18-1 and EYFP-munc18-1_{R39C}. Before the interactions between these fusion proteins and ECFP-syntaxin 1a could be studied *in vivo*, binding studies had to first be carried out *in vitro* to determine whether the addition of the fluorescent tags had any significant effect on their interaction. This required the cloning and bacterial expression of munc18-1-V5-His_6, which was used as a competitor in the binding of [^{35}S]-labelled munc18-1, munc18-1_{R39C}, EGFP-munc18-1 and EGFP-munc18-1_{R39C} to GST-syntaxin 1a constructs.

4.2 PCR amplification of munc18-1, EGFP-munc18-1, munc18-1_{R39C} and EGFP-munc18-1_{R39C} for cloning into pET101/D-TOPO

Genes for EGFP-munc18-1 and EGFP-munc18-1_{R39C} were cloned into a vector that was suitable for bacterial and *in vitro* expression. The pET101/D-TOPO vector was chosen because it contained a T7 promoter and could be used to add on the V5 and His_6 tags. Forward and reverse primers were designed (Figure 4.1), and since 3' A-overhangs were not needed Pfu polymerase (Promega) was used instead. The PCR reaction mix components were assembled (Chapter 2.3.2), then incubated at 95 °C for 1 minute to separate the DNA template strands, then 1 µl Pfu was added followed by two cycles of 95 °C, 30 seconds; 55 °C, 30 seconds; 72 °C, 2 minutes (munc18-1 and munc18-1_{R39C}) or 72 °C, 5 minutes (EGFP-munc18-1 and munc18-1_{R39C}). 25 cycles of 95 °C, 30 seconds; 60 °C, 30 seconds; 72 °C 2 minutes or 5 minutes were then used as above. The PCR reactions were then finished by incubation at 72 °C for 7 minutes then stored at 4 °C until analysed. A parallel negative control reaction was also set up in which only the DNA template was omitted. 5 µl of each

Directional EGFP forward Primer Nhe1

5'- CAC CGT CAG ATC C**GC TAG C**GC TAC CGG TCG CCA CCA TGG T-3'

Directional munc18-1 Forward Primer Xba1

5'-CAC C**TC TAG A**AT GGC CCC CAT TGG CCT CAA GGC GGC GGT GGT

EGFP-munc18-1 Reverse Stop Xba1

5'-**TCT AGA** TTA ACT GCT TAT TTC TTC GTC TGT TTT ATT-3'

EGFP-munc18-1 Reverse No Stop

5'-ACT GCT TAT TTC ATC TGT TTT ATT CAG-3'

Figure 4.1: Sequences of forward and reverse primers for EGFP-munc18-1, EGFP-munc18-1$_{R39C}$, munc18-1 and munc18-1$_{R39C}$

Forward primers that incorporated a 4 bp overhang (shown in red) were required for cloning into the pET101/D-TOPO vector. Reverse primers were designed with and without a stop codon .

PCR product was electrophoresed on a 1 % (w/v) agarose gel along side a 1kb DNA ladder (Figure 4.2). There were no bands present in the negative control lane, but in the munc18-1 and munc18-1_{R39C} lanes there was a band of approximately 2 kb, close to the expected size of 1.8 kb) and a band of approximately 2.5 kb in the EGFP-munc18-1 and EGFP-munc18-1_{R39C} lanes. 2 µl of each PCR mix was used for cloning into pET101/D-TOPO (Invitrogen) according to the manufacturer's instructions. These reaction mixes were then used to transform E.coli TOP10 competent cells (Invitrogen) following the manufacturer's manual. 150 µl of each transformation reaction was plated out on an ampicillin (100 µg/ml)-agar plate before being incubated overnight at 37 °C. Colonies were picked and grown at 37 °C overnight in 5 ml LB-ampicillin media. "Minipreps" (Chapter 2.9.1) were then performed to purify the plasmid DNA. Restriction digestion analysis was used to identify positive clones where 10 µl of each "miniprep was incubated with 10 units Age I for 2 hours at 37 °C for EGFP-munc18-1 and EGFP-munc18-1_{R39C} and 10 units EcoR1 and10 units BamH1 for munc18-1 and munc18-1_{R39C} constructs. 10 % of each digestion product was analysed using a 1 % (w/v) agarose gel (Figure 4.3). The gel illustrates an example of positive clones for EGFP-munc18-1 and EGFP-munc18-1-V5-His_6, with digests giving an insert band of approximately 2.5 kb. The remainder of the 5 ml cultures of positive clones were used (1:100 dilution) to seed a 100 ml LB-ampicillin (100 µg/ml) overnight culture for "maxiprep" (Qiagen) performed according to the manufacturer's instructions.

4.2.1 Sequencing of constructs encoding munc18-1, munc18-1-V5-His_6, munc18-1_{R39C}, munc18-1_{R39C}-V5-His_6, EGFP-munc18-1, EGFP-munc18-1-V5-His_6, EGFP-munc18-1_{R39C} and EGFP-munc18-1_{R39C}-V5-His_6

Since PCR was used during the cloning of these constructs their sequences had to be checked to ensure that no mutations that would alter the amino acid sequence of the proteins had been introduced. These proteins are rather large so it took several sequencing reactions to

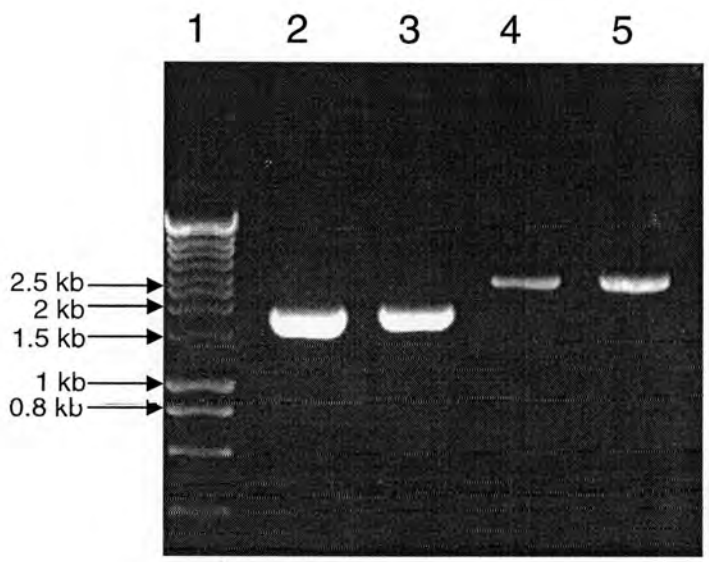

Lane

1: Markers

2: munc18-1 Stop

3: munc18-1_{R39C} Stop

4: EGFP-munc18-1 Stop

5: EGFP-munc18-1_{R39C} Stop

Figure 4.2: PCR of EGFP-munc18-1, EGFP-munc18-1_{R39C}, munc18-1 and munc18-1_{R39C}

5 µl of each PCR reaction mix was analysed by 1 % agarose gel electrophoresis. The stop constructs all contain the proteins stop codon so no tags are added to the end.

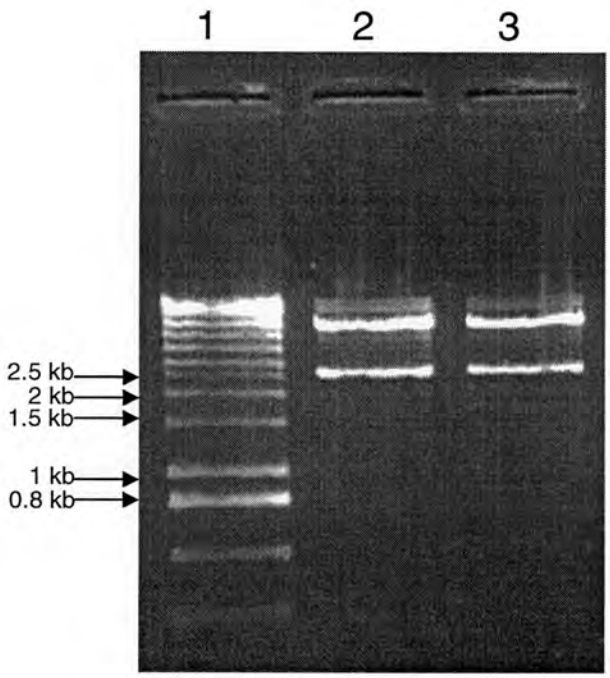

Lane

1: Markers

2: EGFP-munc18-1-V5-His

3: EGFP-munc18-1_{R39C}-V5-His

Figure 4.3: Restriction digestion of EGFP-munc18-1-V5-His and EGFP-munc18-1_{R39C}-V5-His with AgeI

10 µl of each restriction digest was analysed by electrophoresis on a 1 % agarose gel. Positive clones gave inserts of approximately 2.5 kb. Arrows show approximate sizes in kb.

sequence the proteins fully on both strands as each sequencing reaction generates a run of approximately 700 bp, therefore the sequencing was done in stages. First primers were designed to cover the vector/insert junctions and the EGFP/ munc18-1 or munc18-1_{R39C} junction (Appendix 2). The sequencing results were then aligned against the coding sequences of Rat munc18-1 and EGFP. The sequencing of all of the constructs revealed that the junctions in munc18-1-V5-His_6, EGFP-munc18-1-V5-His_6, munc18-1_{R39C}-V5-His_6 and EGFP-munc18-1_{R39C}-V5-His_6 were correct, but that in all the stop variants (i.e. those in which there was no C-terminal tag) the junction between munc18-1 and the vector was altered. In these clones the stop codon had been mutated and there was an insertion of 13 base pairs. The first explanation for this was there may have been a mistake in the reverse primer containing the stop codon so a new primer was ordered and the cloning repeated. On completion the sequencing over the junctions was repeated as before, but the same alteration had occurred. The cloning and the sequencing were then repeated, but again the stop codon was mutated and several base pairs inserted between the munc18-1 and vector junction. The reason for the mutations and the insertion of random base pairs could have been due to the way that the TOPO cloning worked (Chapter 2.4)

During this period the tagged clones were further sequenced by designing primers to overlap the sequence already obtained (Appendix 2.1), until the full sequence of each clone was generated. This revealed that the munc18-1_{R39C}-V5-His_6 and the EGFP-munc18-1_{R39C}-V5-His_6 clones were of the correct sequence, whereas the munc18-1-V5-His_6 and the EGFP-munc18-1-V5-His_6 clones had several point mutations throughout their sequences, presumably introduced during the PCR reaction.

Because of the problems encountered during the initial cloning it was decided to generate the wild-type sequences by back-mutation of the munc18-1_{R39C} constructs, using site-directed mutagenesis.

4.2.2 Site-directed mutagenesis of munc18-1_{R39C}-V5-His_6 and EGFP-munc18-1_{R39C}-V5-His_6.

Site-directed mutagenesis was performed using the Stratagene Quick Change kit (Chapter 2.3.2). Primers were designed (Figure 4.4), complementary to each other and with 15 base pairs on either side of the point mutation. The PCR reaction mixture was assembled (Chapter 2.3.5) then incubated at 95 °C for 1 min, followed by the addition of 1 µl Turbo Pfu (Stratagene), then 18 cycles of 95 °C, 50 seconds; 60 °C, 50 seconds; 68 °C, 8 minutes and 15 seconds. The PCR reaction was completed by 68 °C, 7 minutes then stored at 4 °C until the reaction was analysed by electrophoresis of 5 µl in a 1 % (w/v) agarose gel along side a 1 kb DNA ladder (Figure 4.5), which revealed multiple bands in each lane that could be attributed to the the template DNA or varying amounts of supercoiling of the PCR products. Although multiple bands were seen it was decided to carry on with the protocol. 10 units of the methyl-specific restriction enzyme, Dpn1, was added to each PCR mix to digest the template DNA for 1 h at 37 °C. 2 µl of each digested PCR mix was used to transform *E.coli* XL-10 Gold competent cells according to the manufacturer's instructions (Stratagene), which were then plated on to LB-agar plates containing ampicillin (100 µg/ml) and incubated at 37 °C overnight. Colonies were picked for "minipreps" (Chapter 2.9.1), which were analysed by digestion (total vol of 20 µl) with 10 units Age1, 2 h at 37 °C for EGFP-munc18-1-V5-His_6 "minipreps" or 10 units of both EcoRI and BamHI for 2 h at 37 °C for munc18-1-V5-His_6 'minipreps'. Positive clones were chosen and the remainder of the 5 ml cultures were used to seed 100 ml LB-ampicillin (100 µg/ml) cultures (1:100 dilution) for "maxiprep" (Qiagen) following the manufacturer's instructions. The positive clones of munc18-1-V5-His_6 and EGFP-munc18-1-V5-His_6 were then sent off for sequencing.

Munc18-1$_{R39C}$ → wildtype forward mutagenic primer

5'- GAC CAG TTA AGC ATG **AGG** ATG CTG TCT TCC TGC -3'

Munc18-1$_{R39C}$ → wildtype reverse mutagenic primer

5'- GCA GGA AGA CAG CAT **C**C**T** CAT GCT TAA CTG GTC -3'

Figure 4.4: Sequences of the mutagenic primers used in the production of wildtype munc18-1 constructs from munc18-1$_{R39C}$ constructs

The mutagenic primers were complementary to each other, with 15 bp on either side of the point mutations, which are shown in bold

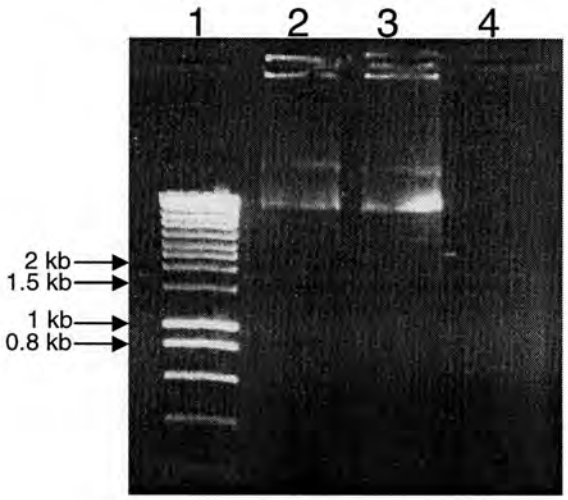

Lane

1: Markers

2: EGFP-munc18-1-V5-His_6

3: munc18-1-V5-His_6

4: negative control

Figure 4.5: Site-directed mutagenesis of munc18-1_{R39C}-V5-His_6 and EGFP-munc18-1-V5-His_6

Site-directed mutagenic PCR was used to revert the munc18-1_{R39C}-V5-His_6 and EGFP-munc18-1-V5-His_6 back to wild-type. 5 µl of each PCR reaction mix was electrophoresed alongside a 1 kb DNA ladder in a 1 % agarose gel. Arrows show approximate sizes in kb

4.2.3 Sequencing of munc18-1-V5-His_6 and EGFP-munc18-1-V5-His_6 constructs

The munc18-1-V5-His_6 and EGFP-munc18-1-V5-His_6 constructs were sent off for sequencing using the same primers that were used before (Chapter 4.2.1, Appendix 2). The sequencing confirmed that the site-directed mutagenesis had been successful and that no other mutations had been introduced by the PCR. These constructs, munc18-1-V5-His_6, EGFP-munc18-1-V5-His_6, munc18-1_{R39C}-V5-His_6 and EGFP-munc18-1_{R39C}-V5-His_6 could then be used for *in vitro* transcription/translation (Chapter 5) and bacterial expression.

4.3 Bacterial Expression of munc18-V5-His_6 in *E.coli* BL21 DE3

To investigate the relative binding affinities between [^{35}S]-munc18-1-V5-His_6 and EGFP-munc18-1-V5-His_6, unlabelled munc18-1 was needed to compete with the radiolabelled protein in binding to GST-syntaxin 1a-(cyt) (Chapter 5). *E.coli* BL21s (DE3) was used to generate soluble munc18-1-V5-His_6, which could then be purified using its oligohistidine tag.

Munc18-1-V5-His_6 was transformed into BL21 DE3 (Chapter 2.8). A colony was picked and grown in a 5 ml LB-ampicillin (100 µg/ml) overnight culture at 37 °C. This was then used to seed two 100 ml cultures (1 in 100 dilution) containing 100 µg/ml ampicillin, for induction (Chapter 2.13.1). One culture was induced at 37 °C for 4 h and the other culture was induced overnight at 16 °C using 1 mM IPTG, but before induction a 1 ml non-induced sample was collected. Following induction 1 ml samples of the cultures were taken and the bacteria harvested by centrifugation and lysed with Bugbuster (Chapter 2.13.2). The lysates were separated into soluble and insoluble fractions by centrifugation at 14000 rpm for 20 minutes. Samples were then made for SDS PAGE analysis with Coomassie staining. The Coomassie stained gel contained no obvious band corresponding to munc18-V5-His_6, so western blotting was carried out, (Chapter 2.13) using anti-munc18-1 to detect the product. The western blot revealed that there was some protein expression, but that the product was

mostly insoluble (Figure 4.6). Because of the poor expression of munc18-1-V5-His_6 and the gift of a munc18-1-His_6 construct from Prof Alan Morgan that was known to be well expressed it was decided to make use of this construct for bacterial expression of munc18-His_6.

4.4 Expression and purification of Munc18-1-His_6 in *E.coli* M15[pREP4]

Munc18-His_6 cloned into pQE plasmid (Qiagen) was obtained already transformed into *E.coli* M15[pREP4] cells. These cells contain a pREP4 plasmid encoding the *lacI* repressor, which allows tight control of recombinant protein expression from a *lac* promoter. Protein expression was carried out following the instructions that came with the plasmid. An overnight 5 ml culture containing ampicillin (100 µg/ml) and kanamycin (30 µg/ml) was set up and used to seed a 100 ml Supermedia-antibiotic culture (100 fold dilution). The bacteria were grown at 37 °C to A_{600}= 0.6-0.8 before being induced with 1 mM IPTG and incubated at 37 °C for 4 h. Following the 4 h induction the bacteria were lysed using Bugbuster (Chapter 2.14.2) and separated into soluble and insoluble fractions by centrifugation at 14000 rpm for 20 min. Samples were made for SDS PAGE followed by Coomassie staining (Figure 4.7). The gel revealed that munc18-His_6 was highly expressed, but that most of it was insoluble. In an attempt to produce soluble protein the grow-up was repeated using LB-media, which has less nutrients, and therefore should result in a reduced growth rate and hence slower protein production. This induction was performed, as before, at 37 °C for 4 h and also at 16 °C overnight. Samples were lysed, separated into soluble and insoluble fractions then analysed by SDS PAGE and Coomassie staining. Growth under these conditions resulted in less recombinant protein production, and it was still insoluble. Lower IPTG concentrations and expression at 16 °C were also investigated, but the munc18-His_6 was still insoluble. It was reasoned that since growth on Supermedia at 37 °C and induction for 4 h with 1 mM IPTG produced a higher yield of munc18-1-His_6 these conditions may

Lane

1: Markers

2: Uninduced, 37 °C, pellet fraction

3: Uninduced, 37 °C, soluble fraction

4: Induced, 37 °C, pellet fraction

5: Induced, 37 °C, soluble fraction

6: Induced, 16 °C, O/N, pellet fraction

7: Induced, 16 °C, O/N, soluble fraction

8: Positive control, purified munc18-1-His_6

Figure 4.6: Expression of munc18-1-V5-His_6

Western blot analysis of munc18-1-V5-His_6 expression in BL21 DE3 at 37 °C for 4 h and 16 °C overnight. Products visualised using anti-munc18-1

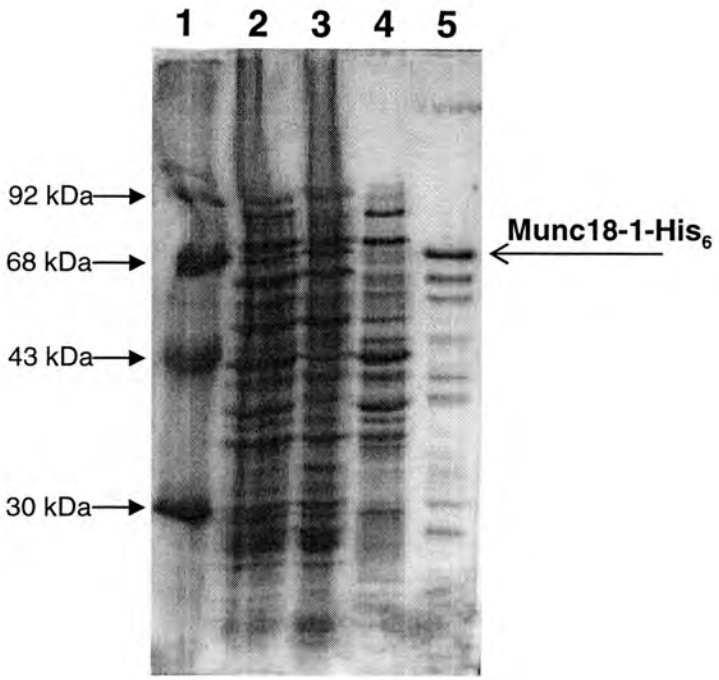

Lane

1: Markers

2: Bacterial lysate

3: Pellet fraction

4: Soluble fraction

5: Positive control, purified munc18-1-His_6

Figure 4.7: Expression of munc18-1-His_6

Coomassie blue stained gel of munc18-1-His_6 expression in M15[pREP4] in Supermedia at 37 °C for 4 h

have produced a useful level of soluble protein, even though the bulk of the product was insoluble. An attempt was made to purify soluble munc18-1-His_6 after induction under these conditions, using a HiTrap affinity column (Amersham) (Chapter 2.14.3.1). Samples from each of the fractions were taken for SDS PAGE analysis followed by Coomassie staining (Figure 4.8 A-B). The gel revealed that some munc18-1-His_6 had been purified, but it was eluted over a wide range of imidazole concentrations (50 – 500 mM). There was also a contaminant protein band at ~40 kDa present in larger quantities than munc18-1-His_6 itself, which was not recognised by the munc18-1 antibody. To try and improve the purification process various different washing strategies were investigated, for example washing with a large volume of 25 mM imidazole followed by elution with 500 mM imidazole or washing with 70 mM imidazole and eluting with 500 mM imidazole. None of these processes improved the purification or removed the ~40 kDa contaminant so a different affinity matrix for purifying His_6-tagged proteins, BD Talon (BD Biosciences), was tried (Chapter 2.14.3.2). Munc18-1- His_6 expression was carried out as before, using Supermedia and inducing at 37 ^{o}C for 4 h with 1 mM IPTG. Analysis of the eluates by SDS PAGE and Coomassie staining revealed that the ~40 kDa contaminant protein was still present.

Since the greatest problem in producing munc18-1-His_6 was that insufficient soluble protein was produced, we attempted to resolubilise munc18-1-His_6 from *E.coli* lysates. The method used was treatment with a non-detergent sulphobutane (NDSB) 3-(1-pyridinio)-1-propanesulphonate, which has been shown to aid in the solubilisation of proteins in a biologically active form (Vuillard, Braun-Breton et al. 1995) (Chapter 2.16.1). Solubilised protein was purified using the BD TALON resin in the same way as with the soluble munc18-1-His_6 and fractions analysed by SDS PAGE and Coomassie staining (Figure 4.9 A-B). The gels revealed that munc18-1-His_6 had been solubilised, but to determine whether the protein was in a biologically active form, the folded state of the protein was investigated using Circular Dichroism spectroscopy (CD) (Chapter 2.17). The CD spectrum (Figure 4.10) revealed that the solubilised munc18-1-His_6 had some secondary structure, but

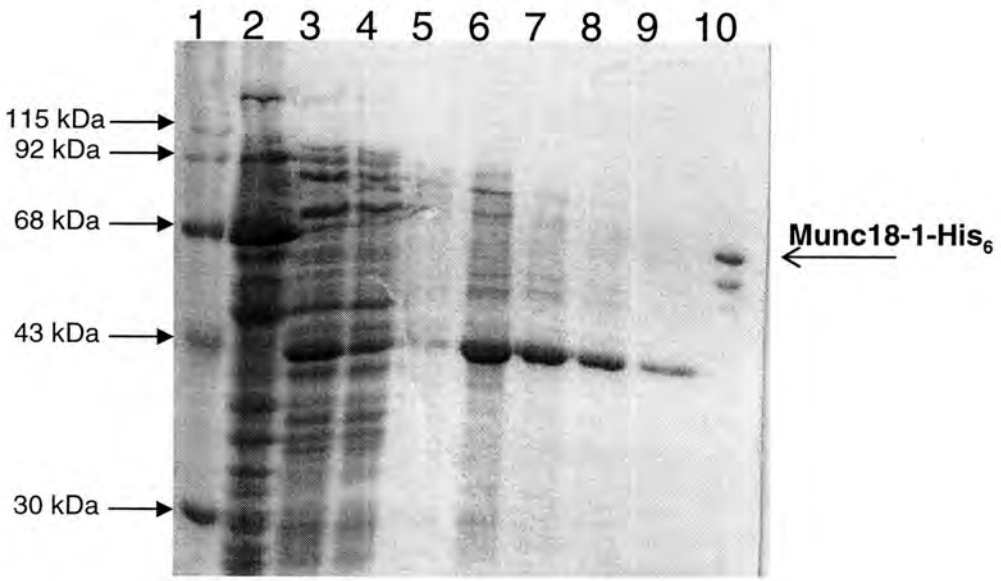

Lane

1: Markers

2: bacterial lysate

3: Pellet fraction

4: Soluble fraction

5: Flow through

6: Fraction 1, 25 mM Imidazole

7: Fraction 2, 25 mM Imidazole

8: Fraction 3, 25 mM Imidazole

9: Fraction4, 25 mM Imidazole

10: positive control, purified munc18-1-His_6

Figure 4.8A: Purification of munc18-1-His_6

Coomassie blue-stained gel of fractions in the purification of munc18-1-His_6. The arrow indicates the band corresponding to munc18-1-His_6. A stepwise imidazole gradient (25, 50, 50, 100 mM) was used to elute the protein from the column.

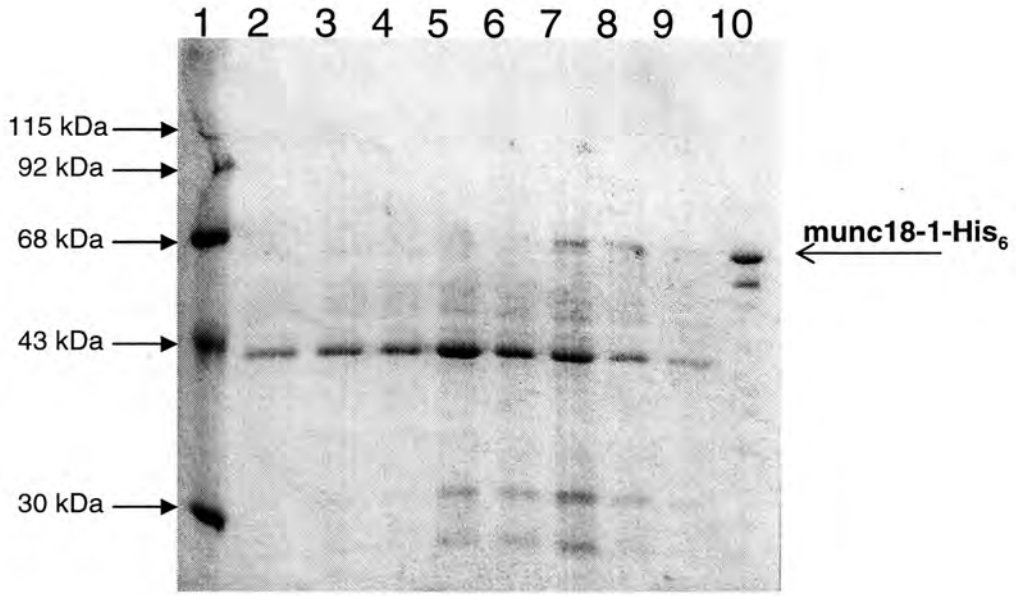

Lane

1: Marker

2: Fraction 5, 25 mM Imidazole

3: Fraction 6, 50 mM Imidazole

4: Fraction 7, 50 mM Imidazole

5: Fraction 8, 50 mM Imidazole

6: Fraction 9, 100 mM Imidazole

7: Fraction 10, 100 mM Imidazole

8: Fraction 11, 100 mM Imidazole

9: Fraction 12, 100 mM Imidazole

10: Positive control, purified munc18-1-His_6

Figure 4.8B: Purification of munc18-1-His_6

Coomassie blue-stained gel of fractions from the purification of munc18-1-His_6 using a HiTrap column (Amersham).

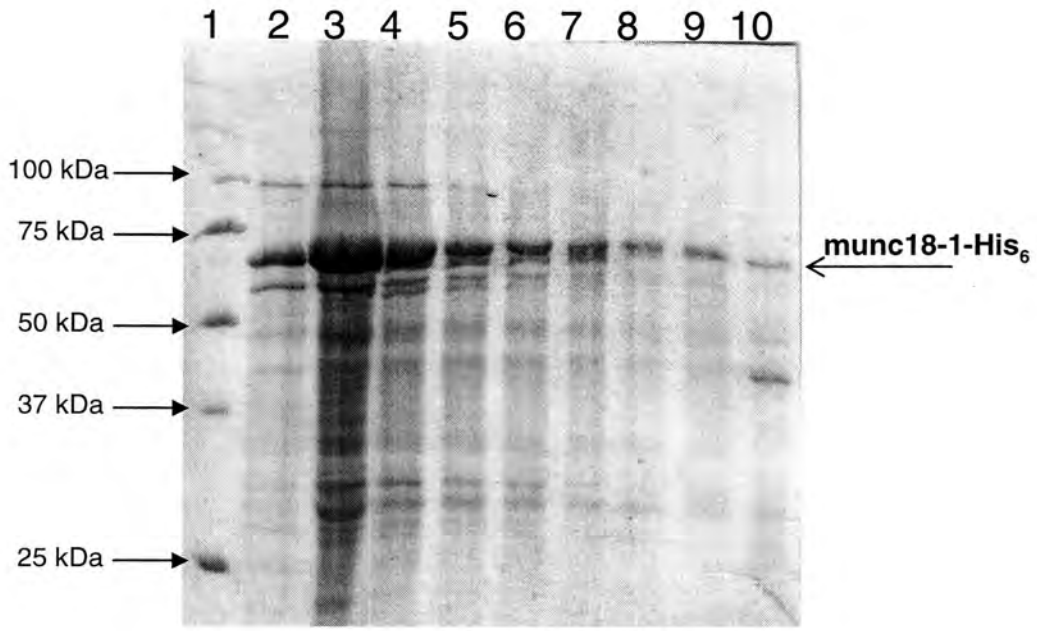

Lane

1:Markers

2: Inclusion Bodies

3: Soluble protein after guanidine treatment

4:Insoluble pellet after guanidine treatment

5: Soluble protein after NDSB

6: Soluble protein after dialysis

7: Flow through

8: Fraction 1, 500 mM Imidazole

9: Fraction 2, 500 mM Imidazole

10: Positive control, purified munc18-1-His_6

Figure 4.9A: Attempted solubilisation of munc18-1-His_6

Coomassie blue- stained gel showing the attempted solubilisation of munc18-1-His_6 from inclusion bodies with a non-detergent sulphobetaine and purification using a BD Talon column.

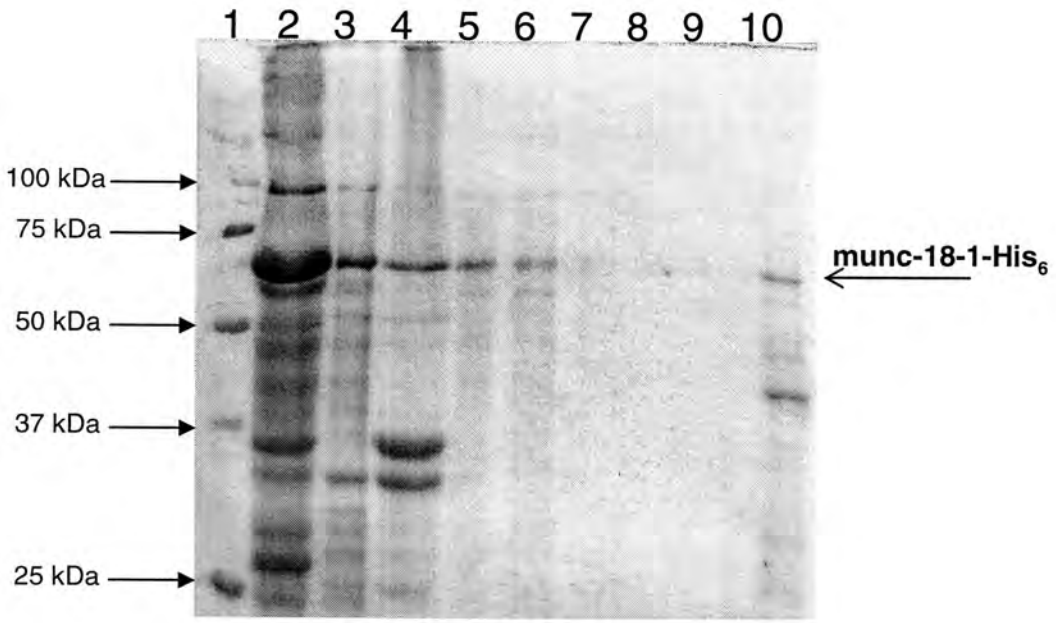

Lane

1: Markers

2: Fraction 3, 500 mM Imidazole

3: Fraction 4, 500 mM Imidazole

4: Fraction 5, 500 mM Imidazole

5: Fraction 6, 500 mM Imidazole

6: Fraction 7, 500 mM Imidazole

7: Fraction 8, 500 mM Imidazole

8: Fraction 9, 500 mM Imidazole

9: Fraction 10, 500 mM Imidazole

10: Positive control, purified munc18-1-His_6

Figure 4.9B: Attempted solubilisation and Purification of munc18-1-His_6

Coomassie stained gel analysing the attempted solubilisation of munc18-1-His_6 with a non-detergent sulphobetaine and purification on a BD Talon column. The arrow shows the munc18-1-His_6 band.

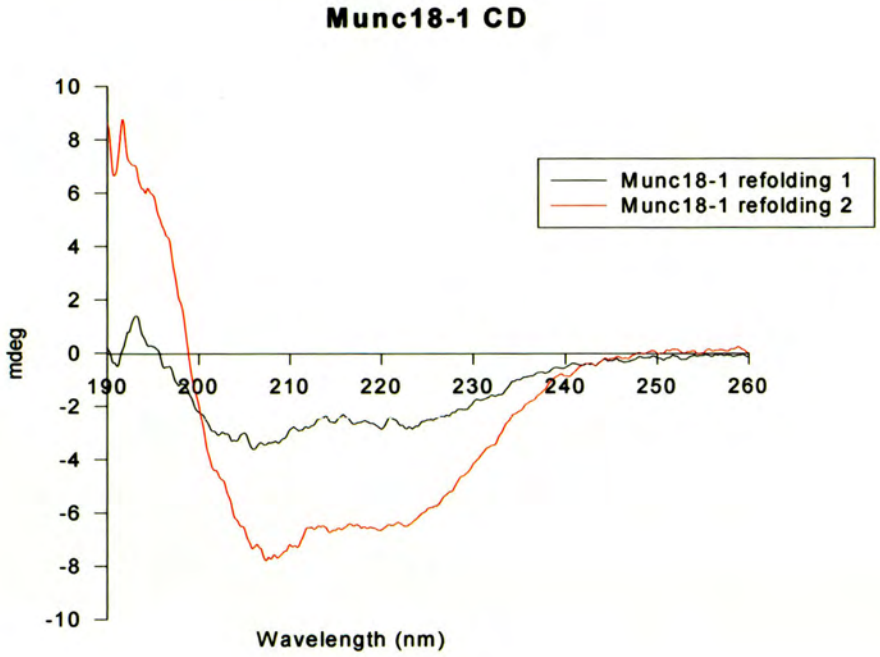

Figure 4.10: CD Spectra of the solubilised munc18-1-His_6

Following solubilisation and refolding, the folded state of munc18-1 was investigated using circular dichroism, revealing that the second solubilisation protocol used, where the inclusion bodies were washed more stringently using an inclusion body wash buffer (Appendix 1.9.2) resulted in the munc18-1-His_6 containing more secondary structures

included a high proportion of unordered structure (with 18 % α-helical, 17 % β-strands, 18 % turns and 47 % unordered). In attempt to improve the folded state of the munc181-His_6 the isolated inclusion bodies were washed three times with inclusion body wash buffer (Appendix 1.9.2) followed by centrifugation at 30000 x g for 30 mins before being solubilised, refolded and purified as before. CD spectroscopy was used to analyse the folded state of the munc18-1-His_6 revealing that there was more secondary structure present (Figure 4.10; 61 % α-helical, 10 % β-strand, 11 % turns and 18 % unordered). To determine whether it was in a biologically active form a binding experiment was set up using solubilised munc18-1-His_6 and immobilised GST-syntaxin 1a-(cyt) as follows:

100 µl of GST-syntaxin 1a-(cyt)-coupled Glutathione Sepharose 4B was incubated with 25, 50, 75 and 100 µg of solubilised munc18-1-His_6 in 200 µl binding buffer (Appendix 1.9.2) for 2 h at 4 °C with rolling. The beads were harvested by centrifugation at 1000 x g for 2 minutes followed by washing five times with binding buffer with rolling at 4 °C for 15 minutes. Following the final wash the residual binding buffer was removed with tissue paper, and the beads resuspended in 15 µl SDS loading buffer. The gel revealed that the munc18-1-His_6 had not bound significantly to GST-syntaxin 1a-(cyt), suggesting that the solubilised munc18-1-His_6 was biologically inactive.

4.5 Expression of munc18-1-V5-His_6 and purification using Qiagen Ni-NTA superflow column

The problems encountered when expressing munc18-1-His_6 in M15[pREP4] *E.coli* cells, and particularly the presence of the ~40 kDa contaminant protein, led to work on expressing munc18-1-V5-His_6 in pET101/D-TOPO and the use of Ni-NTA Superflow columns (Qiagen) for protein purification. Expression was initially carried out in LB medium (Chapter 4.2) and a relatively small amount of soluble munc18-1-V5-His_6 was produced. Expression was repeated using Supermedia to increase the yield of soluble protein, induction

being with 1 mM IPTG, either at 37 °C for 4 h or 16 °C overnight. After induction samples of the cultures were taken, lysed with Bugbuster (Chapter 2.14.2) and separated into soluble and insoluble fractions by centrifugation at 13000 rpm for 20 minutes. SDS loading buffer was added to the soluble and insoluble fractions and the protein expression was analysed by SDS PAGE followed by Western blotting (Chapter 2.13) using anti-munc18-1. The western blot revealed that the best condition for inducing expression of soluble munc18-1-V5-His_6 was 37 °C for 4 h with 1 mM IPTG in Supermedia.

Following the determination of the optimum expression conditions, a 1 litre induction was set up in Supermedia containing ampicillin (100 µg/ml) and munc18-1-V5-His_6 was induced using 1 mM IPTG for 4 h at 37 °C. Purification of munc18-1-V5-His_6 was carried out according to the manufacturer's instructions (Qiagen) (Chapter 2.14.3.3). The bacteria were harvested by centrifugation, 10 min at 5000 x g and resuspended in lysis buffer (Appendix 1.5.3.1) then incubated on ice for 1 h. The bacterial lysate was then sonicated (Soniprep 150), 8 x 10 secs at amplitude = 6 microns then separated into soluble and insoluble fractions by centrifugation at 12000 x g for 30 min. The soluble fraction was then incubated with 1 ml of the NTA Ni resin for 2 h at 4 °C with rolling before being packed into a gravity flow Supercolumn. The resin was washed with 10 ml of binding buffer (10 mM imidazole, Appendix 1.5.3.2), then 50 ml of wash buffer 1 (20 mM imidazole, Appendix 1.5.3.3), followed by 6 ml of wash buffer 2 (50 mM imidazole, Appendix 1.5.3.4), collected as 1 ml fractions. The protein was eluted in 3 ml of elution buffer (250 mM imidazole, Appendix 1.5.3.5), collected as 0.5 ml fractions. Samples were prepared for SDS PAGE followed by Coomassie staining. The gel revealed (Figure 4.11 A-B) that soluble munc18-1-V5-His_6 had been purified; however there was a contaminant band of approximately 70 kDa that could not be separated from the munc18-1-V5-His_6. To determine whether the munc18-1-V5-His_6 could be used in future binding experiments binding to GST-syntaxin 1a-(cyt) was tested in the same way as described in Chapter 4.3. It was again found that the munc18-1-V5-His_6 did not interact with GST-syntaxin 1a-(cyt). The reason for this could that the 70 kDa

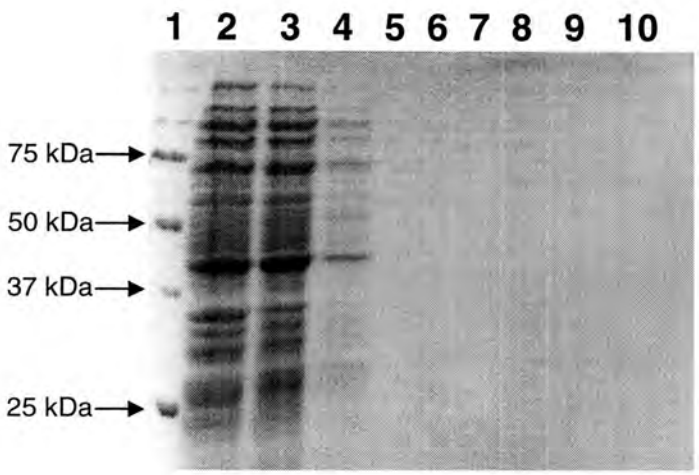

Lane

1: Markers

2: Flow through

3: Wash 1, 20 mM imidazole

4: Wash 2, 20 mM imidazole

5: Wash 3, 20 mM imidazole

6: Wash 4, 20 mM imidazole

7: Wash 5, 20 mM imidazole

8: Fraction 1, 50 mM imidazole

9: Fraction 2, 50 mM imidazole

10: Fraction 3, 50 mM imidazole

Figure 4.11A: Purification of munc18-1-V5-His_6

Coomassie blue stained gel of the purification of munc18-1-V5-His_6 using a Quiagen Ni-NTA superflow column.

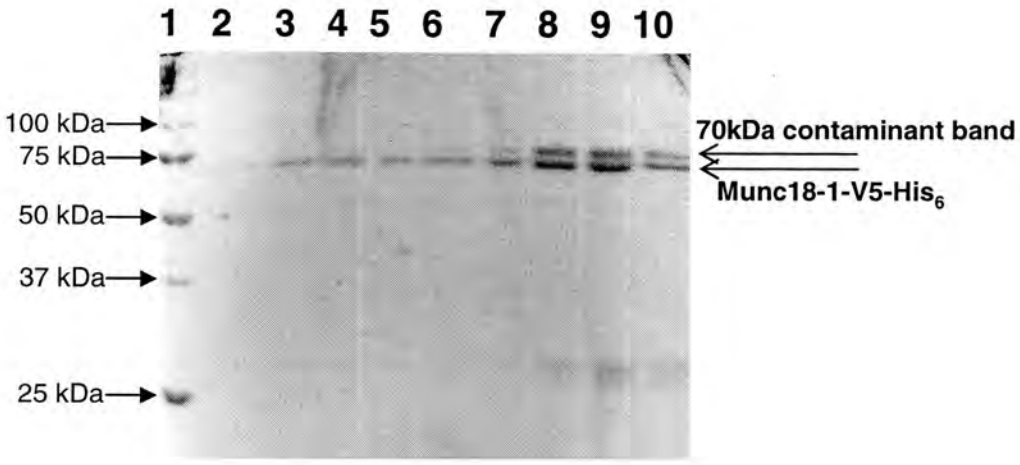

Lane

1: Markers

2: Fraction 4, 50 mM imidazole

3: Fraction 5, 50 mM imidazole

4: Fraction 6, 50 mM imidazole

5: Fraction 7, 250 mM imidazole

6: Fraction 8, 250 mM imidazole

7: Fraction 9, 250 mM imidazole

8: Fraction 10, 250 mM imidazole

9: Fraction 11, 250 mM imidazole

10: Fraction 12, 250 mM imidazole

Figure 4.11B: Purification of munc18-1-V5-His_6

Coomassie blue stained gel of the purification of munc18-1-V5-His_6 using a Quiagen Ni-NTA Superflow column. The gel shows the presence of the 70 kDa contaminant band that could not be separated from the munc18-1-V5-His_6.

contaminant was binding tightly to munc18-1-V5-His_6 and thus preventing its interaction with GST-syntaxin 1a-(cyt). If this was the case the 70 kDa contaminant protein could be Hsc70, which is a bacterial chaperone protein that may interact with the munc18-1-V5-His_6 and aid in its folding. To test this hypothesis the binding experiment between GST-syntaxin 1a-(cyt) and munc18-1-V5-His_6 was repeated in the presence of 2 mM ATP and 5 mM $MgSO_4$, since MgATP is required by chaperone proteins to release proteins. Under these conditions munc18-1-His_6 still did not
interact with GST-syntaxin 1a-(cyt), suggesting that the 70 kDa contaminant protein was not Hsc70.

4.6 Purification of munc18-1-His_6 on Qiagen Ni-NTA Superflow

Since the purification of munc18-1-V5-His_6 on the Qiagen Ni-NTA superflow column was unsuccessful it was decided to try to purify munc18-1-His_6 using the Quiagen Ni-NTA superflow column. The protein was expressed in *E.coli* M15(pREP4) (Chapter 4.3) in 1 litre of Supermedia containing ampicillin (100 µg/ml) induced at 37 °C for 4 h with 1 mM IPTG. Following expression the protein was purified in the same way as detailed in Chapter 4.4 and analysed by SDS PAGE and Coomassie staining (Figure 4.12 A-B). The gel revealed that munc18-1-His_6 had been successfully purified, eluting from the column in fractions 8-10. Approximately 95 % of the protein eluted from the column was munc18-1-His_6 and the 70 kDa contaminant protein was not present in this protein preparation. To check that the munc18-1-His_6 was folded correctly its interaction with GST-syntaxin 1a-(cyt) was investigated as before (Chapter 4.3) revealing that the munc18-1-His_6 was bound to the GST-syntaxin 1a-(cyt) (Figure 4. 13). The purified munc18-1-His_6 could now be used as a competitor in binding experiments.

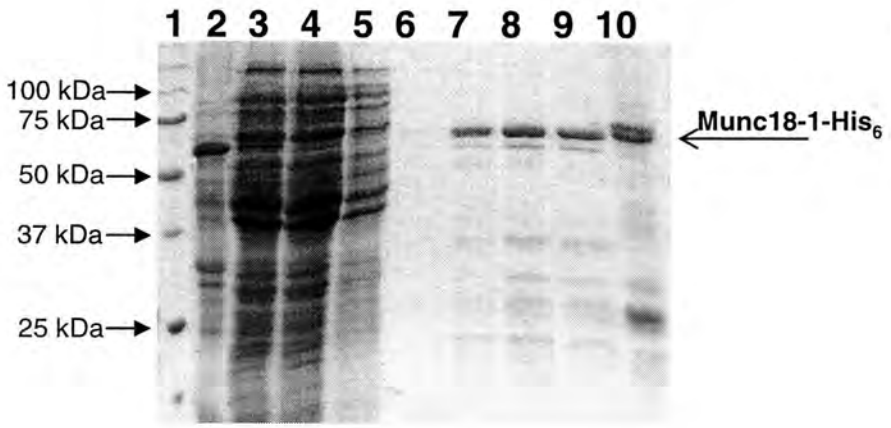

Lane

1: Markers

2: Pellet fraction

3: Soluble fraction

4: Flow through

5: Wash 1, 20 mM imidazole

6: Fraction 1, 50 mM imidazole

7: Fraction 2, 50 mM imidazole

8: Fraction 3, 50 mM imidazole

9: Fraction 4, 50 mM imidazole

10: Positive control, purified munc18-1-V5-His_6

Figure 4.12A: Purification of munc18-1-His_6

Coomassie blue stained gel of purification of munc18-1-His_6 purification using a Qiagen Ni-NTA Superflow column

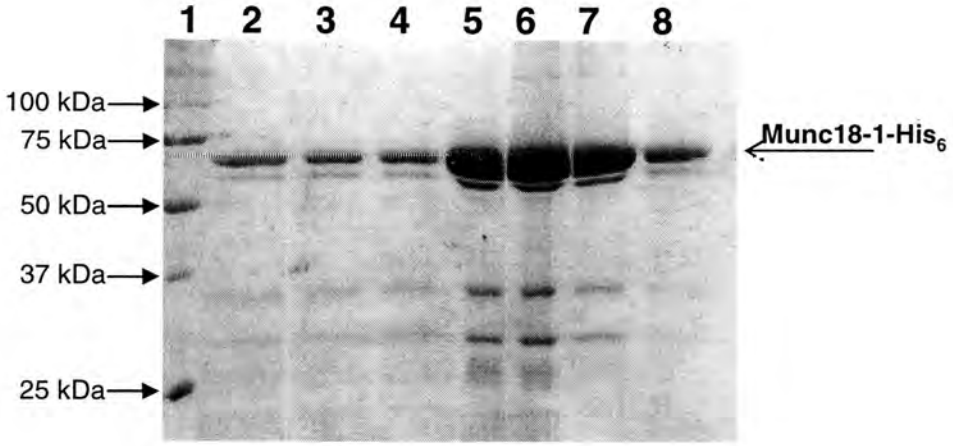

Lane

1: Markers

2: Fraction 5, 50 mM imidazole

3: Fraction 6, 250 mM imidazole

4: Fraction 7, 250 mM imidazole

5: Fraction 8, 250 mM imidazole

6: Fraction 9, 250 mM imidazole

7: Fraction 10, 250 mM imidazole

8: Fraction 11, 250 mM imidazole

Figure 4.12B : Purification of munc18-1-His_6

Coomassie blue stained gel of munc18-1-His_6 purification using the Quiagen Ni-NTA superflow columns. Eluted munc18-1-His_6 was mainly in fractions 5 - 8.

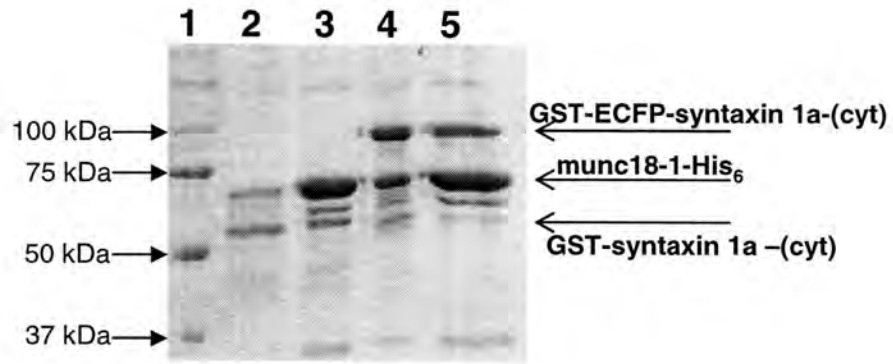

Lane

1: Markers

2: GSH-GST-syntaxin 1a-(cyt)

3: Supernatant

4: GSH-GST-ECFP-syntaxin 1a-(cyt)

5: Supernatant

Figure 4.13: Binding experiment between purified munc18-1-His_6 and GST-syntaxin 1a-(cyt) or GST-ECFP-syntaxin 1a-(cyt)

Coomassie blue stained gel of binding experiments set up between munc18-1-His_6 and either GST-syntaxin 1a-(cyt) or GST-ECFP-syntaxin 1a-(cyt), where soluble munc18-1-His_6 was incubated with Glutathione Sepharose 4B coupled with either GST-syntaxin 1a-(cyt) or GST-ECFP-syntaxin 1a-(cyt). The beads were harvested and the supernatants removed. Both the pellet and supernatant fractions were analysed by SDS PAGE revealing that the purified proteins do interact with each other

4.7 Cloning of EGFP-munc18-1 and EGFP-munc18-1_{R39C} into a Mammalian expression vector.

To investigate the interaction between munc18-1 and syntaxin 1a *in vivo* by expression in cultured mammalian cells, the EGFP-munc18-1 sequence had to be moved into a mammalian expression vector. The expression vector chosen was pcDNA3 (Invitrogen). In order to accomplish this subcloning, restriction sites had to be added on either side of the gene sequence by PCR, present in pcDNA3. Initially EGFP-munc18-1 and EGFP-munc18-1_{R39C} were cloned into the vector pCR2.1 (Invitrogen) using blunt cloning, then sub-cloned into pcDNA3 using the restriction enzymes. This approach was used because excision of the insert from a vector ensured that it been cut by the restriction enzymes, whereas this cannot be guaranteed if a PCR product is digested.

4.7.1 PCR of EGFP-munc18-1 and EGFP-munc18-1_{R39C} to add restriction sites for Xba1

EGFP-munc18-1 and EGFP-munc18-1_{R39C} were first cloned into pCR2.1. This required the addition of 3' A-overhangs, so the Expand High Fidelity PCR System (Roche) was used. An EGFP forward primer, containing and Xba1 site and a reverse primer, also incorporating an Xba1 site, were used (Figure 4.14). The components of the PCR reaction mix were assembled as before and the same PCR conditions used (Chapter 4.2.1). PCR products were analysed by electrophoresis on a 1 % (w/v) agarose gel alongside a 1 kb DNA ladder. The gel contained a band of approximately 2.5 kb for both EGFP-munc18-1 and EGFP-munc18-1_{R39C} as expected and the negative control lane was empty. The DNA concentration of the PCR products was also estimated from this gel, and used to calculate the amount of the PCR products required for the ligation.

EGFP Forward Primer Xba1

5'-GTC AGA TCC **TCT AGA** GCT ACC GGT CGC CAC CAT GGT GAG CAA GG-3'

EGFP-munc18-1 Reverse Stop Xba1

5'-**TCT AGA** TTA ACT GCT TAT TTC TTC GTC TGT TTT ATT-3'

Figure 4.14: Sequences of forward and reverse munc18-1 PCR primers

Primers used for munc18-1 PCR so that it could be cloned into the mammalian expression vestor pcDNA3

4.7.2 Cloning of EGFP-munc18-1 and munc18-1_{R39C} into pCR2.1

Once the DNA concentration on the PCR products of EGFP-munc18-1 and EGFP-munc18-1_{R39C} was estimated the following equation was used to calculate the volume of each of the PCR products required for the ligation, following the manufacturer's instructions

$$X = 50N/V$$

where X = amount of PCR product (ng), N = size of PCR product (bp) and V = size of pCR2.1 vector (~3900bp)

The ligation reaction mix was set up containing the correct volume of PCR product, 1 µl of ligation buffer, 2 µl pCR2.1 vector, 1 µl T4 DNA Ligase and made up to 10 µl with dH_2O. The reaction was then incubated overnight at 16 °C before being transformed into competent *E.coli* TOP10 cells (Chapter 2.8). The transformed bacteria were spread on an LB-Agar plate containing ampicillin and incubated at 37 °C overnight. Colonies were analysed using PCR to screen for positive clones, where the components were assembled into a master mix on ice (Chapter 2.3.3) and thoroughly mixed, then 49 µl was aliquoted into PCR tubes. 10 colonies were picked and each one was dipped into a different PCR tube several times before being spotted on to an LB-Agar plate containing ampicillin (100 µg/ml). 1 µl of template DNA was added to one of the remaining PCR tubes for a positive control and the other was used as a negative control containing no DNA. The heating block of the PCR machine was brought to 95 °C before the samples were placed inside and incubated for 1 min to lyse the bacteria and separate the DNA strands. The same PCR conditions were used as before (Chapter 4.2.2). The LB-agar plate with spotted colonies was incubated at 37 °C. The PCR reaction products were analysed by electrophoresis on a 1 % (w/v) agarose gel alongside a 1 kb DNA ladder and lanes containing a band of ~2500 bp indicated the colonies that were positive clones. One of the positive clones was chosen and the corresponding colony that had grown on the LB-Agar plate was used to seed an overnight 100 ml LB-ampicillin (100

μg/ml) culture for a "Maxiprep". The "Maxiprep" (Qiagen) was done following the manufacturer's instructions.

4.7.3 Sequencing of EGFP-munc18-1 and EGFP-munc18-1_{R39C} in pCR2.1

Since PCR had been used during cloning of EGFP-munc18-1 and EGFP-munc18-1_{R39C} into pCR2.1 the sequence had to be checked for mutations. Samples were prepared (Chapter 2.11) and the same primers used as before (Appendix 2) to fully sequence the clones. DNA sequencing revealed that no mutations had been introduced into the sequences of EGFP-munc18-1 and EGFP-munc18-1_{R39C} during the PCR reaction. These could now be excised from pCR2.1 by restriction digestion and sub-cloned in pcDNA3.

4.7.4 Cloning of EGFP-munc18-1 and EGFP-munc18-1_{R39C} into pcDNA3

The restriction enzyme used to clone EGFP-munc18-1 and EGFP-munc18-1_{R39C} into pcDNA was XbaI. 3 μg of EGFP-munc18-1, EGFP-munc18-1_{R39C} and pcDNA3 vector were digested by 10 units of XbaI for 2 h at 37 °. The restriction digests were analysed by electrophoresis of the entire restriction digest reaction mix in a 1 % (w/v) agarose gel. The bands corresponding to EGFP-munc18-1, EGFP-munc18-1_{R39C} and pcDNA were excised from the gel and the DNA purified using a gel extraction kit (Eppendorf) following the manufacturer's instructions. 10 % (v/v) of each of the purified DNA samples was analysed by 1 % (w/v) agarose gel to estimate their concentration. The DNA concentrations were then used to calculate the amount of the vector and each of the insert required for the ligation reactions (Chapter 2.6)

Three ligation reaction mixes for EGFP-munc18-1 and EGFP-munc18-1_{R39C}were set up with vector:insert ratios of 1:1, 3:1 and 1:3 containing 1 μl Ligase buffer, 1 μl T4 DNA Ligase (Promega) and made up to 10 μl with dH_2O. One control was also set up containing no T4 DNA ligase to show whether any of the pcDNA3 vector was undigested. These reaction

mixes were incubated overnight at 4 °C then transformed into competent *E.coli* TOP10 cells (Chapter 2.8). Colonies were picked and grown overnight at 37 °C in 5 ml LB-ampicillin (100 μg/ml) cultures for "minipreps" to purify the plasmid DNA. The "minipreps" were done (Chapter 2.9.1) and positive clones containing EGFP-munc18-1 and EGFP-munc18-1_{R39C} inserted in the correct orientation were determined by restriction digestion. 10 μl of each "miniprep" was digested with 10 units of NotI for 2 h at 37 °C followed by digestion with 10 units of BamH1 for 2 h at 37 °C and the results were analysed by 1 % (w/v) agarose gel alongside a 1 kb DNA ladder. Lanes containing a band ~ 2500 bp represented positive clones, one of which was chosen for each EGFP-munc18-1 and EGFP-munc18-1_{R39C} and using the remainder of their 5 ml "miniprep" culture to seed a 100 ml (1:100 dilution) LB-ampicillin (100 μg/ml) culture grown overnight at 37 °C for "maxiprep". The "maxiprep" (Qiagen) was made according to the manufacturer's instructions. Samples were then prepared for sequencing over the vector/insert junctions, to check that the EGFP-munc18-1 and EGFP-munc18-1_{R39C} had been ligated properly into pcDNA3, using the sequencing primers T7 forward and EGFP Reverse (Appendix 2) for the N-terminal junction and munc18-1 Forward 3 and BGH reverse for the C-terminal junction. The sequencing revealed that the ligations had been successful and the constructs could then be used to transfect mammalian cells.

4.8 Transfection of mammalian cells with EGFP-munc18-1 and EGFP-munc18-1_{R39C}

HEK293 cells and AtT20 cells were transfected with both EGFP-munc18-1 and EGFP-munc18-1_{R39C} to investigate the expression of these proteins and the interaction between EGFP- munc18-1 and EGFP-munc18-1_{R39C} with native syntaxin 1a. This work is discussed more fully in Chapter 6. In AtT20 cells endogenous syntaxin 1a was immuno-stained using a commercial monoclonal antibody and second antibody conjugated with Alexa Fluor 546.

Although there was colocalisation of munc18-1 and syntaxin 1a no FRET was detected. Two possible reasons for the lack of FRET were that the Alexa 546 fluorophor was highly quenched during excitation, or the distance between EGFP and the antibody conjugated flurophor was too large for FRET to occur. To overcome this problem exogenous ECFP-syntaxin 1a was used instead, but this required EGFP on munc18-1 to be replaced by EYFP, which is a better FRET acceptor for ECFP than is EGFP.

4.9 Exchange of EGFP for EYFP to produce EYFP-munc18-1 and EYFP-munc18-1_{R39C} in pcDNA3

The easiest way to exchange EGFP for EYFP was to remove EGFP by restriction digestion and replace it with EYFP from pEYFP-N1 (Clontech) and since EGFP and EYFP sequences only differ from each other by several base pairs an appropriate internal restriction site was used. The restriction enzymes chosen were Kpn1, which was found in both pcDNA3 and pEYFP-N1 upstream of EGFP and EYFP, and BsrG1 for which there was one site in both the EGFP and the EYFP genes, located 46 bp from the C-terminus. Accordingly, 3 µg each of EGFP-munc18-1, EGFP-munc18-1_{R39C} in pcDNA3 and pEYFP-N1 was digested with 10 units of Kpn1 for 2 h at 37 °C (total volume = 20 µl) followed by incubation for a further 2 h at 37 °C with 10 units of BsrG1 (total volume = 50 µl). The whole volume of each restriction digest was loaded for electrophoresis on a 1 % (w/v) agarose gel, alongside a 1 kb DNA ladder. The DNA bands corresponding to munc18-1-pcDNA3, munc18-1_{R39C}-pcDNA3 and EYFP were excised and the DNA purified using a gel extraction kit (Eppendorf) following the manufacturer's instructions. The concentration of the extracted DNA was estimated by comparison with the ladder on 1 % (w/v) agarose gel electrophoresis so that the ligations of EYFP into munc18-1-pcDNA and munc18-1_{R39C}-pcDNA could be set up as before (Chapter 4.4.4). The reaction mixes were incubated at 4 °C overnight preceded by transformation in competent *E.coli* TOP10 cells (Chapter 2.8). Colonies were then

screened for positive clones using PCR (Chapter 4.4.2) which would gave a product of ~2500 bp if the cloning had been successful. Positive clones of EYFP-munc18-1 and EYFP-munc18-1_{R39C} were chosen and used to seed overnight 100 ml LB-ampicillin (100 μg/ml) cultures for "maxipreps" (Qiagen), which were made according to the manufacturer's instructions. Samples were sent for sequencing (Chapter 2.11) to ensure that EGFP had been replaced by EYFP.

4.9.1 Sequencing of EYFP-munc18-1 and EYFP-munc18-1_{R39C} in pcDNA3

The clones were sequenced to ensure that EGFP had been replaced by EYFP in frame. The sequencing primers used were; T7 Forward, EGFP Forward, and munc18-1/EGFP junction Reverse and EGFP Reverse (Appendix 2). Sequencing results revealed that the cloning had been successful, producing EYFP-munc18-1 and EYFP-munc18-1_{R39C} in pcDNA3 that could now be used to transfect mammalian cells.

4.9.2 Transfection of mammalian cells with EYFP-munc18-1 and EYFP-munc18-1_{R39C} in pcDNA3

Transfections were done in HEK293 cells to investigate the interactions between EYFP-munc18-1 and EYFP-munc18-1_{R39C} with ECFP-syntaxin 1a and are discussed in Chapter 6.

4.10 Summary

This chapter outlines the production of various munc18-1 constructs for bacterial expression, *in vitro* transcription/translation and transfection of mammalian cells.

During the building of these constructs several time-consuming problems were encountered, such as the mutations introduced during PCR amplification and the unexpected deletion of the munc18-1 sequence during the TOPO cloning. These problems were eventually

overcome, allowing the production of munc18-1 constructs that could be used both for bacterial expression and *in vitro* transcription/translation. These constructs produced usable radiolabelled products on *in vitro* transcription/translation, however bacterial expression of munc18-1-V5-His_6 was problematic. Even when a successful expression protocol was devised, purification of the His-tagged protein by three different purification protocols was unsuccessful. However, a munc18-1-His_6 construct, a gift from Prof Alan Morgan, was successfully expressed and the protein purified, although only one of the purification methods was successful in generating native protein that could then be used in future experiments. In addition to the munc18-1 constructs produced for the *in vitro* expression of munc18-1, munc18-1 fused to variant GFP fusion proteins were successfully produced, and expressed in mammalian cells. The use of these is described in the next chapters.

Chapter 5

In vitro Binding of munc18-1 constructs to syntaxin 1a constructs

5.1 Introduction

The principal aim of this thesis was to investigate the interaction in cells between the SNARE protein syntaxin 1a and the SNARE regulator munc18-1, and to study their respective roles in exocytosis using both *in vitro* and *in vivo* approaches.

With the production of fluorescent (ECFP, EGFP, EYFP) fusion proteins and the use of high-resolution imaging systems involving FRET and FLIM, the interaction between syntaxin 1a and munc18-1 can be investigated within secretory cells in response to various stimuli, in order to further elucidate their role in exocytosis. However this approach had to be validated by carrying out *in vitro* binding experiments, to check that fusion of the fluorescent proteins to munc18-1 and syntaxin 1a did not significantly affect their interaction. This chapter describes the *in vitro* binding studies that were performed, using radiolabelled munc18-1 constructs and immobilised syntaxin 1a.

First the effect, if any, of the addition of fluorescent GFP variants to syntaxin 1a and munc18-1 on their interaction had to be determined. This involved comparing the relative binding affinities of the wild-type and the fluorescently labelled proteins. The approach taken in this thesis was to quantify the binding of [^{35}S]-munc18-1 and [^{35}S]-EGFP-munc18-1 to GST-syntaxin 1a-(cyt) and GST-ECFP-syntaxin 1a-(cyt), using competition by unlabelled, bacterially expressed munc18-1-His_6 to determine the relative binding affinities. The syntaxin 1a constructs were derived from the cytoplasmic domain of syntaxin 1a, N-terminally fused to glutathione S-transferase (Figure 5.1): These were bound to GST-Sepharose, and used in 'pull-down' assays. [^{35}S]-munc18-1 and [^{35}S]-EGFP-munc18-1 were produced using a cell-free protein translation system. This enables a specific protein of interest to be transcribed from its cDNA under the control of a T7 promoter, and then translated with the incorporation of a radiolabelled amino acid ([^{35}S]-methionine) allowing quantification of the bound protein after separation by SDS-PAGE.

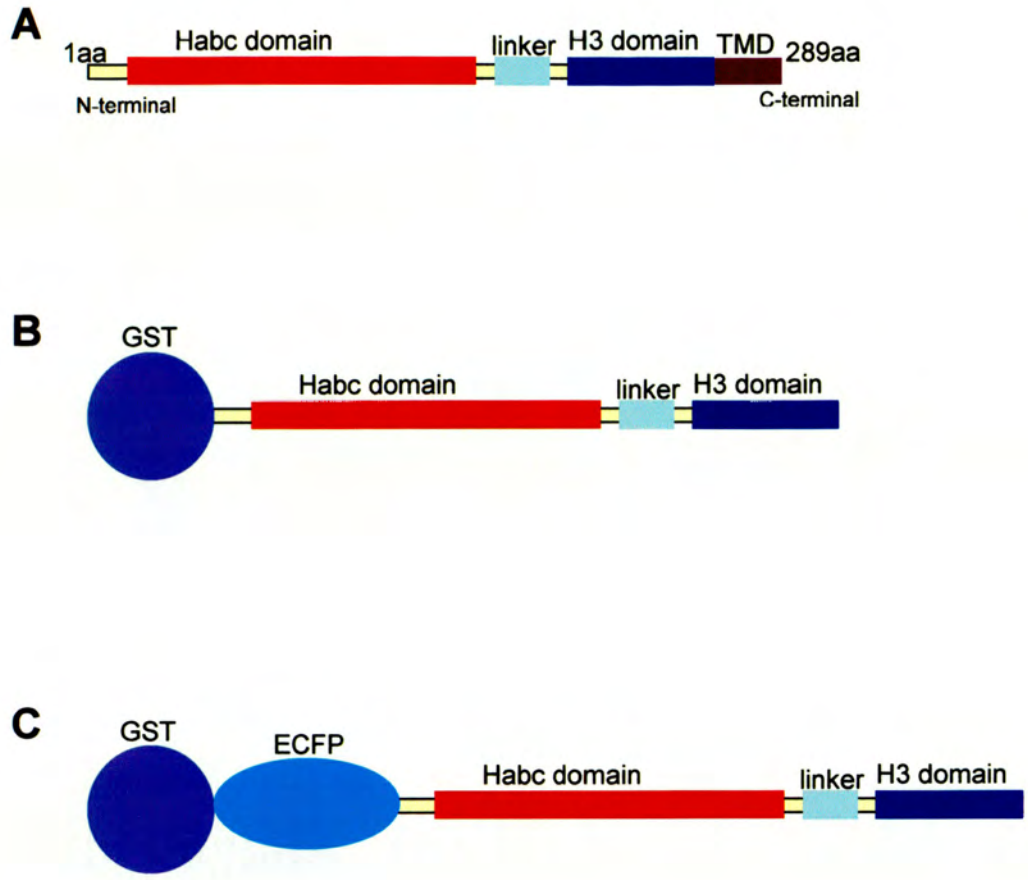

Figure 5.1: Diagram of the GST-syntaxin 1a fusion proteins

A: Full length syntaxin 1a

B: GST-syntaxin 1a (cyt)

C: GST-ECFP-syntaxin 1a-(cyt)

5.2 *In vitro* transcription/translation of munc18-1-V5-His_6, EGFP-munc18-1-V5-His_6, munc18-1_{R39C}-V5-His_6 and EGFP-munc18-1_{R39C}-V5-His_6

For production of [^{35}S]-labelled munc18-1 through transcription and translation of its cDNA by the TnT Coupled Reticulocyte Lysate system (Promega), the reaction was carried out as described in Chapter 2.18 and 5 µl of each reaction product was analysed by SDS PAGE followed by autoradiography (Figure 5.2). The autoradiogram revealed that munc18-1, EGFP-munc18-1, munc18-1_{R39C} and EGFP-munc18-1_{R39C} were *in vitro* transcribed/translated well, appearing as a doublet (not well resolved in Figure 5.2 – see Figure 5.6A), which could then be used in binding experiments. Recombinant munc18-1 has been shown to run as a doublet during electrophoretic separation (Barclay, Craig et al. 2003), thought to be due to some limited proteolysis, and the two forms were found to behave identically in their binding assays (but see section 5.4).

5.3 [^{35}S]-labelled munc18-1, EGFP-munc18-1, munc18-1_{R39C} and EGFP-munc18-1_{R39C} binding to GST-syntaxin 1a-(cyt)

Initially it was decided to investigate whether each of the munc18-1 constructs associated with the syntaxin 1a-(cyt) before measuring their relative binding affinities. [^{35}S]-munc18-1, [^{35}S]-EGFP-munc18-1, [^{35}S]-munc18-1_{R39C} and [^{35}S]-EGFP-munc18-1_{R39C} were produced by *in vitro* transcription/translation reactions (Chapter 2.18) and binding reaction mixes were set up in triplicate for each one, using either GST-syntaxin 1a-(cyt) or GST (used as a control) coupled to Glutathione Sepharose 4B. 5 µl of protein coupled beads was incubated with 5 µl of the *in vitro* transcription/translation reaction in binding buffer (Appendix 1.11.1, total volume of 50 µl) for 2h at 4 °C with rolling. The beads were then washed 5 times with 500 µl of binding buffer (Chapter 2.18.1). The samples were then analysed by SDS PAGE, but before being dried the gels were stained with Coomassie Blue R (Figure 5.3) so that the amount of syntaxin 1a used in each experiment could be estimated by densitometry and the binding normalised.

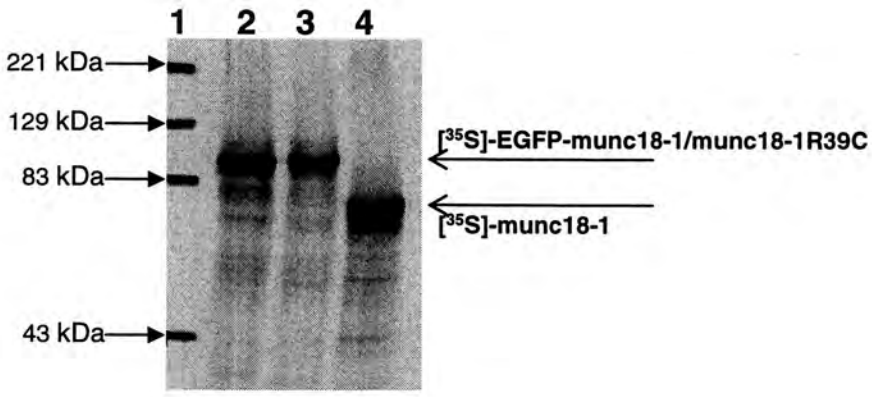

Lane

1: Markers

2: EGFP-munc18-1

3: EGFP-munc18-1_{R39C}

4: munc18-1

Figure 5.2: *In vitro* transcription/translation

Autoradiograph of a 10 % Polyacrylamide-SDSgel showing the production of [^{35}S] munc18-1, [^{35}S] EGFP-munc18-1 and [^{35}S] EGFP-munc18-1_{R39C}.

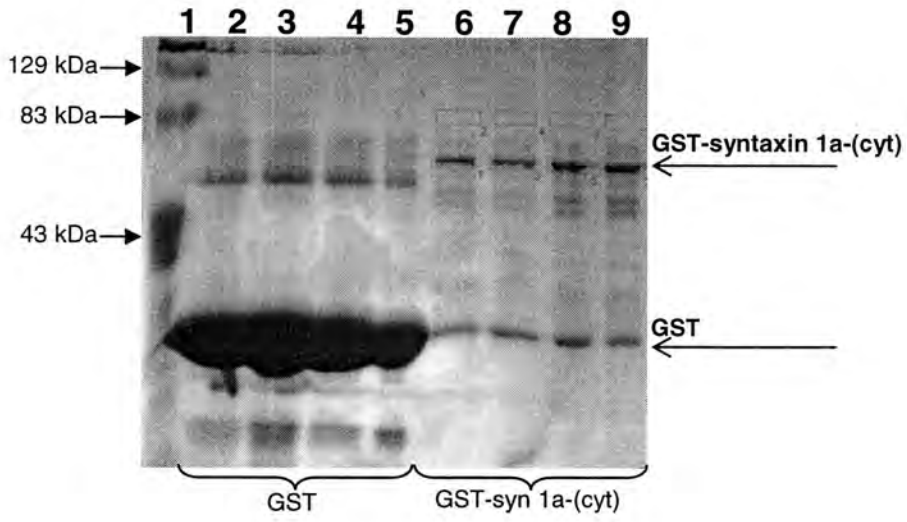

Lane

1: Markers

2: [^{35}S]-munc18-1

3: [^{35}S]-EGFP-munc18-1

4: [^{35}S]-munc18-1$_{R39C}$

5: [^{35}S]-EGFP-munc18-1$_{R39C}$

6: [^{35}S]-munc18-1

7: [^{35}S]-EGFP-munc18-1

8: [^{35}S]-Munc18-1$_{R39C}$

9: [^{35}S]-EGFP-munc18-1$_{R39C}$

Figure 5.3: Assessment of amount of GST-syntaxin 1a–(cyt) in binding mixes

Coomassie blue stained gel of components of an experiment to study the binding of [^{35}S] munc18-1s to either GST or GST-syntaxin 1a-(cyt). Each lane contained the translation mix shown and either GST or GST-syntaxin 1a (cytoplasmic domain) An autoradiograph of this gel is shown in Fig. 5.3

The gels were dried and analysed by autoradiography (Figure 5.4) and a phosphor imager (Chapter 2.20) to quantify the amount of [^{35}S]-labelled protein bound to the protein-coupled glutathione. Once the amount of [^{35}S]-labelled protein had been determined there were several corrections that had to be done before the quantification was complete. These were:

1. A correction for transcription/translation efficiency – these differed between the different munc18-1 constructs used and between the same constructs produced on different days.
2. The number of methionine residues in each protein had to be taken into account since the EGFP variants contain 12 methionines whereas the untagged munc18-1 variants contain 8. Consequently the EGFP variants incorporated more [^{35}S]-methionine and a correction was made for this.
3. The amount of protein-coupled Glutathione Sepharose 4B present in each binding reaction had to be normalised because this would affect how much [^{35}S]-labelled protein had bound. Although this was meant to be identical in each binding reaction, in practice accurate pipetting of suspensions of Sepharose is difficult, so a correction was made for variations between samples.

The results (Figure 5.4) revealed that both [^{35}S]-munc18-1 and [^{35}S]-EGFP-munc18-1 bound to the GST-syntaxin 1a-(cyt) whereas binding of [^{35}S]-munc18-1$_{R39C}$ and [^{35}S]-EGFP-munc18-1$_{R39C}$ was not significantly above background levels. To get a more accurate comparison of the binding affinities competition experiments were done to investigate the relative binding affinities of [^{35}S]-munc18-1 and [^{35}S]-EGFP-munc18-1 with GST-syntaxin 1a-(cyt), since these were the variants that bound significantly above background levels. Initially this was attempted using a munc18-1-derived peptide as a competitor with [^{35}S]-munc18-1 variants. Relatively short munc18-1-derived peptides have been reported to block the munc18-1 – syntaxin 1a interaction (Dresbach, Burns et al, 1998), and since, at this time problems were being encountered in expressing and purifying munc18-1-V5-His$_6$ from bacteria it was decided to try using synthetic peptides as competitors. However once the

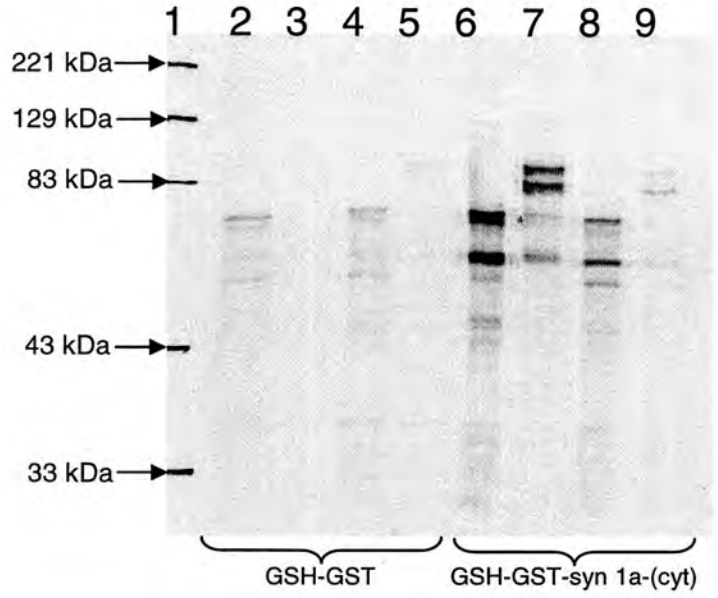

Lane

1: Markers

2: [^{35}S]-munc18-1

3: [^{35}S]-EGFP-munc18-1

4: [^{35}S]-munc18-1$_{R39C}$

5: [^{35}S]-EGFP-munc18-1$_{R39C}$

6: [^{35}S]-munc18-1

7: [^{35}S]-EGFP-munc18-1

8: [^{35}S]-Munc18-1$_{R39C}$

9: [^{35}S]-EGFP-munc18-1$_{R39C}$

Figure 5.4: [^{35}S] Munc18-1 constructs binding to GST-syntaxin 1a-(cyt)

An autoradiogram of and SDS-polyacrylamide gel showing binding of [^{35}S]-munc18-1, [^{35}S]-EGFP-munc18-1, [^{35}S]-munc18-1$_{R39C}$ and [^{35}S]-EGFP-munc18-1$_{R39C}$ to either GST or GST-syntaxin 1a-(cyt)

problems of munc18-1 expression had been overcome, subsequent experiments involved competition of purified munc18-1 with the [^{35}S]-labelled constructs.

5.4 Competition between [^{35}S]-munc18-1 or [^{35}S]-EGFP-munc18-1 and a munc18-1 peptide for binding to GST-syntaxin 1a-(cyt)

Studies in squid axon have shown that short munc18-derived peptides inhibit the interaction between the squid syntaxin (s-syntaxin) and munc18 (s-Sec1) homologues. s-Sec1 has 66 % sequence identity with munc18-1, throughout the entire sequence. A dose response curve of one such peptide (secpep3) revealed a half-maximal inhibition of binding to s-syntaxin at 75μM (Dresbach, Burns et al. 1998). Based on the secpep3 peptide sequence a 24-aminoacid peptide (Figure 5.5) was designed that covered the same region in the mammalian munc18-1 sequence (amino acids 463 – 487) to be used in competitive binding experiments. The binding experiment outlined in Chapter 5.3 was repeated with the inclusion of increasing concentrations (0 – 260 μM) of this munc18-1 peptide or a scrambled peptide, as a control, made up in binding buffer (Appendix 1.11.1), total volume of 50 μl (Figure 5.6 A-B). The results were analysed by SDS PAGE followed by Coomassie Staining, autoradiography and using the phosphorimager, and showed that the munc18-1 peptide did not fully displace the [^{35}S]-munc18-1, removing only the lower band in the doublet. This appears to be the only reported incidence of a difference in behaviour between the two forms of recombinant munc18-1 that are resolved by SDS-PAGE, in that the two bands are not equally displaced from syntaxin 1a by the competing peptide. The experiment was repeated with the concentration of competitive peptide doubled, the highest concentration used being 520 μM, but this also failed fully to compete off the [^{35}S]-munc18-1. A 'scrambled' version of this peptide had no significant effect on the binding of [^{35}S]-munc18-1 to GST-syntaxin 1a-(cyt) (Figure 5.6B). Since the munc18-1 peptide failed to act as a satisfactory competitor for [^{35}S]-munc18-1 this experiment was not extended to [^{35}S]-EGFP-munc18-1. The outcome of this experiment confirmed that there was no alternative to using bacterially

Munc18-1 competitive peptide

RKERISEQTYSRWTPIIKDIME

Scrambled munc18-1 peptide

RFKLWDKFESRTIDTSQPIMREEA

Figure 5.5: Sequences of the munc18-1-derived competitive peptide and the 'scrambled' peptide.

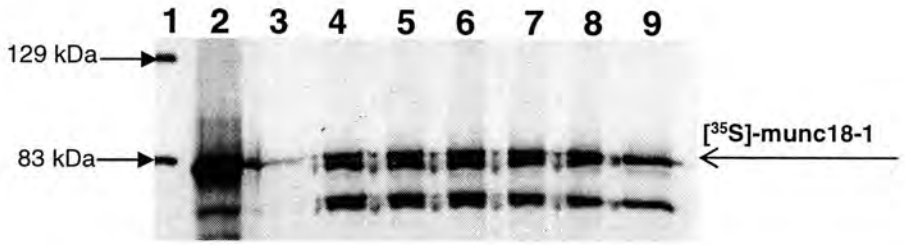

Lane

1: Markers

2: [^{35}S]-munc18-1

3: GST

4: GST-syn 1a-(cyt), 0 peptide 1

5: GST-syn 1a-(cyt), 26 μM peptide 1

6: GST-syn 1a-(cyt), 65 μM peptide 1

7: GST-syn 1a-(cyt), 130 μM peptide 1

8: GST-syn 1a-(cyt), 260 μM peptide 1

9: GST-syn 1a-(cyt), 520 μM peptide 1

Figure 5.6A: Displacement of [^{35}S]-munc18-1 from its complex with GST-syntaxin 1a-(cyt) by a munc18-1 derived peptide

Autoradiogram of bound [^{35}S]-munc18-1 in the presence of increasing concentrations of competitive peptide-1

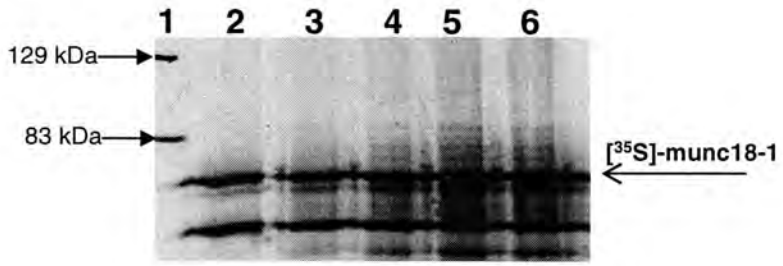

Lane

1: Markers

2: GST-syn 1a-(cyt), 0 peptide-2

3: GST-syn1a-(cyt), 26 μM peptide-2

3: GST-syn 1a-(cyt), 65 μM peptide-2

4: GST-syn1a-(cyt), 130 μM peptide-2

5: GST-syn 1a-(cyt), 260 μM peptide-2

6: GST-syn1a-(cyt), 520 μM peptide-2

Figure 5.6B: Effect of the 'scrambled' munc18-1 derived peptide-2 on binding of [^{35}S]-munc18-1 to GST-syntaxin 1a-(cyt)

Autoradiogram showing binding of [^{35}S]-Munc18-1 in the presence of increasing concentrations of the 'scrambled' peptide -2

expressed unlabelled munc18-1 protein, in order to determine the relative binding affinities of [^{35}S]-munc18-1 for GST-syntaxin 1a-(cyt) and [^{35}S]-EGFP-munc18-1 for GST-ECFP-syntaxin 1a-(cyt).

5.5 Competition between [^{35}S]-munc18-1 or [^{35}S]-EGFP-munc18-1 and bacterially expressed munc18-1-His$_6$ for binding to GST-syntaxin 1a-(cyt) or GST-ECFP-syntaxin 1a-(cyt) respectively

Experiments in AtT20 cells led to the conclusion that FLIM could not be used to study the interaction between immuno-labelled endogenous syntaxin 1a and EGFP-munc18-1, so the interaction between ECFP-syntaxin 1a and EYFP-munc18-1 was investigated in HEK293 cells (Chapter 6), which lack endogenous syntaxin 1a. To validate these experiments it had to be determined whether the addition of GFP variants to both syntaxin 1a and munc18-1 interfered with their interaction, so a comparison was made between the binding affinity of GST-syntaxin 1a-(cyt) for [^{35}S]-munc18-1 with that of GST-ECFP-syntaxin 1a-(cyt) for [^{35}S]-EGFP-munc18-1. Binding experiments (Chapter 5.4) were set up with GST-syntaxin 1a-(cyt) and [^{35}S]-munc18-1 alongside binding experiments with GST-ECFP-syntaxin 1a-(cyt) and [^{35}S]-EGFP-munc18-1 in the presence of increasing concentrations [0 - 3 μM] of bacterially expressed, purified munc18-1-His$_6$, which was diluted in binding buffer (Appendix 1.11.1) to the appropriate concentration (stock munc18-1-His$_6$ = 22 μM, total binding reaction volume = 50 μl, Chapter 2.18.3)

Analysis of bound protein, by Coomassie staining, autoradiography and the phosphorimager as before (Figure 5.7), revealed that the bacterially expressed purified munc18-1-His$_6$ successfully competed with [^{35}S]-munc18-1 for binding to GST-syntaxin 1a-(cyt) and with [^{35}S]-EGFP-munc18-1 for binding to GST-ECFP-syntaxin 1a. This data is shown in a graph (Figure 5.8) of radioactive counts vs. [munc18-1-His$_6$], revealing that as the concentration of unlabelled munc18-1-His$_6$ increased, the amount of bound [^{35}S]-munc18-1 and [^{35}S]-EGFP-munc18-1 decreased. However when these competitive binding experiments were repeated

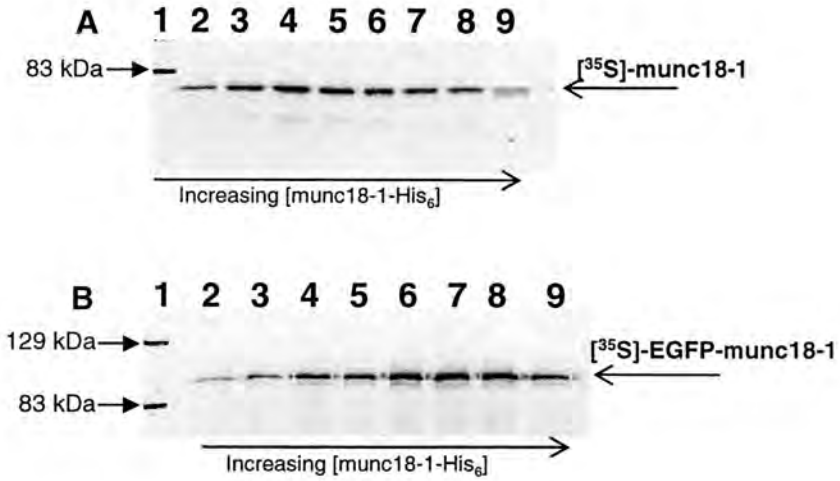

A	B
Lane	**Lane**
1: Markers	1: Markers
2: 0 μM munc18-1-His_6	2: 0 μM munc18-1-His_6
3: 0.06 μM munc18-1-His_6	3: 0.15 μM munc18-1-His_6
4: 0.16 μM munc18-1-His_6	4: 0.37 μM munc18-1-His_6
5: 0.32 μM munc18-1-His_6	5: 0.75 μM munc18-1-His_6
6: 0.48 μM munc18-1-His_6	6: 1.12 μM munc18-1-His_6
7: 0.64 μM munc18-1-His_6	7: 1.50 μM munc18-1-His_6
8: 0.96 μM munc18-1-His_6	8: 2.24 μM munc18-1-His_6
9: 1.28 μM munc18-1-His_6	9: 2.98 μM munc18-1-His_6

Figure 5.7: Competitive binding experiments

A: Autoradiograph of SDS-polyacrylamide gel showing [^{35}S]-munc18-1 bound to GST-syntaxin 1a(cyt) in the presence of increasing concentrations of bacterially expressed munc18-1-His_6

B: Autoradiograph of SDS-polyacrylamide gel showing [^{35}S]-EGFP-munc18-1 bound to GST-ECFP-syntaxin 1a-(cyt) in the presence of increasing concentrations of bacterially expressed munc18-1-His_6

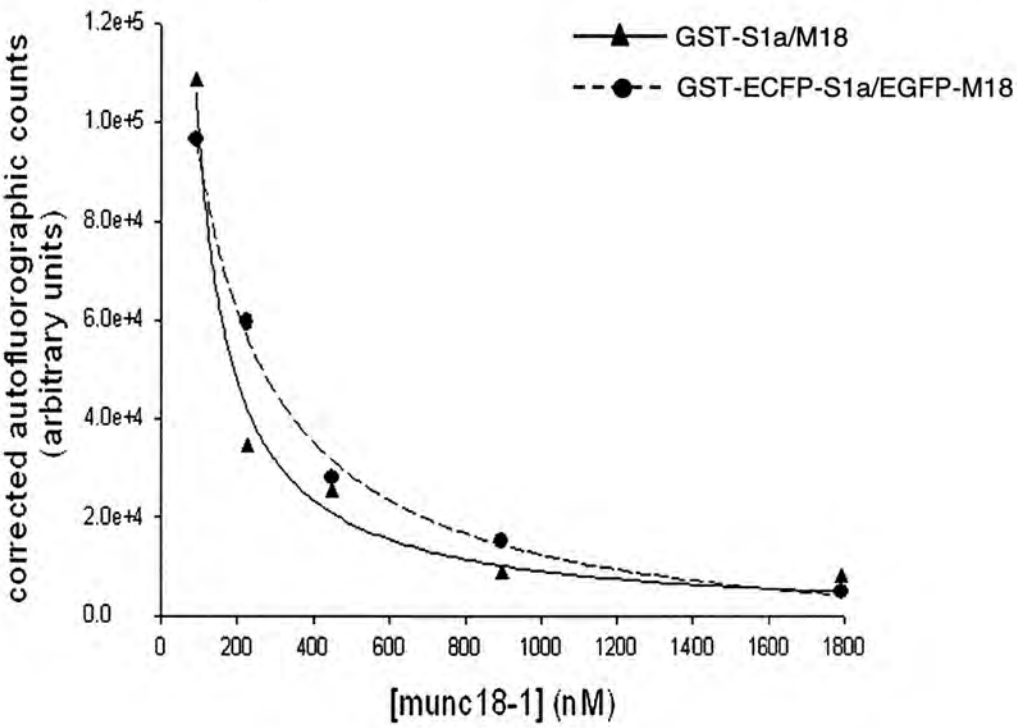

Figure 5.8: Displacement of munc18-1 variants from complex with syntaxin

Triangle trace: Displacement of [^{35}S]munc18-1 from GST-syntaxin 1a-(cyt) by bacterially expressed munc18-1-His6

Circle trace: Displacement of [^{35}S]-EGFP-munc18-1 from GST-ECFP-syntaxin 1a-(cyt) by bacterially expressed munc18-1-His_6

on different occasions, there was a variation in the concentration of the cold munc18-1-His_6 required to successfully compete off the radiolabelled protein, which can be seen in Figure 5.7, which shows the results of competition experiments carried out on different days. One possible explanation for these differences could be that when the cold munc18-1-His_6 was thawed, after storage in aliquots at -80 °C, some of the protein came out of solution. Accordingly, the concentration of the protein remaining in solution was determined before each binding experiment, but measuring the protein concentration does not indicate the stability of the soluble protein, some of which might not have been folded properly, and might therefore not bind to syntaxin. This could result in a higher concentration of the cold munc18-1 being required for successful competition. The munc18-1-His_6 could have been unstable because it was frozen as it came off the column in a buffer containing 250 mM imidazole, thus in future purifications the imidazole should be removed before freezing the munc18-1-His_6. Furthermore, as the concentration of munc18-1-His_6 was increased from zero, there was an initial enhancement of radiolabelled protein binding before it was competed off. This effect is thought to be an artefact; it could be due to the presence in the *in vitro* transcription/translation reaction mix of some component with a high affinity and low binding capacity for the radiolabelled munc18s, which sequesters some of the protein making it unavailable for binding to syntaxin 1a. When a small amount of cold munc18-1-His_6 was added to the reaction it would displace the radiolabelled munc18-1 from this factor, making it available to syntaxin and resulting in the initial enhancement of binding. Curiously, this effect appeared to increase with successive binding experiments performed, where higher concentrations of cold munc18-1-His_6 were required to overcome this enhancement, which could be a result of an increase in age of the *in vitro* transcription/translation mixes used. Even with such variations seen between experiments done on different days, comparisons could be made between the tagged and untagged proteins' binding affinities done on the same day.

A convenient way of treating binding data, when the concentration of a competitive inhibitor can be varied but the concentration of the binding component cannot, is to use the Dixon plot (Dixon 1953). This was originally devised for displaying enzyme inhibition data, but is equally applicable to simple ligand binding. The theory is given in Appendix 3. In enzyme assays the total enzyme concentration is usually much less than the concentration of substrate. The situation in the experiments described here is different in that the amount of ligand used is much less than the amount of protein binding it – it is calculated that each binding mix contains approximately 1 pmol of GST-syntaxin 1a-(cyt) and 0.06 pmol of [^{35}S]-munc18-1; however the equation is still valid (see Appendix 3). A plot of the reciprocal of the amount of bound ligand ([^{35}S]-munc18-1, in this case) against the competitor (unlabelled munc18-1) should be a straight line, where:

$$\frac{1}{B} = \frac{L_T + B_{max} + K_D}{B_{max}.L_T} + [I]\frac{K_D}{K_I.B_{max}.L_T}$$

This predicts that a plot of 1/B against [I] will be a straight line of slope $K_D/K_I.B_{max}.L_T$. In this expression B_{max} is the concentration of GST-syntaxin 1a-(cyt), which is the same in each experiment; and L_T is the amount of [^{35}S]-munc18-1, which is the same in each titration but may vary between titrations, depending on the efficiency of the transcription/translation system. Assuming that L_T is approximately constant, the relative slopes of the plots will depend on K_D/K_I, the ratio of dissociation constants of [^{35}S]-munc18 (or [^{35}S]-EGFP-munc18-1) and munc18-His$_6$ from GST-syntaxin 1a-(cyt) (or GST-ECFP-syntaxin 1a-(cyt)). For binding of munc18-1 the value of K_D/K_I should be 1; the ratio of the slopes of the plots gives the value of K_D/K_I for binding of EGFP-munc18 to ECFP-syntaxin 1a, which is also close to 1.

Two Dixon plots were drawn for competitive binding experiments done on two separate occasions (Figures 5.9 and 5.10), one of which contained all the binding data obtained in each competition and one in which the binding data was normalised so that each data point

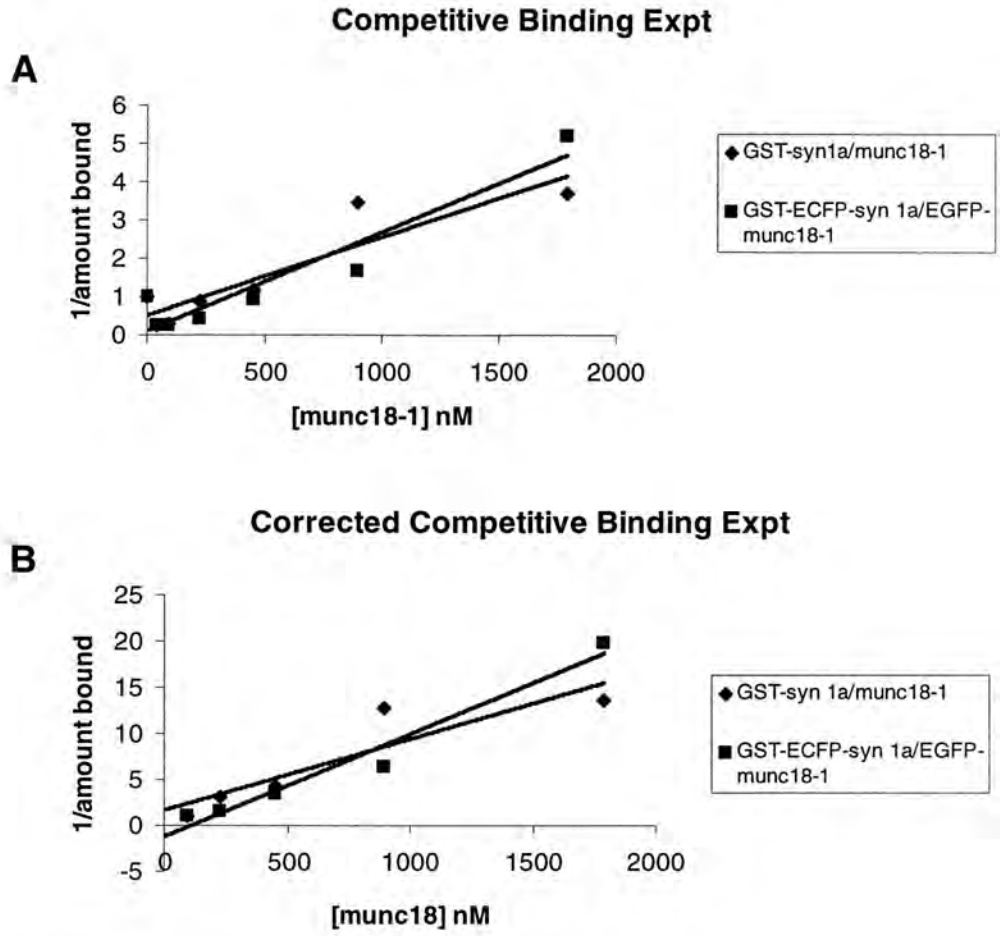

Figure 5.9: Dixon plots of competitive binding experiments

A: Dixon plot of all the data showing competition

1. between [^{35}S]-munc18-1 and munc18-1-His_6 for binding to GST-syntaxin 1a-(cyt), and

2. between [^{35}S]-EGFP-munc18-1 and munc18-1-His_6 for binding to GST-ECFP-syntaxin1a –(cyt)

B: Dixon plot of the dame data, but normalised to the maximal value for radiolabelled munc18-1 binding to their respective syntaxin 1a-coupled beads

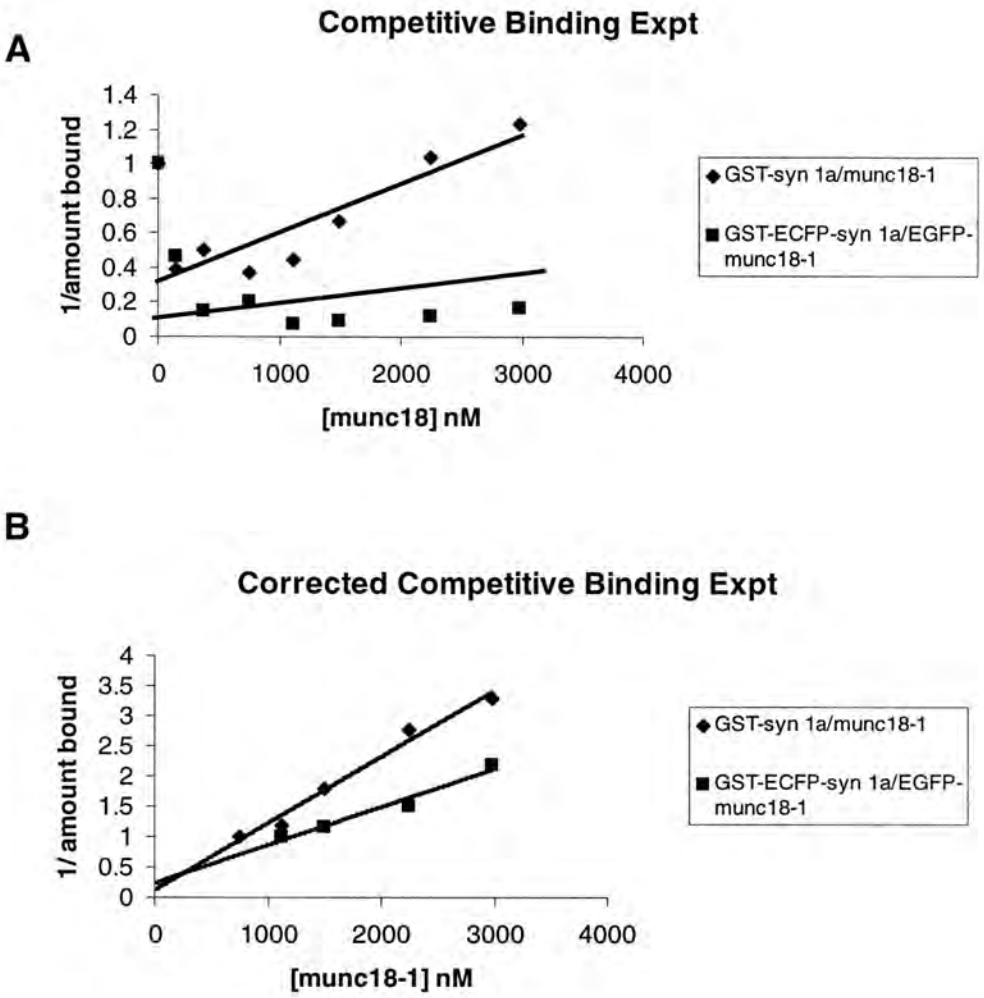

Figure 5.10: Dixon plots of competitive binding experiments

A: Dixon plot of all the data showing competition

1. between [^{35}S]-munc18-1 and munc18-1-His$_6$ for binding to GST-syntaxin 1a-(cyt), and

2. between [^{35}S]-EGFP-munc18-1 and munc18-1-His$_6$ for binding to GST-ECFP-syntaxin1a –(cyt)

B: Dixon plot of the dame data, but normalised to the maximal value for radiolabelled munc18-1 binding to their respective syntaxin 1a-coupled beads

was expressed as a percentage of the point where the highest binding of radiolabelled protein was detected. Figure 5.9A shows all the binding data obtained in the two competition experiments: the slopes of the plots for [35S]-munc18-1 binding to GST-syntaxin 1a-(cyt) and [35S]-EGFP-munc18-1 binding to GST-ECFP-syntaxin 1a-(cyt) were similar (gradient = 0.002 and 0.0026 respectively). When the binding data were normalised (Figure 5.9B) both slopes are again very similar (gradient = 0.0077 and 0.011 respectively) suggesting that the relative binding affinities between the tagged and the untagged proteins are not significantly different. Dixon plots were drawn for competitive binding experiments done at later date (Figure 5.10) and although the enhancement of radiolabelled protein binding was found to be much greater, when the data were normalised as before (Figure 5.9B) the gradients of these lines were similar. To compare the competition experiments done on different days the gradients from the normalised Dixon plots were averaged (Figure 5.11) revealing that the gradient of the GST-syntaxin 1a-(cyt)/munc18-1 competition was 0.010±0.0012 and the gradient of the GST-ECFP-syntaxin 1a-(cyt)/EGFP-munc18-1 was 0.0045±0.006, which were found to be not significantly different (P = 0.1918, t-test). From these experiments it was concluded that the addition of fluorescent fusions to both syntaxin 1a-(cyt) and munc18-1 had no significant effect on their interaction.

5.6 Comparison between the binding of [^{35}S]-EGFP-munc18 and its mutants; [^{35}S]-EGFP-$_{R39C}$, EYFP-munc18-1$_{S306E:S313E}$ and EYFP-munc18-1$_{R39C:S306E:S313E}$ to GST-ECFP-syntaxin 1a-(cyt)

As *in vitro* controls for experiments in HEK293 cells (Chapter 6), the binding of several other EGFP/EYFP-munc18-1 mutants to GST-ECFP-syntaxin 1a-(cyt) was studied. These experiments were carried out by Dr Rory Duncan and Dr David Apps, using constructs and proteins described here. A plate based assay (Chapter 2, (Craig, Evans et al. 2003) was used in which GST-ECFP-syntaxin 1a-(cyt) was immobilised on glutathione-coated plates and incubated with *in vitro* translated [^{35}S]munc18-1 variants: EGFP-munc18-1, EGFP-

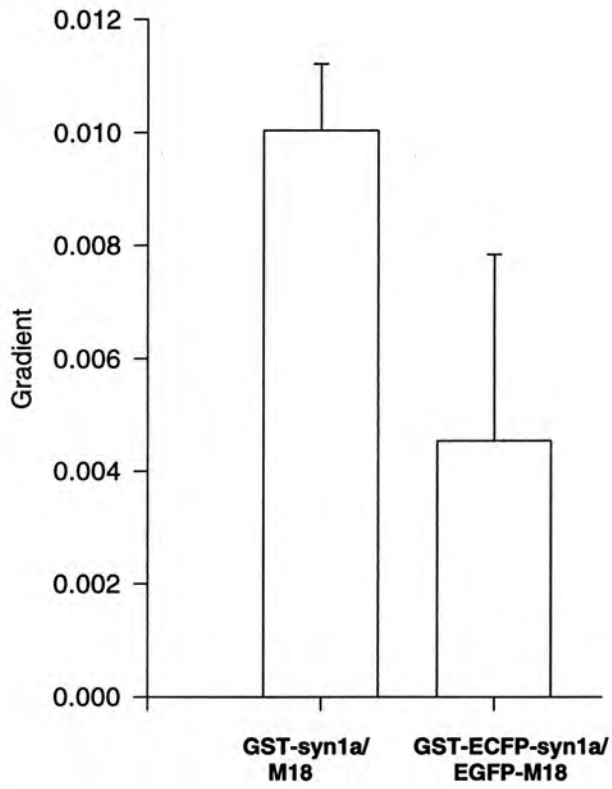

Figure: 5.11: Dixon plot gradients from the competitive binding experiments

Dixon plots were drawn for each of the GST-syntaxin 1a-(cyt)/munc18-1 and GST-ECFP-syntaxin 1a-(cyt)/EGFP-munc18-1 competition experiments and the gradients from the plots averaged to compare their relative binding experiments (n = 3 for each experiment)

munc18-1_{R39C}, the phosphomimetic double mutant EYFP-munc18-$1_{S306E:S313E}$ and the triple mutant EYFP-munc18-$1_{R39C:S306E:S313E}$.

These binding experiments revealed (Figure 5.12) that the presence of the R39C mutation in munc18-1 resulted in an approximately 8-fold reduction in binding to GST-ECFP-syntaxin 1a-(cyt). Binding of the phosphomimetic S306E:S313E munc18-1 mutant to GST-ECFP-syntaxin 1a-(cyt) was stronger than that of the R39C mutant, but when both the R39C and phosphomimetic mutations are present in munc18-1, their effects are additive, resulting in the EYFP-munc18-$1_{R39C:S306E:S313E}$ mutant having negligible binding to GST-ECFP-syntaxin 1a-(cyt).

5.7 Summary

This chapter reports the use of *in vitro* GST-pull-down assays to investigate the syntaxin 1a – munc18-1 bimolecular complex and to determine whether the fusion of GFP variants to the N-terminus of these proteins has any effect on their interaction. In initial experiments the binding of various munc18-1 constructs to either GST-syntaxin 1a-(cyt) or GST-ECFP-syntaxin 1a-(cyt) was investigated. As discussed earlier, several corrections had to be applied to the data before direct comparisons of the munc18-1 variants could be made. After these corrections had been applied, the binding data revealed that there were differences in the affinity of the different munc18-1 constructs for syntaxin 1a: the binding of the EGFP-munc18-1_{R39C} mutant was barely detectable above background, and the phosphomimetic mutants also showed reduced binding to syntaxin 1a. However when comparisons were made between experiments done with different preparations of [^{35}S]-munc18, variations were seen in the absolute amount of munc18 bound. To try and overcome this variability it was decided to carry out competition assays to determine the relative binding affinities of the untagged syntaxin 1a and munc18-1 in comparison with the GFP-tagged fusion proteins. Because of problems in the production of bacterially expressed munc18-1, munc18-1-derived peptides were initially employed to compete with munc18 itself in binding to

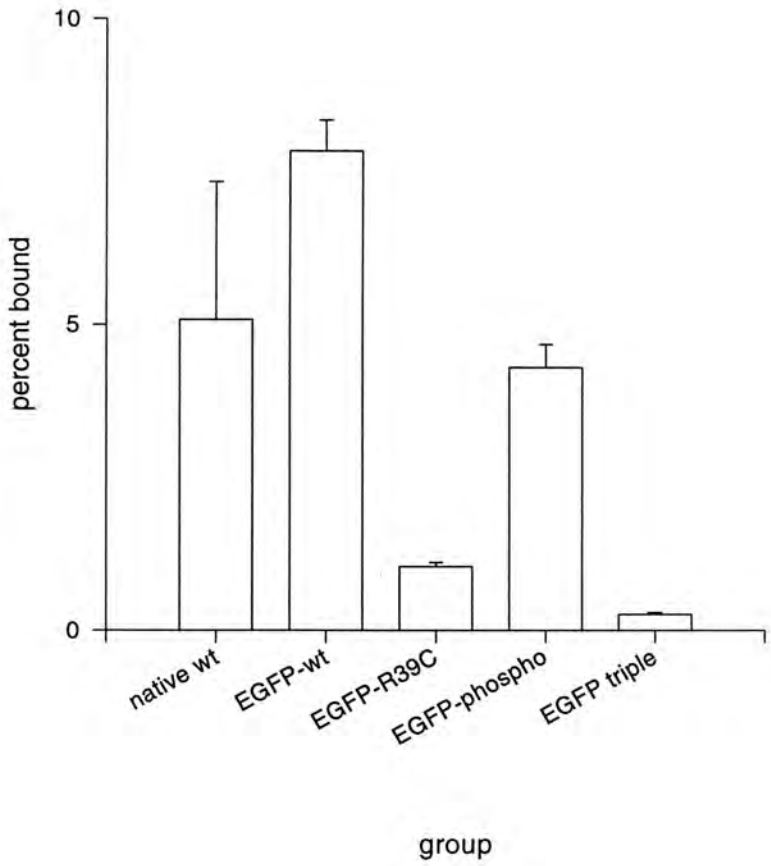

Figure 5.12: Comparison between the various [^{35}S]-EGFP/EYFP-munc18-1 constructs binding to GST-ECFP-syntaxin 1a-(cyt)

A plate based assay (Craig et al, 2004) was used to investigate the binding of a range of different [^{35}S]-EGFP/EYFP-munc18-1 mutants to GST-ECFP-syntaxin 1a-(cyt), where the percentage of bound radiolabelled protein with respect to total radiolabelled protein was calculated (n = 8 for each experiment).

syntaxin 1a. The corresponding peptide had been previously shown to inhibit the binding of the squid homologue of munc18 to squid syntaxin with a Ki of about 100 μM, but in our assay the munc18-1 competitive peptide was unsuccessful in competing off the [^{35}S]-munc18-1 from GST-syntaxin 1a-(cyt), even at concentrations above 500 μM. Only one of the forms of munc18-1 was successfully competed off, which is unusual since both forms of munc18-1 have been found to behave identically in previous studies. A possible explanation that different munc18s have been shown to bind to their respective syntaxins in different ways, therefore s-Sec1 may interact with s-syntaxin differently from munc18-1 and syntaxin 1a. It is assumed that the two bands within the doublet arise through proteolysis, and therefore that the two sub-forms differ by a short stretch of the aminoacids at the N- or C-terminal. The syntaxin-competitive peptide lies within the munc18-1 sequence (aminoacids 463 – 487)

With the availability of bacterially expressed munc18-1-His_6 from the laboratory of Prof Alan Morgan and the development of a protocol for the expression and purification of munc18-1-His_6, experiments could be done using cold munc18-1-His_6 as the competitor. These revealed that the addition of the GFP tags to both syntaxin 1a and munc18-1 had no significant effect on their interaction. However this assay was very time-consuming so for a comparison between the binding, to syntaxin 1a, of a range different munc18-1 mutants a plate based assay (Craig, Evans et al. 2003) was used. This assay was chosen since it is much quicker, potentially more reproducible and a large number of samples can be processed at the same time. It was not used to compare the binding of munc18-1 to syntaxin 1a and EGFP-syntaxin 1a because it is not possible to quantitate the amount of native GST-syntaxin immobilized in each well, making the comparison between two different syntaxin variants difficult. These plate based experiments revealed that introduction of either the R39C or the phosphomimetic mutation resulted in similar reduction in the binding affinity of munc18-1 for syntaxin 1a and that these mutations are additive resulting in an even lower affinity for syntaxin 1a (Figure 5.12). These results however, do not indicate the relative Kd

of the various mutants because in such experiments the major contributing factor the Kd of an interaction is the off rates of the protein. Therefore in the case of these mutants, if the binding affinity is reduced by a factor of 100, then the k_{off} time is greatly reduced so that the proteins would dissociate during the washing, resulting in an underestimation of weak binding in the plate based assay.

Although the plate-based assay has the advantages over the more traditional GST-pull-down assay of high speed, reproducibility and the large number of data points that can be generated it does have some disadvantages. In this assay only total radioactive counts (bound and unbound) are measured and *in vitro* transcription/translation produces not only full length protein, but also some truncated forms. These may bind differently to the immobilised protein and in this method, which measures only free and bound counts, it is impossible to distinguish between truncations and full-length proteins. In contrast the full-length protein is quantified in the GST-pull-downs, by measuring a specific band on a gel. Such *in vitro* binding experiments provide valuable information, but the relevance of such data to cellular conditions can be disputed. In the case of syntaxin 1a and munc18-1 *in vitro* binding experiments, only the cytoplasmic domain of syntaxin 1a is used because it is difficult to express full length syntaxin 1a in bacteria. The transmembrane domain of syntaxin 1a is important for some of its protein interactions (Lewis, Dong et al. 2001), so the removal of this domain may alter syntaxin 1a's binding properties. Furthermore, in cells syntaxin 1a is associated with membranes, however, in these *in vitro* binding experiments syntaxin 1a has no transmembrane domain and no membranes are present, which may also have implications in syntaxin 1a's binding properties. Finally, the ionic conditions may be rather different, in the *in vitro* experiments, from those within cells. Although the *in vitro* approach can be justified as a basis for comparing the affinities of different fusion proteins under the same conditions, and indeed is an essential control for the *in vivo* studies, it must be borne in mind that the findings may not be quantitatively applicable to intracellular interactions between munc18 and syntaxin 1a.

Chapter 6

Localisation of the syntaxin 1a – munc18-1 complex in cells

6.1 Introduction

Syntaxin 1a can exist in at least two conformational states: the 'open' conformation, in which it can interact with other SNAREs to form the ternary complex that leads to membrane fusion, and the 'closed' conformation in which it forms a bimolecular complex with munc18-1 and is thus sequestered from binding to the other SNARE proteins (Misura, Scheller et al. 2000; Margittai, Fasshauer et al. 2003). For exocytosis to occur the syntaxin 1a – munc18-1 complex must be dissociated; however the molecular mechanism by which this occurs remains unclear.

Exocytosis in bovine adrenal chromaffin cells has been shown to be directly regulated by phorbol ester (PE)/diacylglycerol-mediated protein kinase C (PKC) phosphorylation of munc18-1 (Barclay, Craig et al. 2003). Munc18-1 phosphorylation on serines 306 and 313 results in a reduced affinity for syntaxin 1a and alters the kinetics of catecholamine release. Another residue, arginine 39 (R39), has been shown to make an electrostatic interaction with syntaxin 1a and with other amino acids within each of the domains of munc18-1, thereby stabilising the syntaxin 1a – munc18-1 bimolecular complex (Misura, Scheller et al. 2000). If R39 is mutated to cysteine (R39C) it can no longer participate in these important interactions and this mutant also has a reduced affinity for syntaxin 1a, resulting in altered release kinetics, such as an increase in the rate of opening and closing of the fusion pore, which could lead to an increase in the rate of neurotransmitter release. This idea was further supported in *Drosophila*, in which the Rop F3 mutant (R50, equivalent to R39 in munc18-1) produced an increase in postsynaptic current. Furthermore, the effect of expression of munc18-1_{R39C} in cells is identical to the effect of activation of protein kinase C (Wu, Littleton et al. 1998; Fisher, Pevsner et al. 2001).

Immunocytochemical investigation of the localisation of endogenous syntaxin 1a in rat phaeochromocytoma (PC12) cells, using monoclonal anti-syntaxin 1a and confocal laser scanning microscopy, revealed intense staining at the cell periphery, with significant staining of intracellular structures (Jennifer Greaves, personal communication). In cells treated with

100nM phorbol myristoyl acetate (PMA) for 15 minutes there was significant redistribution of syntaxin 1a from intracellular structures to the plasma membrane. However, whether the phorbol ester modulation of exocytosis is mediated through PKC or munc13s remains controversial (Rhee, Betz et al. 2002; Barclay, Craig et al. 2003). Therefore to further elucidate the molecular mechanisms responsible for the PMA-mediated translocation of syntaxin 1a, confocal laser scanning microscopy (CLSM), in conjunction with time-correlated single photon counting (TCSPC)-based fluorescence lifetime imaging microscopy, was used to quantify localisation and fluorescence resonance energy transfer (FRET) between fluorescent protein constructs. Most of these experiments were performed in HEK293 cells, chosen because they do not express synaptic exocytotic proteins, such as the SNAREs, munc18, and munc13s and therefore the interpretation of the images was not complicated by possible interaction of the transfected fluorescent proteins with such endogenous proteins (Groffen, Brian et al. 2004). Some experiments were also carried out on AtT-20 (mouse anterior pituitary corticotroph) cells, in which endogenous syntaxin 1a could be detected immunologically.

6.2 AtT20 cells transfected with EGFP-munc18-1 and immuno-stained for native syntaxin 1a

AtT20 cells were plated out on glass coverslips in 12-well dishes (Chapter 2.22) and incubated overnight before transfection with 1 μg of EGFP-munc18-1 or plasmid DNA using Lipofectamine 2000 (Chapter 2.22). The cells were incubated for 48 h before being fixed with 4 % (w/v) paraformaldehyde then either mounted on microscope slides in Mowiol immediately, or immunostained using commercial monoclonal anti-syntaxin 1a (anti-HPC-1) (Chapter 2.23) before CLSM.

6.2.1 Co-localisation analysis between EGFP-munc18-1 or and native syntaxin 1a

Images were acquired of AtT-20 cells transfected with EGFP-munc18-1, and immuno-stained for endogenous syntaxin 1a. In cells transfected with EGFP-munc18-1 alone the heterologous EGFP-munc18-1 was distributed throughout the cytoplasm of the cell (Figure 6.1).

To investigate whether the EGFP-munc18-1 co-localised with native syntaxin 1a an image stack was acquired of AtT20 cells transfected with EGFP-munc18-1 and immuno-stained with monoclonal anti-syntaxin 1a and Alexa-546-conjugated second antibody, using multi-tracking (Chapter 2.24). The image data were deconvoluted using Huygens II software and the relative amount of co-localisation quantified in a 3D pixel-by-pixel manner using Imaris Colocalisation software (Chapter 2.24). These images revealed (Figure 6.2) that 52.4±6.74 % of EGFP-munc18-1 colocalised with 13.7±2.09 % of native syntaxin 1a, located throughout the cells. There was also a large fraction (47.6±8.83 %) of EGFP-munc18-1 not co-localised with the syntaxin 1a, presumably because endogenous munc18-1 interacted with the endogenous syntaxin 1a, and the overexpression of EGFP-munc18-1 resulted in an excess of EGFP-munc18-1 over syntaxin 1a within the cell.

6.2.2 FRET/FLIM of EGFP-munc18-1 and endogenous syntaxin 1a in AtT-20 cells

Since the preceding analysis revealed co-localisation of exogenous EGFP-munc18-1 and endogenous syntaxin 1a in AtT-20 cells, FLIM was used to quantify FRET in order to determine whether the proteins were interacting, by measuring the fluorescent lifetime of the EGFP-munc18-1 in the presence and absence of immunostained native syntaxin 1a. If the proteins were interacting a decrease in the fluorescence lifetime of the EGFP-munc18-1 should be seen compared to non-immunostained control samples. Imaging was performed (Chapter 2.25), but no FRET was detected. There were several possible reasons for this, for

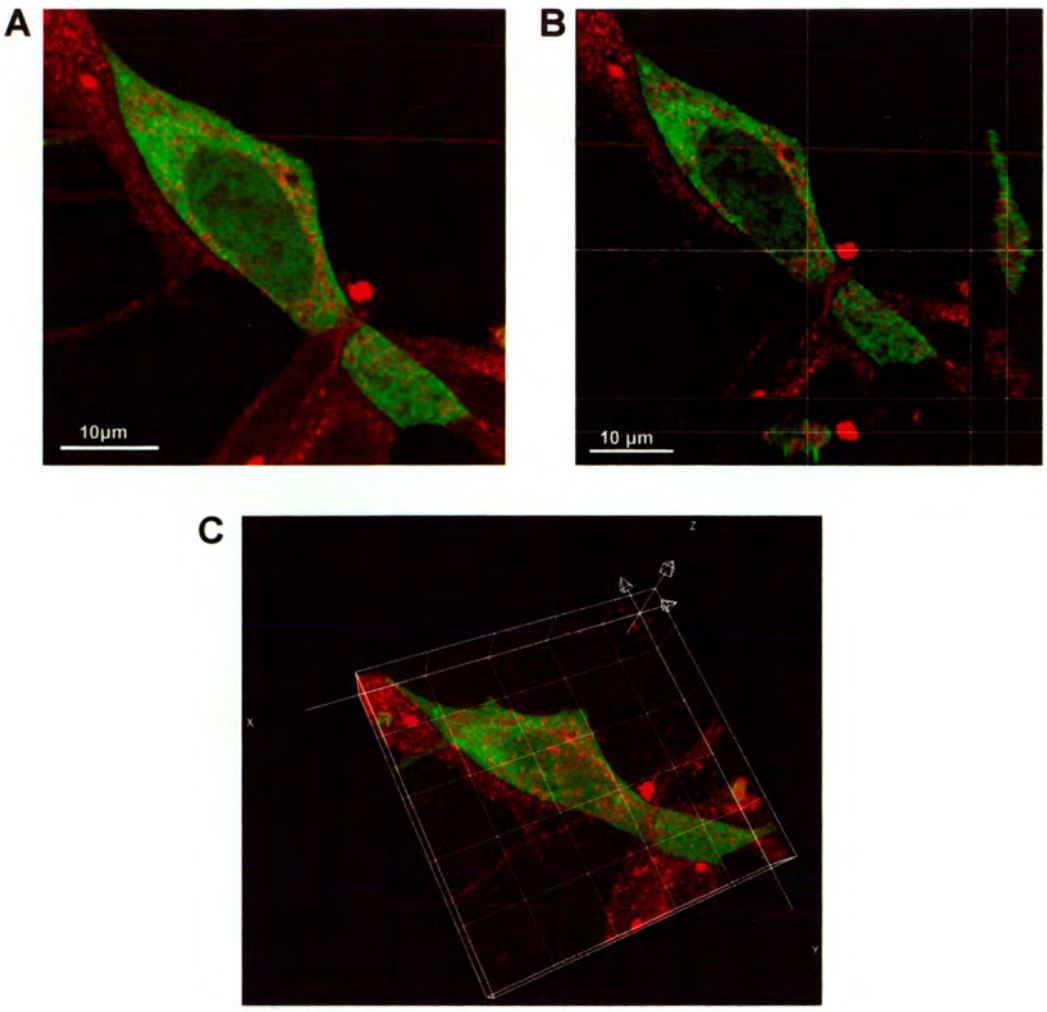

Figure 6.1: AtT20 cells transfected with EGFP-munc18-1 and immuno-stained for endogenous syntaxin 1a

Paraformaldehyde fixed AtT20 cells were imaged by CLSM followed data deconvolution using Huygens II software. EGFP-munc18-1 is shown in green and native syntaxin 1a is shown in red

A: middle slice of the z-stack image

B: orthoslicer view of the image stack showing the middle slice and looking at the image in XY, YZ and XZ side views

C: 3D reconstruction of the image stack with a 10 µM grid; see attached CD for accompanying movie

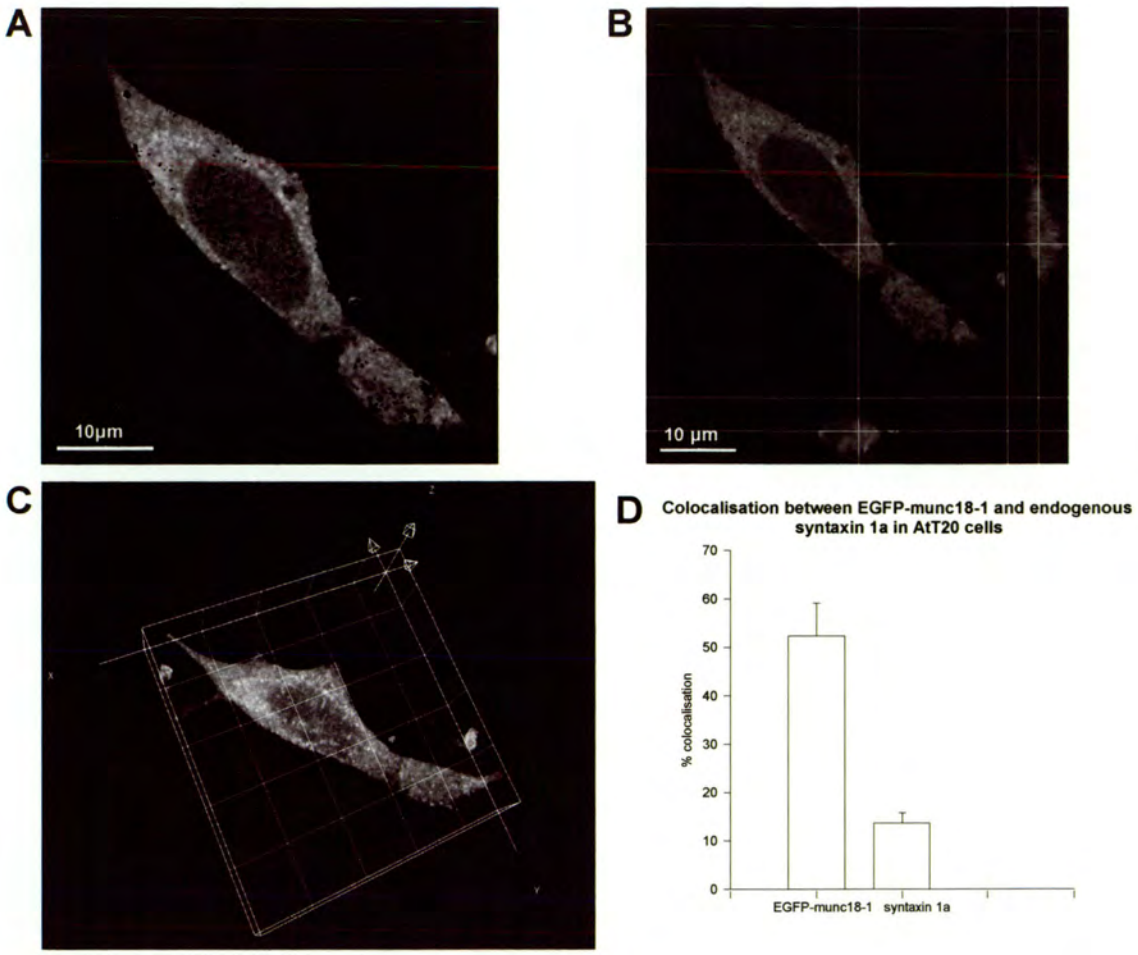

Figure 6.2: AtT20 cells transfected with EGFP-munc18-1 and immuno-stained for endogenous syntaxin 1a

Colocalisation analysis of the AtT20 cell transfected with EGFP-munc18-1 and immuno-stained for endogenous syntaxin 1a shown in figure 6.1. Quantification was on a 3D pixel-by-pixel basis, using Imaris Colocalisation software, where pixels containing both EGFP-munc18-1 and native syntaxin were extracted and displayed.

A: middle slice of the image z-stack

B: orthoslicer view of the image stack

C: 3D reconstruction of the image stack with a 10 µM grid, see accompanying CD for movie

D: Histogram of the amount of both EGFP-munc18-1 (52.4±6.74 %) and endogenous syntaxin 1a (13.7±2.09 %) colocalising with each other

example, Alexa546 became photo-bleached quickly resulting in a low number of photons being transferred, making it difficult to acquire FLIM data. Furthermore in a recent publication (Rickman and Davletov 2005) it was shown that the monoclonal antibody HPC-1 does not recognise syntaxin 1a when it is in complex with munc18-1, therefore no FRET will occur between the antibody-conjugated fluorophore and the EGFP fused to munc18-1. Since, no FRET could be detected, and due to the pronounced photo-bleaching when using immuno-stained syntaxin 1a, it was decided to cotransfect fluorescently-labelled munc18-1 with ECFP-syntaxin 1a. In addition, EGFP is a poor FRET acceptor for ECFP fluorescence resonance energy, so the EGFP was replaced by EYFP as detailed in Chapter 4.9.2. It was also decided to investigate the interaction between these proteins in HEK293 cells instead of AtT20 cells so that the interactions could be investigated without an endogenous protein background, and because HEK293s have a high transfection efficiency.

6.3 HEK293 cells transfected with ECFP-syntaxin 1a, EYFP-munc18-1 or EYFP-munc18-1_{R39C}

HEK293 cells were plated out on glass coverslips in the same way as the AtT20 cells and were transfected after 24h with 1µg DNA encoding, ECFP-syntaxin 1a, EYFP-munc18-1 or EYFP-munc18-1_{R39C}, using Lipofectamine 2000 (Chapter 2.22). Following transfection the cells were incubated for 48 h before fixing with 4 % (w/v) buffered paraformaldehyde and mounting in Mowiol (Chapter 2.22.1), then stored at 4 °C before CLSM analysis.
The subcellular distribution of each of the transfected constructs was investigated, and it was found that ECFP-syntaxin 1a was localised throughout the cell and on the plasma membrane (Figure 6.3), whereas the EYFP-munc18-1 and EYFP-munc18-1_{R39C} were distributed throughout the cell with a large fraction in the cytoplasm.

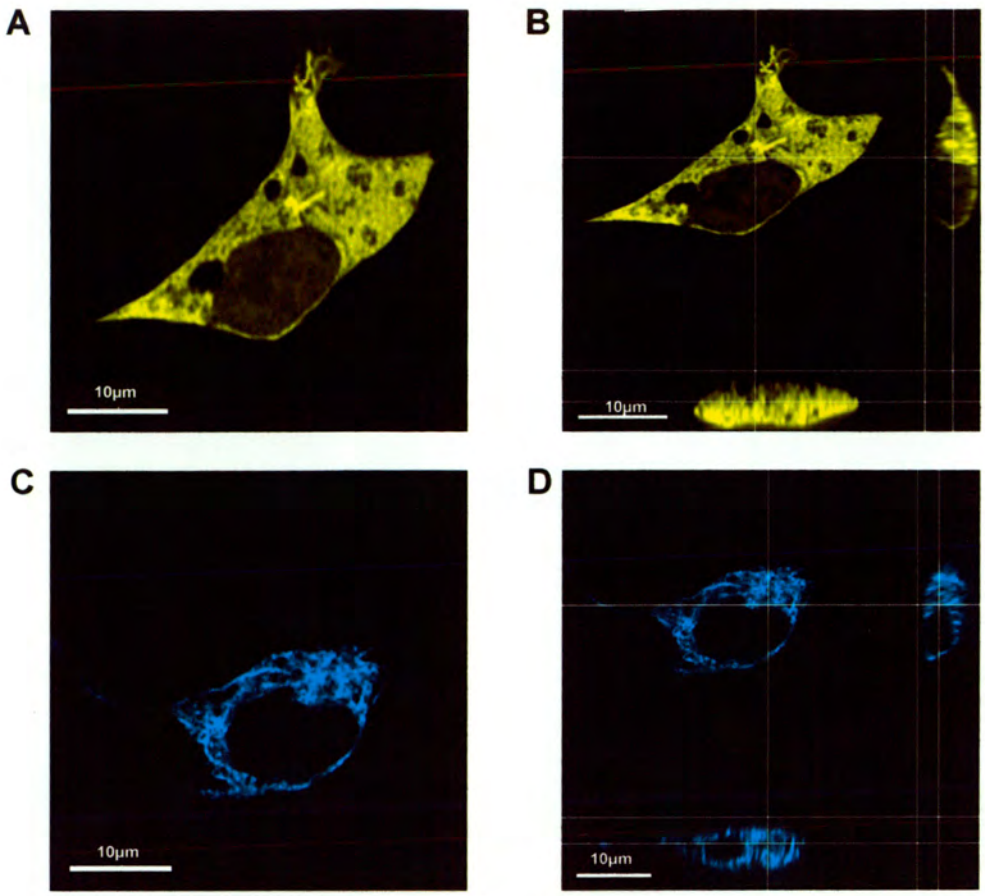

Figure 6.3: HEK293 cells transfected either with EYFP-munc18-1 or with ECFP-syntaxin 1a

Paraformaldehyde-fixed HEK293 cells were imaged by CLSM and deconvoluted using Huygens II software

A: middle slice of an image stack of a HEK293 cell transfected with EYFP-munc18-1

B: orthoslicer view of a HEK293 cell transfected with EYFP-munc18-1

C: middle slice from an image stack of a HEK293 cell transfected with ECFP-syntaxin 1a

D: orthoslicer view of a HEK293 cell transfected with ECFP-syntaxin 1a

6.3.1 HEK293 cells cotransfected with ECFP-syntaxin 1a and either EYFP-munc18-1 or EYFP-munc18-1_{R39C}

For co-transfected cells, ECFP-syntaxin 1a was transfected together with either EYFP-munc18-1 or EYFP-munc18-1_{R39C}, with 0.5 μg of each of the constructs per well. Following transfection images were acquired using a multi-tracking, sequential scanning protocol. The image data were deconvolved (Chapter 2.24) followed by 3D reconstruction.

In HEK293 cells cotransfected with ECFP-syntaxin 1a and EYFP-munc18-1 (Figure 6.4) both of the proteins were seen in puncta on the plasma membrane, suggesting that their interaction may cause redistribution from the predominantly intracellular location that each exhibited when expressed on its own.

In contrast, however, ECFP-syntaxin 1a and EYFP-munc18-1_{R39C} proteins appeared to be located in intracellular structures (Figure 6.5) implying that the presence of the R39C mutation in munc18-1 resulted in the intracellular trapping of both proteins. Since ECFP-syntaxin 1a and the EYFP-munc18-1s had overlapping distributions within the HEK293 cells this was quantified by colocalisation analysis.

6.3.2 Colocalisation analysis of HEK293 cells cotransfected with ECFP-syntaxin 1a and either EYFP-munc18-1 or EYFP- munc18-1_{R39C}

The images for co-localisation analysis were acquired by 3D pixel-by-pixel colocalisation of deconvoluted, CLSM data (Chapter 2.24) and the amount of syntaxin 1a colocalising with the different munc18 1 variants was quantified, since the syntaxin 1a is constant throughout all the experiments performed. The co-localisation analysis (Figure 6.6) revealed that 52±8.81 % of the ECFP-syntaxin 1a co-localised with the EYFP-munc18-1. Co-localisation data in isolation indicated the percentage of each protein interacting with each other, but did not indicate where in the cells the proteins were colocalising, so as well as obtaining whole-cell data; colocalisation was examined in each individual section throughout the cell. However problems with this method of analysis became apparent, where during image

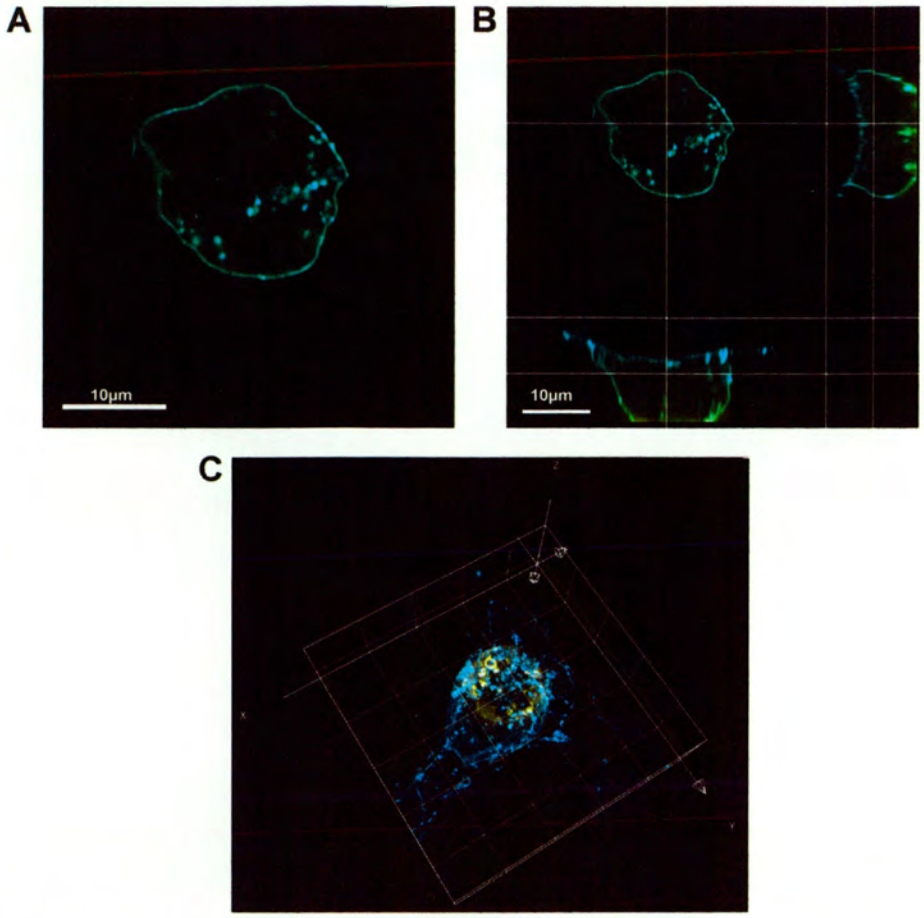

Figure 6.4: HEK293 cell cotransfected with ECFP-syntaxin 1a and EYFP-munc18-1

Paraformaldehyde-fixed HEK293 cells were imaged by CLSM followed by deconvolution using Huygens II software. ECFP-syntaxin 1a is displayed in blue and EYFP-munc18-1 is shown in yellow

A: middle slice through the image stack

B: orthoslicer view

C: 3D reconstruction of the image stack, with a 10 µM see accompanying CD for movie

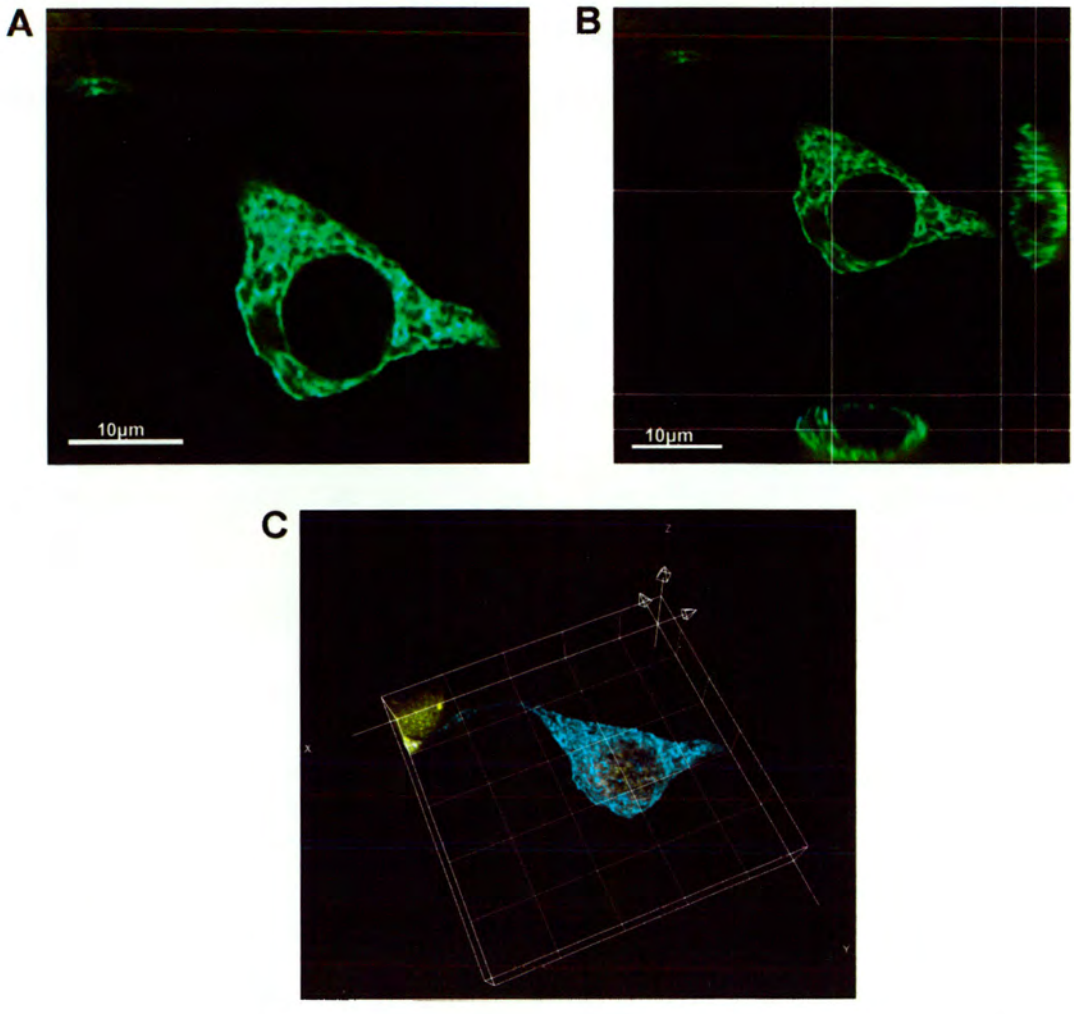

Figure 6.5: HEK293 cell cotransfected with ECFP-syntaxin 1a and EYFP-munc18-1$_{R39C}$

HEK293 cells were fixed in paraformaldehyde before being imaged by CLSM followed by deconvolution using Huygens II software. ECFP-syntaxin 1a is shown in blue and EYFP-munc18-1$_{R39C}$ in yellow.

A: middle slice of the image stack

B: orthoslicer view of the image stack

C: 3D reconstruction of the image stack, with a 10 µM grid; see accompanying CD for the appropriate movie

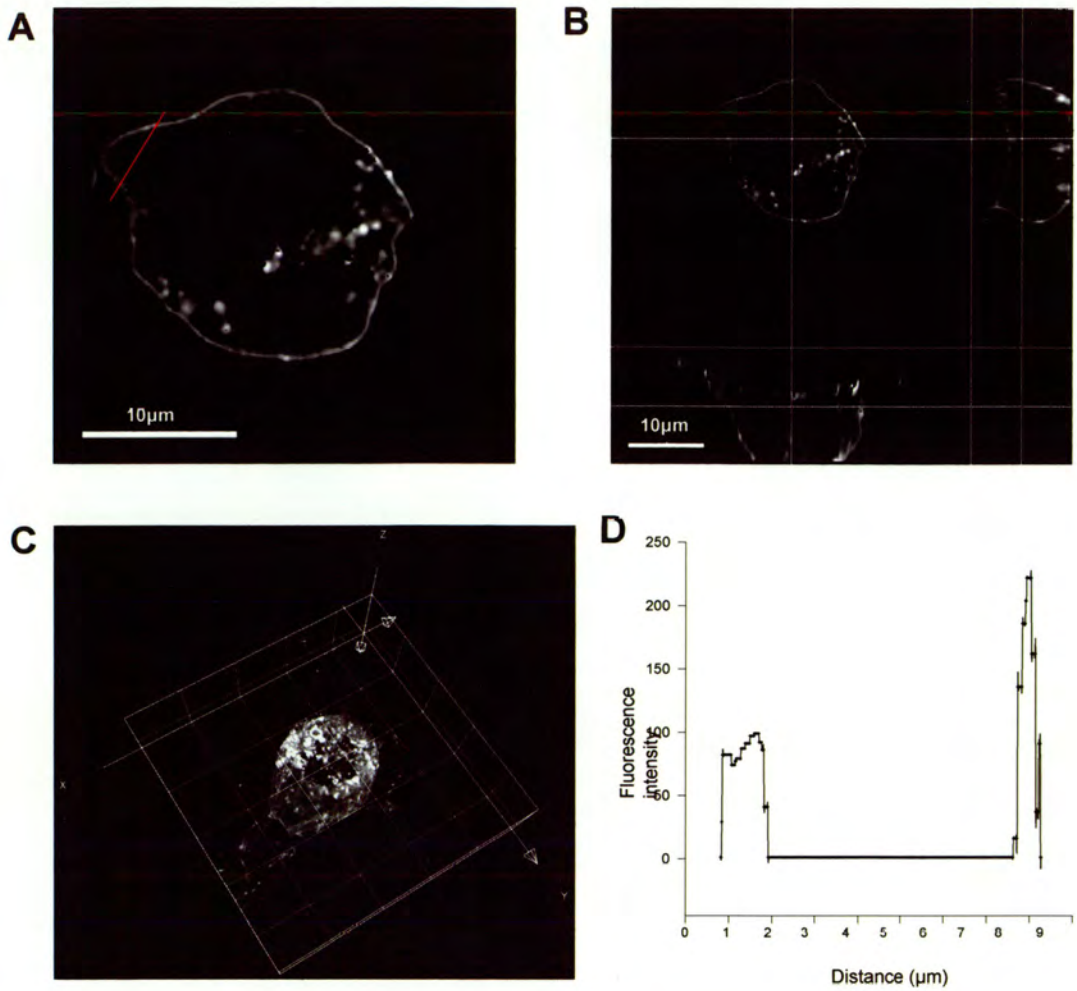

Figure 6.6: Colocalisation analysis of a HEK293 cell cotransfected with ECFP-syntaxin 1a and EYFP-munc18-1

Colocalisation was quantified in a 3D pixel-by pixel manner using Imaris Colocalisation software

A: colocalisation between ECFP-syntaxin 1a and EYFP-munc18-1 in the middle section of the image stack. The red line illustrates how the lines were drawn to investigate where the colocalisation was localised within the cell

B: orthoslicer view of the colocalisation between ECFP-syntaxin 1a and EYFP-munc18-1

C: 3D reconstruction of the image showing all the pixels in which colocalisation was dectected with a 10 µM grid, see accompanying CD for the movie

D: plot of the distribution of colocalisation between the two proteins, within a line drawn through the middle section of the image stack covering two membranes and the cytoplasm (see Figure 6.6A).

acquisition the fluorescent proteins became bleached toward the top of the cell resulting in a reduction in the signal obtained, so that in a plot of colocalisation against confocal section the colocalisation tailed off, skewing the results. To avoid this problem another method was used to quantify the spatial distribution of the colocalisation within the cell. The middle 'z' section of the extracted colocalisation image was chosen, and four straight lines were drawn randomly through the cell, cutting membranes but avoiding the nucleus (Figure 6.6A). The software Zeiss LSM image analyser used creates a plot of intensity vs distance (Figure 6.6D) and a table containing the relative amount of colocalisation in a scale of 0-255 fluorescence intensity units at corresponding points on the line. The tabulated data was then taken and normalised to the background of the individual cell in Microsoft excel, then grouped as either plasma membrane, by taking the first and last 60 data points (approximately 1μm) from where the signal starts and ends respectively, or intracellular (cytoplasmic) which included all the other data points in between. A ratio of colocalisation on the plasma membrane and intracellular was calculated by dividing the mean colocalisation intensity value for the plasma membrane points by the median of the intracellular points. A distribution ratio >1 showed more colocalisation on the plasma membrane than inside the cell and a ratio less than <1 showed more colocalisation within the cell than on the plasma membrane. This analysis produced a ratio of 5.73±1.3 for the wild-type proteins confirming that colocalisation of ECFP-syntaxin 1a and EYFP-munc18-1 occurs mainly on the plasma membrane, suggesting that both syntaxin 1a and munc18-1 are required for the proper targeting of these proteins to the plasma membrane.

When cells cotransfected with ECFP-syntaxin 1a and EYFP-munc18-1_{R39C} were analysed in a similar way (Figure 6.7), ECFP-syntaxin 1a was found to be extensively colocalised (53.7 ±11.2 %) with EYFP-munc18-1_{R39C}. However, when the colocalisation was investigated as above, there was a ratio of 0.94 ± 0.14 suggesting that the proteins were not properly targeted to the plasma membrane of the cells (Figure 6.7D).

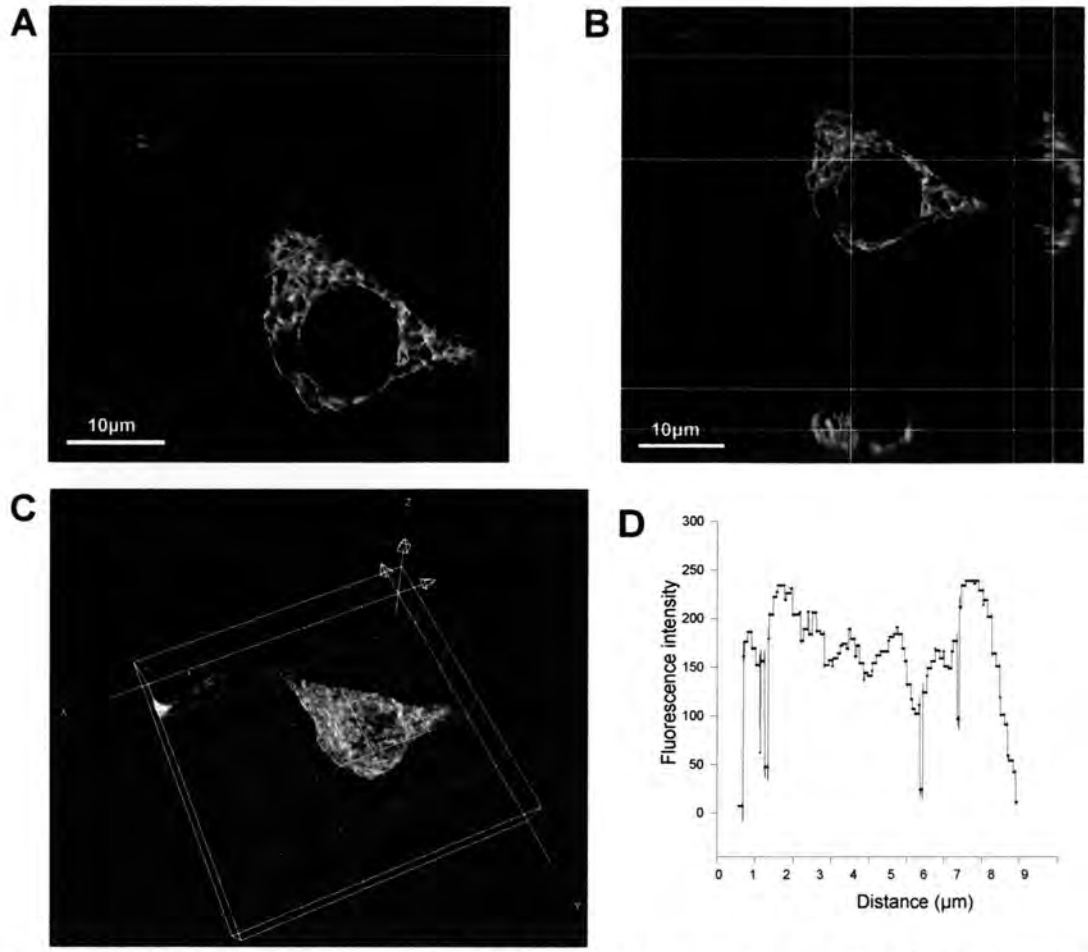

Figure 6.7: Colocalisation analysis in HEK293 cell cotransfected with ECFP-syntaxin 1a and EYFP-munc18-1_{R39C}

Colocalisation was quantified in a 3D pixel-by-pixel manner using Imaris Colocalisation software where pixels containing both ECFP-syntaxin 1a and EYFP-munc18-1_{R39C} were extracted.

A: colocalisation between ECFP-syntaxin 1a and EYFP-munc18-1_{R39C} in the middle slice of the Image stack. The red line illustrates where the lines were drawn through the images to investigate the distribution of the colocalisation.

B: orthoslicer view of the colocalisation between ECFP-syntaxin 1a and EYFP-munc18-1_{R39C}

C: 3D reconstruction of the pixels in the image which had colocalisation between ECFP-syntaxin 1a and EYFP-munc18-1_{R39C} with a 10 μM grid, see accompanying CD for movie.

D: plot of the distribution of colocalisation between the two proteins, within a line drawn through the middle section of the image stack covering two membranes and the cytoplasm.

Control experiments were performed in which ECFP-syntaxin 1a was transfected along with EYFP to ensure that the fluorescent proteins themselves did not interact, since it has been reported that EGFP can form dimers (Zacharias 2002). These experiments confirmed that the EYFP on its own did not localise with the ECFP-syntaxin 1a suggesting that syntaxin 1a and munc18-1 specifically co-localise.

6.4 FRET and FLIM analyses of ECFP-syntaxin 1a and EYFP-munc18-1 or EYFP-munc18-1_{R39C} transfected HEK293 cells

In these experiments ECFP was used as the donor fluorophore and EYFP as the acceptor. First, the fluorescence lifetime of the ECFP-syntaxin 1a alone was determined, which gave a weighted mean lifetime of 2.1±0.2 ns, which was slightly longer than previously reported (Duncan, Bergmann et al. 2004), possibly as a result of the ECFP being attached to the syntaxin 1a. The fluorescence decay for ECFP fused to syntaxin 1a was found to be fit by a bi-exponential function as previously described (Duncan, Bergmann et al. 2004), in non-FRET and FRET systems. All data here are presented as the weighted mean of the two (FRET or non-FRET) components.

First, FRET was investigated between ECFP-syntaxin 1a and EYFP-munc18-1 (Figure 6.8). Three distinct populations of ECFP, with different fluorescence lifetimes, were detected. The data were best fit by a triple-Gaussian frequency distribution plot describing the whole FLIM image. A population with long fluorescence lifetime was found in the region of the cells where there was no colocalisation. This lifetime was identical to that of ECFP-syntaxin 1a alone, indicating that no FRET occurred. Although FRET was not detected this does not necessarily mean that the proteins are not interacting, simply that the two fluorophores are too far apart or in an unfavourable orientation for FRET to occur. The fluorescence lifetimes of the other two populations were shorter, as a result of FRET. These were located exclusively on the plasma membrane (0.9±0.05 ns - 'short') and on both perinuclear structures reminiscent of Golgi membranes and the plasma membrane (1.4±0.1 ns -

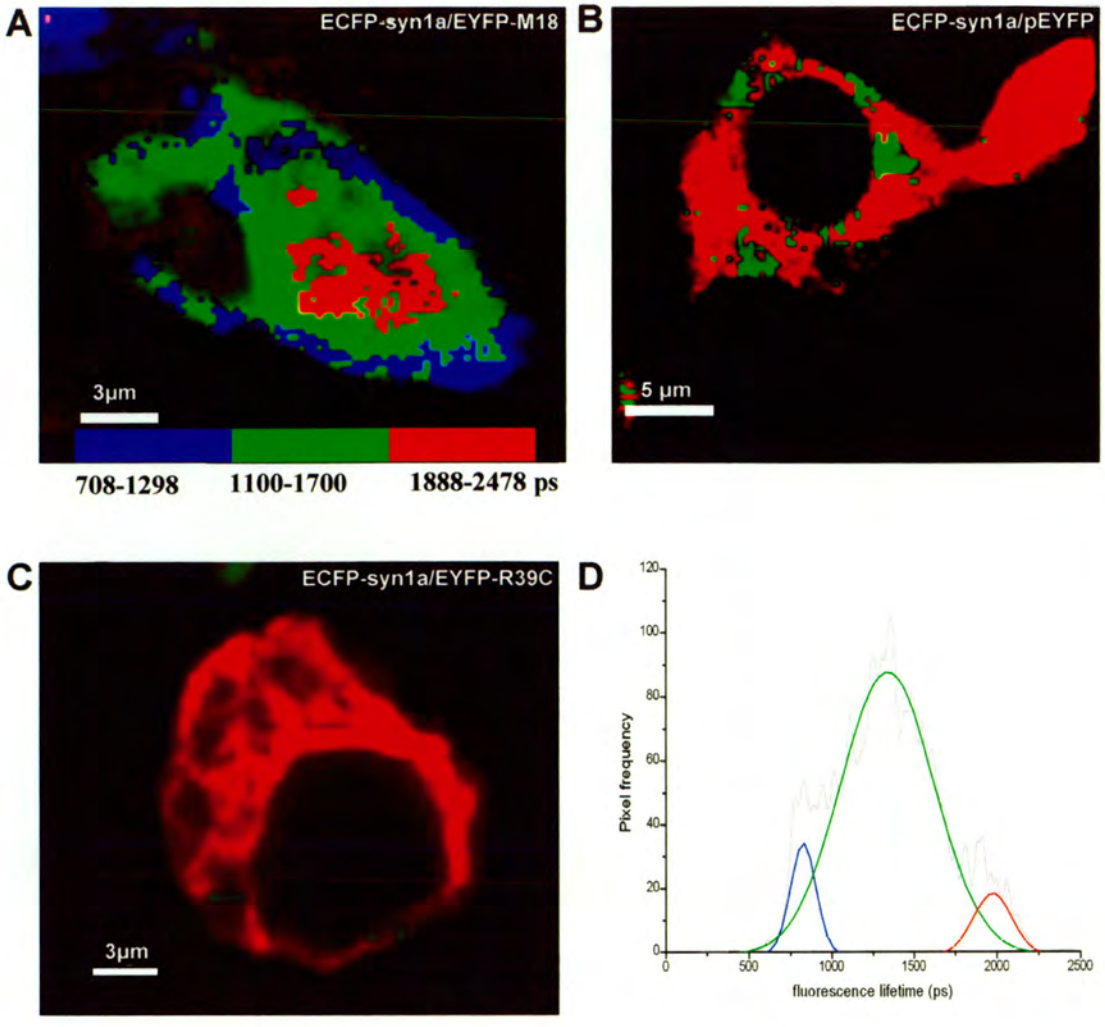

Figure 6.8: HEK293 cells cotransfected with ECFP-syntaxin 1a and EYFP-munc18-1, with ECFP-syntaxin 1a and pEYFP or with ECFP-syntaxin 1a and EYFP-munc18-1_{R39C}

FLIM data were acquired on parafolmaldehyde fixed HEK293 cells

A: FLIM map of HEK293 cell cotransfected with ECFP-syntaxin 1a and EYFP-munc18-1

B: FLIM map of HEK293 cell cotransfected with ECFP-syntaxin 1a and pEYFP

C: FLIM map of HEK293 cell cotransfected with ECFP-syntaxin 1a and EYFP-munc18-1_{R39C}

D: Frequency distribution plot of ECFP lifetimes measured for HEK293 cells cotransfected with ECFP-syntaxin 1a and EYFP-munc18-1

'intermediate'). The presence of two weighted mean lifetimes suggests that the distance between, or orientation of, the fluorophores is different in the two populations and therefore that the ECFP-syntaxin 1a and EYFP-munc18-1 are interacting in different ways or that the bimolecular complex has two different conformations, that are specific to intracellular locations. In the conformation with the short lifetime the fluorophores must be closer together or preferentially orientated, with more efficient energy transfer than in the conformation with the intermediate lifetime.

A parallel control was performed, as with the co-localisation analysis, in which cells were transfected with ECFP-syntaxin 1a and EYFP itself (Figure 6.8B). In these cells no FRET was detected (weighted mean lifetime = 2.2±0.1 ns), confirming that the syntaxin 1a - munc18-1 interaction is specific.

When FRET between ECFP-syntaxin 1a and EYFP-munc18-1_{R39C} was investigated, no FRET was detected (mean lifetime 2.2±0.1 ns; Figure 6.8C), suggesting that if these proteins were interacting, their conformation was such that the fluorophores were not close enough for energy transfer to occur (> ~6 nm in this system), or else that their dipoles were not in a favourable mutual orientation.

6.4.1 FRET and FLIM analysis of ECFP-syntaxin 1a and EYFP-munc18-1 or EYFP-munc18-1_{R39C} in the presence of Phorbol Ester

Previous studies (Barclay, Craig et al. 2003) have shown that when munc18-1 is phosphorylated *in vitro* by PKC its interaction with syntaxin 1a is weakened and in bovine adrenal chromaffin cells exocytosis has been shown to be regulated by phorbol ester/diacylglycerol-mediated PKC phosphorylation of munc18-1, which can only occur when munc18-1 is free of syntaxin 1a (Fujita, Sasaki et al. 1996; Rickman and Davletov 2005). Furthermore, experiments in this laboratory with rat phaeochromocytoma (PC12) cells suggested (J. Greaves, personal communication) that endogenous syntaxin 1a was translocated to the plasma membrane in response to treatment of the cells with phorbol ester.

To investigate the role of phosphorylation in the interaction between munc18-1 and syntaxin 1a in cells we employed FLIM. This was accomplished by incubating the transfected cells with 100 nM PMA for 15 mins to activate PKC and hence phosphorylate munc18-1, before fixing and mounting them in the usual way (Duncan, Betz et al. 1999).

In cells that had been transfected with ECFP-syntaxin 1a and EYFP-munc18-1 (Figure 6.9A) treatment with PMA resulted in a change in the fluorescence lifetimes. The plasma membrane-located population with the short fluorescence lifetime (highest FRET efficiency) disappeared, and was replaced by a population of intermediate fluorescence lifetime (1.5±0.05 ns), equal to that observed predominantly in internal locations in untreated cells. This corresponded to a reduction in FRET efficiency, an increase in the donor lifetime and hence a change in the distance and/or orientation of the fluorophores and was confirmed by the frequency distribution plot of the entire image. This suggested that the phosphorylated form of munc18-1 still interacts with syntaxin 1a, but had prevented the formation of the conformation that brought the fluorophores the closest together.

Interestingly, when the PMA treatment was repeated in cells transfected with ECFP-syntaxin 1a and EYFP-munc18-1_{R39C} (Figure 6.9B), FRET, which was undetectable before the addition of PMA, could now be detected throughout the cell, with the same efficiency as in the population of intermediate fluorescence lifetime (1.6±0.06 ns) seen for ECFP-syntaxin 1a and EYFP-munc18-1. This suggested that the phosphorylated form of munc18-1_{R39C} interacts with syntaxin 1a in a way that brings the fluorophores closer together than in the absence of the PMA. This implied that in the absence of the PMA, the ECFP-syntaxin 1a and the EYFP-munc18-1_{R39C} may still be interacting with each other but in a conformation or orientation where the fluorophores are too far apart, or aligned in an unfavourable manner, for FRET to occur, but when the munc18-1_{R39C} is phosphorylated the proteins interact with an altered conformation. Furthermore, although the R39 residue of munc18-1 is essential for the conformation of munc18-1 and for its interaction with syntaxin 1a (Misura, Scheller et al. 2000; Fisher, Pevsner et al. 2001), our FLIM data suggests that PKC phosphorylation of

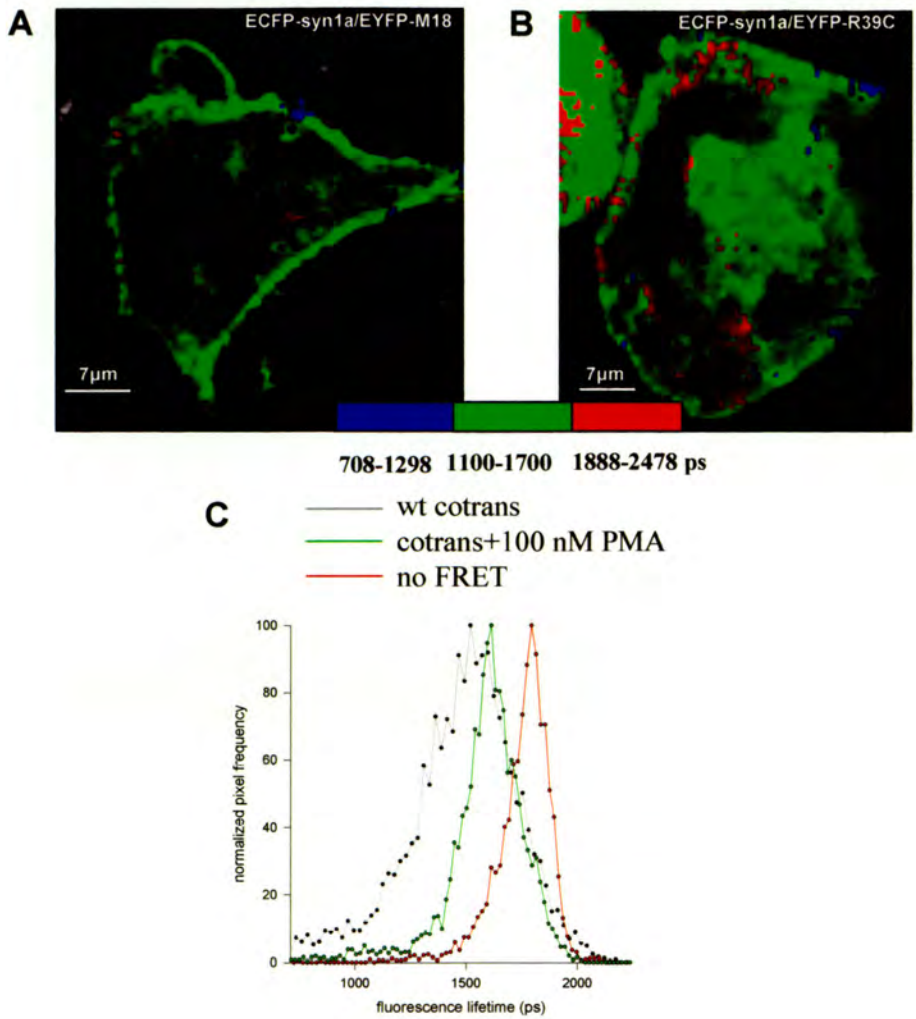

Figure 6.9: HEK293 cells cotransfected either with ECFP-syntaxin 1a and EYFP-munc18-1 or with ECFP-syntaxin 1a and EYFP-munc18-1_{R39C}

FLIM data were acquired from HEK293 cells that had been treated with 100 nM PMA before being fixed in paraformaldehyde.

A: FLIM map of a HEK293 cell cotransfected with ECFP-syntaxin 1a and EYFP-munc18-1

B: FLIM map of a HEK293 cell cotransfected with ECFP-syntaxin 1a and EYFP-munc18-1_{R39C}

C: Frequency distribution plot of the different ECFP lifetimes measured, revealing the short, intermediate and non-FRET lifetime populations

munc18-1 bypasses the requirement for R39 in the syntaxin 1a – munc18-1 complex; in other words, it rescues the R39C mutant form of munc18-1.

Parallel controls were set up to check that the changes in the fluorescence lifetime of the ECFP-syntaxin 1a were not a direct effect of adding the PMA. Cells transfected with ECFP-syntaxin1a alone were treated with PMA and the fluorescence lifetime of the ECFP-syntaxin 1a measured. It was found to be the same as in the absence of PMA. HEK293 cells transfected with ECFP-syntaxin 1a and EYFP were also treated with PMA, which again had no effect on the lifetime of the ECFP-syntaxin 1a. Therefore the changes in the fluorescence lifetimes detected on treatment with PMA were the result of changes in conformation of the complex formed by the two proteins, altering the distance between the fluorophores and hence the efficiency of FRET. In other control experiments, done to confirm that the effect seen due to the addition of phorbol ester was mediated via the activation of PKC, the cells were treated with an inactive phorbol ester, -phorbol 4α-myristoyl acetate (4α-PMA), (100 nM) for 15 minutes prior to fixing as before. This had no effect on the fluorescent lifetimes measured for ECFP-syntaxin 1a in the presence on either EYFP-munc18-1 or EYFP-munc18-1_{R39C}, suggesting that the phorbol ester effect seen is specific.

6.5 FRET and FLIM analyses of cells cotransfected with ECFP-syntaxin 1a and either EYFP-munc18-$1_{S306E:S313E}$ or EYFP-munc18-$1_{R39C:S306E:S313E}$

To further investigate whether the changes in fluorescence lifetime produced by PMA treatment of cells was due to phosphorylation of munc18-1 and munc18-1_{R39C} on Serines 306 and 313, as previously reported (Barclay, Craig et al. 2003), phosphomimetic mutants, made by site-directed mutagenesis, (kind gift of Dr Rory Duncan) were studied. The mutations changed these serines into glutamic acids, in which the negative charge mimics the effect of phosphorylation of EYFP-munc18-1 and EYFP-munc18-1_{R39C}. The munc18-$1_{S306E:S313E}$ phosphomimetic (double mutant) has previously been shown (Barclay, Craig et al. 2003) to

have weakened affinity for syntaxin 1a *in vitro*, comparable with that of phosphorylated munc18-1. Its expression also modified the kinetics of catecholamine release from bovine adrenal chromaffin cells in a similar, but not identical way to phorbol ester treatment of the cells.

FLIM data for HEK293 cells cotransfected with ECFP-syntaxin 1a and EYFP-munc18-$1_{S306E:S313E}$ (Figure 6.10A) were generated in the same way as above and showed that with the phosphomimetic munc18-1 mutant, the shortest lifetime (plasma membrane) population was not detectable, however the intermediate (predominantly non-plasma membrane) lifetime population (1.7±0.06 ns) was found uniformly throughout the cells. This gives support to the idea that the phosphorylation of munc18-1 is responsible for the reduction in the observed FRET efficiency, presumably through a change in the conformation of the syntaxin 1a – munc18-1 complex.

Similar experiments were performed with a phosphomimetic mutant of EYFP-munc18-1_{R39C}. FLIM data for HEK293 cells transfected with ECFP-syntaxin 1a and EYFP-munc18-$1_{R39C:S306E:S313E}$ (triple mutant, Figure 6.10B) showed levels of FRET (1.6±0.07 ns) identical to those seen in PMA-treated cells expressing EYFP-munc18-1_{R39C} and in cells expressing the phosphomimetic mutant.

The observation that PKC-directed phosphorylation of munc18-1 on serines 306 and 313 results in a reduction of FRET between the two fluorophores implies that there is a change in the conformation of the syntaxin 1a – munc18-1 complex that results either in an increase in the interdipole distance or in an unfavourable dipole orientation. Significantly, this effect is restricted to munc18-1/syntaxin 1a resident on the plasma membrane.

Controls were also performed in which the cells were treated either with 100 nM PMA or 100 nM 4α-PMA 15 mins before fixing. Treatment with the latter had no effect on the FLIM data acquired.

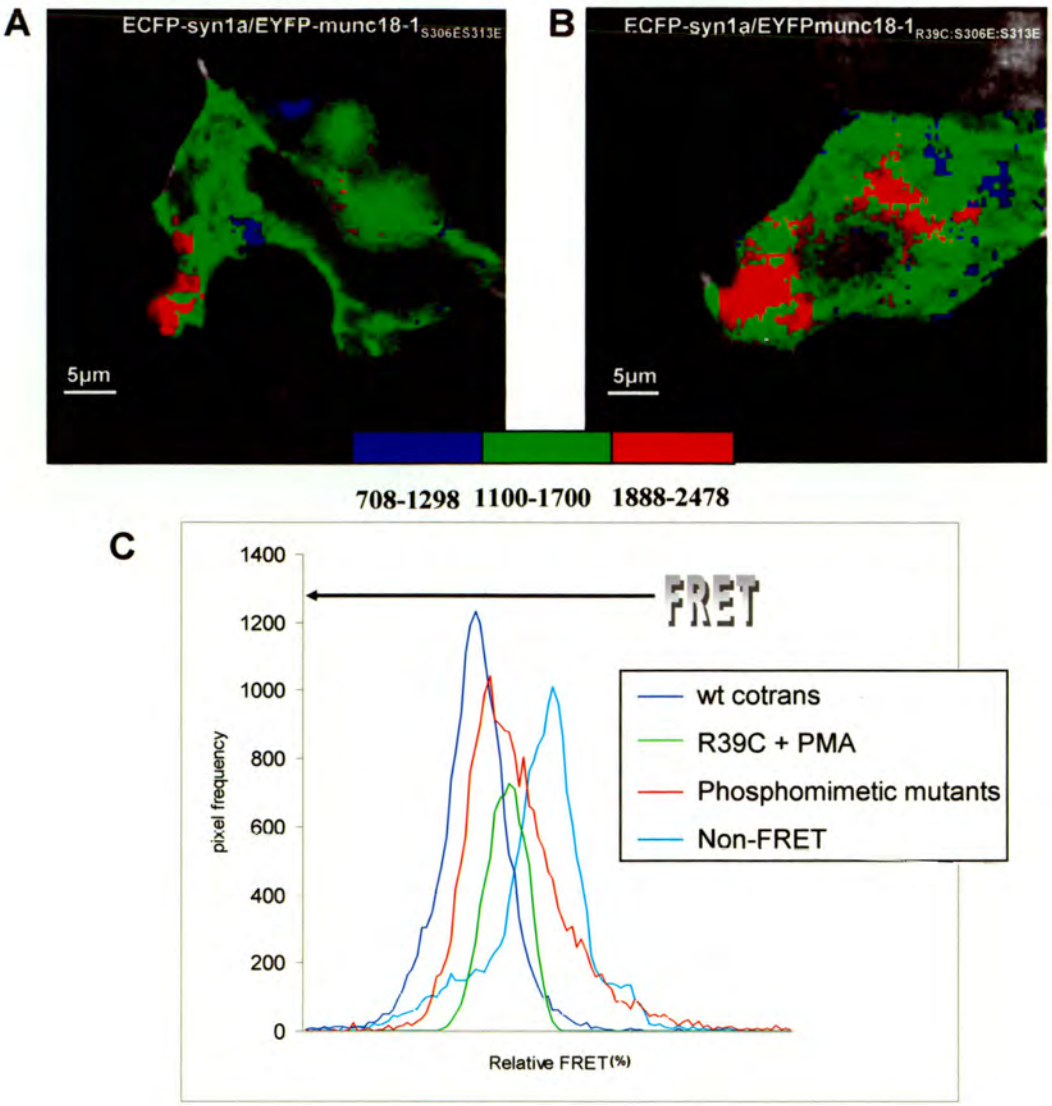

Figure 6.10: HEK293 cells cotransfected either with ECFP-syntaxin 1a and EYFP-munc18-1$_{S306E:S313E}$ or with ECFP-syntaxin 1a and EYFPmunc18-1$_{R39C:S306E:S313E}$

FLIM data were acquired on paraformaldehyde fixed HEK293 cells

A: FLIM map of HEK293 cell cotransfected with ECFP-syntaxin 1a and EYFP-munc18-1$_{S306E:S313E}$

B: FLIM map of HEK293 cell cotransfected with ECFP-syntaxin 1a and EYFP-munc18-1$_{R39C:S306E:S313E}$

C: Frequency distribution plot of the global analysis of the ECFP fluorescent lifetimes measured

6.6 Colocalisation analysis of HEK293 cells cotransfected with ECFP-syntaxin 1a and either EYFP-munc18-1 or EYFP-munc18-1_{R39C} treated with 100 nM PMA

Since the effects of munc18-1 phosphorylation appeared to be restricted to the plasma membrane of the cells, it was investigated whether phosphorylation had any effect on colocalisation of the proteins.

HEK293 cells transfected with ECFP-syntaxin 1a and EYFP-munc18-1 were treated with 100 nM PMA for 15 mins, then fixed and mounted (Chapter 2.22.1). Laser scanning confocal microscopy was used to generate image stacks, which were deconvolved and reconstructed as before (Figure 6.11), showing that both ECFP-syntaxin 1a and EYFP-munc18-1 were on the plasma membrane. 3D pixel-by-pixel colocalisation analysis was performed (Figure 6.12) on these images revealing that 39.7± 11.8% of the ECFP-syntaxin 1a colocalised with the EYFP-munc18-1. When the spatial distribution of the colocalisation was investigated a ratio of 4.73±1.73 was found suggesting there was more colocalisation on the plasma membrane of the cell than in the cytoplasm. These results were similar to those obtained with untreated cells.

Interestingly, when the same analysis was done on cells cotransfected with ECFP-syntaxin 1a and EYFP-munc18 1_{R39C} and treated with PMA, in the reconstructed images (Figure 6.13), a fraction of both proteins appeared to be on the plasma membrane and therefore had reached their correct intracellular destination. Colocalisation analysis (Figure 6.14) revealed that 44.6±9.7 % of the ECFP-syntaxin 1a colocalised with the EYFP-munc18-1_{R39C}, and, in contrast to untreated cells, when the location of the colocalisation was quantified the distribution ratio was 4.44±1.64, revealing that there was more colocalisation on the plasma membrane than in the cytoplasm. Control experiments were performed in which the cells were treated with 100 nM 4α-PMA instead of PMA to check that the effects seen were specifically PMA-mediated (Figure 6.15 & 6.16). In cells cotransfected with ECFP-syntaxin

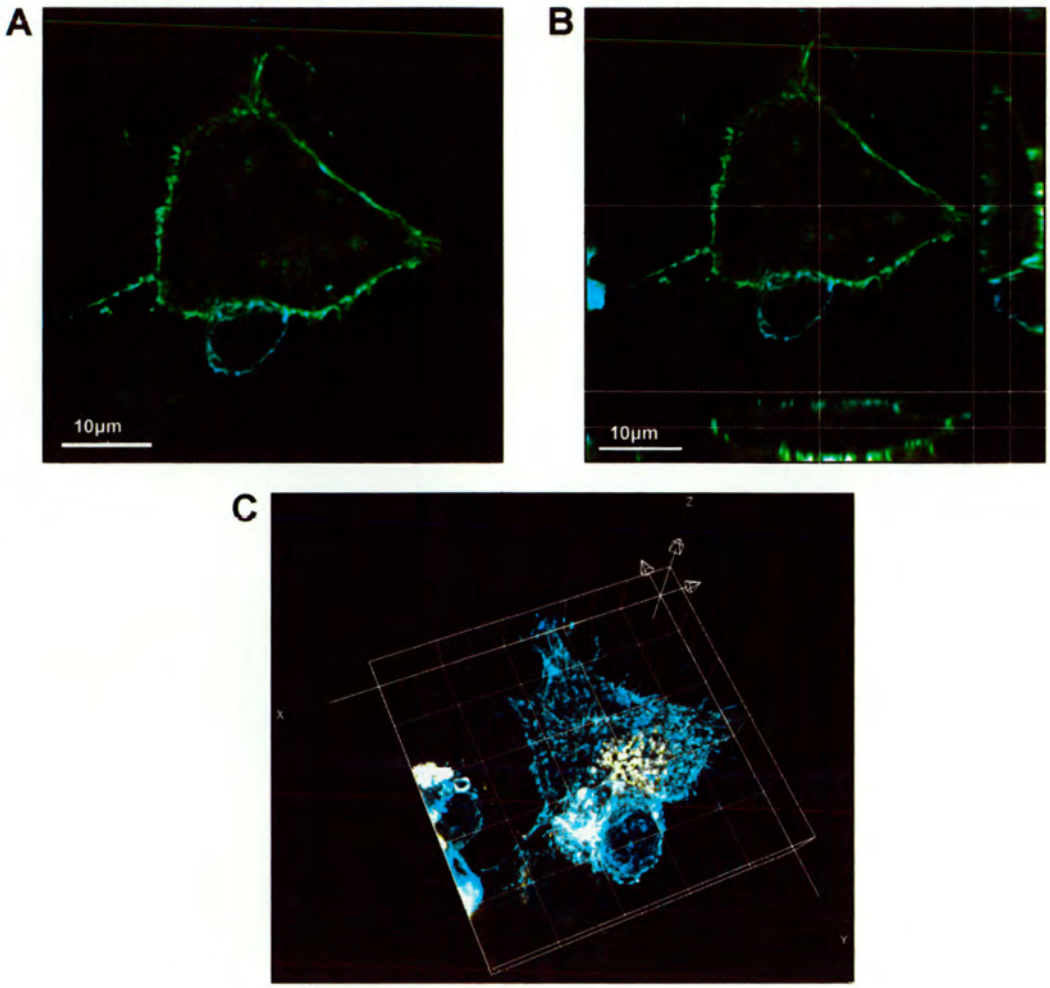

Figure 6.11: HEK293 cell cotransfected with ECFP-syntaxin 1a and EYFP-munc18-1

HEK293 cells were treated with 10nM PMA before being fixed in paraformaldehyde and imaged using CLSM followed by deconvolution with Huygens II software. The ECFP-syntaxin 1a is shown in blue and EYFP-munc18-1 in yellow

A: middle slice through the image stack

B: orthoslicer view of the image stack

C: 3D reconstruction of image stack with a 10µM grid; see accompanying CD for movie

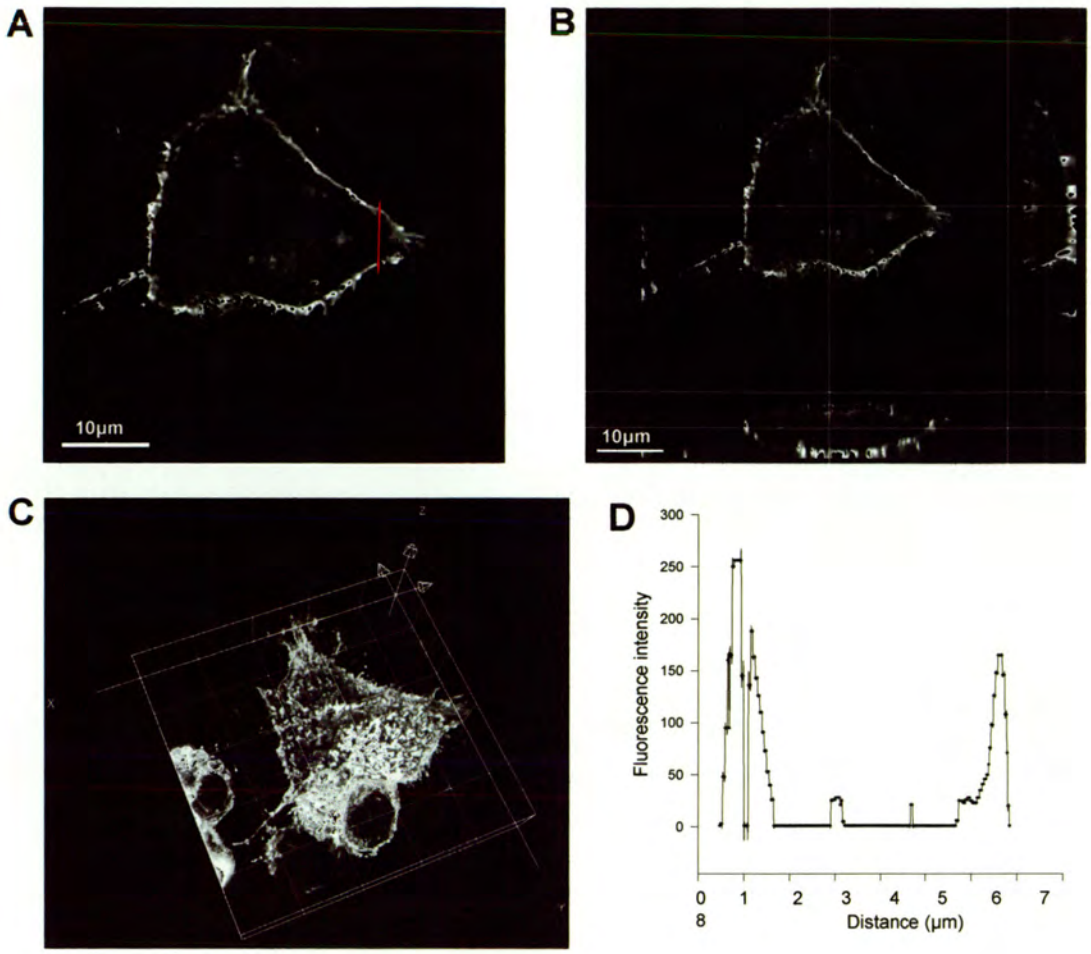

Figure 6.12: HEK293 cell cotransfected with ECFP-syntaxin 1a and EYFP-munc18-1

Colocalisation was quantified on a 3D pixel-by-pixel basis, using Imaris Colocalisation software. HEK293 cells were treated with 100 nM PMA before being fixed in paraformaldehyde

A: middle slice of an image stack containing an example of a line drawn for investigating the distribution of colocalisation within in the cell.

B: orthoslicer view of image stack

C: 3D reconstruction of image stack with a 10 µM grid, see accompanying CD for movie

D: Plot of colocalisation along a line drawn (see Fig 6.12A) through the middle section of the image stack

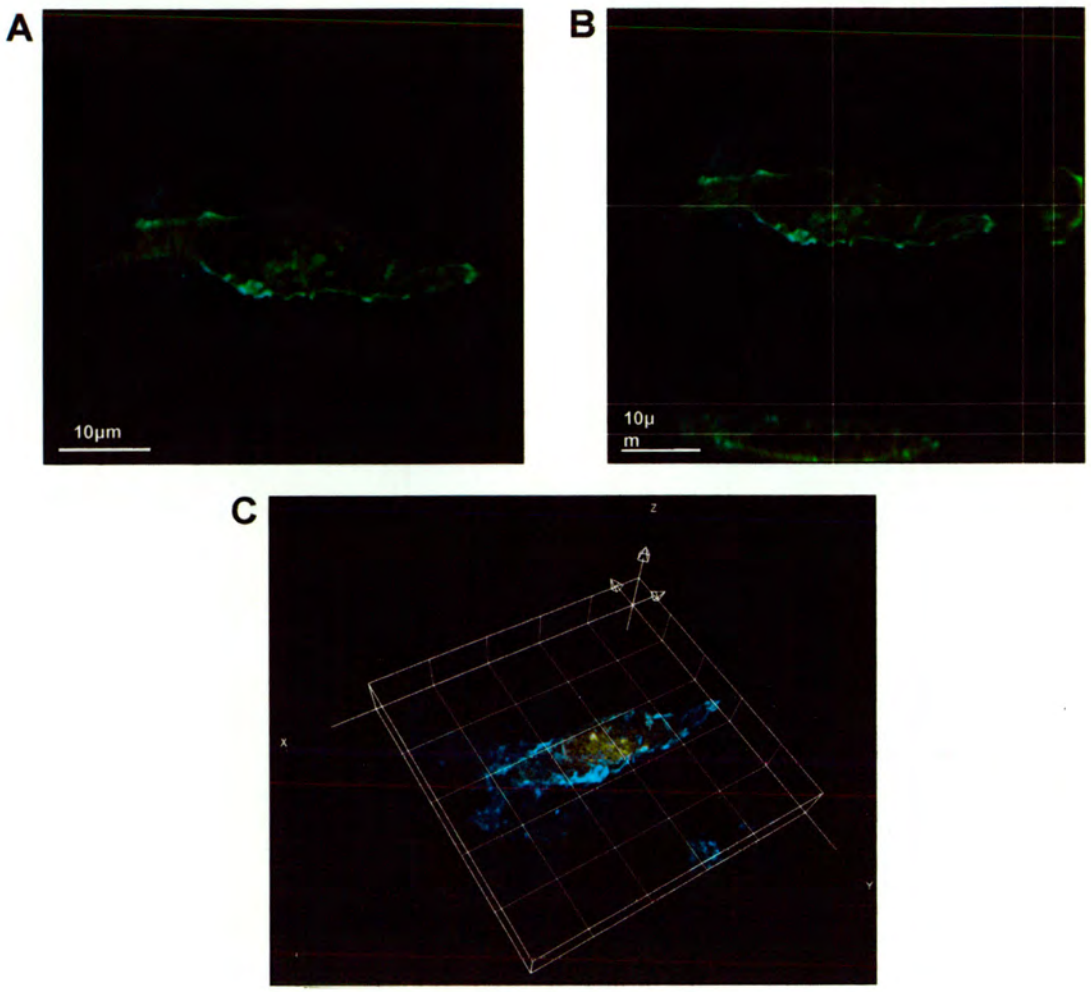

Figure 6.13: HEK293 cell cotransfected with ECFP-syntaxin 1a and EYFP-munc18-1_{R39C}

HEK293 cells were treated with 100 nM PMA before being fixed in paraformaldehyde and imaged by CLSM followed by deconvolution with Huygens II software. ECFP-syntaxin 1a is shown in blue and EYFP-munc18-1_{R39C} in yellow

A: middle slice of an image stack

B: orthoslicer view of the image stack

C: 3D reconstruction of image stack with a 10 µM grid ; see accompanying CD movie

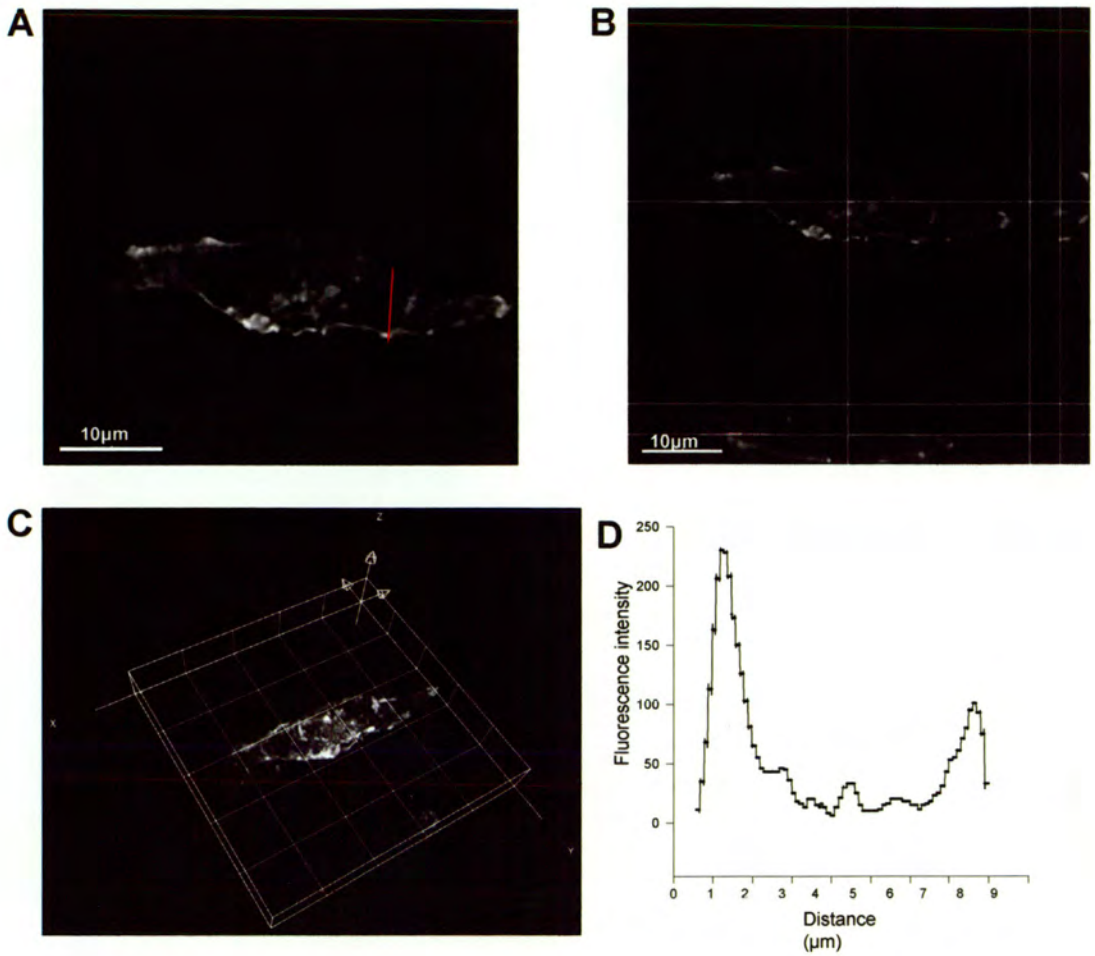

Figure 6.14: HEK293 cell cotransfected with ECFP-syntaxin 1a and EYFP-munc18-1$_{R39C}$

Colocalisation in the cell shown in Figure 6.13 was quantified on a 3D pixel-by-pixel basis that had been treated with 100 nM PMA before being fixed in paraformaldehyde

A: middle slice of an image stack with an example of how the lines were drawn to investigate the distribution of the colocalisation.

B: orthoslicer view of the image stack

C: 3D reconstruction of the image stack with a 10 µM grid; see accompanying CD for movie

D: plot of colocalisation intensity measured on a line drawn (see Figure 6.14A) through the middle section of the colocalised image stack.

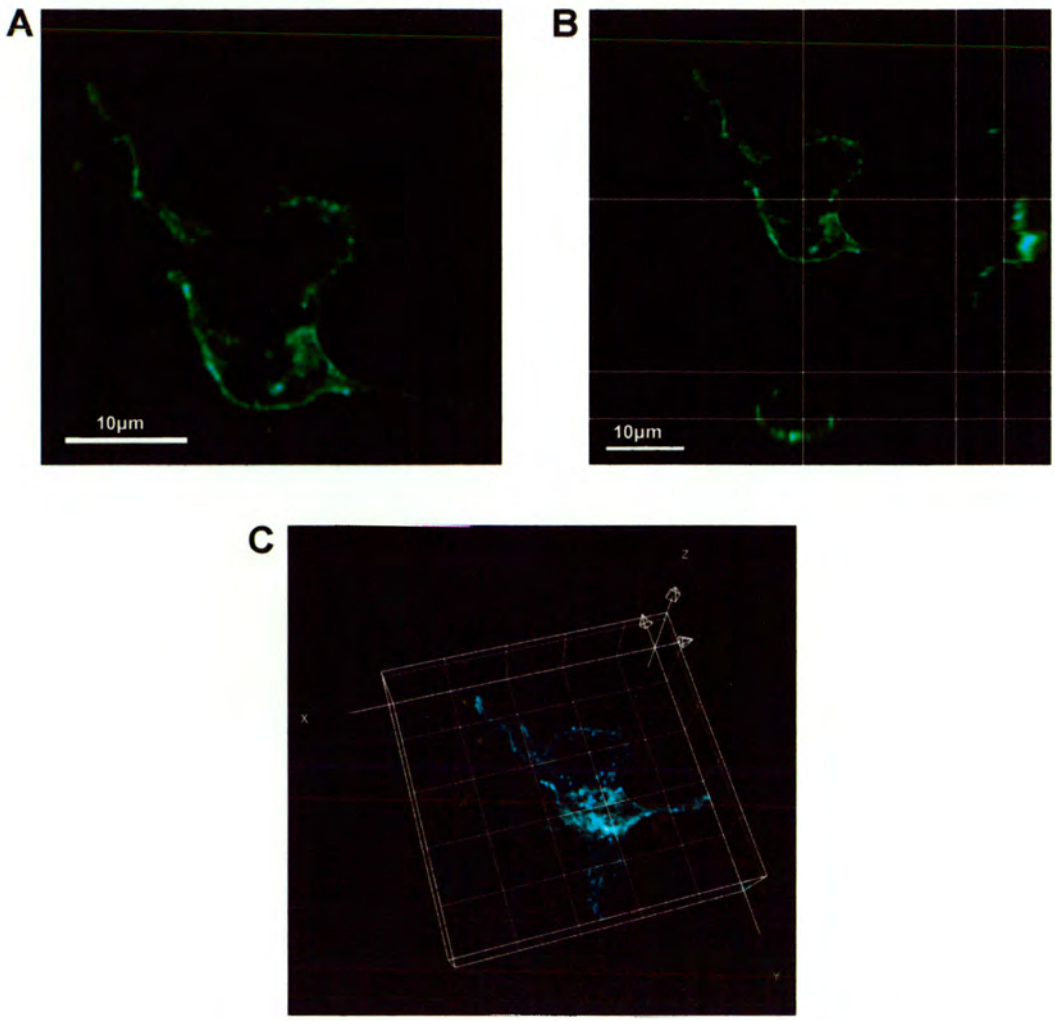

Figure 6.15: HEK293 cell cotransfected with ECFP-syntaxin 1a and EYFP-munc18-1

HEK293 cells were treated with 100 nM 4α-PMA for 15min before being fixed and imaged by CLSM. Image data were deconvolved using Huygens II software. ECFP-syntaxin 1a is displayed in blue and EYFP-munc18-1 in yellow.

A: middle section an image stack

B: orthoslicer view of the image stack

C: 3D reconstruction of the image stack with a 10 µM grid, see accompanying CD for movie.

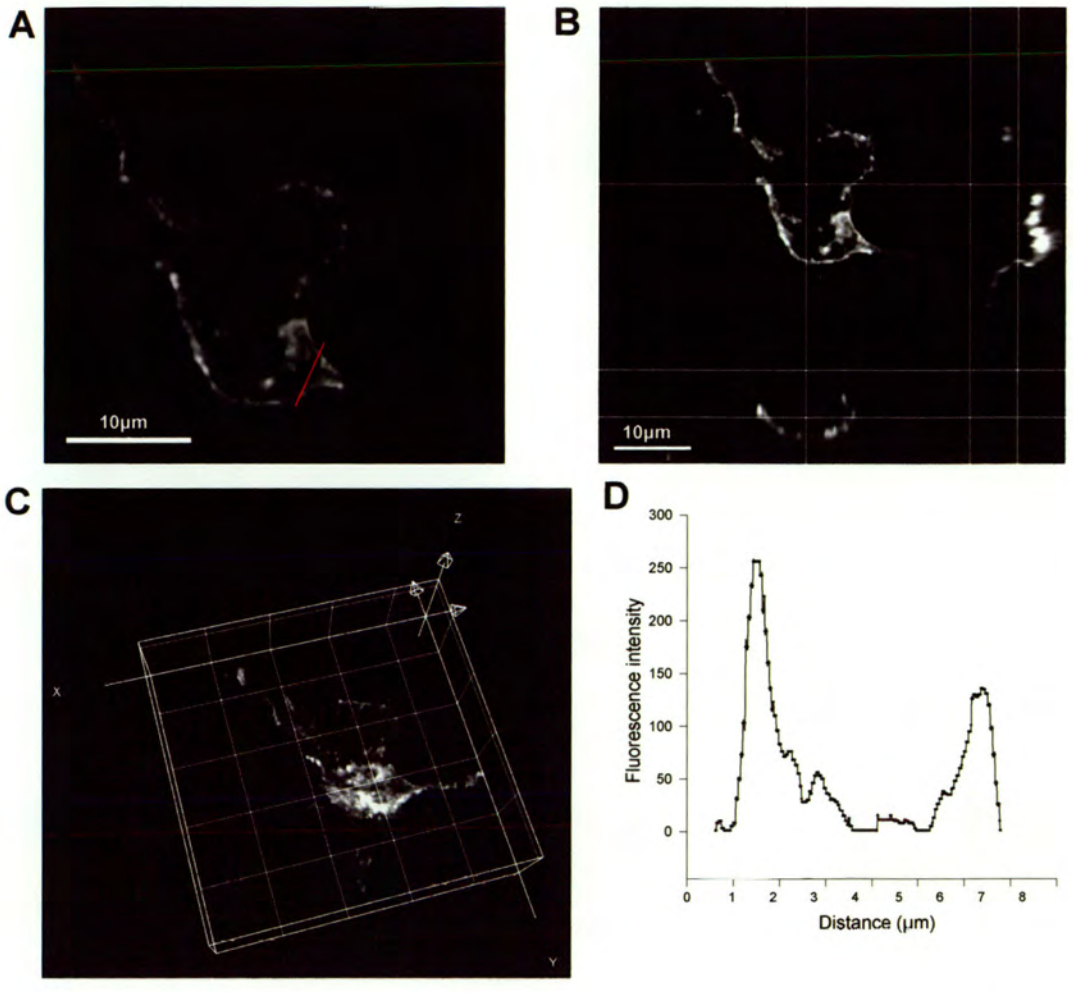

Figure 6.16: HEK293 cell cotransfected with ECFP-syntaxin 1a and EYFP-munc18-1

3D pixel-by-pixel colocalisation analysis was done on HEK293 cell transfected and treated with 10nM 4α–PMA for 15min prior to fixing shown in Figure 6.15.

A: middle section of the colocalisation image stack containing an example of the lines drawn to investigate the distribution of the colocalisation

B: orthoslicer view of the colocalisation image

C: 3D reconstruction of the colocalised pixels in the image stack with a 10 µM grid, see accompanying CD for movie.

D: plot of colocalisation intensity measured on a line drawn through the middle section of the colocalised image stack.

1a and EYFP-munc18-1 there was 38.3±3.9 % colocalisation of the syntaxin 1a with the munc18-1 and this colocalisation had a distribution ratio of 2.37±0.81, suggesting that most of the proteins were colocalising on the plasma membrane as in untreated cells.

When cells cotransfected with ECFP-syntaxin 1a and EYFP-munc18-1_{R39C} were treated with 100 nM 4α-PMA (Figure 6.17 &6.18), 48.9±9.5 % of the syntaxin 1a colocalised with the munc18-1_{R39C} and the distribution ratio was 0.48±0.04, so most of the protein complex was located intracellularly, as was seen in untreated cells.

These results suggested that phosphorylation of munc18-1 on serines 306 and 313 bypasses the requirement for interactions involving R39, and therefore rescues the R39C mutation, allowing proper targeting of the syntaxin 1a – munc18-1 complex to the plasma membrane.

6.7 Colocalisation analysis of HEK293 cells cotransfected with ECFP-syntaxin 1a and either EYFP-munc18-$1_{S306E:S313E}$ or EYFP-munc18-$1_{R39C:S306E:S313E}$

To further understand the role of phosphorylation on the syntaxin 1a – munc18-1 complex, the colocalisation of ECFP-syntaxin 1a and the phosphomimetic mutants was investigated. HEK293 cells were cotransfected with either, ECFP-syntaxin 1a and EYFP-munc18-$1_{S306E:S313E}$ or ECFP-syntaxin 1a and EYFP-munc18-$1_{R39C:S306E:S313E}$ in the same way as before (Chapter 6.2) then imaged using CLSM.

In cells cotransfected with ECFP-syntaxin 1a and EYFP-munc18-$1_{S306E:S313E}$ (Figure 6.19) the proteins were found to be both cytoplasmic and on the plasma membrane. The same was seen in cells cotransfected with ECFP-syntaxin 1a and EYFP-munc18-$1_{R39C:S306E:S313E}$ (Figure 6.20).

The amount of colocalisation between the proteins was quantified in a 3D pixel-by-pixel manner using Imaris colocalisation software and the spatial distribution of the colocalisation was determined to investigate whether the phosphomimetic mutations had any effect.

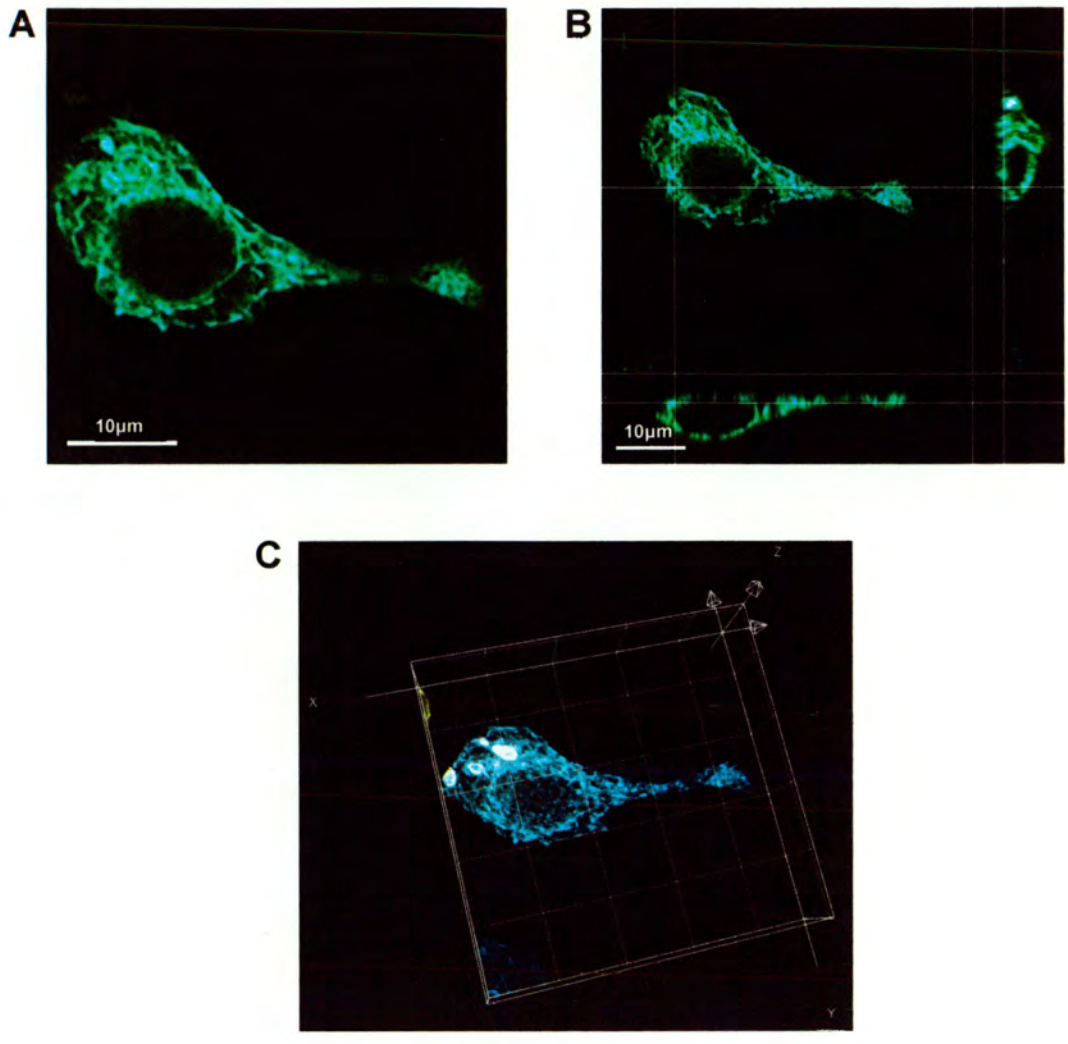

Figure 6.17: HEK293 cell cotransfected with ECFP-syntaxin 1a and EYFP-munc18-1_{R39C}

Cells were treated with 100 nM 4α-PMA for 15min before fixing and imaging by CLSM. The image data were then deconvolved using Huygens II software. ECFP-syntaxin 1a is displayed in blue and EYFP-munc18-1_{R39C} in yellow

A: middle section of a cell image stack

B: orthoslicer view of the image stack

C: 3D reconstruction of the image stack with a 10 µM grid, see accompanying CD for movie.

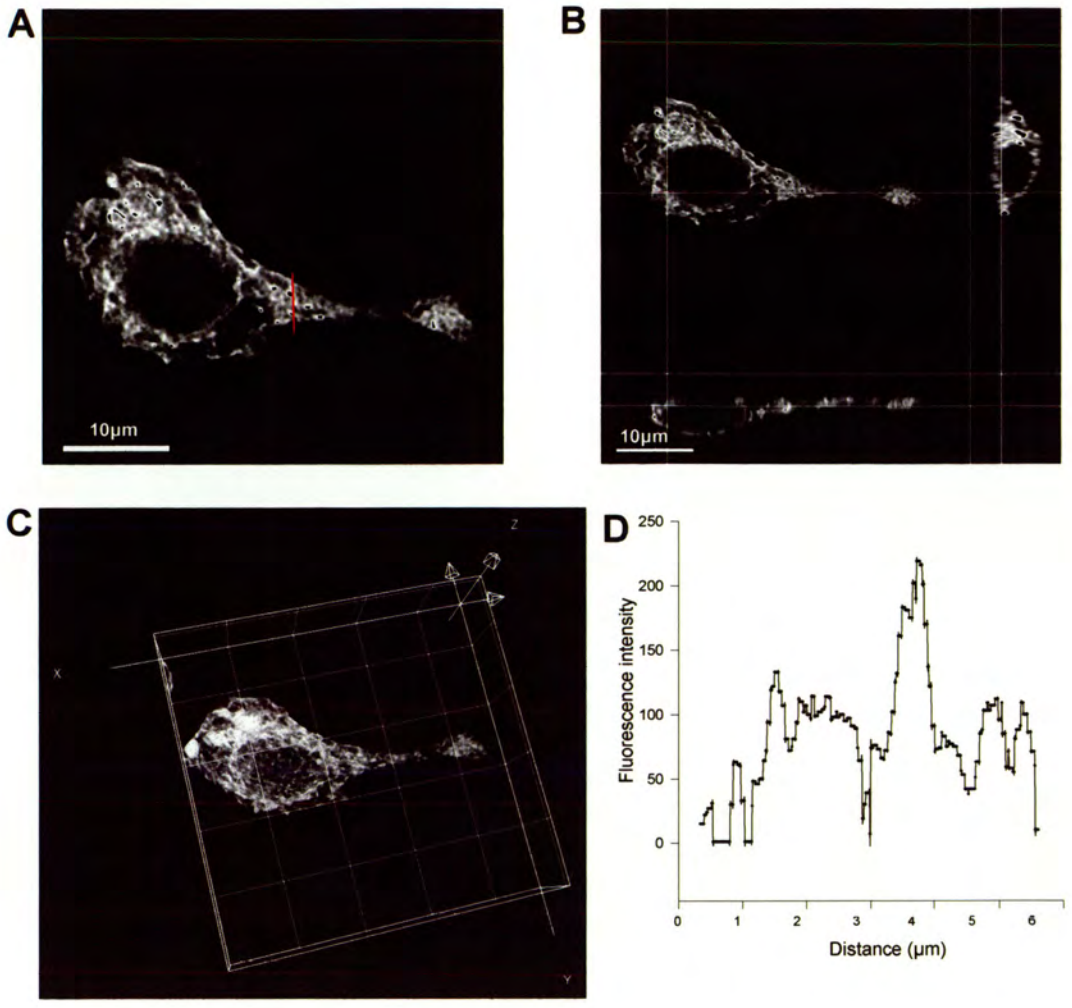

Figure 6.18: HEK293 cell cotransfected with ECFP-syntaxin 1a and EYFP-munc18-1$_{R39C}$

Colocalisation analysis was performed on a 3D pixel-by-pixel basis using Imaris colocalisation software on cells treated with 4α-PMA for 15min before fixation.

A: middle section of the colocalisation image stack containing an example of the lines drawn in the investigation of the distribution of the colocalisation.

B: orthoslicer view of the colocalisation image stack

C: 3D reconstruction of the colocalised pixels of the image stack with a 10 µM grid, see accompanying CD for movie.

D: plot of colocalisation intensity measured on a line drawn through the middle section of the colocalised image stack.

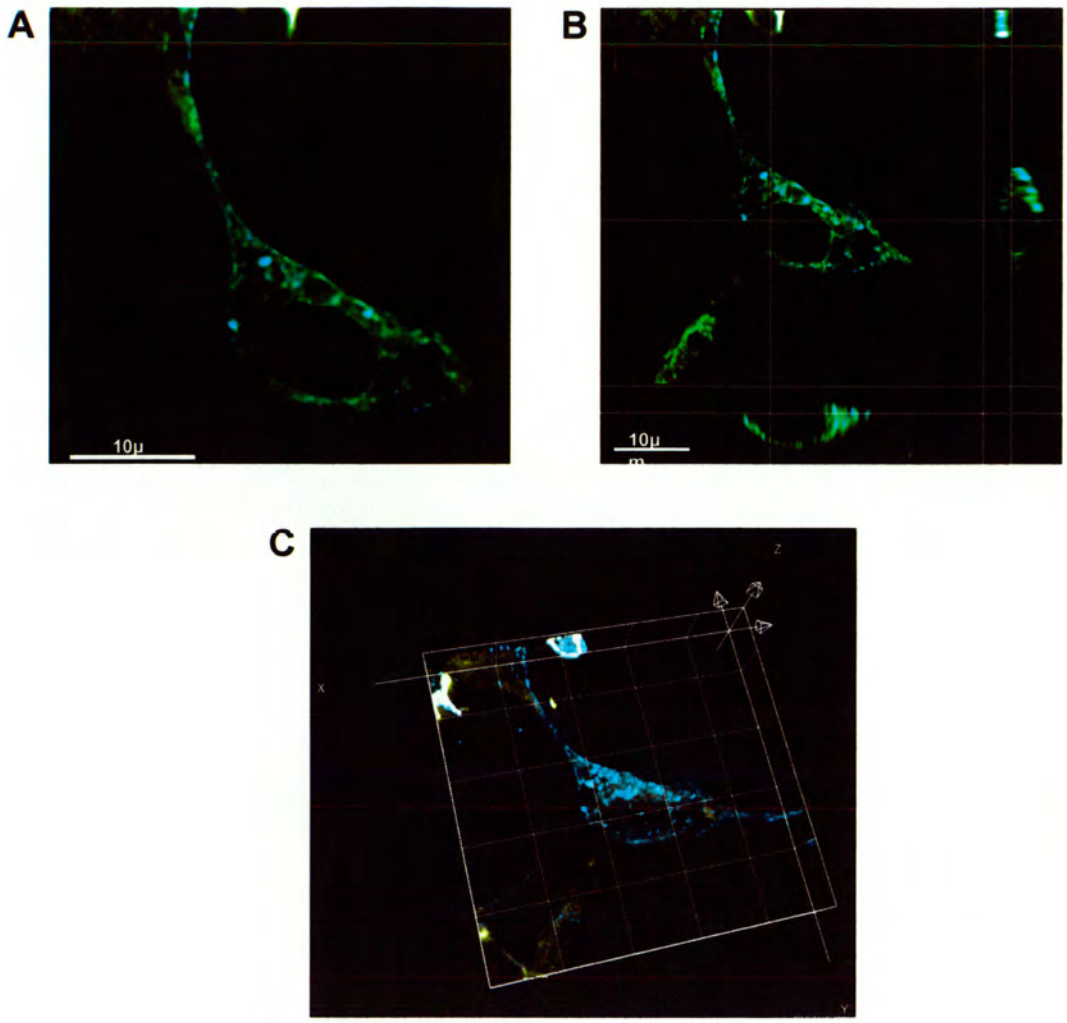

Figure 6.19: HEK293 cell cotransfected with ECFP-syntaxin 1a and EYFP-munc18-1$_{S306E:S313E}$

Transfected HEK293 cells were fixed in 4 % (w/v) paraformaldehyde then imaged using CLSM followed by deconvolution using Huygens II software. The ECFP-syntaxin 1a is shown in blue and the EYFP-munc18-1$_{S306E:S313E}$ in yellow

A: middle section of the image stack

B: orthoslicer view of the confocal image stack

C: 3D reconstruction of the deconvolved image stack with a 10 µM grid, see accompanying CD for movie.

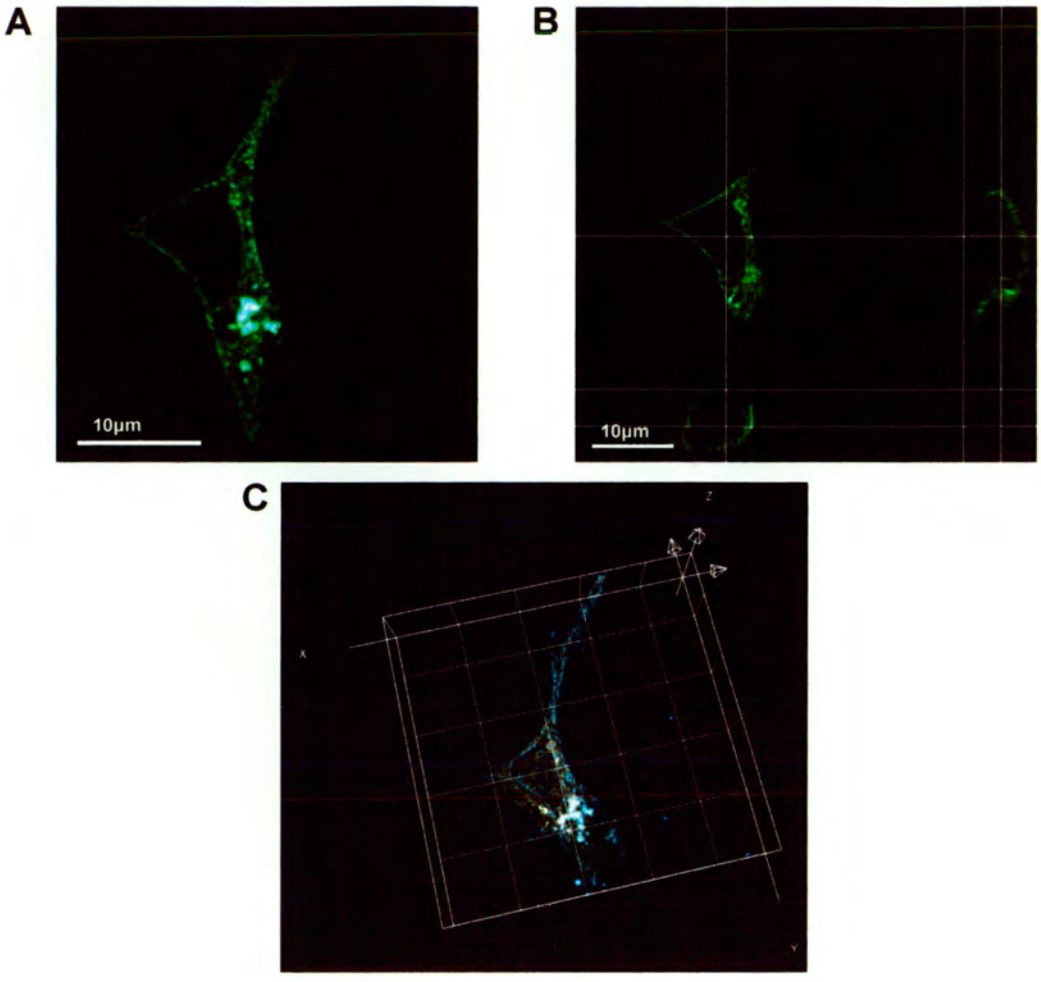

Figure 6.20: HEK293 cell cotransfected with ECFP-syntaxin 1a and EYFP-munc18-1$_{R39C:S306E:S313E}$

Transfected HEK293 cells were fixed in 4 % (w/v) paraformaldehyde and imaged using CLSM followed by deconvolution using Huygens II software. ECFP-syntaxin 1a is displayed in blue and EYFP-munc18-1$_{R39C:S306E:S313E}$ in yellow.

A: middle section through a confocal image stack

B: orthoslicer view of the confocal image stack

C: 3D reconstruction of the confocal image stack with a 10 µM grid, see accompanying CD for movie.

In HEK293 cells cotransfected with ECFP-syntaxin 1a and EYFP-munc18-$1_{S306E:S313E}$, 42±4.81 % of the ECFP-syntaxin 1a colocalised with EYFP-munc18-$1_{S306E:S313E}$, which is not significantly different from the colocalisation seen with wild-type proteins (Figure 6.21). The distribution of the colocalisation in the cell was also investigated (Chapter 6.3.2); the distribution ratio was 1.53±0.64 % suggesting that slightly more of the protein complex was found on the plasma membrane than intracellularly. This is, however, different to wild-type proteins in cells treated with PMA, in which a much higher percentage of the protein is localised to the plasma membrane than in the cytoplasm. A possible reason for this difference is a folding problem with the phosphomimetic mutant, such that the presence of the glutamic acids at positions 306 and 313 may result in inefficient folding of a fraction of the munc18-1, resulting in the formation of a syntaxin 1a – munc18-1 bimolecular complex that is trapped intracellularly; where the munc18-$1_{S306E:S313E}$ has folded correctly the syntaxin 1a – munc18-$1_{S306E:S313E}$ complex is correctly targeted to the plasma membrane. This is in contrast to phosphorylation of wild-type munc18-1, which obviously must occur following folding.

In HEK293 cells cotransfected with ECFP-syntaxin 1a and EYFP-munc18-$1_{R39C:S306E:S313E}$ the colocalisation analysis revealed (Figure 6.22) that 53.2±7.04 % of the ECFP-syntaxin 1a colocalised with the EYFP-munc18-$1_{R39C:S306E:S313E}$ which is not significantly different from the colocalisation seen in cells transfected with wild-type proteins. When the distribution of the colocalised proteins was investigated as before, the distribution ratio was 1.85±0.53 %, revealing that slightly more of the complex was localised on the plasma membrane than intracellularly. Although this result differs from that obtained in cells cotransfected with ECFP-syntaxin 1a and EYFP-munc18-1_{R39C}, it is also different to the result obtained in cells cotransfected with ECFP-syntaxin 1a and EYFP-munc18-1_{R39C} treated with 100 nM PMA, in which trafficking of the complex to the plasma membrane is restored. Again the reason for a difference in these results could be due to the mis-folding of some of the munc18-1 containing the phosphomimetic mutations. Another possibility is that

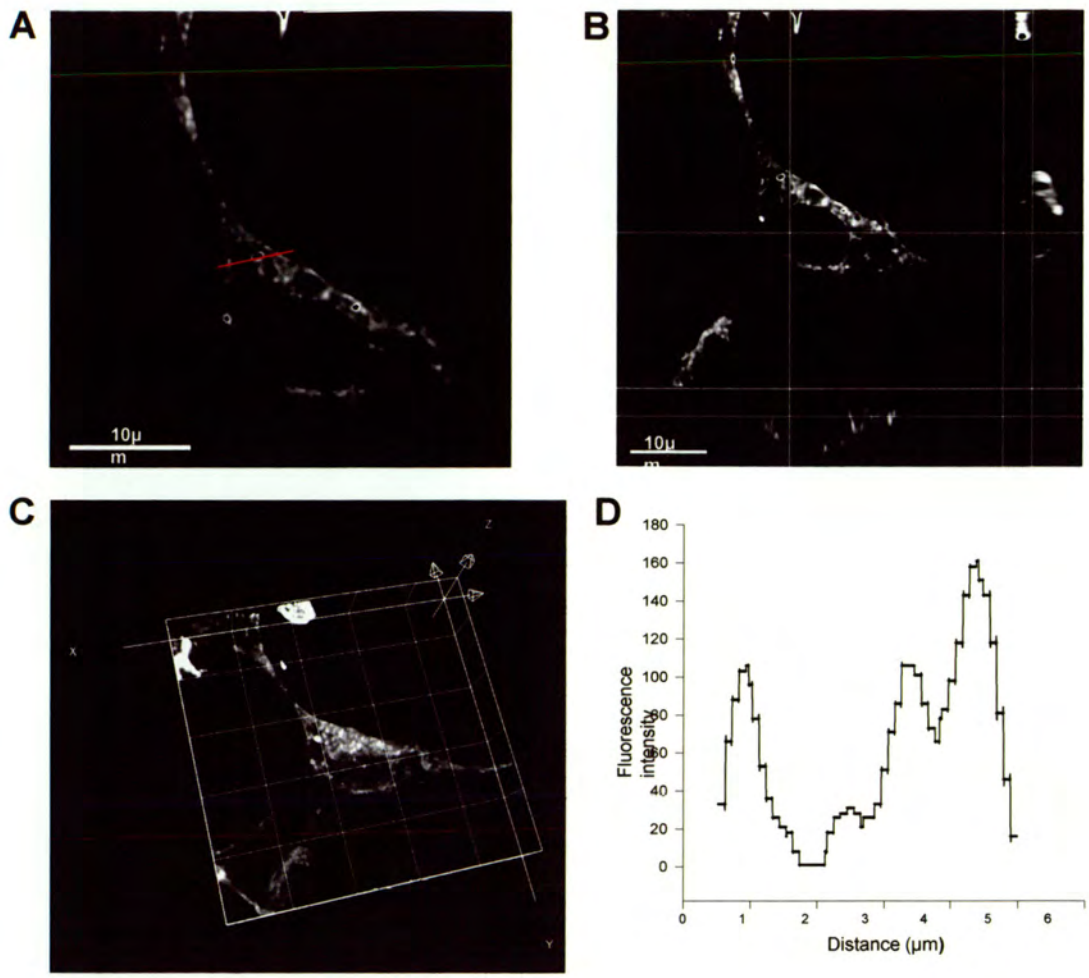

Figure: 6.21: HEK293 cell transfected with ECFP-syntaxin 1a and EYFP-munc18-1$_{S306E:S313E}$

3D pixel-by-pixel colocalisation analysis was carried out using Imaris imaging software on the cell shown in Figure 6.20

A: middle section of the colocalisation image stack with a example of the lines drawn to investigate the distribution of the colocalisation

B: orthoslicer view of the image stack

C: 3D reconstruction of the colocalised pixels with a 10 µM grid, see accompanying CD for movie.

D: A plot of colocalisation along a line drawn through the middle section of the image stack.

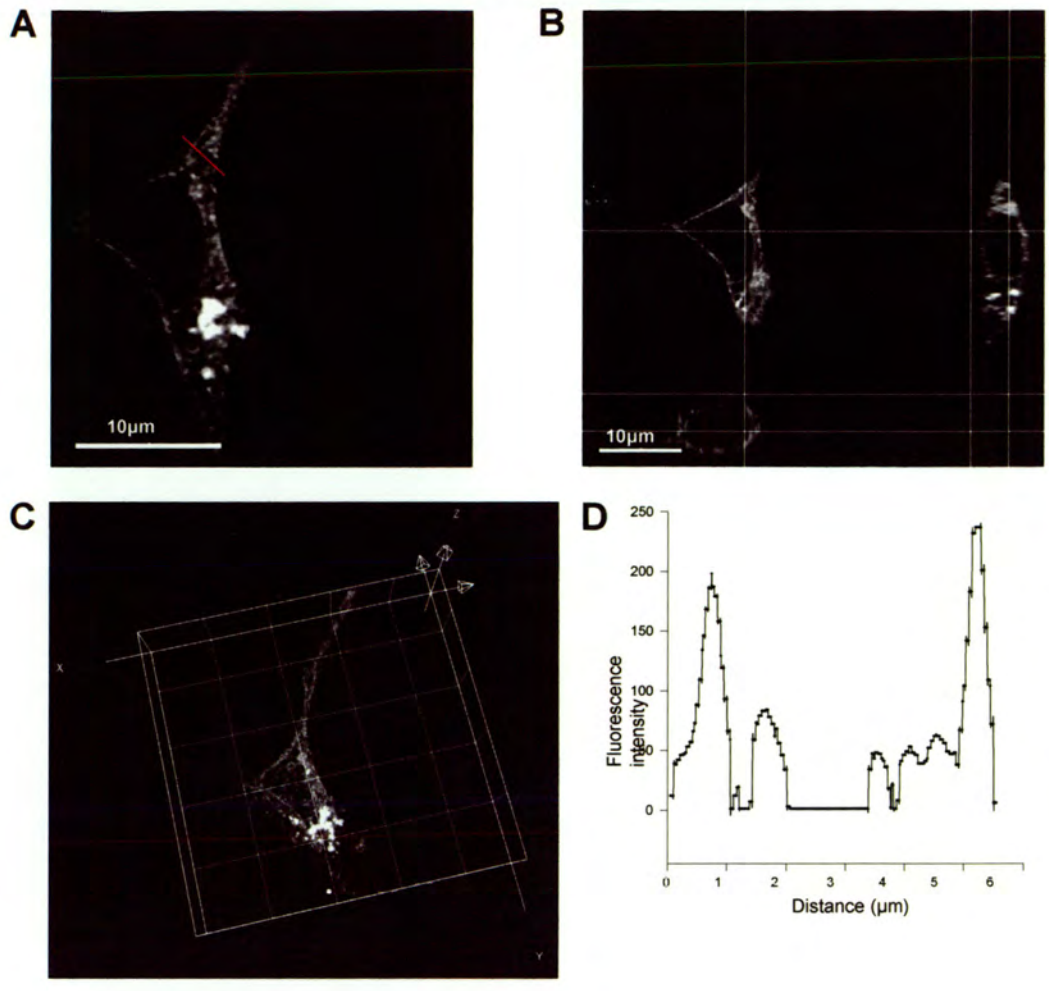

Figure 6.22: HEK293 cell transfected with ECFP-syntaxin 1a and EYFP-munc18-1$_{R39C:S306E:S313E}$

Colocalisation analysis was performed on a 3D pixel-by-pixel basid using Imaris colocalisation software

A: middle section of the image slice with an example of the lines drawn to investigate the distribution of the colocalisation within the cell

B: orthoslicer view of the colocalisation image stack

C: 3D reconstruction of the colocalised pixels with a 10 µM grid, see accompanying CD for movie.

D: A plot of the amount of colocalisation found in a line drawn through the middle section of the colocalisation image stack

the glutamic acids do not accurately mimic the electrostatics of PO_4^{2-} groups therefore do not rescue the R39C mutation as well as PKC phosphorylation does.

Similar experiments were done with cells treated with 100 nM 4α-PMA for 15 mins prior to fixing, which had no effect on the amount and distribution of the colocalisation calculated. In cells cotransfected with ECFP-syntaxin 1a and EYFP-munc18-$1_{S306E:S313E}$ and treated with 4α-PMA, 55.2±5.15 % of the ECFP-syntaxin 1a was found to colocalise with the EYFP-munc18-$1_{S306E:S313E}$ phosphomimetic mutant with a ratio of 0.95±0.33, both of which are not significantly different to the results obtained in untreated cells. With cells cotransfected with ECFP-syntaxin 1a and EYFP-munc18-$1_{R39C:S306E:S313E}$ treated with 4α-PMA, 56.6±6.9 % of the ECFP-syntaxin 1a colocalised with the EYFP-munc18-$1_{R39C:S306E:S313E}$ with a ratio of 1.25±0.19 and therefore not significantly different to the results obtained with untreated cells.

6.8 Summary

This chapter demonstrates that both syntaxin 1a and munc18-1 had to be co-expressed in cells together in order for the bimolecular complex to be properly targeted. These proteins, when expressed together, were found to colocalise specifically at the plasma membrane; approximately 50 % of syntaxin 1a colocalises with munc18-1, with a plasma membrane:intracellular colocalisation ratio >3, (Figure 6.23). Colocalisation analysis however, does not by itself reveal whether two proteins are interacting. For this TCSPC-FLIM was employed to investigate specifically the syntaxin 1a – munc18-1 interaction in HEK293 cells.

In cells cotransfected with ECFP-syntaxin 1a and EYFP-munc18-1, FLIM data showed the presence of three different ECFP-syntaxin 1a populations; a long-lifetime, non FRET population, which corresponded to regions of the cell in which no colocalisation was detected, and two FRET populations, of short and intermediate lifetimes. The short lifetime

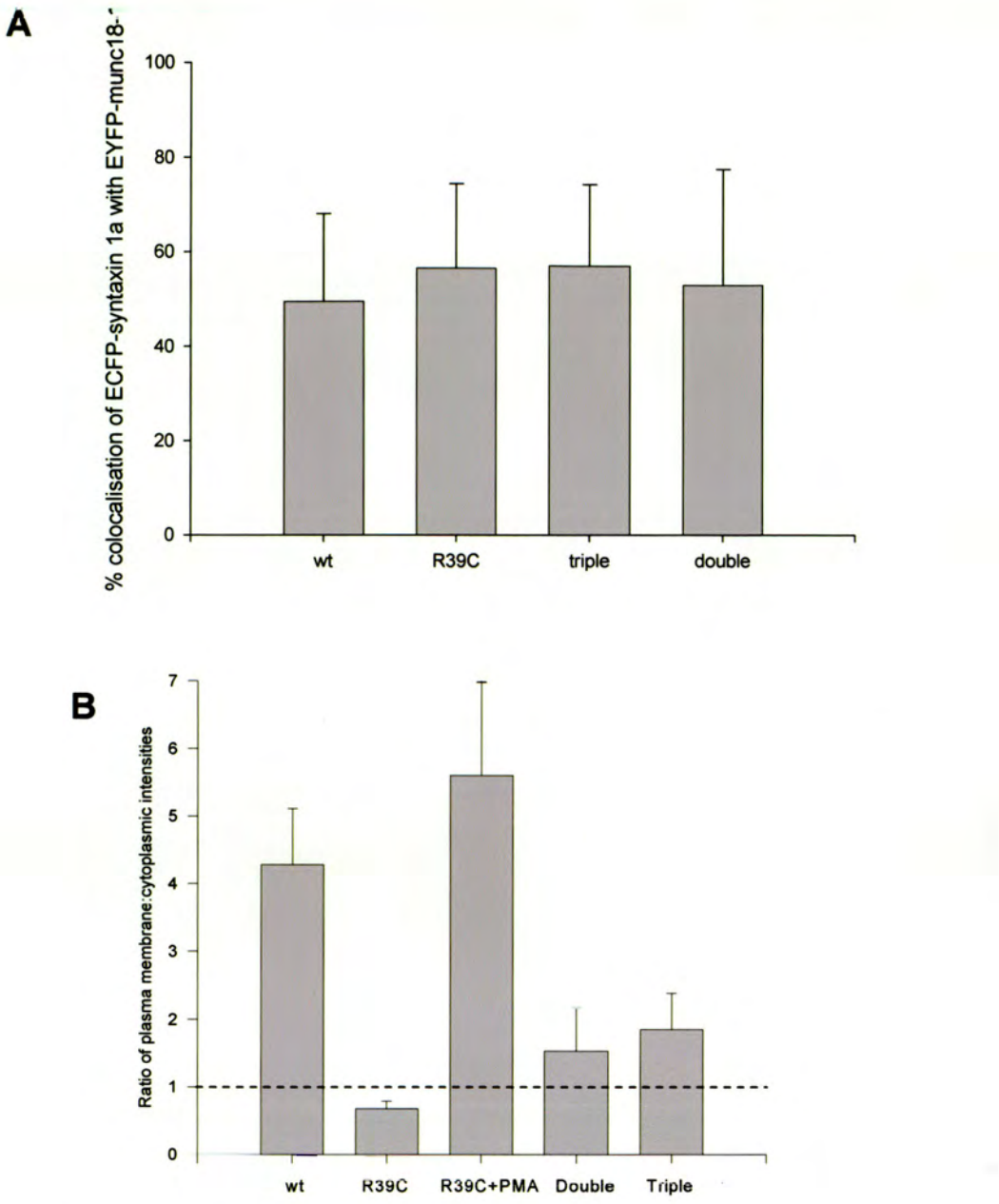

Figure 6.23: Colocalisation of syntaxin 1a with the different munc18 variantss

A: Histogram of the total colocalisation of ECFP-syntaxin with the various EYFP-munc18-1s including all treatments used (n = 3 for each group)

B: Histogram of colocalisation distribution ratios (plasma membrane/cytoplasmic intensities) (n = 3 in each group)

Double: ECFP-S1a/EYFP-M18-$1_{S306E:S313E}$

Triple: ECFP-S1a/EYFP-M18-$1_{R39C:S306E:S313E}$

population, in which the fluorophores are closest together, was localised exclusively to the plasma membrane of the cell and the intermediate lifetime population was found mainly in intracellular structures with some located to the plasma membrane. The presence of these two populations, with different FRET lifetimes, is suggestive of two distinct conformations of the syntaxin 1a – munc18-1 complex that are spatially restricted within the cell.

When the effect of munc18-1 PKC phosphorylation on serines 306 and 313 was investigated by incubating the cells with PMA, TCSPC-FLIM revealed that the population with the shortest FLIM lifetime had disappeared from the plasma membrane and was replaced by one with intermediate lifetime. This suggested that the phosphorylation of munc18-1 resulted in a change in the conformation of the syntaxin 1a – munc18-1 complex, altering the proximity of the fluorophores.

When the role of R39 was investigated by use of the munc18-1_{R39C} mutant, similar amounts of syntaxin 1a were found to localise with munc18-1_{R39C} (figure 6.23), however the proteins were mainly trapped in intracellular structures. TCSPC-FLIM analysis revealed only the presence of the non-FRET population, indicating that if the proteins were interacting they were doing so in a way that the fluorophores were either too far apart or in an unfavourable orientation for FRET to occur.

Interestingly, when these cells were treated with PMA the population of intermediate FRET lifetime could be detected. Furthermore, when the spatial distribution of the colocalisation between ECFP-syntaxin 1a and EYFP-munc18-1_{R39C} was investigated in the presence of PMA the proteins were found to colocalise largely on the plasma membrane (Figure 6.23). These results implied that when R39 is mutated to a cysteine it results in an altered conformation of the syntaxin 1a – munc18-1 complex that is not trafficked correctly to the plasma membrane, but phosphorylation of munc18-1 causes a conformational change, so that interactions involving R39 are not required and therefore the complex can be properly targeted.

To confirm that the effects seen were indeed due to phosphorylation of munc18-1 on Ser306 and Ser313, phosphomimetic mutants were made in which these serines were mutated to glutamic acids. TCSPC-FLIM analysis of cells cotransfected with either, ECFP-syntaxin 1a and EYFP-munc18-$1_{S306E:S313E}$ or ECFP-syntaxin 1a and EYFP-munc18-$1_{R39C:S306E:S313E}$ revealed the presence only of the population of intermediate lifetime and not that with the shortest FLIM lifetime, suggesting that phosphorylation on Ser306 and Ser313 is capable of altering the syntaxin 1a – munc18-1 complex conformation.

When the localisation of the ECFP-syntaxin 1a – EYFP-munc18-$1_{S306E:S313E}$ complex was investigated, differences were seen from the phosphorylated wild-type proteins. This complex was found slightly more on the plasma membrane than intracellularly, rather than being predominantly on the plasma membrane like the wild-type protein complex. In cells cotransfected with ECFP-syntaxin 1a and EYFP-munc18-$1_{R39C:S306E:S313E}$, the complex was also found in larger amounts on the plasma membrane than inside the cell, which was different to the localisation of the complex, both in cells cotransfected with ECFP-syntaxin 1a and EYFP-munc18-1_{R39C}, where the complex is trapped intracellularly, and in these cells after treatment with PMA, in which the complex is found predominantly on the plasma membrane. A reason for the differences in the spatial distribution of the phosphomimetic mutants could be due to the effect of the glutamic acid substitution on the folding of munc18-1, so that a fraction of munc18-1 is mis-folded the syntaxin 1a – munc18-1 complex is trapped intracellularly, but when the munc18-1 folds folds properly, the complex is correctly targeted to the plasma membrane, this seems plausible since PKC phophorylation of munc18-1 can only occur following folding, and the presence of the negatively charged amino acids at positions 306 and 313 may interfere with folding process.

Chapter 7

Summary and Discussion

7.1 Discussion and Future Work

Munc18-1 and its homologues, known as the Sec1/munc18 (SM) proteins are believed to be key regulators of membrane fusion steps throughout the secretory pathway, and to have both positive and negative regulatory roles in exocytosis. Many SM proteins share a common feature of interacting with their corresponding syntaxin homologue, leading to the suggestion that SM proteins may function by acting as a chaperone for their cognate syntaxin. This idea was strongly supported by studies in the yeast *S.cerevisiae* lacking the munc18 orthologue, Vps45p, where its syntaxin binding partner, Tlg2p was severely down-regulated through rapid proteasomal degradation (Bryant and James 2001). However the yeast munc18 homologue Sec1p does not bind to monomeric Sso1p, a syntaxin homologue, although it does bind to a ternary complex containing homologues of VAMP and SNAP-25 (Carr, Grote et al. 1999). In addition, in PC12 cells syntaxin is unable to leave the Golgi in the absence of munc18 (Rowe, Calegari et al. 2001) and a recent reanalysis of the munc18-1 null mutant mouse revealed that syntaxin 1a levels were reduced by up to 70% (Toonen, de Vries et al. 2005), providing a simple explanation for the reduction in neurotransmission seen. Therefore, munc18-1 may function by transporting newly synthesised syntaxin 1a, in an inhibited state, to sites of exocytosis, where the syntaxin 1a – munc18-1 complex dissociates, allowing SNARE complex formation and eventually exocytosis (Rickman and Davletov 2005). Such a role could explain both the positive and negative effects seen in the various SM protein mutants. However, this leads to a further question: how is syntaxin 1a released from its tight complex with munc18-1?

To date several possible candidates for the dissociation of the syntaxin 1a – munc18-1 complex have been investigated; UNC13/munc13 proteins, Rab and Rab effectors, Tomosyn, munc18-1 phosphorylation and, more recently, arachidonic acid and Mint1 (Okamoto and Sudhof 1997; Biederer and Sudhof 2000; Rickman, Hu et al. 2005). The work reported in this thesis focussed on the effects of phosphorylation by PKC, which has been shown to stimulate Ca^{2+}-dependent exocytosis in various types of secretory cell. PKC was found to

phosphorylate free munc18-1 on Ser306 and Ser313 *in vitro*, with a reduction in its affinity for syntaxin 1a, although munc18-1 was not phosphorylated when in complex with syntaxin 1a (Fujita, Sasaki et al. 1996). In this study however, the detergent CHAPS, which is capable of dissociating the syntaxin 1a – munc18-1 complex, was included in the reaction buffer (Rickman, Hu et al. 2005).

In rat brain synaptic terminals munc18-1 is almost completely dephosphorylated and inhibition of protein phosphatases results in a 250 % increase in phosphorylation, which is then increased by a further 1500 % on additional, direct PKC activation by phorbol esters (de Vries, Geijtenbeek et al. 2000). Also, phosphorylation of munc18-1 increased by 50 %, in a Ca^{2+}-dependent manner, within 5 seconds of K^+-evoked depolarisation, and activation of endogenous PKC in nerve terminals inhibited the interaction of munc18-1 with syntaxin 1a by 50 % (de Vries, Geijtenbeek et al. 2000).

In intact bovine chromaffin cells munc18-1 has been shown to be phosphorylated in response to treatment with phorbol ester or histamine and in permeabilised bovine chromaffin cells in response to elevation of $[Ca^{2+}]$, altering the release kinetics of exocytosis. These results were mimicked in chromaffin cells overexpressing a munc18-1 phosphomimetic mutant in which both Ser306 and Ser313 were mutated to glutamates (Barclay, Craig et al. 2003; Craig, Evans et al. 2003).

In this thesis the role of munc18-1 phosphorylation in the dimeric syntaxin 1a – munc18-1 complex was investigated by expressing fluorescent fusion proteins and various munc18-1 mutants in HEK293 cells, which were chosen since they do not contain endogenous munc18-1, syntaxin 1a or several other exocytotic proteins. Initial binding experiments were performed *in vitro*, comparing the relative binding affinities of wild-type syntaxin 1a and munc18-1 with those of N-terminally fluorescence-tagged syntaxin 1a and munc18-1, and it was concluded that the attachment of the fluorescent proteins had no significant effect on their interaction. HEK293 cells were then cotransfected with ECFP-syntaxin and either EYFP-munc18-1 or the munc18-1 mutant, EYFP-munc18-1_{R39C}. R39 is thought to be an

important residue in munc18-1-syntaxin interactions, since it not only makes electrostatic contacts with syntaxin 1a, but also coordinates intra-molecular interactions with other amino acids within each of the domains of munc18-1, suggesting that it is essential for stabilising both munc18-1 and the syntaxin 1a – munc18-1 complex structures. When R39 is mutated to cysteine all of these contacts are lost, and overexpression of this mutant in bovine chromaffin cells was reported to alter granule release kinetics (Fisher, Pevsner et al. 2001). In recent work with PC12, cells, however, no such effect was found (Schutz, Zilly et al. 2005). In this context, the possibility that syntaxin 1a is extensively localised in cholesterol-rich rafts (Salaun, Gould et al. 2005) may be relevant, as the amperometric studies of Fisher et al were performed in digitonin-permeabilized chromaffin cells, and the permeabilization process itself may have altered the distribution of syntaxin, thereby altering the release kinetics.

In these transfectants most of the proteins were localised intracellularly, with some of the ECFP-syntaxin 1a found on the plasma membrane. However, when HEK293 cells were cotransfected with ECFP-syntaxin 1a and EYFP-munc18-1 they were found to colocalise predominantly on the plasma membrane supporting the data from PC12 cells (Rowe, Calegari et al. 2001) and yeast (Bryant and James 2001), which suggested that munc18-1 has to be present for the correct plasma membrane targeting of syntaxin 1a. Interestingly, in HEK293 cells cotransfected with ECFP-syntaxin 1a and EYFP-munc18-1_{R39C} both proteins were found to be trapped on intracellular structures and not properly targeted to the plasma membrane, suggesting that the predominant effect of the munc18-1_{R39C} mutation is on targeting. This is in agreement with a recent report on the effect of the R39C mutation in PC12 cells (Schutz, Zilly et al. 2005). These workers also studied another munc18-1 variant, D34N, which binds negligibly to syntaxin 1a; paradoxically, while munc18-1_{R39C} inhibited exocytosis in PC12 cells, munc18-1_{D34N} was found to be stimulatory. This was attributed to its strong interaction with Mint1, which has been reported to form a trimeric complex with munc18 and syntaxin (Okamoto and Sudhof 1997).

These data strongly suggest an interaction between the two proteins, but since colocalisation of proteins does not necessarily prove their direct interaction, TCSPC-FLIM was used. This revealed the presence in HEK293 cells cotransfected with ECFP-syntaxin 1a and EYFP-munc18-1 of three ECFP-syntaxin 1a populations with distinct fluorescence lifetimes; a long-lifetime, non-FRET population in regions of the cells where no colocalisation was detected and two others, of short and intermediate FRET lifetimes. The population of highest FRET efficiency (short fluorescent lifetime) was detected exclusively on the plasma membrane and the population of lower FRET efficiency (intermediate fluorescent lifetime) was detected both on the plasma membrane and in intracellular structures. The finding of two FLIM lifetimes suggests two distinct conformational states of the bimolecular syntaxin 1a – munc18-1 complex; one in which the fluorophores are closer together or in a more favourable orientation, having a higher FRET efficiency, a shorter fluorescence lifetime and therefore probably a tighter interaction, than in the other conformation, because FRET is a direct measurement of the interdipole distance between the two fluorophores. In HEK293 cells cotransfected with ECFP-syntaxin 1a and EYFP-munc18-1_{R39C} only the non-FRET lifetime was detected suggesting that if the proteins were interacting they were doing so in a conformation in which the fluorophores were too far apart (>6nm in this system) or in a unfavourable orientation for FRET to occur.

Next, the effect of munc18-1 phosphorylation was investigated by treating the cells with phorbol ester before fixing. Analysis of colocalisation between ECFP-syntaxin 1a and EYFP-munc18-1 showed that the proteins were found mainly on the plasma membrane of the cells, with no significant difference in distribution from untreated cells. However, the FLIM data revealed that the population of shortest fluorescence lifetime, residing exclusively on the plasma membrane in untreated cells, had disappeared and been replaced by population with the intermediate fluorescence lifetime, suggesting that the phosphorylation of munc18-1 had altered the conformation of the syntaxin 1a – munc18-1 complex so that the two fluorophores were further apart. Interestingly, when FLIM data was acquired from HEK293

cells cotransfected with ECFP-syntaxin 1a and EYFP-munc18-1_{R39C} and then treated with PMA, the intermediate FRET lifetime was also detectable, implying that the phosphorylation of munc18-1 altered the conformation of the munc18-1_{R39C} and/or the ECFP-syntaxin 1a – EYFP-munc18-1_{R39C} complex so that the fluorophores were now able to participate in FRET. Furthermore, colocalisation analysis showed that the complex was predominantly on the plasma membrane, so its proper targeting had been restored by phosphorylation of EYFP-munc18-1_{R39C}. This suggests that if R39 is mutated to cysteine the conformation of munc18 and/or of the syntaxin 1a – munc18-1 complex is destabilized and that as a result it is no longer properly targeted; but that this is rescued by phosphorylation of munc18-1.

To confirm that the changes seen on addition of phorbol ester were indeed due to phosphorylation of munc18-1 the experiments were repeated using phosphomimetic mutants, in which Ser306 and Ser313 were mutated to glutamates. FLIM data from cells cotransfected with ECFP-syntaxin 1a and either EYFP-munc18-$1_{S306E:S313E}$ or EYFP-munc18-$1_{R39C:S306E:S313E}$ revealed the presence of a complex of intermediate fluorescence lifetime throughout the cells, suggesting that the negative charge on Ser306 and Ser313, arising either from phosphorylation or from mutation to glutamate, in munc18-1 is sufficient to change the conformation of the dimeric complex so that the fluorophores are further apart than when the shortest lifetime was detected. When colocalisation analysis was performed on these cells in both cases the syntaxin 1a – munc18-1 complex was found in roughly equal amounts on the plasma membrane and inside the cell, with slightly more on the plasma membrane, which was different from results obtained from cells cotransfected with wild-type proteins, either in the presence or the absence of phorbol ester, and from cells cotransfected with ECFP-syntaxin 1a and EYFP-munc18-1_{R39C} after treatment with phorbol ester. One possible explanation for this is that the phosphorylation of munc18-1 necessarily occurs post-translationally and after the protein has folded, while in contrast, the substitution of negatively charged glutamates for serines in positions 306 and 313 may affect the folding efficiency of the overexpressed munc18-1. Thus, if the phosphomimetic munc18-1s fold

correctly then the dimeric complex is targeted correctly to the plasma membrane, and if not then the complex is trapped intracellularly. Alternatively it is possible that the serine-to-glutamate substitution does not fully mimic the effect of phosphorylation.

Taken together these data suggest that the syntaxin 1a – munc18-1 complex can exist in two conformations that are spatially restricted within the cell (Figure 7.1) and that these conformations can be modulated by PKC-catalysed phosphorylation of munc18-1; the consequent conformational changes are reflected in the FLIM signal. In untreated cells the complex of shortest fluorescence lifetime, and presumably tightest interaction, was located exclusively on the plasma membrane, with the weaker complex, of intermediate fluorescent lifetime, located both on the plasma membrane and intracellularly. Upon PMA treatment, resulting in PKC activation and hence enhanced munc18-1 phosphorylation, the plasma membrane population of shortest fluorescence lifetime was replaced by one of intermediate fluorescence lifetime. This suggests that the fluorescence lifetime of ECFP-syntaxin 1a in complex with munc18-1 is indicative of the phosphorylation state of munc18-1. Therefore, the shortest fluorescent lifetime corresponds to the population of the complex containing non-phosphorylated munc18-1 and the intermediate fluorescent lifetime corresponds to syntaxin 1a – munc18-1 complexes containing phosphorylated munc18-1. This suggests that phosphorylation of munc18-1 is required for the targeting of the syntaxin 1a – munc18-1 complex to the plasma membrane, but that upon reaching the plasma membrane, munc18-1 is dephosphorylated, resulting in the appearance of the tightest complex, which holds syntaxin 1a in an inactive conformation until it is dissociated by some other factor, possibly arachidonic acid (Rickman and Davletov 2005), allowing exocytosis to proceed. This theory is further supported by the data obtained from cells overexpressing ECFP-syntaxin 1a and EYFP-munc18-1_{R39C}, in which the proteins either do not interact or are in a conformation that prevents the correct targeting of the complex; however upon phosphorylation of munc18-1 the conformation of the complex changes so that the requirement for R39 in stabilising the munc18-1 and/or syntaxin 1a – munc18-1 complex is bypassed, allowing its

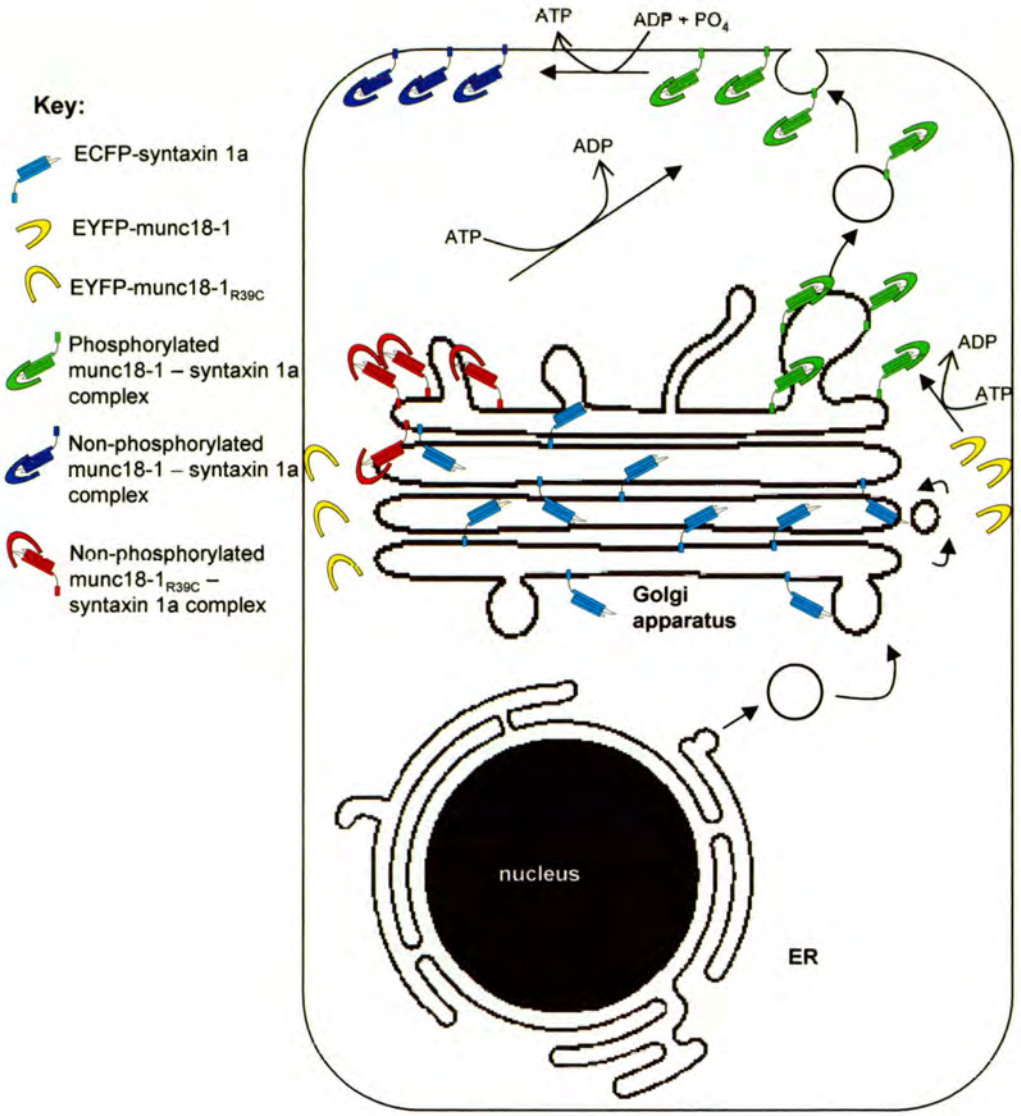

Figure 7.1: The targeting of the munc18-1 – syntaxin 1a complex in cells

Phosphorylated munc18-1 and syntaxin 1a form a complex in the Golgi apparatus. The bimolecular complex is then transported to the plasma membrane, where the munc18-1 is dephosphorylated. The complex remains on the plasma membrane until upon activation it is dissociated by some factor allowing syntaxin 1a to participate in SNARE complex formation and exocytosis to occur.

The munc18-1_{R39C} – syntaxin 1a complex remains trapped in the Golgi, where no FRET can be detected between the fluorophores. Upon phosphorylation, FRET is measured and the complex is properly targeted to the plasma membrane

proper targeting to the plasma membrane. Again this hypothesis is supported by the data seen with the phosphomimetic variants, in which the presence of glutamates at positions 306 and 313 is sufficient to alter the conformation of the complex so as to give the intermediate fluorescence lifetime and partially to rescue trafficking to the plasma membrane.

To further test this hypothesis and to confirm the role of munc18-1 phosphorylation in exocytosis these experiments should be repeated using a non-phosphorylatable munc18-1 mutant, created by mutating Ser306 and Ser313 to alanines. If this hypothesis is correct then the complex of munc18-$1_{S306A:S313A}$ with syntaxin 1a would be trapped intracellularly and exhibit the shortest fluorescence lifetime inside the cell. In addition the phosphorylation state of munc18-1 could be investigated using antibodies specific for phosphorylated munc18-1, raised against phosphorylated munc18-1-derived peptides. This would reveal whether the complex of intermediate fluorescence lifetime is phosphorylated, and the complex with the shortest lifetime is dephosphorylated. A further prediction, which could be tested *in vitro,* is that the phosphorylated, bimolecular syntaxin 1a – munc18-1 complex can be dephosphorylated.

The recent demonstration (Schutz, Zilly et al. 2005) that Mint1 may be directly involved in syntaxin 1a – munc18-1 complex formation suggests that an investigation of the effect of munc18 phosphorylation on its interactions with Mint1 is necessary. Finally, it is not known how trafficking of the bimolecular complex is carried out, and it remains to be investigated which cellular components interact with this complex in a conformation-dependent manner.

Appendices

Appendix I

Solutions

1.1 Electrophoretic separation and detection of proteins solutions

2.1.1 SDS-PAGE separating gel

component	*ml*
30:0.8 % (w/v) acrylamide/bis-acrylamide	2.0
1.5 M Tris-HCl, 8 mM EDTA, 0.4 % SDS pH8.8	1.5
H_2O	1.5
3 % Polyacrylamide, 1mM NaN_3, 1 mM NaF	1.0
TEMED	0.006
10 % (w/v) ammonium persulfate	0.06

1.1.1 SDS-PAGE stacking gel

component	*ml*
30:0.8% (w/v) acrylamide/bis-acrylamide	0.6
0.5 M Tris-HCl, 8 mM EDTA, 0.4 % SDS, pH6.5	1.0
H_2O	1.7
3 % Polyacrylamide, 1 mM NaN_3, 1 mM NaF	0.65
TEMED	0.006
10 % (w/v) ammonium persulfate	0.06

1.1.2 1 X SDS sample buffer

50 mM Tris-HCl pH6.5, 5 % (w/v) SDS, 10 % (w/v) glycerol, 10 mM DTT, 50 µg/ml bromophenol blue

1.1.3 Electrophoresis running buffer

0.05 M Tris-base, 0.384 M Glycine, 0.1 % SDS, 0.2 mM EDTA

1.2 Coomassie Blue R Staining

1.2.1 Fixing solution

50 % (v/v) methanol, 10 % (v/v) acetic acid

1.2.2 Coomassie Blue R Stain

0.25 % (w/v) Coomassie Brilliant Blue R dissolved in 50 % (v/v) methanol

10 % (v/v) acetic acid

1.2.3 Destaining solution

10 % (v/v) methanol, 7 % (v/v) acetic acid

1.3 Silver staining solutions

1.3.1 Solution A

dissolve 0.4 g $AgNO_3$ in 2 ml of H_2O

1.3.2 Solution B

mix 21 ml 0.36 % NaOH with 1.4 ml 14.8 M NH_4OH make up to 100 ml

1.3.3 Solution C

solution A added dropwise to solution B with vigorous stirring

1.3.4 Solution D

mix 2.5 ml 1 % acetic acid with 0.25 ml formaldehyde (38 % stock) and make up to 500 ml with H_2O

1.4 Western blotting solutions

1.4.1 Transfer Buffer

20 mM Na_2HPO_4, 20 % (v/v) methanol, 0.02 % (w/v) SDS

1.4.2 Tris buffered saline (TBS)

0.01 M Tris-HCl pH7.5, 0.15 M NaCl

1.4.3 TBST

0.01 M Tris-HCl pH7.5, 0.15 M NaCl, 0.5 % (v/v) Tween 20

1.4.4 Primary antibody solution

TBS, 0.1 % (v/v) NaN_3, 1 % (v/v) BSA, 10 % (v/v) Calf Serum, 0.05 % (v/v) Tween 20

1.4.5 ECL solution 1

1.0 ml stock luminol (250 mM in DMSO), 0,44 ml stock p-coumaric acid (90 mM in DMSO), 10 ml 1 M Tris-HCl pH8.5 made up to 100 ml with H_2O

1.4.6 ECL solution 2

64 µl 30 % H_2O_2, 10 ml 1 M Tris-HCl pH8.5 made up to 100 ml with H_2O

1.5 Purification of oligohistidine-tagged protein solutions

1.5.1 HiTrap affinity column solutions

1.5.1.1 Wash buffer

0.02 M phosphate, 0.5 M NaCl pH7.4

1.5.1.2 Elution buffer

0.02 M phosphate, 0.5 M NaCl, 50-500 mM Imadazole pH7.4

1.5.2 BD Talon™ resin solutions

1.5.2.1 Wash buffer

50 mM phosphate, 300 mM NaCl pH7.0

1.5.2.2 Elution buffer

50 mM NaH_2PO_4, 300 mM NaCl, 50-500 mM imadazole pH7.0

1.5.3 Ni-NTA Superflow columns solutions

1.5.3.1 Lysis buffer

50 mM NaH_2PO_4, 300 mM NaCl, 10 mM Imadazole, pH8.0

1.5.3.2 Wash buffer

50 mM NaH_2PO_4, 300 mM NaCl, 20 mM Imadazole, 0.5 % Triton X-100, pH8.0

1.5.3.3 Elution buffer

50 mM NaH_2PO_4, 300 mM NaCl, 250 mM Imadazole, pH8.0

1.6 Purification of GST-tagged proteins solutions

1.6.1 Wash buffer

PBS, 5 mM DTT, 0.1 % Triton X-100 pH7.5

1.7 Bradford method solutions

1.7.1 Bradfords reagent

50 mg Coomassie blue G250 dissolved in 25 ml 95 % (v/v) ethanol, 50 ml 85 % (v/v) phosphoric acid was added and then made up to 500 ml with H_2O

1.8 Lowry method solutions

1.8.1 Solution A

200 mM Na_2CO_3, 100 mM NaOH, 7 mM sodium tartate, 1 % (w/v) SDS

1.8.2 Solution B

4 % (w/v) $CuSO_4.5H_2O$

1.8.3 Solution C

100 µl solution B added to 10 ml solution A

1.8.4 Solution D

1:1 dilution H_2O:Folin reagent

1.9 Solubilisation and refolding of insoluble fusion proteins solutions using non detergent sulforbutane

1.9.1 Solubilising solution

50 mM HEPES-NaOH pH 7.5, 6 M guanidine HCl, 25 mM DTT

1.9.2 Inclusion body wash buffer

50 mM Tris, 1 mM EDTA, 100 mM NaCl, 2 M Urea, 1 % Triton X-100

1.9.3 Refolding buffer

50 mM HEPES pH7.5, 0.2 M NaCl, 1 mM DTT, 1 M NDSN256

1.9.4 Phosphate buffer

50 mM sodium phosphate, 300 mM NaCl pH7.0

1.10 Solubilising and refolding of insoluble GST-fusion proteins using Q-Sepharose

1.10.1 Buffer A

50 mM Tris-HCl pH8, 50 mM NaCl, 1 mM EDTA, 1 mM DTT, 1 mM phenylmethyl sulfonyl fluoride, 10 % glycerol

1.10.2 High salt buffer A

50 mM Tris-HCl pH8, 1 mM EDTA, 1 mM DTT, 1 mM phenylmethyl sulfonyl fluoride, 10 % glycerol, 250-750 mM NaCl

1.11 Binding experiment solutions

1.11.1 Binding/wash buffer

PBS, 100 mM HEPES, 5 mM DTT, 0.1 % Triton X-100 pH7.5

Appendix II

Sequencing Primers

2.2 Munc18-1 variants sequencing primers

2.2.1 Forward sequencing primers

T7: 5'-TAA TAC GAC TCA CTA TAG GG-3'

Munc18-1 Forward 1: 5'-AAC GAG AAG CGC GAT CAC AT-3'

Munc18-1 Forward 2: 5'-AGT ACA AGG ACA ATG CCT TG-3'

Munc18-1 Forward 3: 5'-AGA AGA CAG TGA GAT CAT CA-3'

EGFP Forward 1: 5'-CTG CTG CCC GAC AAC CAC TA-3'

EGFP – Munc18-1 junction: 5'-GAC GGC AGC GTG CAG CTC GC-3'

Munc18-1 – Vector junction: 5'-GGG GAG TAC CGC AGC GGT CC-3'

M13 uni (-43): 5'-AGG GTT TTC CCA GTC ACG ACG TT-3'

2.2.2 Reverse sequencing primers

T7 Reverse: 5'-CTA GTT ATT GCT CAG CGG T

Munc18-1 Reverse 1: 5'-TTT GTA TCC AGT TTG TCT TC-3'

Munc18-1 Reverse 2: 5'-ATG TTG GTG ATG ATC TCA CT-3'

Munc18-1 Reverse 3: 5'-TTG CTA GAG GAA AAG TCC TT-3'

EGFP Reverse 1: 5'-ATG CCG TTC TTC TGC TTG TC-3'

Munc18-1 – EGFP junction: 5'-GCT CTC GGG GCT TGT TGA TGA TA-3'

M13 rev (-49): 5'- GAG CGG ATA ACA ATT TCA CAC AGG-3'

2.3 Syntaxin 1a variants sequencing primers

2.3.1 Forward sequencing primers

T7: 5'-TAA TAC GAC TCA CTA TAG GG-3'

Syntaxin 1a – Vector junction: 5'-AGA GCC AGG GGG AGA TGA TT-3'

GST – ECFP junction: 5'-TCT TGA TGT TGT TTT ATA CA-3'

ECFP – Syntaxin 1a junction: 5'-GAC GGC AGC GTG CAG CTC GC-3'

2.3.2 Reverse sequencing primers

Syntaxin 1a – Vector junction: 5'- GGT TCG GGG AGG CCA GGA TG-3'

Reverse: 5'-AAC GCA ATT AAT GTG AGT TA-3'

Syntaxin 1a – ECFP junction: 5'-TCA GCA ATC TTG TCA ATA AA-3'

pGex Reverse: 5'-CGC TTA CAG ACA AGC TGT GA-3'

Appendix III

Dixon Equation

3.1 Derivation of the equation describing the Dixon Plot (Dixon 1953)

Consider a protein, P, that binds a ligand, L and a competitor, I, at the same binding site.

The binding equiilibria are defined as follows:

$$K_D = \frac{[P][L]}{[PL]}$$

$$K_I = \frac{[P][I]}{[PI]}$$

Denoting the total concentrations of protein, ligand and inhibitor as P_T, L_T and I_T, and assuming $I_T >> P_T$ but that $L_T \sim P_T$

$$P_T = [P] + [PL] + [PI]$$

$$[P] = \frac{K_D[PL]}{L_T - [PL]}$$

$$[PI] = \frac{K_D[PL][I]}{(L_T - [PL])K_I}$$

$$P_T = \frac{K_D[PL]}{L_T - [PL]} + [PL] + \frac{K_D[PL][I]}{(L_T - [PL])K_I}$$

This can be expanded to give the expression

$$P_T L_T - P_T[PL] = K_D[PL] + L_T[PL] - [PL]^2 + [PL][I]\frac{K_D}{K_I}$$

If [PL] is replaced by B, the concentration of bound ligand, and P_T by B_{max}, the concentration bound at saturation; and if the term $[PL]^2$ is neglected because it is small, this expression simplifies to:

$$L_T.B_{max} = B(K_D + B_{max} + L_T + [I]\frac{K_D}{K_I})$$

$$B = \frac{B_{max}.L_T}{L_T + B_{max} + K_D + [I]\frac{K_D}{K_I}}$$

$$\frac{1}{B} = \frac{L_T + B_{max} + K_D}{B_{max}.L_T} + [I]\frac{K_D}{K_I.B_{max}.L_T}$$

This predicts that a plot of 1/B against [I] will be a straight line of slope $K_D/K_I.B_{max}.L_T$

Appendix IV

Vector maps

4.1 Syntaxin 1a vector maps

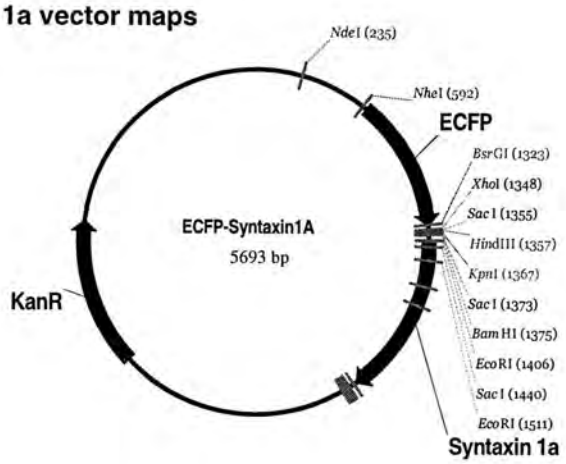

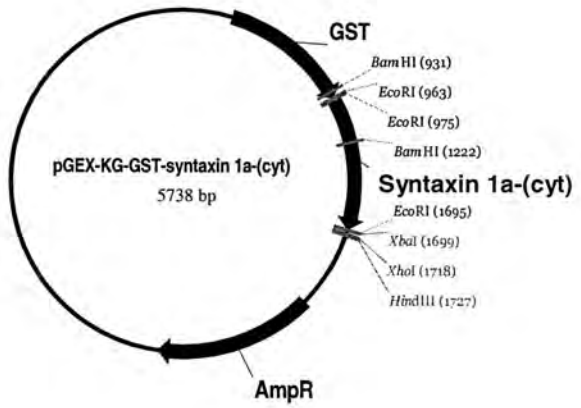

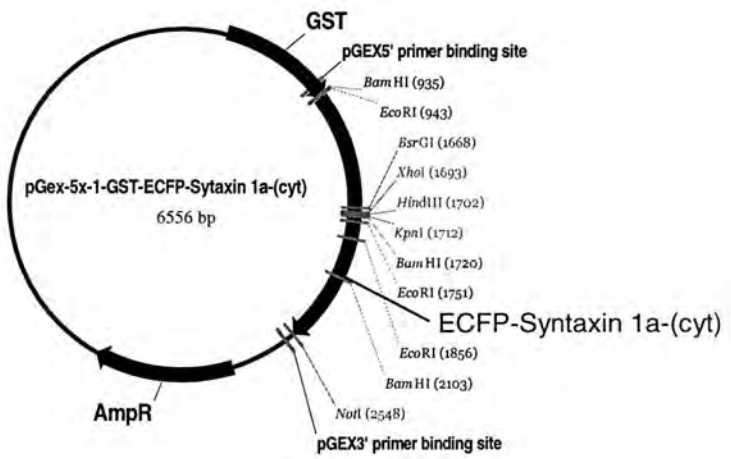

4.2 Munc18-1 vector maps

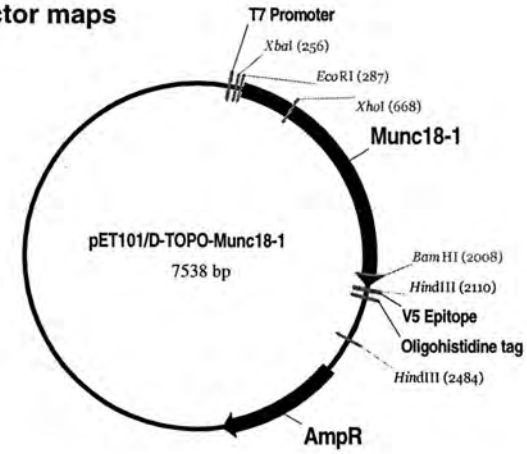

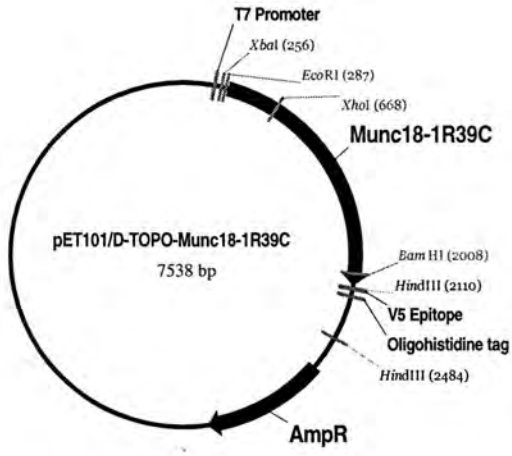

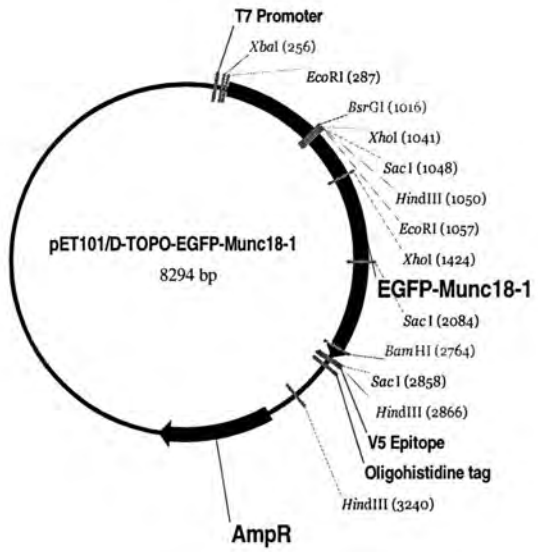

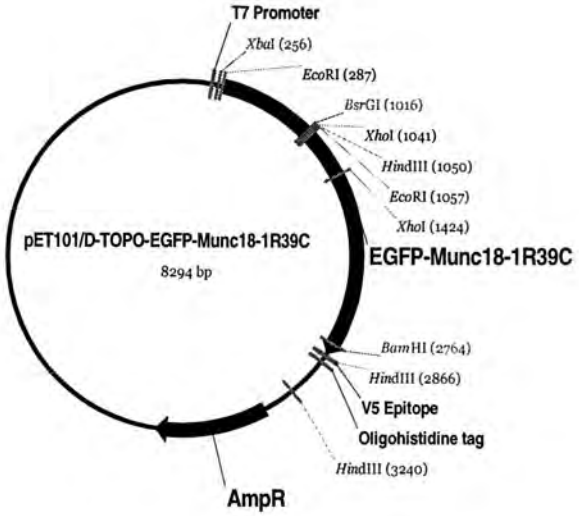
T7 Promoter
XbaI (256)
EcoRI (287)
BsrGI (1016)
XhoI (1041)
HindIII (1050)
EcoRI (1057)
XhoI (1424)
pET101/D-TOPO-EGFP-Munc18-1R39C
8294 bp
EGFP-Munc18-1R39C
BamHI (2764)
HindIII (2866)
V5 Epitope
Oligohistidine tag
HindIII (3240)
AmpR

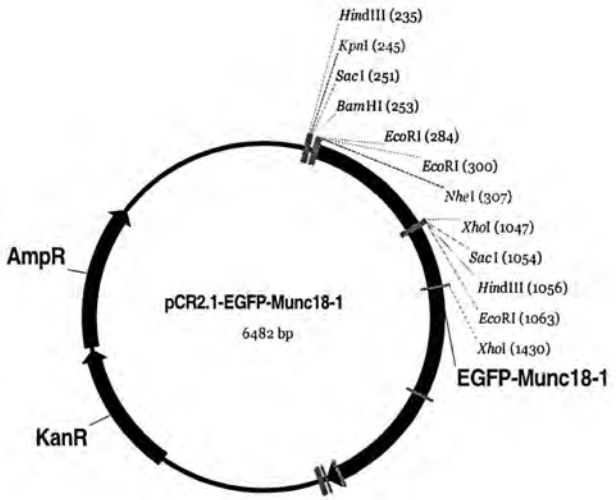
HindIII (235)
KpnI (245)
SacI (251)
BamHI (253)
EcoRI (284)
EcoRI (300)
NheI (307)
XhoI (1047)
SacI (1054)
HindIII (1056)
EcoRI (1063)
XhoI (1430)
AmpR
pCR2.1-EGFP-Munc18-1
6482 bp
EGFP-Munc18-1
KanR

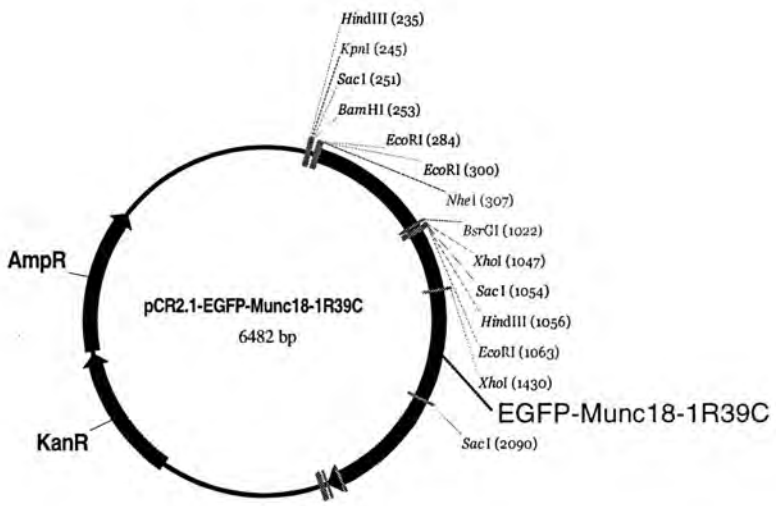
HindIII (235)
KpnI (245)
SacI (251)
BamHI (253)
EcoRI (284)
EcoRI (300)
NheI (307)
BsrGI (1022)
XhoI (1047)
SacI (1054)
HindIII (1056)
EcoRI (1063)
XhoI (1430)
AmpR
pCR2.1-EGFP-Munc18-1R39C
6482 bp
EGFP-Munc18-1R39C
KanR
SacI (2090)

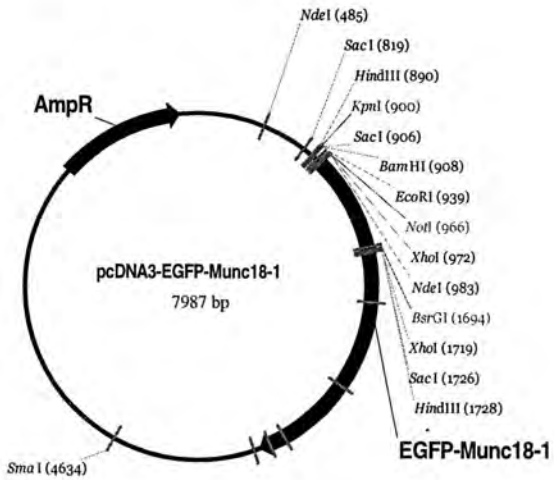
NdeI (485)
SacI (819)
HindIII (890)
KpnI (900)
SacI (906)
BamHI (908)
EcoRI (939)
NotI (966)
XhoI (972)
NdeI (983)
BsrGI (1694)
XhoI (1719)
SacI (1726)
HindIII (1728)
AmpR
pcDNA3-EGFP-Munc18-1
7987 bp
EGFP-Munc18-1
SmaI (4634)

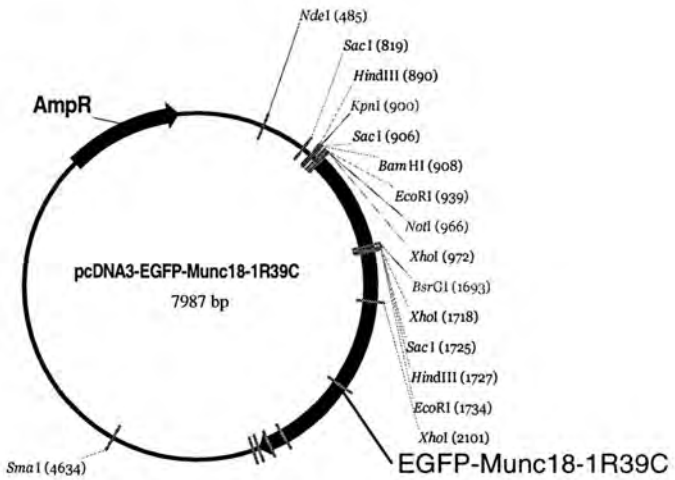
NdeI (485)
SacI (819)
HindIII (890)
KpnI (900)
SacI (906)
BamHI (908)
EcoRI (939)
NotI (966)
XhoI (972)
BsrGI (1693)
XhoI (1718)
SacI (1725)
HindIII (1727)
EcoRI (1734)
XhoI (2101)
AmpR
pcDNA3-EGFP-Munc18-1R39C
7987 bp
EGFP-Munc18-1R39C
SmaI (4634)

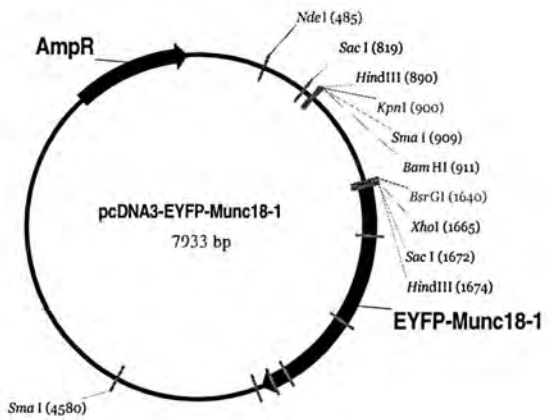
NdeI (485)
SacI (819)
HindIII (890)
KpnI (900)
SmaI (909)
BamHI (911)
BsrGI (1640)
XhoI (1665)
SacI (1672)
HindIII (1674)
AmpR
pcDNA3-EYFP-Munc18-1
7933 bp
EYFP-Munc18-1
SmaI (4580)

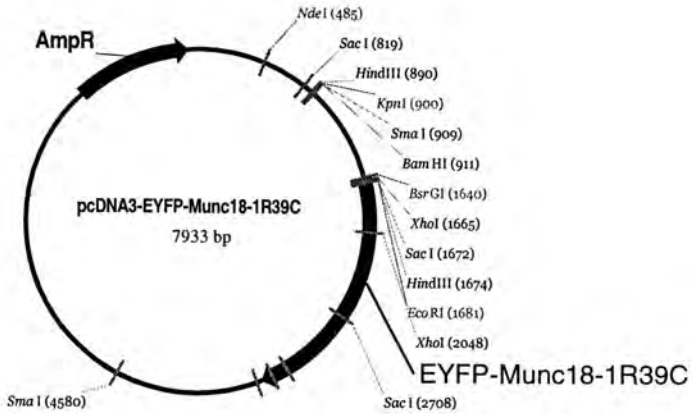
AmpR
NdeI (485)
SacI (819)
HindIII (890)
KpnI (900)
SmaI (909)
BamHI (911)
BsrGI (1640)
XhoI (1665)
SacI (1672)
HindIII (1674)
EcoRI (1681)
XhoI (2048)
pcDNA3-EYFP-Munc18-1R39C
7933 bp
EYFP-Munc18-1R39C
SmaI (4580)
SacI (2708)

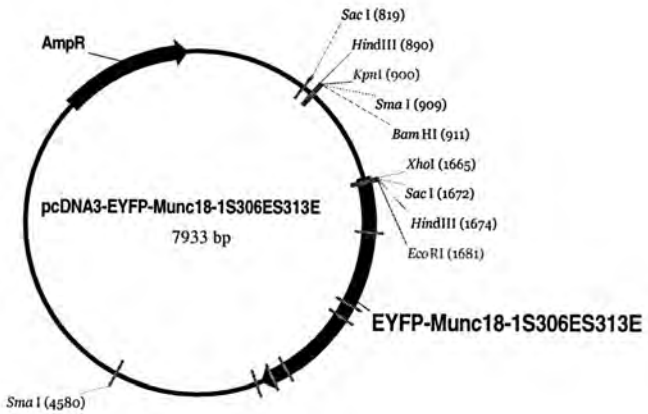
AmpR
SacI (819)
HindIII (890)
KpnI (900)
SmaI (909)
BamHI (911)
XhoI (1665)
SacI (1672)
HindIII (1674)
EcoRI (1681)
pcDNA3-EYFP-Munc18-1S306ES313E
7933 bp
EYFP-Munc18-1S306ES313E
SmaI (4580)

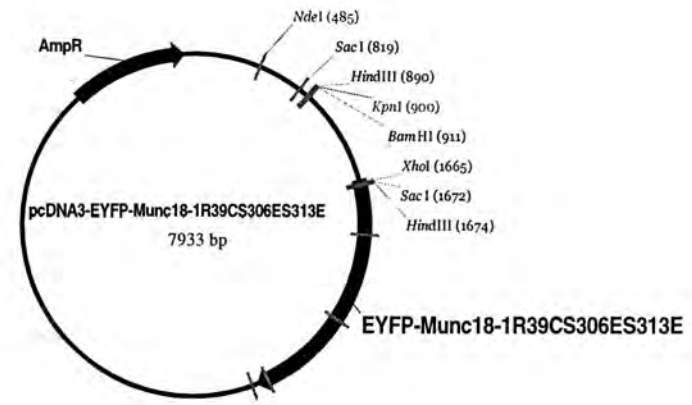
AmpR
NdeI (485)
SacI (819)
HindIII (890)
KpnI (900)
BamHI (911)
XhoI (1665)
SacI (1672)
HindIII (1674)
pcDNA3-EYFP-Munc18-1R39CS306ES313E
7933 bp
EYFP-Munc18-1R39CS306ES313E

Bibliography

Andersson, H., T. Baechi, et al. (1998). "Autofluorescence of living cells." J Microsc **191 (Pt 1)**: 1-7.

Apps, D. K., Cousin, M.A., Duncan, R.R., Wiegand, U.K., Shipston, M.J. (2004). The life cycle of secretory vesicles: implications for dendritic transmitter release. Dendritic Neurotranmitter Release. M. Ludwig, Plenum Press: 35-53.

Aubin, J. E. (1979). "Autofluorescence of viable cultured mammalian cells." J Histochem Cytochem **27**(1): 36-43.

Bai, J., P. Wang, et al. (2002). "C2A activates a cryptic Ca(2+)-triggered membrane penetration activity within the C2B domain of synaptotagmin I." Proc Natl Acad Sci U S A **99**(3): 1665-70.

Baird, G. S., D. A. Zacharias, et al. (2000). "Biochemistry, mutagenesis, and oligomerization of DsRed, a red fluorescent protein from coral." Proc Natl Acad Sci U S A **97**(22): 11984-9.

Bajno, L. and S. Grinstein (1999). "Fluorescent proteins: powerful tools in phagocyte biology." J Immunol Methods **232**(1-2): 67-75.

Banerjee, A., V. A. Barry, et al. (1996). "N-Ethylmaleimide-sensitive factor acts at a prefusion ATP-dependent step in Ca2+-activated exocytosis." J Biol Chem **271**(34): 20223-6.

Barclay, J. W., T. J. Craig, et al. (2003). "Phosphorylation of Munc18 by protein kinase C regulates the kinetics of exocytosis." J Biol Chem **278**(12): 10538-45.

Barg, S., C. S. Olofsson, et al. (2002). "Delay between fusion pore opening and peptide release from large dense-core vesicles in neuroendocrine cells." Neuron **33**(2): 287-99.

Beckers, C. J., M. R. Block, et al. (1989). "Vesicular transport between the endoplasmic reticulum and the Golgi stack requires the NEM-sensitive fusion protein." Nature **339**(6223): 397-8.

Bennett, M. K., N. Calakos, et al. (1992). "Syntaxin: a synaptic protein implicated in docking of synaptic vesicles at presynaptic active zones." Science **257**(5067): 255-9.

Benson, R. C., R. A. Meyer, et al. (1979). "Cellular autofluorescence--is it due to flavins?" J Histochem Cytochem **27**(1): 44-8.

Betz, A., U. Ashery, et al. (1998). "Munc13-1 is a presynaptic phorbol ester receptor that enhances neurotransmitter release." Neuron **21**(1): 123-36.

Betz, A., P. Thakur, et al. (2001). "Functional interaction of the active zone proteins Munc13-1 and RIM1 in synaptic vesicle priming." Neuron **30**(1): 183-96.

Biederer, T. and T. C. Sudhof (2000). "Mints as adaptors. Direct binding to neurexins and recruitment of munc18." J Biol Chem **275**(51): 39803-6.

Bittner, M. A. and R. W. Holz (1992). "A temperature-sensitive step in exocytosis." J Biol Chem **267**(23): 16226-9.

Blobel, G., P. Walter, et al. (1979). "Translocation of proteins across membranes: the signal hypothesis and beyond." Symp Soc Exp Biol **33**: 9-36.

Bock, J. B., H. T. Matern, et al. (2001). "A genomic perspective on membrane compartment organization." Nature **409**(6822): 839-41.

Bock, J. B. and R. H. Scheller (1999). "SNARE proteins mediate lipid bilayer fusion." Proc Natl Acad Sci U S A **96**(22): 12227-9.

Booth, C., L. Tian, et al. (1998). "Dissociation of early glucocorticoid inhibition of ACTH secretion and glucose uptake in mouse AtT20 D16:16 corticotrophs." J Neuroendocrinol **10**(6): 447-52.

Brenner, S. (1974). "The genetics of Caenorhabditis elegans." Genetics **77**(1): 71-94.

Brunger, A. T. (2000). "Structural insights into the molecular mechanism of Ca(2+)-dependent exocytosis." Curr Opin Neurobiol **10**(3): 293-302.

Bryant, N. J. and D. E. James (2001). "Vps45p stabilizes the syntaxin homologue Tlg2p and positively regulates SNARE complex formation." Embo J **20**(13): 3380-8.

Burgoyne, R. D. and A. Morgan (2003). "Secretory granule exocytosis." Physiol Rev **83**(2): 581-632.

Burke, N. V., W. Han, et al. (1997). "Neuronal peptide release is limited by secretory granule mobility." Neuron **19**(5): 1095-102.

Cahalan, M. D., I. Parker, et al. (2002). "Two-photon tissue imaging: seeing the immune system in a fresh light." Nat Rev Immunol **2**(11): 872-80.

Carr, C. M., E. Grote, et al. (1999). "Sec1p binds to SNARE complexes and concentrates at sites of secretion." J Cell Biol **146**(2): 333-44.

Chalfie, M., Y. Tu, et al. (1994). "Green fluorescent protein as a marker for gene expression." Science **263**(5148): 802-5.

Chamberlain, L. H., D. Roth, et al. (1995). "Distinct effects of alpha-SNAP, 14-3-3 proteins, and calmodulin on priming and triggering of regulated exocytosis." J Cell Biol **130**(5): 1063-70.

Chapman, E. R., P. I. Hanson, et al. (1995). "Ca2+ regulates the interaction between synaptotagmin and syntaxin 1." J Biol Chem **270**(40): 23667-71.

Cheek, T. R. and R. D. Burgoyne (1987). "Cyclic AMP inhibits both nicotine-induced actin disassembly and catecholamine secretion from bovine adrenal chromaffin cells." J Biol Chem **262**(24): 11663-6.

Ciufo, L. F., J. W. Barclay, et al. (2005). "Munc18-1 regulates early and late stages of exocytosis via syntaxin-independent protein interactions." Mol Biol Cell **16**(2): 470-82.

Cline, J., J. C. Braman, et al. (1996). "PCR fidelity of pfu DNA polymerase and other thermostable DNA polymerases." Nucleic Acids Res **24**(18): 3546-51.

Cody, C. W., D. C. Prasher, et al. (1993). "Chemical structure of the hexapeptide chromophore of the Aequorea green-fluorescent protein." Biochemistry **32**(5): 1212-8.

Compton, L. A. and W. C. Johnson, Jr. (1986). "Analysis of protein circular dichroism spectra for secondary structure using a simple matrix multiplication." Anal Biochem **155**(1): 155-67.

Craig, T. J., G. J. Evans, et al. (2003). "Physiological regulation of Munc18/nSec1 phosphorylation on serine-313." J Neurochem **86**(6): 1450-7.

Cubitt, A. B., R. Heim, et al. (1995). "Understanding, improving and using green fluorescent proteins." Trends Biochem Sci **20**(11): 448-55.

Dascher, C., R. Ossig, et al. (1991). "Identification and structure of four yeast genes (SLY) that are able to suppress the functional loss of YPT1, a member of the RAS superfamily." Mol Cell Biol **11**(2): 872-85.

de Vries, K. J., A. Geijtenbeek, et al. (2000). "Dynamics of munc18-1 phosphorylation/dephosphorylation in rat brain nerve terminals." Eur J Neurosci **12**(1): 385-90.

Dixon, M. (1953). "The determination of enzyme inhibitor constants." Biochem J **55**(1): 170-1.

Doyle, A., J. B. Griffiths, et al. (1994). Cell and Tissue Culture: Laboratory Procedures. Chichester, UK., Wiley and Sons.

Dresbach, T., M. E. Burns, et al. (1998). "A neuronal Sec1 homolog regulates neurotransmitter release at the squid giant synapse." J Neurosci **18**(8): 2923-32.

Dulubova, I., S. Sugita, et al. (1999). "A conformational switch in syntaxin during exocytosis: role of munc18." Embo J **18**(16): 4372-82.

Duncan, R. R., D. K. Apps, et al. (2000). "Is double C2 protein (DOC2) expressed in bovine adrenal medulla? A commercial anti-DOC2 monoclonal antibody recognizes a major bovine mitochondrial antigen." Biochem J **351**(Pt 1): 33-7.

Duncan, R. R., A. Bergmann, et al. (2004). "Multi-dimensional time-correlated single photon counting (TCSPC) fluorescence lifetime imaging microscopy (FLIM) to detect FRET in cells." J Microsc **215**(Pt 1): 1-12.

Duncan, R. R., Bergmann, A., Cousin, M. A., Apps, D. K., Shipston, M. J (2003). Multi-dimensional time-correlated single photon counting (TCSPC) fluorescence lifetime imaging microscopy (FLIM) to detec FRET in cells.

Duncan, R. R., A. Betz, et al. (1999). "Transient, phorbol ester-induced DOC2-Munc13 interactions in vivo." J Biol Chem **274**(39): 27347-50.

Duncan, R. R., J. Greaves, et al. (2003). "Functional and spatial segregation of secretory vesicle pools according to vesicle age." Nature **422**(6928): 176-80.

Elangovan, M., R. N. Day, et al. (2002). "Nanosecond fluorescence resonance energy transfer-fluorescence lifetime imaging microscopy to localize the protein interactions in a single living cell." J Microsc **205**(Pt 1): 3-14.

Eliasson, L., E. Renstrom, et al. (1997). "Rapid ATP-dependent priming of secretory granules precedes Ca(2+)-induced exocytosis in mouse pancreatic B-cells." J Physiol **503 (Pt 2)**: 399-412.

Fasshauer, D., D. Bruns, et al. (1997). "A structural change occurs upon binding of syntaxin to SNAP-25." J Biol Chem **272**(7): 4582-90.

Fasshauer, D., R. B. Sutton, et al. (1998). "Conserved structural features of the synaptic fusion complex: SNARE proteins reclassified as Q- and R-SNAREs." Proc Natl Acad Sci U S A **95**(26): 15781-6.

Fernandez, I., D. Arac, et al. (2001). "Three-dimensional structure of the synaptotagmin 1 C2B-domain: synaptotagmin 1 as a phospholipid binding machine." Neuron **32**(6): 1057-69.

Fernandez, I., J. Ubach, et al. (1998). "Three-dimensional structure of an evolutionarily conserved N-terminal domain of syntaxin 1A." Cell **94**(6): 841-9.

Ferro-Novick, S. and R. Jahn (1994). "Vesicle fusion from yeast to man." Nature **370**(6486): 191-3.

Fisher, R. J., J. Pevsner, et al. (2001). "Control of Fusion Pore Dynamics During Exocytosis by Munc18." Science **291**(5505): 875-878.

Fix, M., T. J. Melia, et al. (2004). "Imaging single membrane fusion events mediated by SNARE proteins." Proc Natl Acad Sci U S A **101**(19): 7311-6.

Fletcher, A. I., R. Shuang, et al. (1999). "Regulation of exocytosis by cyclin-dependent kinase 5 via phosphorylation of Munc18." J Biol Chem **274**(7): 4027-35.

Fujita, Y., T. Sasaki, et al. (1996). "Phosphorylation of Munc-18/n-Sec1/rbSec1 by protein kinase C: its implication in regulating the interaction of Munc-18/n-Sec1/rbSec1 with syntaxin." J Biol Chem **271**(13): 7265-8.

Fujita, Y., H. Shirataki, et al. (1998). "Tomosyn: a syntaxin-1-binding protein that forms a novel complex in the neurotransmitter release process." Neuron **20**(5): 905-15.

Fukuda, M., E. Kanno, et al. (2002). "Slp4-a/granuphilin-a regulates dense-core vesicle exocytosis in PC12 cells." J Biol Chem **277**(42): 39673-8.

Gaudin, Y., R. W. Ruigrok, et al. (1995). "Low-pH induced conformational changes in viral fusion proteins: implications for the fusion mechanism." J Gen Virol **76 (Pt 7)**: 1541-56.

Gerber, S. H. and T. C. Sudhof (2002). "Molecular determinants of regulated exocytosis." Diabetes **51 Suppl 1**: S3-S11.

Gerst, J. E. (1999). "SNAREs and SNARE regulators in membrane fusion and exocytosis." Cell Mol Life Sci **55**(5): 707-34.

Gladycheva, S. E., C. S. Ho, et al. (2004). "Regulation of syntaxin1A-munc18 complex for SNARE pairing in HEK293 cells." J Physiol **558**(Pt 3): 857-71.

Greengard, P., F. Valtorta, et al. (1993). "Synaptic vesicle phosphoproteins and regulation of synaptic function." Science **259**(5096): 780-5.

Groffen, A. J., E. C. Brian, et al. (2004). "Ca(2+)-induced recruitment of the secretory vesicle protein DOC2B to the target membrane." J Biol Chem **279**(22): 23740-7.

Grote, E., C. M. Carr, et al. (2000). "Ordering the final events in yeast exocytosis." J Cell Biol **151**(2): 439-52.

Gurskaya, N. G., A. F. Fradkov, et al. (2001). "GFP-like chromoproteins as a source of far-red fluorescent proteins." FEBS Lett **507**(1): 16-20.

Halachmi, N. and Z. Lev (1996). "The Sec1 family: a novel family of proteins involved in synaptic transmission and general secretion." J Neurochem **66**(3): 889-97.

Han, X., C. T. Wang, et al. (2004). "Transmembrane segments of syntaxin line the fusion pore of Ca2+-triggered exocytosis." Science **304**(5668): 289-92.

Hanson, P. I. (2000). "Sec1 gets a grip on syntaxin." Nat Struct Biol **7**(5): 347-9.

Harter, C., P. James, et al. (1989). "Hydrophobic binding of the ectodomain of influenza hemagglutinin to membranes occurs through the "fusion peptide"." J Biol Chem **264**(11): 6459-64.

Hata, Y., C. A. Slaughter, et al. (1993). "Synaptic vesicle fusion complex contains unc-18 homologue bound to syntaxin." Nature **366**(6453): 347-51.

Hayashi, T., H. McMahon, et al. (1994). "Synaptic vesicle membrane fusion complex: action of clostridial neurotoxins on assembly." Embo J **13**(21): 5051-61.

Heinemann, C., R. H. Chow, et al. (1994). "Kinetics of the secretory response in bovine chromaffin cells following flash photolysis of caged Ca2+." Biophys J **67**(6): 2546-57.

Hess, D. T., T. M. Slater, et al. (1992). "The 25 kDa synaptosomal-associated protein SNAP-25 is the major methionine-rich polypeptide in rapid axonal transport and a major substrate for palmitoylation in adult CNS." J Neurosci **12**(12): 4634-41.

Hoess, A., A. K. Arthur, et al. (1988). "Recovery of soluble, biologically active recombinant proteins from total bacterial lysates using ion exchange resin." Biotechnology **6**: 1214-1217.

Holz, R. W., M. A. Bittner, et al. (1989). "MgATP-independent and MgATP-dependent exocytosis. Evidence that MgATP primes adrenal chromaffin cells to undergo exocytosis." J Biol Chem **264**(10): 5412-9.

Hsu, S. F. and M. B. Jackson (1996). "Rapid exocytosis and endocytosis in nerve terminals of the rat posterior pituitary." J Physiol **494 (Pt 2)**: 539-53.

Inoue, A., K. Obata, et al. (1992). "Cloning and sequence analysis of cDNA for a neuronal cell membrane antigen, HPC-1." J Biol Chem **267**(15): 10613-9.

Jahn, R. (2000). "Sec1/Munc18 proteins: mediators of membrane fusion moving to center stage." Neuron **27**(2): 201-4.

Jahn, R. and T. C. Sudhof (1999). "Membrane fusion and exocytosis." Annu Rev Biochem **68**: 863-911.

Kaiser, C. A. and R. Schekman (1990). "Distinct sets of SEC genes govern transport vesicle formation and fusion early in the secretory pathway." Cell **61**(4): 723-33.

Krasnoperov, V. G., M. A. Bittner, et al. (1997). "alpha-Latrotoxin stimulates exocytosis by the interaction with a neuronal G-protein-coupled receptor." Neuron **18**(6): 925-37.

Lehman, K., G. Rossi, et al. (1999). "Yeast homologues of tomosyn and lethal giant larvae function in exocytosis and are associated with the plasma membrane SNARE, Sec9." J Cell Biol **146**(1): 125-40.

Lewis, J. L., M. Dong, et al. (2001). "The transmembrane domain of syntaxin 1A is critical for cytoplasmic domain protein-protein interactions." J Biol Chem **276**(18): 15458-65.

Li, L. and L. S. Chin (2003). "The molecular machinery of synaptic vesicle exocytosis." Cell Mol Life Sci **60**(5): 942-60.

Lin, R. C. and R. H. Scheller (2000). "MECHANISMS OF SYNAPTIC VESICLE EXOCYTOSIS." Annu. Rev. Cell Dev. Biol. **16**(1): 19-49.

Lindau, M. and G. Alvarez de Toledo (2003). "The fusion pore." Biochim Biophys Acta **1641**(2-3): 167-73.

Liu, J., S. A. Ernst, et al. (2004). "Fluorescence resonance energy transfer reports properties of syntaxin1a interaction with Munc18-1 in vivo." J Biol Chem **279**(53): 55924-36.

Lobley, A., L. Whitmore, et al. (2002). "DICHROWEB: an interactive website for the analysis of protein secondary structure from circular dichroism spectra." Bioinformatics **18**(1): 211-2.

Manavalan, P. and W. C. Johnson, Jr. (1987). "Variable selection method improves the prediction of protein secondary structure from circular dichroism spectra." Anal Biochem **167**(1): 76-85.

Marek, K. W. and G. W. Davis (2002). "Transgenically encoded protein photoinactivation (FlAsH-FALI): acute inactivation of synaptotagmin I." Neuron **36**(5): 805-13.

Margittai, M., D. Fasshauer, et al. (2003). "The Habc domain and the SNARE core complex are connected by a highly flexible linker." Biochemistry **42**(14): 4009-14.

Margittai, M., J. Widengren, et al. (2003). "Single-molecule fluorescence resonance energy transfer reveals a dynamic equilibrium between closed and open conformations of syntaxin 1." Proc Natl Acad Sci U S A **100**(26): 15516-21.

Matz, M. V., A. F. Fradkov, et al. (1999). "Fluorescent proteins from nonbioluminescent Anthozoa species." Nat Biotechnol **17**(10): 969-73.

McMahon, H. T., M. Missler, et al. (1995). "Complexins: cytosolic proteins that regulate SNAP receptor function." Cell **83**(1): 111-9.

McNew, J. A., F. Parlati, et al. (2000). "Compartmental specificity of cellular membrane fusion encoded in SNARE proteins." Nature **407**(6801): 153-9.

Misura, K. M., R. H. Scheller, et al. (2000). "Three-dimensional structure of the neuronal-Sec1-syntaxin 1a complex." Nature **404**(6776): 355-62.

Morise, H., O. Shimomura, et al. (1974). "Intermolecular energy transfer in the bioluminescent system of Aequorea." Biochemistry **13**(12): 2656-62.

Nelson, B. A., K. A. Robinson, et al. (2002). "Insulin acutely regulates Munc18-c subcellular trafficking: altered response in insulin-resistant 3T3-L1 adipocytes." J Biol Chem **277**(6): 3809-12.

Niswender, K. D., S. M. Blackman, et al. (1995). "Quantitative imaging of green fluorescent protein in cultured cells: comparison of microscopic techniques, use in fusion proteins and detection limits." J Microsc **180 (Pt 2)**: 109-16.

Nonet, M. L., O. Saifee, et al. (1998). "Synaptic transmission deficits in Caenorhabditis elegans synaptobrevin mutants." J Neurosci **18**(1): 70-80.

Novick, P. and R. Schekman (1979). "Secretion and cell-surface growth are blocked in a temperature-sensitive mutant of Saccharomyces cerevisiae." Proc Natl Acad Sci U S A **76**(4): 1858-62.

Oheim, M., D. Loerke, et al. (1998). "The last few milliseconds in the life of a secretory granule. Docking, dynamics and fusion visualized by total internal reflection fluorescence microscopy (TIRFM)." Eur Biophys J **27**(2): 83-98.

Oheim, M., D. Loerke, et al. (1999). "Multiple stimulation-dependent processes regulate the size of the releasable pool of vesicles." Eur Biophys J **28**(2): 91-101.

Okamoto, M. and T. C. Sudhof (1997). "Mints, Munc18-interacting proteins in synaptic vesicle exocytosis." J Biol Chem **272**(50): 31459-64.

Ormo, M., A. B. Cubitt, et al. (1996). "Crystal structure of the Aequorea victoria green fluorescent protein." Science **273**(5280): 1392-5.

Ossig, R., C. Dascher, et al. (1991). "The yeast SLY gene products, suppressors of defects in the essential GTP-binding Ypt1 protein, may act in endoplasmic reticulum-to-Golgi transport." Mol Cell Biol **11**(6): 2980-93.

Parlati, F., J. A. McNew, et al. (2000). "Topological restriction of SNARE-dependent membrane fusion." Nature **407**(6801): 194-8.

Pelham, H. R. (1999). "SNAREs and the secretory pathway-lessons from yeast." Exp Cell Res **247**(1): 1-8.

Peng, R. and D. Gallwitz (2002). "Sly1 protein bound to Golgi syntaxin Sed5p allows assembly and contributes to specificity of SNARE fusion complexes." J Cell Biol **157**(4): 645-55.

Pepperkok, R., A. Squire, et al. (1999). "Simultaneous detection of multiple green fluorescent proteins in live cells by fluorescence lifetime imaging microscopy." Curr Biol **9**(5): 269-72.

Peterson, G. L. (1977). "A simplification of the protein assay method of Lowry et al. which is more generally applicable." Anal Biochem **83**: 346-356.

Pollok, B. A. and R. Heim (1999). "Using GFP in FRET-based applications." Trends Cell Biol **9**(2): 57-60.

Pouli, A. E., E. Emmanouilidou, et al. (1998). "Secretory-granule dynamics visualized in vivo with a phogrin-green fluorescent protein chimaera." Biochem J **333**(Pt 1): 193-9.

Prasher, D. C., V. K. Eckenrode, et al. (1992). "Primary structure of the Aequorea victoria green-fluorescent protein." Gene **111**(2): 229-33.

Presley, J. F., N. B. Cole, et al. (1997). "ER-to-Golgi transport visualized in living cells." Nature **389**(6646): 81-5.

Provencher, S. W. and J. Glockner (1981). "Estimation of globular protein secondary structure from circular dichroism." Biochemistry **20**(1): 33-7.

Rhee, J. S., A. Betz, et al. (2002). "Beta phorbol ester- and diacylglycerol-induced augmentation of transmitter release is mediated by Munc13s and not by PKCs." Cell **108**(1): 121-33.

Richmond, J. E., R. M. Weimer, et al. (2001). "An open form of syntaxin bypasses the requirement for UNC-13 in vesicle priming." Nature **412**(6844): 338-41.

Rickman, C. and B. Davletov (2005). "Arachidonic Acid Allows SNARE Complex Formation in the Presence of Munc18." Chem Biol **12**(5): 545-53.

Rickman, C., K. Hu, et al. (2005). "Self-assembly of SNARE fusion proteins into star-shaped oligomers." Biochem J **388**(Pt 1): 75-9.

Rizo, J. and T. C. Sudhof (2002). "Snares and Munc18 in synaptic vesicle fusion." Nat Rev Neurosci **3**(8): 641-53.

Rowe, J., F. Calegari, et al. (2001). "Syntaxin 1A is delivered to the apical and basolateral domains of epithelial cells: the role of munc-18 proteins." J Cell Sci **114**(Pt 18): 3323-32.

Salaun, C., G. W. Gould, et al. (2005). "Lipid raft association of SNARE proteins regulates exocytosis in PC12 cells." J Biol Chem **280**(20): 19449-53.

Sambrook, J., E. F. Fritsch, et al. (1989). Molecular Cloning: A Laboratory Manual. NJ, Cold Spring Harbour Laboratory Press.

Sassa, T., S. Harada, et al. (1999). "Regulation of the UNC-18-Caenorhabditis elegans syntaxin complex by UNC-13." J Neurosci **19**(12): 4772-7.

Sato, T. K., P. Rehling, et al. (2000). "Class C Vps protein complex regulates vacuolar SNARE pairing and is required for vesicle docking/fusion." Mol Cell **6**(3): 661-71.

Schoch, S., F. Deak, et al. (2001). "SNARE function analyzed in synaptobrevin/VAMP knockout mice." Science **294**(5544): 1117-22.

Schulze, K. L., K. Broadie, et al. (1995). "Genetic and electrophysiological studies of Drosophila syntaxin-1A demonstrate its role in nonneuronal secretion and neurotransmission." Cell **80**(2): 311-20.

Schulze, K. L., J. T. Littleton, et al. (1994). "rop, a Drosophila homolog of yeast Sec1 and vertebrate n-Sec1/Munc-18 proteins, is a negative regulator of neurotransmitter release in vivo." Neuron **13**(5): 1099-108.

Schutz, D., F. Zilly, et al. (2005). "A dual function for Munc-18 in exocytosis of PC12 cells." Eur J Neurosci **21**(9): 2419-32.

Sevrioukov, E. A., J. P. He, et al. (1999). "A role for the deep orange and carnation eye color genes in lysosomal delivery in Drosophila." Mol Cell **4**(4): 479-86.

Shimomura, O., F. H. Johnson, et al. (1962). "Extraction, purification and properties of aequorin, a bioluminescent protein from the luminous hydromedusan, Aequorea." J Cell Comp Physiol **59**: 223-39.

Shuman, S. (1991). "Recombination mediated by vaccinia virus DNA topoisomerase I in Escherichia coli is sequence specific." Proc Natl Acad Sci U S A **88**(22): 10104-8.

Shuman, S. (1994). "Novel approach to molecular cloning and polynucleotide synthesis using vaccinia DNA topoisomerase." J Biol Chem **269**(51): 32678-84.

Sollner, T., M. K. Bennett, et al. (1993). "A protein assembly-disassembly pathway in vitro that may correspond to sequential steps of synaptic vesicle docking, activation, and fusion." Cell **75**(3): 409-18.

Sreerama, N. and R. W. Woody (2000). "Estimation of protein secondary structure from circular dichroism spectra: comparison of CONTIN, SELCON, and CDSSTR methods with an expanded reference set." Anal Biochem **287**(2): 252-60.

Steyer, J. A. and W. Almers (1999). "Tracking single secretory granules in live chromaffin cells by evanescent-field fluorescence microscopy." Biophys J **76**(4): 2262-71.

Steyer, J. A., H. Horstmann, et al. (1997). "Transport, docking and exocytosis of single secretory granules in live chromaffin cells." Nature **388**(6641): 474-8.

Sudhof, T. C. (1995). "The synaptic vesicle cycle: a cascade of protein-protein interactions." Nature **375**(6533): 645-53.

Sudhof, T. C. (2004). "The synaptic vesicle cycle." Annu Rev Neurosci **27**: 509-47.

Sutton, R. B., D. Fasshauer, et al. (1998). "Crystal structure of a SNARE complex involved in synaptic exocytosis at 2.4 A resolution." Nature **395**(6700): 347-53.

Tahara, M., J. R. Coorssen, et al. (1998). "Calcium can disrupt the SNARE protein complex on sea urchin egg secretory vesicles without irreversibly blocking fusion." J Biol Chem **273**(50): 33667-73.

Terrian, D. M. and M. K. White (1997). "Phylogenetic analysis of membrane trafficking proteins: a family reunion and secondary structure predictions." Eur J Cell Biol **73**(3): 198-204.

Toonen, R. F., K. J. de Vries, et al. (2005). "Munc18-1 stabilizes syntaxin 1, but is not essential for syntaxin 1 targeting and SNARE complex formation." J Neurochem **93**(6): 1393-400.

Toonen, R. F. and M. Verhage (2003). "Vesicle trafficking: pleasure and pain from SM genes." Trends Cell Biol **13**(4): 177-86.

Towbin, H., T. Staehelin, et al. (1979). "Electrophoretic transfer of proteins from polyacrylamide gels to nitrocellolose sheets: procedure and some applications." Proc.Nat.Acad.Sci.USA **76**: 4350-4354.

Tramier, M., I. Gautier, et al. (2002). "Picosecond-hetero-FRET microscopy to probe protein-protein interactions in live cells." Biophys J **83**(6): 3570-7.

Tucker, W. C., T. Weber, et al. (2004). "Reconstitution of Ca2+-regulated membrane fusion by synaptotagmin and SNAREs." Science **304**(5669): 435-8.

Ubach, J., X. Zhang, et al. (1998). "Ca2+ binding to synaptotagmin: how many Ca2+ ions bind to the tip of a C2-domain?" Embo J **17**(14): 3921-30.

Ungermann, C., K. Sato, et al. (1998). "Defining the functions of trans-SNARE pairs." Nature **396**(6711): 543-8.

van Kuppeveld, F. J., W. J. Melchers, et al. (2002). "Homomultimerization of the coxsackievirus 2B protein in living cells visualized by fluorescence resonance energy transfer microscopy." J Virol **76**(18): 9446-56.

Verhage, M., A. S. Maia, et al. (2000). "Synaptic assembly of the brain in the absence of neurotransmitter secretion." Science **287**(5454): 864-9.

Vitale, M. L., E. P. Seward, et al. (1995). "Chromaffin cell cortical actin network dynamics control the size of the release-ready vesicle pool and the initial rate of exocytosis." Neuron **14**(2): 353-63.

Voets, T., T. Moser, et al. (2001). "Intracellular calcium dependence of large dense-core vesicle exocytosis in the absence of synaptotagmin I." Proc Natl Acad Sci U S A **98**(20): 11680-5.

Vuillard, L., C. Braun-Breton, et al. (1995). "Non-detergent sulphobetaines: a new class of mild solubilization agents for protein purification." Biochem.J. **305**: 337-343.

Washbourne, P., P. M. Thompson, et al. (2002). "Genetic ablation of the t-SNARE SNAP-25 distinguishes mechanisms of neuroexocytosis." Nat Neurosci **5**(1): 19-26.

Weber, T., B. V. Zemelman, et al. (1998). "SNAREpins: minimal machinery for membrane fusion." Cell **92**(6): 759-72.

Weimbs, T., S. H. Low, et al. (1997). "A conserved domain is present in different families of vesicular fusion proteins: a new superfamily." Proc Natl Acad Sci U S A **94**(7): 3046-51.

Weimbs, T., K. Mostov, et al. (1998). "A model for structural similarity between different SNARE complexes based on sequence relationships." Trends Cell Biol **8**(7): 260-2.

Weimer, R. M., J. E. Richmond, et al. (2003). "Defects in synaptic vesicle docking in unc-18 mutants." Nat Neurosci **6**(10): 1023-30.

Wiegand, U. K., A. Don-Wauchope, et al. (2002). "Exocytosis studies in a chromaffin cell-free system: imaging of single-vesicle exocytosis in a chromaffin cell-free system using total internal reflection fluorescence microscopy." Ann N Y Acad Sci **971**: 257-61.

Wiegand, U. K., R. R. Duncan, et al. (2003). "Red, yellow, green go! - a novel tool for microscopic segregation of secretory vesicle pools according to their age." Biochem Soc Trans **31**(4): 851-6.

Wilson, D. W., S. W. Whiteheart, et al. (1992). "A multisubunit particle implicated in membrane fusion." J Cell Biol **117**(3): 531-8.

Wilson, D. W., C. A. Wilcox, et al. (1989). "A fusion protein required for vesicle-mediated transport in both mammalian cells and yeast." Nature **339**(6223): 355-9.

Wray, W., T. Boulikas, et al. (1981). "Silver staining of proteins in polyacrylamide gels." Anal.Biochem. **118**: 197-203.

Wu, M. N., J. T. Littleton, et al. (1998). "ROP, the Drosophila Sec1 homolog, interacts with syntaxin and regulates neurotransmitter release in a dosage-dependent manner." Embo J **17**(1): 127-39.

Xu, T., B. Rammner, et al. (1999). "Inhibition of SNARE complex assembly differentially affects kinetic components of exocytosis." Cell **99**(7): 713-22.

Yang, F., L. G. Moss, et al. (1996). "The molecular structure of green fluorescent protein." Nat Biotechnol **14**(10): 1246-51.

Zacharias, D. A., J.DViolin, et al (2002). "Partitioning of Lipid-Modified Monomeric GFPs into Membrane Microdomains of Live Cells." Science **296**: 913-916.